TU Delft

Delft University of Technology

Document Version
Final published version

Licence
CC BY

Citation (APA)
Megill, L. (2026). *Assessing Contrail Climate Impacts and Metrics with OpenAirClim*. [Dissertation (TU Delft), Delft University of Technology]. https://doi.org/10.4233/uuid:54158d90-3779-4d9a-ba42-c9288a2a6bce

Important note
To cite this publication, please use the final published version (if applicable).
Please check the document version above.

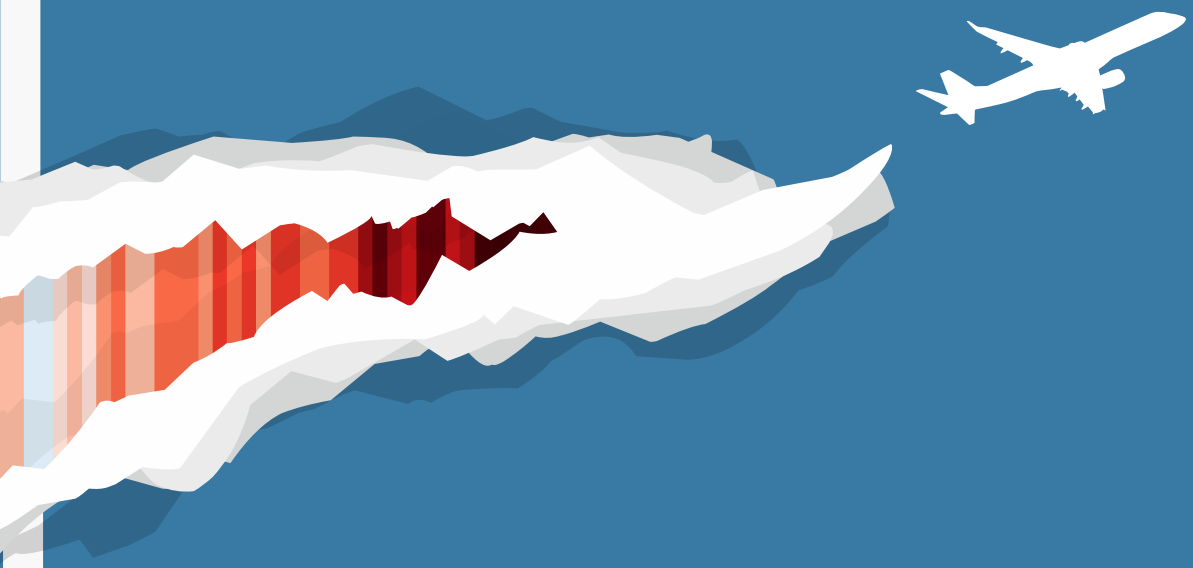
Copyright
In case the licence states “Dutch Copyright Act (Article 25fa)”, this publication was made available Green Open Access via the TU Delft Institutional Repository pursuant to Dutch Copyright Act (Article 25fa, the Taverne amendment). This provision does not affect copyright ownership.
Unless copyright is transferred by contract or statute, it remains with the copyright holder.

Sharing and reuse
Other than for strictly personal use, it is not permitted to download, forward or distribute the text or part of it, without the consent of the author(s) and/or copyright holder(s), unless the work is under an open content license such as Creative Commons.

Takedown policy
Please contact us and provide details if you believe this document breaches copyrights.
We will remove access to the work immediately and investigate your claim.

This work is downloaded from Delft University of Technology.

Assessing Contrail Climate Impacts and Metrics with OpenAirClim



Liam Megill

Assessing Contrail Climate Impacts and Metrics with OpenAirClim

William Alexander MEGILL

Assessing Contrail Climate Impacts and Metrics with OpenAirClim

Dissertation

for the purpose of obtaining the degree of doctor
at Delft University of Technology
by the authority of the Rector Magnificus,
Prof.dr.ir. H. Bijl,
chair of the Board for Doctorates
to be defended publicly on
Friday, 27 November 2026, 10:00

by

William Alexander MEGILL

This dissertation has been approved by the (co)promotors.

Composition of the doctoral committee:

Rector Magnificus,	chairperson
Prof.dr. V. Grewe,	Delft University of Technology, *promotor*
Dr. F. Yin,	Delft University of Technology, *copromotor*

Independent members:

Prof.dr. A. Gangoli Rao,	Delft University of Technology
Prof.dr. M.E.J. Stettler,	Imperial College London
Dr. S. Unterstraßer,	Deutsches Zentrum für Luft- und Raumfahrt
Prof.dr.ir. L.L.M. Veldhuis,	Delft University of Technology
Prof.dr. L.L.A. Vermeersen,	Delft University of Technology, *reserve member*

This doctoral research was supported by the DINA2030+ and 328H2-FC projects of the German Aviation Research Program LuFo VI-2 as well as a joint DLR-Airbus project for the development of the OpenAirClim response model.

Keywords: OpenAirClim, contrails, aviation non-CO_2, climate metrics

Cover by: Turkuaz Nacafi Knol & W.A. Megill. The Climate Stripes are adapted from https://showyourstripes.info/ by Prof. Ed Hawkins (University of Reading), used under CC-BY 4.0

Copyright: 2026 W.A. Megill

An electronic version of this dissertation is available at https://repository.tudelft.nl/.

"Words of encouragement."
"You can't just say 'words of encouragement'."
"Words of great encouragement."

Andy Weir, *Project Hail Mary*

Make sure the information in your sentence is useable even if you get run over by a tram part way throu...

Anna Lanteri

Your. sentences. need. full. stops.

Roosa Joensuu

I feel like some of the findings could have been approximated through physical reasoning.

Reviewer #3

If you're not having fun, it's half your fault.

Doug Dietz

I hate the way things are.
But more than that, I hate change.

Ben Edgar

You can't go around building a better world for people.
Only people can build a better world for people.
Otherwise it's just a cage.

Terry Pratchett, *Witches Abroad*

SUMMARY

International civil aviation is the cornerstone of global mobility and trade, enabling the efficient movement of people and goods across long distances. At the same time, global air transport operations contribute to anthropogenic climate change through carbon dioxide (CO_2) emissions and a range of non-CO_2 emissions and effects. Particularly important is the increased cloudiness due to the formation of condensation trails, or contrails, which is estimated to account for around half of aviation's total radiative forcing. As the industry continues to grow and its climate impact increases, policymakers are increasingly considering the inclusion of aviation non-CO_2 effects within regulatory frameworks. This poses a significant challenge, because these emissions and effects vary strongly with emission location, altitude, season and time of day, have very different atmospheric lifetimes and efficacies and remain subject to considerable scientific uncertainty.

A number of alternative aviation fuels, propulsion technologies and operational concepts have been proposed to reduce the aviation industry's climate impact. Quantifying their long-term effects requires tools capable of simulating large scenario ensembles while adequately representing both CO_2 and non-CO_2 emissions and effects. Comprehensive climate models offer high fidelity but are computationally expensive, making them impractical for the systematic evaluation of large numbers of aviation scenarios. Response models such as AirClim provide a practical alternative by using pre-computed responses and statistical relationships derived from simulations with more comprehensive climate models. However, existing response models are limited in their applicability to emerging propulsion systems and alternative aviation fuels. This dissertation addresses this challenge through the development and application of the open-source response model OpenAirClim, with a particular focus on contrails. The research has three main objectives: (1) to improve the understanding and modelling of persistent contrail formation within a climatological framework; (2) to enable the consistent assessment of future aviation industry scenarios; and (3) to assess the suitability of climate metrics for representing CO_2 and non-CO_2 climate effects on a common scale within policy frameworks.

The dissertation begins by investigating the environmental and aircraft-design-dependent factors controlling persistent contrail formation. Using 10 % of all hourly reanalysis data on conventional flight levels within the 2010 decade, the relative importance of these factors is analysed on a climatological timescale for a wide range of aviation fuels and propulsion technologies. Ice supersaturation is found to be the dominant limiting factor for all engine and fuel combinations, underscoring the importance of accurately predicting ice supersaturated regions.

Nevertheless, the introduction of novel aviation fuels and propulsion technologies is found to have substantial influence on persistent contrail formation. Compared with a state-of-the-art conventional aircraft, envisioned water vapour extraction technologies could reduce the formation of persistent contrails by up to 85 %, whereas hydrogen-powered aircraft could increase formation by around 50 %. The study demonstrates that the probability of persistent contrail formation can be robustly parameterised as a function of aircraft design and flight altitude, which is a necessary first step for developing a consistent climate assessment for different aviation technologies.

Building on this foundation and using dedicated simulations of the general circulation model ECHAM5-CCMod, a new contrail module is developed for the open-source response model OpenAirClim. The module enables the efficient simulation and attribution of stratospheric-adjusted radiative forcing through a modelling chain that links emission inventories, persistent contrail formation, contrail-cirrus coverage and radiative forcing. The framework allows multiple aircraft and fuels to be simultaneously represented within the same emission inventory and scenario. To quantify the climate impact of emerging propulsion technologies and fuels, the module also includes a first representation of the low-soot regime. A comparison with literature demonstrates its ability to reproduce saturation behaviour under high future air traffic scenarios.

The resulting modelling framework is then applied to integrated aviation scenarios developed by the International Civil Aviation Organization (ICAO) to test its ability to simulate complex, multi-fuel and multi-aircraft scenarios. These scenarios represent a wide range of possible technology and fuel transition pathways for the industry. Global mean temperature change from contrails and CO_2 is found not to stabilise within the study horizon for any of the ICAO scenarios, even under the most ambitious transition pathways. The impacts of contrails and CO_2 are found to have opposing trends: While improvements in overall propulsion efficiency and the increasing use of alternative aviation fuels reduce lifecycle net CO_2 emissions, the probability of persistent contrail formation increases. Therefore, the contrail climate benefit of switching to alternative fuels strongly depends on the modelling approach for the low-soot regime. The results demonstrate that an effective reduction in aviation's climate impact requires the introduction of alternative fuels to be accompanied by dedicated non-CO_2 mitigation measures.

Finally, to allow for a complete analysis chain from emissions to policy, the suitability of existing physical climate metrics for representing aviation CO_2 and non-CO_2 emissions and effects is systematically evaluated. The neutrality, temporal stability, policy compatibility and simplicity of alternatives to the conventional Global Warming Potential (GWP) are investigated using the response model AirClim. The historical dominance of the GWP is found to result in a natural bias towards climate metrics that behave similarly. However, more accurate assessments of existing and future aircraft powered by novel aviation fuels can be

achieved using the Average Temperature Response (ATR) or Efficacy-weighted Global Warming Potential (EGWP). While the ATR performs best overall, the EGWP represents a practical compromise and has recently been introduced into European aviation policy.

Overall, this dissertation contributes to the scientific understanding of aviation climate impacts by improving knowledge of the factors governing persistent contrail formation, developing a robust response modelling framework for contrails and identifying suitable climate metrics for use in aviation policy. A central outcome is the OpenAirClim contrail module, an open-source and computationally efficient tool that can be readily adapted and extended. Together with ongoing developments of the OpenAirClim framework, this work is an important step towards enabling consistent and transparent assessments of aviation climate impacts across a wide range of industry scenarios, thereby supporting both scientific analysis and policy implementation.

SAMENVATTING

De internationale luchtvaart is een fundamenteel onderdeel van de wereldwijde mobiliteits- en handelssector. Tegelijkertijd draagt deze echter ook bij aan de antropogene klimaatverandering door de uitstoot van CO_2 en een reeks niet-CO_2-emissies en -effecten. De toegenomen bewolking als gevolg van de vorming van condensatiestrepen, ofwel contrails, vormt een van de belangrijkste factoren van deze laatste categorie, aangezien dit naar schatting verantwoordelijk is voor ongeveer de helft van de stralingsforcering van luchtvaartoperaties. Naarmate de sector blijft groeien en de klimaateffecten toenemen, overwegen beleidsmakers in toenemende mate om niet-CO_2-effecten van de luchtvaart op te nemen in wettelijke regelgeving. Dit vormt een aanzienlijke uitdaging, omdat de atmosferische levensduur en klimaateffectiviteit van deze emissies sterk variëren met de emissielocatie, vlieghoogte, het seizoen en het tijdstip. Bovendien bestaat er grote wetenschappelijke onzekerheid in de kwantificatie van deze effecten.

Er zijn reeds verschillende alternatieve luchtvaartbrandstoffen, voortstuwingstechnologieën en operationele concepten voorgesteld om de klimaatimpact van de luchtvaart te verminderen. Het kwantificeren van de langetermijneffecten van deze maatregelen vereist modellen die in staat zijn complexe scenario's te simuleren, waarin zowel de CO_2- als niet-CO_2-emissies en -effecten adequaat worden gerepresenteerd. Uitgebreide klimaatmodellen bieden een hoge mate van fysische nauwkeurigheid, maar hebben een hoge computationele kost, waardoor zij ongeschikt zijn voor de systematische evaluatie van grote aantallen luchtvaartscenario's. Responsmodellen zoals AirClim bieden een praktisch alternatief door gebruik te maken van vooraf berekende responsfuncties en statistische relaties die zijn afgeleid uit eerdere simulaties met uitgebreidere klimaatmodellen. Bestaande responsmodellen zijn echter beperkt in hoeverre zij toegepast kunnen worden op nieuwe voortstuwingssystemen en alternatieve luchtvaartbrandstoffen. Dit proefschrift pakt deze uitdaging aan door de ontwikkeling en toepassing van het open-source responsmodel OpenAirClim, met daarin een focus op contrails. Het onderzoek heeft drie hoofddoelstellingen: (1) het verbeteren van het begrip en de modellering van persistente contrailvorming binnen een klimatologisch kader; (2) het ontwikkelen van een consistente evaluatiemethode voor toekomstige luchtvaartscenario's; en (3) het beoordelen van de toepasbaarheid van klimaatmetrics voor het doeltreffend representeren van de klimaatimpact van CO_2- en niet-CO_2-emissies, om vergelijkingen binnen beleidskaders mogelijk te maken.

Het proefschrift begint met een onderzoek naar de omgevings- en vliegtuigontwerpafhankelijke factoren die verantwoordelijk zijn voor het vormen van persistente contrails. Met behulp van reanalysedata uit de jaren 2010 wordt de rela-

tieve bijdrage van deze factoren op klimatologische tijdschalen onderzocht. IJs-oververzadiging blijkt de dominante beperkende factor te zijn, wat de noodzaak van een nauwkeurige voorspelling van ijs-oververzadigde gebieden benadrukt. Daarnaast wordt de impact van de introductie van nieuwe luchtvaartbrandstoffen en voortstuwingstechnologieën onderzocht. In vergelijking met een hedendaags vliegtuig zouden toekomstige waterdampafscheidingstechnologieën de vorming van persistente contrails met tot wel 85 % kunnen verminderen, terwijl vliegtuigen met waterstofaandrijving de vorming met ongeveer 50 % zouden kunnen vergroten. De studie laat zien dat de kans op persistente contrailvorming betrouwbaar kan worden geparametriseerd als functie van vliegtuigontwerp en vlieghoogte. Dit vormt een noodzakelijke eerste stap voor het ontwikkelen van een consistent klimaatbeoordeling voor verschillende luchtvaarttechnologieën.

Voortbouwend op deze resultaten en met behulp van simulaties met het circulatiemodel ECHAM5-CCMod wordt een nieuwe contrailmodule ontwikkeld voor het open-source responsmodel OpenAirClim. Deze module maakt een efficiënte simulatie van stratosferisch aangepaste stralingsforcering mogelijk met een methode die emissie-inventarissen, de vorming van persistente contrails, contrail-cirrusbedekking en stralingsforcering met elkaar verbindt. Deze nieuwe methode maakt het mogelijk om meerdere vliegtuigtypen en brandstoffen binnen hetzelfde emissie-inventaris en scenario te analyseren. Om de klimaatimpact van deze opkomende voortstuwingstechnologieën en brandstoffen te kwantificeren, bevat de module bovendien een eerste beschrijving van het zogenaamde lage-roetregime. Een vergelijking met bestaande literatuur toont aan dat het model in staat is verzadigingspatronen te reproduceren onder toekomstscenario's met een grote hoeveelheid luchtverkeer.

Het hiermee ontwikkelde framework wordt vervolgens toegepast op luchtvaartscenario's ontwikkeld door de International Civil Aviation Organization (ICAO) om te testen in hoeverre het complexe scenario's met meerdere brandstoffen en vliegtuigtypen accuraat kan representeren. Deze scenario's vertegenwoordigen een breed scala aan mogelijke technologische en brandstoftransitiepaden voor de luchtvaartsector. Voor geen van de ICAO-scenario's stabiliseert de wereldgemiddelde temperatuurverandering als gevolg van contrails en CO_2 binnen de beschouwde tijdshorizon, zelfs niet met de meest ambitieuze aanpak. De effecten van contrails en CO_2 vertonen tegenovergestelde trends: terwijl verbeteringen in voortstuwingsefficiëntie en het toenemende gebruik van alternatieve luchtvaartbrandstoffen de netto CO_2-emissies over de levenscyclus verminderen, neemt de kans op vorming van persistente contrails toe. Het klimaateffect van de overstap naar alternatieve brandstoffen hangt daarom sterk af van de definitie van het lage-roetregime. De resultaten tonen aan dat, naast het gebruik van alternatieve brandstoffen, het ook noodzakelijk is om de effecten van niet-CO_2 te verminderen om een significante vermindering van de klimaatinvloed van de luchtvaart te bereiken.

Ten slotte wordt de toepasbaarheid van bestaande klimaatmetrics voor de

indicatie van CO_2- en niet-CO_2-emissies in de luchtvaart systematisch geëvalueerd. De neutraliteit, tijdsonafhankelijkheid, beleidsrelevantie en eenvoud van toepassing van alternatieven voor het conventionele Global Warming Potential (GWP) worden onderzocht met behulp van het responsmodel AirClim. De historische tendens in het gebruik van het GWP blijkt te leiden tot een vertekend beeld, met een voorkeur voor klimaatmetrics die zich op een vergelijkbare manier gedragen. Nauwkeurigere beoordelingen voor huidige en toekomstige vliegtuigen die worden aangedreven door nieuwe luchtvaartbrandstoffen kunnen echter worden gemaakt met behulp van de Average Temperature Response (ATR) of het Efficacy-weighted Global Warming Potential (EGWP). Hoewel de ATR over het algemeen het beste presteert, biedt het EGWP een praktisch compromis en is het recent opgenomen in het Europese luchtvaartbeleid.

Dit proefschrift draagt bij aan het wetenschappelijke begrip van klimaateffecten van de luchtvaart door het inzicht in de vormingsprocessen van contrails te vergroten, een robuust responsmodelleringraamwerk voor contrails te ontwikkelen en geschikte klimaatmetrics voor toepassing in luchtvaartbeleid te identificeren. Een belangrijk resultaat is de ontwikkelde OpenAirClim-contrailmodule, een open-source en computationeel efficiënt model dat eenvoudig kan worden aangepast en uitgebreid. In combinatie met de voortdurende ontwikkeling van het OpenAirClim-raamwerk vormt dit werk een belangrijke stap richting consistente en onderbouwde beoordelingen van de klimaateffecten van de luchtvaart over een breed domein van luchtvaartscenario's, wat zowel verdere wetenschappelijke analyse als beleidsontwikkeling kan ondersteunen.

ACKNOWLEDGEMENTS

The PhD is ostensibly a solo journey, but you couldn't defend such a proposition even if you tried. This dissertation would not have been possible without a large number of people. I have tried to thank everyone here, but in my current somewhat scatterbrained state, writing what are hopefully some of the last words of this dissertation, I will inevitably have accidentally forgotten to mention someone. In that case, your best course of enacting sweet, sweet revenge is undoubtedly to embody your internal Reviewer #2 and get in touch to point out a spelling mistake or factual oversight that *really* should have been caught.

First and foremost, I'd like to thank my supervisory team: Volker and Feijia. Thank you for all of your encouragement and support! I learned a lot from you over the past few years, starting all the way back during the DSE. I really appreciate the freedom you gave me to do whatever I felt was necessary, even if what I initially thought was necessary sometimes ended up being long (but interesting!) tangents. Thanks also for putting your trust in me and letting me loose on a number of very interesting projects. Leading the tendering process for the Non-CO_2 MRV project was, in particular, a very interesting and rewarding experience, and I know that this was not an opportunity PhDs typically have.

My thanks goes to Anja Schmidt, who warmly welcomed me to the department of Earth System Modelling and supported me during some frustrating periods. Thanks also to Klaus Gierens, who provided very valuable food for thought and feedback on my work, and Birgit Hassler, Tina Jurkat-Witschas and Luca Bugliaro for providing internal reviews of my papers. For their support with all things organisational and administrative, I thank Anja Blum and Sheena Löffel at the DLR and Lisette Vollmer at the TU Delft, in particular during the first year of my PhD when I was travelling back and forth between Delft and Munich.

This work would not have been possible without the great teamwork with Stefan Völk on the development of OpenAirClim! My thanks also goes to the rest of the core development group, in particular Katrin Dahlmann and Hiroshi Yamashita. Björn Brötz's good advice on working with large datasets and software development was also highly appreciated. For the CCMod simulations used to develop the contrail module, I wish to thank Cornelius Weiß-Rehm, Marius Bickel and Ulrike Burkhardt. Thanks to Simon Unterstraßer, who helped me understand the aircraft size dependence implemented in AS4D and its limitations. At Airbus, I'd like to thank in particular Frédérique Rigal, Charles Renard, Philippe Mattei and Katharina Seeliger for their valuable questions and input.

Within the Non-CO_2 MRV project, I'd like to thank Vincent de Haes and Maarten

Tielrooij (To70), Robert Koster (AerLabs), Dimitar Nikov (DG Clima) and at the DLR Roland Eichinger, Alexander Lau, Sven Maertens, Malte Niklaß, Florian Linke, Martin Plohr, Dennis Piontek, Christiane Voigt and Rizwan Malik. For the DINA2030+ project, Christopher Simson (MTU) and at the DLR Max Mendiguchia Meuser and Milenko Rubin-Zuzic. And for the 328H2-FC project, Engin Yilmaz and Lukas Schnörer.

Where there is thanks, I believe there should also be anti-thanks. In the interest of balance. Therefore, no thanks is given to the Munich S-Bahn for its steadfast refusal to adhere to published timetables. That's not to say that I have not found the extra time that I have spent on board during my PhD enjoyable – it gave me a lot of time to read – it's just that there are other things I would rather have been doing for 2500 minutes (I counted). I explicitly withhold thanks from my email inbox for its seemingly tireless expansion during critical writing phases. Nor do I thank my own past self for procrastination-driven experimental analysis. The amount of time I spent making a graph look "pretty"...

This journey was made more enjoyable and inspiring by my current and former PhD colleagues, both at the DLR and TU Delft. And here lies a real danger that I have forgotten someone. If you think I have, I owe you a drink, I'm sorry. Thank you to: Adrienne, Almut, Andrei, Anna, Anna, Arwin, Camilo, Cornelius, Dario, Dennis, Esther, Federica, Harjot, Irina, Jakob, Johannes, Judith, Julia, Juriaan, Jutta, Karol, Laura, Marius, Monica, Moritz, Patrick, Sheena, Simon, Sina and Thymen. Thanks for making me feel at home both in Oberpfaffenhofen and Delft!

I am indebted to the many wonderful people who have made Munich home. Hannes, for the hockey, Cat Quest and amazing salads. The newly wed Mr. and Mrs. Lanteri, for the board games, karaoke, hiking and all-round good times! Hanna, Merlin, Luna and Oskar, for the Isar barbecue, bowling and Krimidinners. Emre, for the roller-coaster fever and political discussions. John and Aida, for fun evenings with Canadian food, and discussions that keep my aerospace engineering knowledge somewhat honed during my foray into atmospheric physics. A big thank you to Aida for also helping me translate the summary into Dutch. The climbing crew: No pain, no gain, except when you're coming to the end of your first dissertation draft and the pain is in your wrist and typing becomes a problem. Ah well, it worked out somehow.

A big thank you also to my friends outside of Munich, in particular Aïcha, Ines, Kristie, Sarah, Thomas, Thomas and Tom. Thanks to Turkuaz for helping with the cover of this dissertation! And thank you to Auke, Fabian, Graceanne and Thijs for the great time racing submarines in Gosport and Gran Canaria.

I am very grateful for the unwavering support and encouragement from my parents, sister and the rest of my family. This dissertation is dedicated to Grandpa, John and Opa, who will not get to read these words. Thanks also to our visiting cats Pablo and Zeytin who provided plenty of moral support. And of course to

our new feline resident Kismet, who is already an intrinsic part of the family.

Finally, the biggest thank you goes to Roosa, for forcing me to go outside, for our great holidays together, for listening to my complaints and for just always being there for me. After my MSc thesis, I promised you that I would use more full stops. Therefore, I'm happy to announce that where my MSc thesis had an average sentence length of 11 words, this document is down to only 8.3! All joking aside, I could not have done this without your love and support. Thank you!

Liam Megill
München, April 2026

DECLARATION ON THE USE OF AI

I acknowledge the use of Artificial Intelligence (AI) tools to support aspects of this PhD research process. All models and tools were used strictly as supportive aids. All final research decisions, analyses, interpretations and written content presented in this dissertation, as well as the linked code and datasets, are my own.

The following models and tools were used. OpenAI ChatGPT (premium subscription) and Microsoft Copilot Chat (as provided by the TU Delft) were employed for assistance with open-source coding tasks and LaTeX development, language refinement of selected passages and the initial translation of the summary into Dutch. Open-source large language models hosted internally by the DLR were used for coding support involving internal data and proprietary code. The Scite and ResearchRabbit platforms were used for literature discovery.

LIST OF PUBLICATIONS

JOURNAL PAPERS

Megill, L., Deck, K. and Grewe, V.: Alternative climate metrics to the Global Warming Potential are more suitable for assessing aviation non-CO_2 effects, Communications Earth & Environment, 5, 249, doi: 10.1038/s43247-024-01423-6, 2024.

Megill, L. and Grewe, V.: Investigating the limiting aircraft-design-dependent and environmental factors of persistent contrail formation, Atmospheric Chemistry & Physics, 25, 7, doi: 10.5194/acp-25-4131-2025, 2025.

Santos Gabriel, V., Bugliaro, L., Montag, M., Ries, S., Wang, Z., Widmaier, K., Arico, M., Unterstrasser, S., Mayer, J., Menekay, D., Marsing, A., de la Torre Castro, E., **Megill, L.**, Scheibe, M. and Voigt, C.: A manually labeled contrail dataset from MSG/SEVIRI, Earth System Science Data, 18, 3, doi: 10.5194/essd-18-2397-2026, 2026.

Grewe, V., Zhukovska, S., Dahlmann, K., Matthes, S., **Megill, L.**, Betram, P., Ratei, P., Prakasha, P., Linke, F., Niklaß, M., Lührs, B., Terrenoire, E., Novelli, P., Lefebvre, T., Söffing, L., Bucchignani, E. and Solazzo, M.: Review of methods for assessing the climate impacts of aviation technologies and the resulting best practices, CEAS Aeronautical Journal, doi: 10.1007/s13272-026-00980-0, 2026

Völk, S., Yamashita, H., **Megill, L.**, Dahlmann, K. and Grewe, V.: OpenAirClim v0.XX: A framework for assessing the climate impact of aviation emissions, *in prep.*

Megill, L. and Grewe, V.: The OpenAirClim v0.XX contrail response modelling and attribution approach, *in prep.*

CONFERENCE PRESENTATIONS

Megill, L., Deck, K. and Grewe, V.: Selecting a suitable climate metric for aviation policy and aircraft design, 4th ECATS Conference 2023, Delft, The Netherlands, 24–26 October, 2023.

Völk, S., Yamashita, H., **Megill, L.**, Matthes, S., Dahlmann, K. and Grewe, V.: OpenAirClim - A framework for the computation of air traffic climate impact based on response modeling (Poster), 4th ECATS Conference 2023, Delft, The Netherlands, 24–26 October, 2023.

Megill, L. et al.: Non-CO_2 MRV - Support for establishing a monitoring, reporting and verification system, Workshop on aviation non-CO_2 emissions, Brussels, Belgium, 13–14 December, 2023.

Megill, L., Völk, S., Yamashita, H., Dahlmann, K. and Grewe, V.: Open-Source Aviation Climate Response Modelling with OpenAirClim (Poster), 13th OpenSky Symposium, Norrköping, Sweden, 6–7 November, 2025.

SOFTWARE

Völk, S., Yamashita, H., **Megill, L.**, Dahlmann, K. and Grewe, V.: OpenAirClim, doi: 10.5281/zenodo.13682729, GitHub: dlr-pa/oac, 2024.

Megill, L.: Generating Emission Datasets from Aircraft Inventories (GEDAI), GitHub: liammegill/gedai, 2025.

DATASETS

Megill, L., Deck, K. and Grewe, V.: Data and code underlying the publication "Alternative climate metrics to the Global Warming Potential are more suitable for assessing aviation non-CO2 effects", 4TU.ResearchData, doi: 10.4121/344e24ad-b2f5-4ed9-8d49-6efa2081d30c, 2024.

Megill, L. and Grewe, V.: Data and code underlying the publication "Investigating the limiting aircraft-design-dependent and environmental factors of persistent contrail formation", 4TU.ResearchData, doi: 10.4121/cdb4e3bb-d6f4-4422-a715-b6187098a314, 2025.

Santos Gabriel, V., Bugliaro, L., Montag, M., Ries, S., Wang, Z., Widmaier, K., Arico, M., Unterstraßer, S., Mayer, J., Menekay, D., Marsing, A., de la Torre Castro, E., **Megill, L.**, Scheibe, M. and Voigt, C.: Annotated contrail dataset for Meteosat Second Generation (MSG), Zenodo, doi: 10.5281/zenodo.17669444, 2025.

Megill, L., Weiß-Rehm, C., Bickel, M., Burkhardt, U. and Grewe, V.: Data and code underlying the development of the OpenAirClim Contrail Module, 4TU.ResearchData, doi: 10.4121/bf6b471a-3dbb-4ba5-b703-518599d51a7f, 2026.

Megill, L.: Data and code underlying the ICAO scenario analysis with OpenAirClim, 4TU.ResearchData, doi: 10.4121/f016041d-5c71-430e-9358-24b2d5bc5403, 2026.

Megill, L.: Data and code underlying the dissertation "Assessing Contrail Climate Impacts and Metrics with OpenAirClim", 4TU.ResearchData, doi: 10.4121/70e059b5-4c42-4462-b8dd-780d57256cdd, 2026.

ADDITIONAL PUBLICATIONS

de Haes, V., Tielrooij, M., Jesus, M., Rodriguez, E., Rzeplinska, L., Eichinger, R., **Megill, L.**, Dahlmann, K., Grewe, V., Lau, A., Niklaß, M., Piontek, D., Voigt, C., Plohr, M., Wozny, F., Scheelhaase, J., Koster, R., Natera Orozco, L.: Support for establishing a monitoring, reporting and verification system for non-CO2 effects in aviation, stemming from the revision of the ETS Directive. Final Report, 2025.

AWARDS

Megill, L.: Ivar Isaksen Early Career Researcher Prize. 4th ECATS Conference 2023, Delft, Netherlands, 24–26 October, 2023.

CONTENTS

Summary vi

Samenvatting ix

Acknowledgements xii

List of Publications xvi

List of Figures xxii

List of Tables xxv

1 Introduction 1
- 1.1 Dissertation aim . . . 5
- 1.2 Dissertation outline . . . 6
- References . . . 8

2 Background 11
- 2.1 Climate impacts of aviation . . . 12
  - 2.1.1 Radiative forcing and temperature change . . . 12
  - 2.1.2 Contribution of aviation emissions . . . 14
  - 2.1.3 Aviation emission species . . . 15
- 2.2 Contrails . . . 19
  - 2.2.1 Contrail formation and ice nucleation . . . 19
  - 2.2.2 Contrail lifecycle . . . 21
  - 2.2.3 Contrail measurements . . . 22
  - 2.2.4 Contrail climate impacts . . . 25
  - 2.2.5 Contrail mitigation . . . 26
- 2.3 Climate metrics . . . 27
  - 2.3.1 Design of climate metrics . . . 28
  - 2.3.2 Climate metric calculations . . . 29
- References . . . 34

3 Modelling 45
- 3.1 Response modelling with (Open)AirClim . . . 47
- 3.2 Contrail modelling . . . 48
  - 3.2.1 Physical contrail models . . . 48
  - 3.2.2 Contrail response modelling with AirClim . . . 50
- 3.3 Emission inventories and scenarios . . . 52
- 3.4 Attribution methods . . . 55
- 3.A Appendix: Critical analysis of track and slant distances in emission inventories . . . 58
- References . . . 60

4 Limiting Factors of Persistent Contrail Formation **67**
4.1 Introduction . . . 68
4.2 Data and methods . . . 69
4.2.1 Contrail formation and persistence . . . 69
4.2.2 Aircraft definitions . . . 73
4.2.3 Air traffic data . . . 74
4.2.4 ERA5 data and corrections . . . 75
4.2.5 Limiting factors analysis . . . 76
4.2.6 Analysis of persistent contrail formation region boundaries . . . 76
4.2.7 Maximum slope analysis . . . 78
4.3 Results and Discussion . . . 79
4.3.1 Limiting factors of persistent contrail formation . . . 79
4.3.2 Boundaries of persistent contrail formation regions . . . 80
4.3.3 Spatial variability of persistent contrail formation . . . 83
4.3.4 Climatological potential persistent contrail formation . . . 85
4.3.5 Competition between limiting factors . . . 87
4.3.6 Uncertainties and limitations . . . 88
4.4 Conclusion . . . 90
References . . . 97

5 Development of the OpenAirClim Contrail Module **101**
5.1 Introduction . . . 102
5.2 ECHAM5-CCMod model setup . . . 103
5.3 Module development . . . 107
5.3.1 Development process & strategy . . . 107
5.3.2 Emission inventory and simulation configuration . . . 109
5.3.3 Contrail formation . . . 109
5.3.4 Contrail-cirrus coverage . . . 112
5.3.5 Influence of particle emissions . . . 114
5.3.6 Radiative forcing . . . 117
5.3.7 Dependence on aircraft size . . . 119
5.4 Validation . . . 120
5.5 Sensitivity to design parameters . . . 123
5.6 Contrail attribution . . . 125
5.7 Discussion . . . 126
5.8 Summary and outlook . . . 128
References . . . 133

6 Analysis of ICAO Aviation Scenarios with OpenAirClim **137**
6.1 Introduction . . . 138
6.2 Harmonising the ICAO scenarios with OpenAirClim . . . 140
6.2.1 Scenario definitions . . . 140
6.2.2 Fuel demand and CO_2 emissions . . . 141
6.2.3 Aircraft definitions . . . 143
6.2.4 Developing Compatible emission inventories . . . 146
6.2.5 OpenAirClim simulation setup . . . 147

6.3 Results . . . 148
6.4 Contextualisation of the results . . . 152
6.5 Discussion and conclusion . . . 154
References . . . 159

7 Analysis of Climate Metrics **163**
7.1 Introduction . . . 164
7.2 Methods . . . 166
7.2.1 Development of climate metric requirements . . . 166
7.2.2 Development of fuel scenarios . . . 167
7.2.3 Development of aircraft designs . . . 167
7.3 Results . . . 168
7.3.1 REQ 1: Climate metric neutrality with respect to aviation emissions . . . 169
7.3.2 REQ 2: Temporal stability . . . 171
7.3.3 REQ 3: Be compatible with existing climate policy . . . 173
7.3.4 REQ 4: Be simple to understand and implement . . . 174
7.3.5 Choice of climate metric and time horizon . . . 175
7.4 Feedback from the community . . . 176
7.4.1 Non-CO_2 MRV . . . 176
7.4.2 CLAIM . . . 178
7.5 Discussion and conclusion . . . 180
References . . . 187

8 Conclusion and Outlook **191**
8.1 Answering the research questions . . . 193
8.2 Outlook . . . 197
References . . . 200

A OpenAirClim Contrail Module **203**
A.1 Emission inventory and simulation configuration . . . 204
A.2 Contrail formation . . . 206
A.3 Contrail-cirrus coverage . . . 206
A.4 Radiative forcing . . . 208
A.5 Post-processing . . . 209
A.6 Attribution . . . 209
References . . . 210

B Curriculum Vitæ **213**

LIST OF FIGURES

2.1 Cartoon demonstrating different radiative forcing definitions 13
2.2 Best estimates for climate forcing terms from global aviation operations from 1940 to 2018 14
2.3 Spatial and temporal scales of aviation-related emissions and effects 16
2.4 Sketch of the ice formation processes for current rich-quench-lean and lean-burn engine configurations 21
2.5 Cause-effect chain from emissions to damages. 28

3.1 Aviation scenarios and emission inventories considered in this study . 53
3.2 Vertical and latitudinal profiles of various emission inventories 54

4.1 Ambient temperature vs. water vapour partial pressure diagram for an example aircraft mixing line. 70
4.2 Example of the horizontal limiting factors analysis for H2C-40 using fictional data at a single pressure level over the Netherlands. 77
4.3 Global area- and level-weighted potential persistent contrail formation and limiting factor frequency during the 2010 decade. 80
4.4 Normalised and area-weighted global limiting factors of the 2010 decade. 81
4.5 Horizontal and vertical total limiting factor results. 82
4.6 Potential persistent contrail formation as a function of latitude and altitude. 83
4.7 Potential persistent contrail formation as a function of the mixing line slope. 85
4.A.1 Ambient temperature vs. water vapour partial pressure diagram with threshold mixing lines 92
4.A.2 DEPA 2050 progressive scenario for the year 2050 used to weight the potential persistent contrail formation 93
4.A.3 Number of hours randomly selected in ERA5 within the 2010 decade 93
4.A.4 Comparison of the cumulative distribution functions of ERA5 and MOZAIC/IAGOS 94
4.A.5 Potential persistent contrail formation as a function of latitude and altitude for different relative humidity enhancements 94
4.A.6 Effect of relative humidity enhancement on potential persistent contrail formation 95
4.A.7 Effect of temperature enhancement on potential persistent contrail formation 96

5.1 Subsets of the DLR TraK inventory used in the ECHAM5-CCMod simulations for the development of the OpenAirClim contrail module . . 105
5.2 Overview of the OpenAirClim Contrail Module 106
5.3 Development Process for the OpenAirClim Contrail Module 108
5.4 Potential persistent contrail formation as a function of the mixing line slope on a climatological timescale for pressure levels 350 to 150 hPa.110
5.5 Comparison of potential persistent contrail formation from ERA5, ECHAM5-CCMod and ECHAM4-CCMod 112
5.6 Performance of coverage model 30 114
5.7 Normalised RF as a function of the soot number emission index. . . . 116
5.8 Relationship between contrail-cirrus coverage and RF from the ECHAM5-CCMod simulations 118
5.9 Area-weighted (latitude) contrail-cirrus coverage vs. Radiative Forcing 119
5.10 Comparison of global RF from literature and calculated using the OpenAirClim contrail module 121
5.11 Sensitivity of OpenAirClim to changes in cruise altitude 123
5.12 Comparison between the AirClim and OpenAirClim contrail modules. 124
5.13 Sensitivity of the OpenAirClim contrail module to two aircraft design parameters 124
5.14 Comparison of global RF from literature and calculated using a simple distance-dependent model based on Bier et al. (2022) 127
5.A.1 RF-anchored reconstruction of contrail-cirrus coverage 130
5.A.2 Regions of the Radiative Forcing model 130

6.1 Global fuel demand and CO_2 emissions for the three integrated ICAO scenarios 142
6.2 Fleet composition of each aircraft category in scenarios IS2 and IS3 . 145
6.3 Demonstration of creating aircraft generations in lieu of providing evolution files per aircraft 147
6.4 Radiative Forcing and temperature change from CO_2 and contrails for the ICAO scenarios 148
6.5 Temperature change for the ICAO scenarios split by source, aircraft category and fuel used 150
6.6 Sensitivity of the contrail-induced temperature change to the low soot case 151
6.7 Radiative Forcing from CO_2 and contrails per Available Seat Kilometre 152
6.A.1 Assumed fuel efficiency values for ICAO scenarios 156
6.A.2 Vertical and latitudinal profiles of the aircraft categories used in this study 156
6.A.3 Temperature change for the ICAO scenarios split by source, aircraft category and fuel used 157
6.A.4 Sensitivity of the background emission scenario on the temperature change from aviation CO_2 emissions 158
6.A.5 Sensitivity of the technology confidence level on the temperature change 158

7.2 Comparison of the neutrality of different climate metrics to changes in aircraft design. 171
7.3 Comparison of the climate metric responses for full aviation emission scenarios. 172
7.4 CO_2-eq emissions calculated using the GWP^*_{100} method for an example fleet demonstrating the flow-based nature of the GWP*. 174
7.5 Comparison of the GWP, EGWP and ATR responses for time horizons between 0 and 100 years. 177
7.A.1 Comparison of the GWP, EGWP and rATR responses for the CORSIA and FP2050 full aviation emission scenarios 182
7.A.2 Time horizon analysis of the GWP 183
7.A.3 Time horizon analysis of the EGWP 184
7.A.4 Time horizon analysis of the ATR 185
7.A.5 Time horizon analysis of the GTP 186

A.1 Overview of the OpenAirClim Contrail Module 205

LIST OF TABLES

2.1 Calculation methods for all climate metrics used in this research. . . 29

4.1 Definition of aircraft-engine-fuel combinations used in the limiting factors study. . . . 74
4.2 Optimal parameters for potential persistent contrail formation as a function of the mixing line slope. . . . 87
4.A.1 Potential persistent contrail formation p_{pcf} and DEPA 2050 distance-weighted p_{pcf} . . . 92

5.1 Fuels used in the ECHAM5-CCMod simulations . . . 104
5.2 Parameters for the low-soot regime modelling cases . . . 117
5.A.1 Literature used for validation of the OpenAirClim contrail module . . 131
5.A.2 Contrail-cirrus coverage functions . . . 132

6.1 Aircraft category definitions for the ICAO scenarios . . . 143

7.1 Ranges of fleet design parameters for the fleet pairing analysis simulations. . . . 167
7.2 Assumed change of in-flight emissions and emission-related effects for SAF and hydrogen. . . . 168
7.3 Overview of the performance of the analysed climate metrics with respect to each requirement. . . . 175

A.1 Parameters for the low-soot regime modelling cases . . . 208
A.2 Radiative forcing model fit parameters and validity ranges . . . 209

Endangerment.

no insects, no birds,
no forests, no reefs, no people,
the line must go up.

— LM

1

INTRODUCTION

1

International civil aviation is the backbone of global mobility and trade. It enables globalised supply chains and facilitates the movement of people for family, work and tourism. Air traffic has grown rapidly across all world regions, reaching a new high of 4.8 billion passengers[1] in 2025 (IATA, 2025). This trend is expected to continue, with compound annual growth rate forecasts between 3.6 % and 4.2 % (Airbus, 2025; Boeing, 2025; ATAG, 2024). The impact of the COVID-19 pandemic was severe but mostly temporary: The industry surpassed 2019 traffic levels again in 2024.

At the same time, aviation contributes significantly to anthropogenic climate change. Recent best estimates attribute approximately 3.7 % of anthropogenic Effective Radiative Forcing (ERF) in 2018 to aviation operations between 1940 and 2018 (Lee et al., 2021). In addition to carbon dioxide (CO_2) emissions, aviation affects the climate though a range of non-CO_2 emissions and effects, most notably nitrogen oxides (NO_x, Stevenson et al., 2004; Myhre et al., 2011), water vapour (H_2O, Frömming et al., 2012; Wilcox et al., 2012), aerosols (Gettelman and Chen, 2013; Righi et al., 2025; Hendricks et al., 2026) and the formation of contrails (Burkhardt and Kärcher, 2011; Bock and Burkhardt, 2016). Unlike CO_2, these effects are highly dependent on the emission location, altitude, season and time of day (Köhler et al., 2008; Frömming et al., 2021) and remain subject to considerable scientific uncertainty (Lee et al., 2021).

Among the non-CO_2 effects, contrails are of particular importance. A contrail can form behind an aircraft when the hot and humid engine exhaust plume mixes with sufficiently cold ambient air, allowing aerosols in the exhaust to activate into water droplets that subsequently freeze (Schumann, 1996; Kärcher et al., 2015). While most contrails dissipate quickly, under ice supersaturated conditions contrails can persist, slowly spread out and evolve into contrail-cirrus clouds (Haywood et al., 2009; Schumann and Heymsfield, 2017). Contrail-cirrus modify the Earth's radiation balance by scattering incoming shortwave radiation and reducing outgoing longwave radiation (Kärcher, 2018). Recent studies have suggested that contrails could be responsible for around half of the anthropogenic ERF from aviation operations (Lee et al., 2021). However, their climate efficacy is assumed to be substantially lower than that of CO_2, thereby limiting their relative impact on temperature change (Bickel et al., 2025).

Mitigating the climate impact of aviation is challenging for three structural reasons. First, non-CO_2 emissions and effects are highly heterogeneous and their quantification is associated with large uncertainty ranges, complicating the development of mitigation strategies. Second, improvements in aircraft, engine and operational efficiency have been outpaced by the sustained growth in air traffic: an effect often described as the efficiency paradox. Several studies have highlighted the difficulty of meeting climate targets while maintaining high growth

[1] This definition (generally used by the International Air Transport Association, IATA) refers to the number of departing passengers, i.e. origin-to-end-destination trips, not the total number of passenger journeys or the number of unique passengers.

rates (e.g. Aamaas et al., 2025; Arblaster et al., 2025). Achieving deep reductions in aviation's climate impact therefore requires structural changes in aircraft design, propulsion systems, fuels and operations.

The third structural difficulty relates to the industry's international nature: The Paris Agreement does not set emissions targets for specific sectors and international civil aviation is not included in Member States' Nationally Determined Contributions. At the global level, the International Civil Aviation Organisation (ICAO) has introduced the Carbon Offsetting and Reduction Scheme for International Aviation (CORSIA), which aims to achieve carbon-neutral growth by offsetting CO_2 emissions from international flights beyond 85 % of 2019 levels (ICAO, 2023). However, the effectiveness and environmental integrity of offsetting mechanisms remains contested (e.g. Badgley et al., 2022; Trencher et al., 2024) and CORSIA addresses CO_2 emissions only.

Non-CO_2 emissions and effects are increasingly considered at the regional level. In the European Union, a recent revision of the EU Emissions Trading Scheme (ETS) introduced a Monitoring, Reporting and Verification (MRV) framework[2] for aviation non-CO_2 effects, with the possibility of their inclusion in the ETS by 2027. In parallel, the ReFuelEU regulation[3] mandates a steadily increasing minimum share of alternative aviation fuels within the EU fuel mix, rising from 2 % in 2025 to 70 % in 2050. Similar mandates have been introduced in the UK and Singapore. These measures signal the movement towards a broader regulatory landscape encompassing both CO_2 and non-CO_2 emissions and effects.

A key enabler of this transition is the introduction of alternative aviation fuels. These can be categorised as either drop-in or non-drop-in: Drop-in fuels can be directly used by existing aircraft engines or mixed with conventional kerosene, whereas non-drop-in fuels require significant changes to aircraft, engines and fuelling infrastructure. Drop-in fuels that meet certain sustainability criteria are commonly referred to as Sustainable Aviation Fuels (SAFs). The principle benefit of SAF lies in lifecycle CO_2 emission reductions, which varies depending on the feedstock and production pathway (Prussi et al., 2021; Detsios et al., 2023). Additionally, the fuel composition can be tailored, for example to influence contrail properties by reducing sulphur content (Dischl et al., 2025).

A promising non-drop-in fuel is hydrogen (H_2), which can be combusted or used in a fuel cell. It produces no direct CO_2 emissions during operation and can substantially reduce or eliminate emissions of NO_x, soot and other aerosols. However, lifecycle emissions depend on production pathways (often categorised by "colour"; Incer-Valverde et al., 2023) and its altered emission characteristics imply different non-CO_2 climate responses. In particular, increased water vapour emissions increases the probability of contrail formation (Marquart et al., 2001; Kaufmann et al., 2024).

[2]Directive 2023/958 of May 10, 2023 amending Directive 2003/87/EC

[3]Regulation (EU) 2023/2405 of the European Parliament and of the Council of 18 October 2023 on ensuring a level playing field for sustainable air transport (ReFuelEU Aviation)

1

The increasing diversity of fuels, propulsion concepts and operational concepts substantially expands the realm of possible future pathways for the aviation industry. Evaluating their long-term climate impacts requires tools capable of simulating large scenario ensembles while adequately representing both CO_2 emissions and non-CO_2 emissions and effects. Comprehensive climate models provide high physical fidelity but are computationally expensive, making them suitable for fundamental research but impractical for the systematic evaluation of large numbers of technology options, operational strategies or scenarios ensembles. A fundamentally different approach is taken by response models such as AirClim (Grewe and Stenke, 2008; Dahlmann et al., 2016): Rather than explicitly simulating atmospheric processes, pre-computed responses and statistical relationships are derived from targeted simulations using comprehensive climate models. This enables the efficient assessment of long-term scenarios as well as sensitivity and uncertainty analyses. However, AirClim is closed-source and not applicable to many emerging fuels and propulsion technologies.

This dissertation addresses this gap through the development and validation of OpenAirClim (Völk et al., 2025), an open-source response model and successor to AirClim. The central contribution is the development of a new contrail module capable of calculating changes in the contrail-induced global mean stratospheric-adjusted radiative forcing and surface temperature change in response to a given emission inventory and scenario. This work explores methods for simulating and attributing the contrail climate effects of multi-aircraft and multi-fuel scenarios, including propulsion technologies that lie within the low-soot regime, such as lean burn combustion and hydrogen propulsion. The OpenAirClim framework is applied to the ICAO integrated aviation scenarios to quantify both contrail and CO_2 climate impacts under possible development pathways, and compared to a recent, similar study by Aamaas et al. (2025).

Beyond quantifying climate impacts, policymakers and industry stakeholders require a basis for comparing technologies and scenarios within regulatory frameworks. To maintain compatibility with market-based schemes and targets initially only developed for CO_2, non-CO_2 emissions and effects must be expressed on a common scale with CO_2 emissions using a climate metric. However, establishing an adequate equivalence between CO_2 and non-CO_2 is non-trivial due to the highly heterogeneous nature of aviation non-CO_2 emissions and effects. This dissertation therefore systematically analyses the applicability of existing, physical climate metrics for aviation policy and aircraft design by examining their compatibility, methodological simplicity, neutrality and stability. It recommends a derivative of, and an alternative to, the dominant Global Warming Potential (GWP) climate metric, which are both found to provide more accurate assessments of current and future aviation technologies.

1.1. DISSERTATION AIM

The following research questions are addressed within the framework of this dissertation. Also provided are the links between some of the research questions (RQ) and the research projects that supported the work conducted.

RESEARCH QUESTIONS

RQ1 **What aircraft-dependent and environmental factors govern persistent contrail formation and how do they vary spatially and seasonally?**
Deliverable for the DINA2030+ and 328H2-FC LuFo projects.

(a) How do the limiting factors interact?
(b) Can the probability of persistent contrail formation be robustly parameterised within a response modelling framework?

RQ2 **How can the climate impact of contrails be evaluated within a computationally efficient response modelling framework?**
Deliverable for the DLR-Airbus OpenAirClim project.

(a) Which parameters best characterise the relationships between contrail formation, contrail-cirrus coverage and radiative forcing?
(b) How can non-linear saturation effects in contrail-cirrus coverage be modelled?
(c) How can attribution principles be applied to multi-aircraft and multi-fuel scenarios?
(d) How can the low-soot regime be represented within the response modelling framework?

RQ3 **How do alternative aviation fuel pathways affect the relative contributions of contrails and CO_2 to future radiative forcing and temperature change?**

(a) How can complex and integrated scenarios such as those developed by ICAO be harmonised and translated into emission inventories compatible with OpenAirClim?
(b) Does the introduction of novel aviation fuels such as SAF and hydrogen contribute to temperature stabilisation?
(c) What do the results reveal about the capabilities and limitations of the OpenAirClim response modelling framework?

RQ4 **Are alternative climate metrics more suitable for assessing aviation CO_2 and non-CO_2 effects?**
Deliverable for the DINA2030+ LuFo project; results integrated into the CLAIM and Non-CO_2 MRV projects.

(a) How should the performance of climate metrics be evaluated?

(b) How do climate metrics differ in neutrality, temporal stability, policy compatibility and simplicity?
(c) What are the implications of climate metric choice for aviation policy and technology decisions?

MATERIAL OUTCOMES

A primary material outcome of this PhD project is the OpenAirClim contrail module (see Chapter 5), which enables users to calculate the contrail climate impact of aircraft powered by conventional as well as novel aviation fuels and propulsion technologies. During the PhD, work also began on an OpenAirClim-compatible emission inventory generator[4] (GEDAI).

1.2. DISSERTATION OUTLINE

Chapters 2 and 3 establish the scientific background and context of this dissertation. Chapter 2 reviews the primary aviation emission species and provides a detailed overview of contrails, including measurement techniques and operational and technological opportunities for mitigation. It further describes climate metrics relevant to aviation. Climate modelling approaches, emission inventories and attribution methods are presented in Chapter 3.

Chapter 4 addresses RQ1. Using reanalysis data from the 2010 decade, this chapter characterises the limiting aircraft-dependent and environmental factors governing persistent contrail formation and analyses their spatial and seasonal variability. The interplay between the limiting factors is examined and the implications of novel fuels and propulsion technologies are explored. The resulting analysis yields robust climatological relationships describing the probability of persistent contrail formation as a function of pressure levels and Schmidt-Appleman mixing line slope.

Chapter 5 addresses RQ2 through the development of the OpenAirClim contrail module. Building on the climatological relationships identified previously and supported by dedicated ECHAM5-CCMod simulations, the chapter formulates a computationally efficient representation of contrail-induced radiative forcing and temperature change. The module is evaluated against scientific literature and its sensitivities to key input parameters and changes in cruise altitude are examined. Attribution approaches suitable for multi-aircraft and multi-fuel scenarios are also assessed.

Chapter 6 addresses RQ3 by applying the OpenAirClim response modelling framework to the ICAO integrated aviation scenarios. The scenarios are harmonised and translated into compatible emission inventories. The resulting CO_2

[4]https://github.com/liammegill/gedai [Last accessed: 16/02/2026]

and contrail radiative forcing and temperature change responses are analysed and compared, providing insights into their relative contributions for different technology and traffic pathways. The study also reveals strengths and limitations of the OpenAirClim framework when applied to complex and integrated scenarios. The CO_2 and contrail results are compared to a similar analysis of the ICAO scenarios by Aamaas et al. (2025). Other emission species are excluded because their respective modules are still in development at the time of writing.

Chapter 7 addresses RQ4 by evaluating the performance of alternative climate metrics in representing aviation CO_2 and non-CO_2 emissions and effects. Using the AirClim response model, the compatibility, simplicity, neutrality and temporal stability of existing physical climate metrics are assessed and compared with the dominant Global Warming Potential (GWP). The study discusses potential implications for aviation policy and aircraft design, including how the results were used to inform the Non-CO_2 MRV of the European Commission.

Finally, Chapter 8 outlines the findings of the dissertation, discusses their broader scientific and policy implications and outlines suggested directions for further research.

1

REFERENCES

Aamaas, B., Lund, M. T., Fuglestvedt, J. S., Totterdill, A., Owen, B., Skowron, A., and Lee, D. S.: Continued global warming from aviation even under high-ambition mitigation scenarios, One Earth, 101451, doi: 10.1016/j.oneear.2025.101451, 2025.

Airbus: Global Market Forecast 2025-2044, 2025.

Arblaster, T., Thonemann, N., and Steubing, B.: Air traffic growth jeopardises European aviation's climate mitigation efforts despite the substantial potential of hydrogen, Communications Earth & Environment, 6, 976, doi: 10.1038/s43247-025-02935-5, 2025.

ATAG: Aviation: Benefits Beyond Borders 2024, Tech. rep., Air Transport Action Group, Geneva, https://aviationbenefits.org/downloads/aviation-benefits-beyond-borders-2024/, 2024.

Badgley, G., Freeman, J., Hamman, J. J., Haya, B., Trugman, A. T., Anderegg, W. R. L., and Cullenward, D.: Systematic over-crediting in California's forest carbon offsets program, Global Change Biology, 28, 1433–1445, doi: 10.1111/gcb.15943, 2022.

Bickel, M., Ponater, M., Burkhardt, U., Righi, M., Hendricks, J., and Jöckel, P.: Contrail cirrus climate impact: from radiative forcing to surface temperature change, Journal of Climate, 38, 1895–1912, doi: 10.1175/JCLI-D-24-0245.1, 2025.

Bock, L. and Burkhardt, U.: Reassessing properties and radiative forcing of contrail cirrus using a climate model, Journal of Geophysical Research: Atmospheres, 121, 9717–9736, doi: 10.1002/2016JD025112, 2016.

Boeing: Commercial Market Outlook 2025-2044, 2025.

Burkhardt, U. and Kärcher, B.: Global radiative forcing from contrail cirrus, Nature Climate Change, 1, 54–58, doi: 10.1038/nclimate1068, 2011.

Dahlmann, K., Grewe, V., Frömming, C., and Burkhardt, U.: Can we reliably assess climate mitigation options for air traffic scenarios despite large uncertainties in atmospheric processes?, Transportation Research Part D: Transport and Environment, 46, 40–55, doi: 10.1016/j.trd.2016.03.006, 2016.

Detsios, N., Theodoraki, S., Maragoudaki, L., Atsonios, K., Grammelis, P., and Orfanoudakis, N. G.: Recent advances on alternative aviation fuels/pathways: a critical review, Energies, 16, 1904, doi: 10.3390/en16041904, 2023.

Dischl, R., Märkl, R., Sauer, D., Voigt, C., Harlaß, T., Scheibe, M., Hahn, V., Kaufmann, S., Marsing, A., Dörnbrack, A., Roiger, A., Yu, F., Gauthier, M., Renard, C., Swann, P., Johnson, M., Ahrens, D., Sallinen, R., Eckel, G., and Le Clercq, P.: Fuel sulfur content can modulate contrail ice crystal numbers, Communications Earth & Environment, 6, 902, doi: 10.1038/s43247-025-02951-5, 2025.

Frömming, C., Ponater, M., Dahlmann, K., Grewe, V., Lee, D. S., and Sausen, R.: Aviation-induced radiative forcing and surface temperature change in dependency of the emission altitude, Journal of Geophysical Research: Atmospheres, 117, doi: 10.1029/2012JD018204, 2012.

Frömming, C., Grewe, V., Brinkop, S., Jöckel, P., Haslerud, A. S., Rosanka, S., van Manen, J., and Matthes, S.: Influence of weather situation on non-CO2 aviation climate effects: the REACT4C climate change functions, Atmospheric Chemistry and Physics, 21, 9151–9172, doi: 10.5194/acp-21-9151-2021, 2021.

Gettelman, A. and Chen, C.: The climate impact of aviation aerosols, Geophysical Research Letters, 40, 2785–2789, doi: 10.1002/grl.50520, 2013.

Grewe, V. and Stenke, A.: AirClim: An efficient tool for climate evaluation of aircraft technology, Atmospheric Chemistry and Physics, 8, 4621–4639, doi: 10.5194/acp-8-4621-2008, 2008.

Haywood, J. M., Allan, R. P., Bornemann, J., Forster, P. M., Francis, P. N., Milton, S., Rädel, G., Rap, A., Shine, K. P., and Thorpe, R.: A case study of the radiative forcing of persistent contrails evolving into contrail-induced cirrus, Journal of Geophysical Research: Atmospheres, 114, 2009JD012 650, doi: 10.1029/2009JD012650, 2009.

Hendricks, J., Righi, M., Brinkop, S., Dahlmann, K., Mertens, M., Beer, C. G., Grewe, V., Kaiser, C. J., and Ponater, M.: Large present-day and future climate forcing due to non-CO2 emissions from global transport, npj Climate and Atmospheric Science, 9, doi: 10.1038/s41612-026-01383-y, 2026.

IATA: IATA Annual Review, Tech. rep., International Air Transport Association, Montreal, https://www.iata.org/contentassets/c81222d96c9a4e0bb4ff6ced0126f0bb/iata-annual-review-2025.pdf, 2025.

ICAO: Annex 16 - Environmental Protection - Volume IV, Carbon Offsetting and Reduction Scheme for International Aviation (CORSIA), Tech. rep., Interational Civil Aviation Organisation, Montreal, ISBN 978-92-9258-611-9, https://elibrary.icao.int/product/229739, 2023.

Incer-Valverde, J., Korayem, A., Tsatsaronis, G., and Morosuk, T.: "Colors" of hydrogen: Definitions and carbon intensity, Energy Conversion and Management, 291, 117 294, doi: 10.1016/j.enconman.2023.117294, 2023.

Kaufmann, S., Dischl, R., and Voigt, C.: Regional and seasonal impact of hydrogen propulsion systems on potential contrail cirrus cover, Atmospheric Environment: X, 24, 100 298, doi: 10.1016/j.aeaoa.2024.100298, 2024.

Kärcher, B.: Formation and radiative forcing of contrail cirrus, Nature Communications, 9, 1824–1824, doi: 10.1038/s41467-018-04068-0, 2018.

Kärcher, B., Burkhardt, U., Bier, A., Bock, L., and Ford, I. J.: The microphysical pathway to contrail formation, Journal of Geophysical Research: Atmospheres, 120, 7893–7927, doi: 10.1002/2015JD023491, 2015.

Köhler, M. O., Rädel, G., Dessens, O., Shine, K. P., Rogers, H. L., Wild, O., and Pyle, J. A.: Impact of perturbations to nitrogen oxide emissions from global aviation, Journal of Geophysical Research: Atmospheres, 113, 2007JD009 140, doi: 10.1029/2007JD009140, 2008.

Lee, D., Fahey, D., Skowron, A., Allen, M., Burkhardt, U., Chen, Q., Doherty, S., Freeman, S., Forster, P., Fuglestvedt, J., Gettelman, A., De León, R., Lim, L., Lund, M., Millar, R., Owen, B., Penner, J., Pitari, G., Prather, M., Sausen, R., and Wilcox, L.: The contribution of global aviation to anthropogenic climate forcing for 2000 to 2018, Atmospheric Environment, 244, 117 834, doi: 10.1016/j.atmosenv.2020.117834, 2021.

Marquart, S., Sausen, R., Ponater, M., and Grewe, V.: Estimate of the climate impact of cryoplanes, Aerospace Science and Technology, 5, 73–84, doi: 10.1016/S1270-9638(00)01084-1, 2001.

Myhre, G., Shine, K., Rädel, G., Gauss, M., Isaksen, I., Tang, Q., Prather, M., Williams, J., van Velthoven, P., Dessens, O., Koffi, B., Szopa, S., Hoor, P., Grewe, V., Borken-Kleefeld, J., Berntsen, T., and Fuglestvedt, J.: Radiative forcing due to changes in ozone and methane caused by the transport sector, Atmospheric Environment, 45, 387–394, doi: 10.1016/j.atmosenv.2010.10.001, 2011.

Prussi, M., Lee, U., Wang, M., Malina, R., Valin, H., Taheripour, F., Velarde, C., Staples, M. D., Lonza, L., and Hileman, J. I.: CORSIA: The first internationally adopted approach to calculate life-cycle GHG emissions for aviation fuels, Renewable and Sustainable Energy Reviews, 150, 111 398, doi: 10.1016/j.rser.2021.111398, 2021.

Righi, M., Testa, B., Beer, C. G., Hendricks, J., and Kanji, Z. A.: Aviation soot interactions with natural cirrus clouds are unlikely to have a significant impact on global climate, Atmospheric Chemistry and Physics, 25, 18 341–18 353, doi: 10.5194/acp-25-18341-2025, 2025.

Schumann, U.: On conditions for contrail formation from aircraft exhausts, Meteorologische Zeitschrift, 5, 4–23, doi: 10.1127/metz/5/1996/4, 1996.

Schumann, U. and Heymsfield, A. J.: On the life cycle of individual contrails and contrail cirrus, Meteorological Monographs, 58, 3.1–3.24, doi: 10.1175/AMSMONOGRAPHS-D-16-0005.1, 2017.

Stevenson, D. S., Doherty, R. M., Sanderson, M. G., Collins, W. J., Johnson, C. E., and Derwent, R. G.: Radiative forcing from aircraft NOx emissions: mechanisms and seasonal dependence, Journal of Geophysical Research, 109, D17 307, doi: 10.1029/2004JD004759, 2004.

Trencher, G., Nick, S., Carlson, J., and Johnson, M.: Demand for low-quality offsets by major companies undermines climate integrity of the voluntary carbon market, Nature Communications, 15, 6863, doi: 10.1038/s41467-024-51151-w, 2024.

Völk, S., Yamashita, H., Megill, L., Dahlmann, K., and Grewe, V.: OpenAirClim, Zenodo [software], doi: 10.5281/ZENODO.13682728, 2025.

Wilcox, L., Shine, K., and Hoskins, B.: Radiative forcing due to aviation water vapour emissions, Atmospheric Environment, 63, 1–13, doi: 10.1016/j.atmosenv.2012.08.072, 2012.

Strength in numbers.

just three atoms,
drifting through the air,
warming the world.

— LM

2

BACKGROUND

This chapter contains elements from:

Megill, L., Deck, K. and Grewe, V.: Alternative climate metrics to the Global Warming Potential are more suitable for assessing aviation non-CO_2 effects, Communications Earth & Environment, 5, 249, doi: 10.1038/s43247-024-01423-6, 2024.

which is reproduced with permission from Springer Nature.

It also contains elements from:

Megill, L. and Grewe, V.: Investigating the limiting aircraft-design-dependent and environmental factors of persistent contrail formation, Atmospheric Chemistry & Physics, 25, 7, doi: 10.5194/acp-25-4131-2025, 2025.

Völk, S., Yamashita, H., **Megill, L.**, Dahlmann, K. and Grewe, V.: OpenAirClim v0.XX: A framework for assessing the climate impact of aviation emissions, *in prep.*

This chapter presents the scientific background and context of this dissertation. Section 2.1 provides an overview of the climate impacts of aviation, including a review of the primary aviation emission species. It also describes the concepts of radiative forcing, efficacy and their relationship to surface temperature change. A detailed overview of contrails and contrail-cirrus is provided in Section 2.2, including measurement techniques and operational and technological opportunities to reduce their climate impact. Finally, Section 2.3 describes climate metrics, which are used to express all aviation emissions and effects on a common scale for policy decision-making.

2.1. CLIMATE IMPACTS OF AVIATION

International civil aviation is the cornerstone of global mobility and trade, enabling the efficient movement of people and goods across long distances. At the same time, aviation operations contribute to anthropogenic climate change through carbon dioxide (CO_2) emissions and a range of non-CO_2 emissions and effects. Of particular importance are the formation of condensation trails, or contrails, behind aircraft, which can persist and spread to form contrail-cirrus clouds that modify Earth's radiation balance.

The concepts of radiative forcing and efficacy are explained and linked to surface temperature changes in Section 2.1.1. The contribution of aviation emissions to anthropogenic climate change and the relative contribution of each emission species and effect is explored in Section 2.1.2. Finally, the primary emission species (CO_2, NO_x and H_2O) are presented in Section 2.1.3. Since contrails are the main focus of this dissertation, they are described in more detail in Section 2.2.

2.1.1. RADIATIVE FORCING AND TEMPERATURE CHANGE

In a stable climate, the energy received by the Earth from the Sun is approximately in balance with the energy lost to space. A change in this energy balance due to an imposed perturbation, represented as a change in net flux, is referred to as radiative forcing (Hansen et al., 2005). To determine the impact of anthropogenic activities, radiative forcing is often calculated with respect to pre-industrial conditions, generally around the year 1750 (IPCC, 2023).

Alternative definitions of the radiative forcing (RF) have been developed. Three common definitions, as used by the IPCC and in this work, are shown in Figure 2.1 (adapted from Hansen et al., 2005). The *instantaneous* RF ($\mathrm{RF_{inst}}$) refers to the instantaneous change in downward net flux due to an imposed change, determined at the climatological tropopause. The *stratospherically-adjusted* RF ($\mathrm{RF_{adj}}$) is defined as the change in downward net flux at the climatological tropopause after only allowing the stratospheric temperatures to adjust. Unless otherwise stated, in this work "RF" refers to $\mathrm{RF_{adj}}$. Finally, the *effective* RF (ERF) refers to the

change in downward net flux at the top of atmosphere (TOA) after allowing rapid atmospheric adjustments (e.g. atmospheric temperature, water vapour, clouds), but fixing global mean land and/or sea surface temperatures. There are multiple definitions of ERF – in this work, we use the definition of the IPCC, which fixes the sea surface temperature (Myhre et al., 2013).

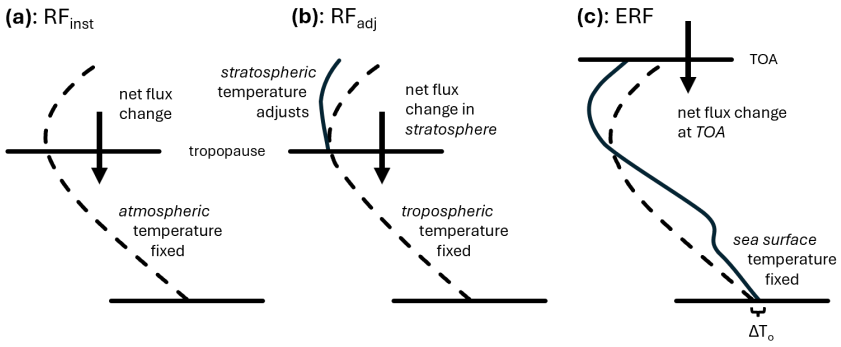


Figure 2.1: Cartoon demonstrating different radiative forcing definitions. (a) Instantaneous RF; (b) stratospherically-adjusted RF; (c) effective RF (ERF), defined as the difference between two simulations with prescribed ocean conditions (IPCC, 2023). ΔT_o represents the land temperature response, which is allowed to vary in this definition. The Figure is based on Hansen et al. (2005) and Myhre et al. (2013).

The fundamental equation linking the radiative forcing to the global mean surface temperature (ΔT_s) is,

$$\Delta T_s = \lambda \cdot \mathrm{RF} \tag{2.1}$$

where λ [$\mathrm{K\,m^2\,W^{-1}}$] is the climate sensitivity parameter. The definition of RF is evolving to best represent this fundamental equation. The equation implicitly assumes that a global radiative forcing will always result in the same change in global mean surface temperature, regardless of what originally caused the forcing (Hansen et al., 2005). However, this assumption does not hold for a range of forcing agents, including for contrails (e.g. Ponater et al., 2021), which are the focus of this work (see Section 2.2). To account for this, Hansen et al. (2005) introduced efficacy factors r, which quantify the relative effectiveness of a certain forcing agent to RF compared to that of CO_2. The above equation can thus be adapted to,

$$\Delta T_s = r \cdot \lambda_{\mathrm{CO_2}} \cdot \mathrm{RF} \tag{2.2}$$

where $\lambda_{\mathrm{CO_2}}$ is the climate sensitivity parameter for CO_2. The closer the efficacy value is to unity, the more closely the response of that forcing agent resembles the response of CO_2. By including a larger number of rapid atmospheric ad-

justments, the efficacy values within the ERF framework generally have a smaller deviation than those within the RF framework (Myhre et al., 2013). The equivalent equation within the ERF framework is,

$$\Delta T_{\mathrm{s}} = r' \cdot \lambda'_{\mathrm{CO_2}} \cdot \mathrm{ERF} \tag{2.3}$$

where r' and $\lambda'_{\mathrm{CO_2}}$ are the efficacy and CO_2 climate sensitivity parameter within the ERF framework respectively.

2.1.2. CONTRIBUTION OF AVIATION EMISSIONS

Aviation contributes to anthropogenic climate change through carbon dioxide (CO_2) emissions and non-CO_2 emissions and effects. A recent study estimates aviation operations from 1940 until 2018 to be responsible for $100.9\ (55, 145)$ $\mathrm{mW\,m^{-2}}$ (ERF; Lee et al., 2021), corresponding to between 3.5 and 4.0 % of global anthropogenic climate change, estimated as $2.72\ (1.96, 3.48)$ $\mathrm{W\,m^{-2}}$ (ERF) by IPCC (2023).

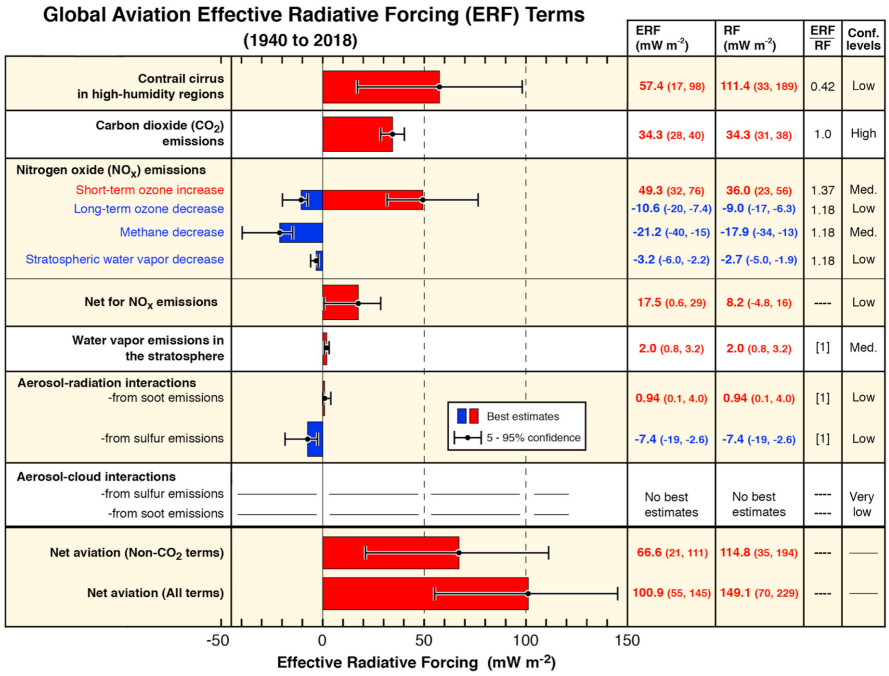


Figure 2.2: Best estimates for climate forcing terms from global aviation operations from 1940 to 2018. The bars and whiskers show ERF best estimates and the 5–95 % confidence intervals respectively. RF corresponds to the stratospheric-adjusted radiative forcing (see Section 2.1.1). Reprinted from Lee et al. (2021), Copyright (2020), with permission from Elsevier.

The contribution of each emission and effect is shown in Figure 2.2 (Lee et al., 2021). In this study, emissions of CO_2 make up around one third of aviation ERF, the remaining two-thirds are due to aviation non-CO_2. Primary among these are contrail-cirrus (Section 2.2) and emissions of nitrogen oxide (NO_x) and water vapour (Section 2.1.3). The relative contribution of non-CO_2 to CO_2 is subject to a high degree of uncertainty. Grewe et al. (2026), for example, find a 12 % likelihood that the CO_2 ERF is larger than the total non-CO_2 ERF for the Lee et al. (2021) study.

Aerosol-cloud interactions likely play a significant role in the climate forcing of aviation, but are associated with a high degree of uncertainty. A recent study found the impact of aviation soot on natural cirrus clouds to be very small, at around $-6.9 \pm 29.8\ \mathrm{mW\,m^{-2}}$, and a statistically significant mean value different from 0 could not be shown (Righi et al., 2025). However, the interaction of sulphur aerosols with natural, lower-level clouds is expected to lead to a substantial cooling effect (Hendricks et al., 2026). Because aircraft emit into comparatively clean conditions at typical cruise levels, the forcing efficiency of aerosols is very high – around 10 to 20 times higher than for road traffic. Accounting for the aerosol-cloud interaction from aviation sulphur and using a different attribution method for aviation NO_x (see Section 3.4), Hendricks et al. (2026) find a global ERF value in 2015 of $27\,\mathrm{mW\,m^{-2}}$, including contributions from all forcing agents – a 73 % reduction compared to Lee et al. (2021).

The spatial and temporal scales of species and effects relevant to aviation emissions vary widely, as shown in Figure 2.3 (Seinfeld and Pandis, 2016). Of these, hydroxyl radicals (OH) have the shortest lifetime (order of seconds) due to their high reactivity with various atmospheric species. On the other end of the spectrum are the globally well-mixed greenhouse gases: Methane (CH_4) has a lifetime of around 10 to 12 years; CO_2 does not have a single lifetime (see the following Section), but can remain in the atmosphere for millennia or longer. The spatial and temporal extent of contrails and contrail-cirrus is highly dependent on the ambient conditions: in ice supersaturated conditions, the increase in cloudiness can be advected over large distances (see Section 2.2).

The wide range of timescales makes it particularly challenging to express the climate impacts of all aviation emissions and effects on a common scale. This complicates the introduction of aviation non-CO_2 emissions into climate policy, which is typically achieved using a climate metric (see Section 2.3). Understanding the implications of this on metric design for aviation climate policy specifically is a core part of this dissertation (RQ4; see Section 7).

2.1.3. AVIATION EMISSION SPECIES

In this section, an overview is provided of the primary aviation emissions and effects and their impacts on the climate. The focus is on the primary drivers, which are carbon dioxide (CO_2), nitrogen oxides (NO_x), water vapour (H_2O) and con-

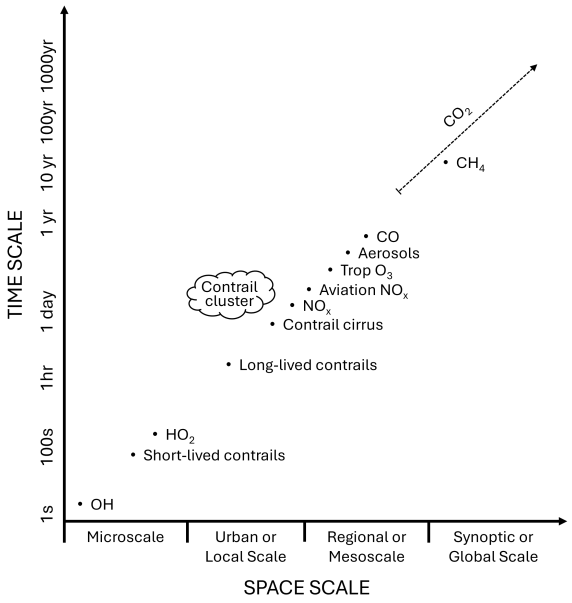


Figure 2.3: Spatial and temporal scales of aviation-related emissions and effects. The time scale represents the lifetime of the species and clouds; the spatial scale how far they are generally transported in the atmosphere. The dashed arrow indicates that it is not possible to define a single lifetime for CO_2 because different removal processes occur on different timescales (see e.g. IPCC, 2001). The contrail, contrail-cirrus and contrail cluster values are adapted from Kärcher (2018). Note that contrail lifetime is highly dependent on ambient conditions (see Section 2.2). The figure is based on Seinfeld and Pandis (2016).

densation trails (contrails). The impact of aerosol-radiation and aerosol-cloud interactions is not considered in this dissertation and thus not further described here. The formation and climate impacts of contrails are described in a separate section (Section 2.2), because they are a particular focus of this dissertation.

Carbon dioxide (CO_2)

The Earth's natural Greenhouse Effect makes life on the planet, as we know and enjoy it, possible. The greenhouse effect refers to the warming of the Earth's surface and lower atmosphere that results from a set of radiative processes, whereby greenhouse gases, clouds and some aerosols absorb and re-emit terrestrial radiation, thereby elevating surface temperatures above what they would otherwise be. Whilst water vapour is responsible for the largest share of the natural greenhouse effect, carbon dioxide (CO_2) is the most prominent anthropogenic greenhouse gas (GHG).

CO_2 is the stoichiometric end-product of complete hydrocarbon combustion, e.g. $\mathrm{C}_x\mathrm{H}_y + (x + y/4)\ \mathrm{O}_2 \rightarrow x\ \mathrm{CO}_2 + (y/2)\ \mathrm{H}_2\mathrm{O}$. Because of humanity's

reliance on the combustion of fossil fuels, the concentration of CO_2 in Earth's atmosphere has increased by 131.6 ppm over the period 1750 to 2019, resulting in a $2.72\,\mathrm{W\,m^{-2}}$ increase in effective radiative forcing (IPCC, 2023). That anthropogenic CO_2 could act as a greenhouse gas and contribute to a global warming has been known for many years: Arrhenius, in 1896, was the first to model climate sensitivity to anthropogenic CO_2 emissions (see also Fig. 1.6 of IPCC, 2023). However, reducing CO_2 emissions and society's reliance on fossil fuels is only a comparatively recent effort, which faces significant industrial, societal and political resistance.

Carbon dioxide is part of the Earth's carbon cycle, which features many different sources and sinks. The transfer of carbon between reservoirs occurs on multiple timescales (see Box 6.1, Table 1 of IPCC, 2013): biosphere (years to centuries), oceans (decades to millennia), marine sedimentation (10^3–10^4 years) and rocks (10^4–10^6 years). A significant fraction of emitted CO_2 thus persists in the atmosphere for millennia. This makes choosing an appropriate time horizon over which to consider the climate impact of CO_2 challenging (see Section 2.3).

Given the complexity of carbon-climate system modelling, reduced-form response models are often used to efficiently approximate the response of the climate system to emissions, including changes in atmospheric concentrations, radiative forcing and temperature. In this work, we primarily make use of the Sausen and Schumann (2000) method, based on Hasselmann et al. (1993), to determine CO_2 concentration changes; the Etminan et al. (2016) method to determine CO_2 radiative forcing; and the Boucher and Reddy (2008) method to determine temperature change. These models form the basis for AirClim and OpenAirClim (see Section 3.1).

Nitrogen oxides (NO_x)

In the context of aviation, NO_x refers to the combination of nitric oxide (NO) and nitrogen dioxide (NO_2). The emission index for NO_x ($EINO_x$) is thus usually given in g NO_2 per kg fuel, where any NO is converted to NO_2 by atomic weight. NO_x is formed as a byproduct of combustion and is generally linked to the temperature within the combustion chamber. This is somewhat problematic, because improved thermodynamic efficiency, for example through increased overall pressure ratio, is linked to increased combustion temperatures. Reduced fuel burn thus tends to lead to higher NO_x, leading to a direct trade-off between CO_2 and NO_x. Global emissions standards for aircraft NO_x are set by the Committee on Aviation Environmental Protection of the International Civil Aviation Organisation (ICAO-CAEP).

Emissions of NO_x non-linearly shift existing balances between species in the atmosphere. We differentiate between four main processes and indicate in each case the sign of the resulting radiative forcing:

- Positive RF: NO_x emissions increase tropospheric ozone (O_3) concentrations, leading to a positive radiative forcing. This results from enhanced ozone production via $HO_2 + NO \longrightarrow NO_2 + OH$, together with reduced ozone loss as lower HO_2 levels suppress the reaction $O_3 + HO_2 \longrightarrow 2\,O_2 + OH$ (Grewe et al., 2002; Lee et al., 2010);
- Negative RF: NO_x emissions reduce methane (CH_4) concentrations, leading to a negative radiative forcing. This is primarily driven by enhanced oxidation through $CH_4 + OH \longrightarrow CH_3 + H_2O$ (Stevenson et al., 2004);
- Negative RF: since methane is an ozone precursor in the troposphere, the reduction in methane concentration leads to a long-term decrease in tropospheric ozone concentration, also called the Primary Mode Ozone (PMO) effect, resulting in a negative radiative forcing (Stevenson et al., 2004);
- Negative RF: the reduction in methane concentration also leads to a long-term decrease in stratospheric water vapour (SWV) concentration, resulting in a negative radiative forcing (Myhre et al., 2007, 2011).

Although NO_x emissions from aviation are substantially lower than from road and ship traffic (Myhre et al., 2011; Righi et al., 2023), NO_x emitted at typical cruise altitudes has a higher ozone production efficiency (e.g. Finney et al., 2016; Hendricks et al., 2026) and thus tends to have a larger relative impact on RF. The sign of net NO_x radiative forcing from aviation operations between 1940 and 2018 was found by Lee et al. (2021) to be positive within 90 % certainty (Lee et al., 2021). However, a number of open questions remain about potential methodological flaws that could result in considerable underestimation of the contribution of aviation NO_x to climate change (Grewe et al., 2019). Notably, by applying a tagging rather than perturbation approach (see Section 3.4 for an overview of attribution methods), Hendricks et al. (2026) find that the cooling and warming ERF effects approximately balance. Addressing these open questions and performing dedicated model intercomparisons (e.g. Cohen et al., 2025) is thus key for understanding and mitigating the climate impact of aviation NO_x.

Water vapour (H_2O)

Water vapour is an unavoidable product of complete hydrocarbon combustion. Relative to the magnitude of fluxes in the natural hydrological cycle, water vapour emissions from global aviation are small (IPCC, 1999). Consistent with this, Frömming et al. (2012) estimate that global aviation perturbs ambient water vapour mixing ratios by less than 1 % of background levels. Consequently, the direct radiative forcing attributable to aviation water vapour is minor for present-day aviation (Lee et al., 2021), in which emissions occur predominantly in the troposphere. The principal climatic relevance of water vapour in the troposphere is indirect: the emission of water vapour is a precursor for the formation of contrails, an effect discussed separately in Section 2.2.

The climatic importance of aviation water vapour depends strongly on the

emission altitude. The stratosphere is markedly drier than the troposphere and removal processes are substantially slower. While water vapour perturbations in the troposphere persist from hours to months, stratospheric perturbations can remain for several years (Grewe and Stenke, 2008; Pletzer, 2024). Pletzer et al. (2022) also showed that photochemistry does not reduce water vapour perturbation even at the highest cruise levels. As a result, the climate impact of water vapour emissions increases with cruise altitude. This sensitivity is amplified for propulsion concepts with higher water vapour emission indices, notably hydrogen combustion. For super- and hypersonic aircraft, which predominantly operate in the stratosphere, water vapour emissions may even become a dominant contributor to total radiative forcing (Pletzer et al., 2022; Pletzer and Grewe, 2024).

2.2. CONTRAILS

Contrails are artificial, line-shaped ice clouds that can form behind aircraft in the upper troposphere and lower stratosphere. Over time and in the right ambient conditions, contrails can persist for many hours, transitioning into contrail-cirrus clouds that can merge and compete with natural cirrus. Contrail-cirrus is widely considered to be one of the most important components of aviation-induced climate impact. Current best estimates suggest that contrails and the resulting aircraft-induced cloudiness could be responsible for around a half of the anthropogenic effective radiative forcing in 2018 stemming from aircraft operations between 1940 and 2018 (Lee et al., 2021). However, such estimates have a substantial associated uncertainty (Zhang et al., 2025).

This section begins by describing contrail formation, including condensation and ice nucleation (Section 2.2.1). The contrail lifecycle is shown in Section 2.2.2. Means of measuring contrails, both in-situ and with remote sensing, are described in Section 2.2.3. Finally, the contrail climate impact and mitigation options are explored in Sections 2.2.4 and 2.2.5.

2.2.1. CONTRAIL FORMATION AND ICE NUCLEATION

Contrails can form behind an aircraft when the hot and humid engine exhaust plume mixes with the ambient air and cools. If, during mixing, the exhaust plume becomes supersaturated with respect to liquid water, water vapour condenses around condensation nuclei in the exhaust, primarily soot (Kärcher and Yu, 2009). If the ambient temperature is below the homogeneous freezing temperature (approx. $235\,\mathrm{K}$), the water droplets freeze to form ice crystals, creating a visible contrail (Kärcher, 2018).

Contrail formation can be approximated using the Schmidt-Appleman Criterion (SAC; Schumann, 1996; see also Schmidt, 1941; Appleman, 1953). The SAC is

a simple thermodynamic model that assumes isobaric mixing in the plume. The actual microphysical mixing pathway is substantially more complex once water droplets form (e.g. Kärcher, 2018), but the SAC has been shown to predict contrail formation with a high degree of confidence. The slope of the isobaric mixing line G is a function of the ambient pressure as well as aircraft engine and fuel-dependent properties. For conventional kerosene (CON), the slope can be calculated using (Schumann, 1996),

$$G_{\text{CON}} = \frac{c_p p_a}{\epsilon} \frac{EI_{H_2O}}{(1-\eta)\, Q} \tag{2.4}$$

where $c_p = 1004\,\mathrm{J\,kg^{-1}\,K^{-1}}$ is the isobaric heat capacity of air, p_a is the ambient pressure [Pa], $\epsilon = 0.622$ is the molar mass ratio of water vapour and dry air, EI_{H_2O} is the emission index of water vapour [$\mathrm{kg\,kg^{-1}(fuel)}$], η is the overall propulsion system efficiency and Q is the lower heating value of the fuel [$\mathrm{MJ\,kg^{-1}}$]. Derivatives of this method for other fuels and propulsion technologies are explored in Section 4.2.1.

As shown in Figure 2.4 (Voigt et al., 2026), a large variety of particles are present in the exhaust plume of aircraft engines. However, not all particles are suitable condensation nuclei. Soot, a by-product of incomplete combustion, acts as the preferential condensation nucleus for conventional aircraft fuelled with kerosene (Kärcher and Yu, 2009; Wong and Miake-Lye, 2010; Kärcher et al., 2015) through the Kelvin effect (Lewellen, 2014). For conventional fossil-based fuels, the inherently low hygroscopicity of soot particles (Popovicheva et al., 2008) is enhanced by the presence of sulphur in the fuel. The fuel sulphur is partially converted into sulphuric acid (H_2SO_4) in the exhaust, which coats the soot particles, thereby making them more effective at capturing water vapour and producing contrail ice crystals (Petzold et al., 2005; Jones and Miake-Lye, 2024; Dischl et al., 2025). However, the presence of sulphur in the fuel is not mandatory for the activation of soot particles, because hydroxyls and nitrates can also interact with soot particles (Kärcher et al., 1996; Grimonprez et al., 2018).

A lack of soot in the exhaust does not prevent condensation. As soot emissions are reduced, (semi-)volatile and organic aerosols such as chemi-ions (Yu and Turco, 1997; Wong and Miake-Lye, 2010; Rojo et al., 2015), ultrafine aqueous particles (UAPs; Kärcher, 2018) and other emissions such as lubrication oil droplets (Fushimi et al., 2019; Ungeheuer et al., 2022; Ponsonby et al., 2024) become more relevant (see Figure 2.4). This was recently demonstrated with in-situ measurements by Voigt et al. (2026, see also Section 2.2.3), who found substantial contrail ice crystal formation even when the soot particle emission index was reduced by three orders of magnitude. This finding is particularly relevant as emerging propulsion technologies such as lean-burn combustion aviation fuels such as SAF and hydrogen are increasingly introduced (see also Section 2.2.5).

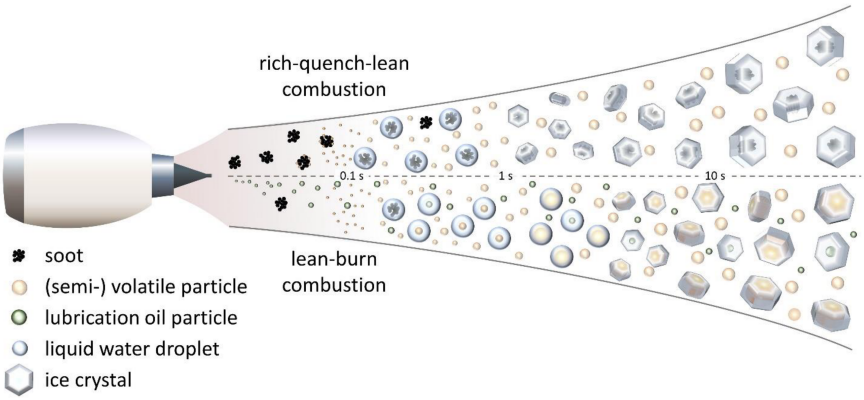


Figure 2.4: Sketch of the ice formation processes for current rich-quench-lean and lean-burn engine configurations. Rich-Quench-Lean combustion is used by the majority of contemporary passenger jet aircraft. Lean-burn combustion reduces soot emissions by up to three orders of magnitude. Current lean-burn engine configurations vent lubrication oils into the exhaust, resulting in substantial ice crystal formation. The figure was published by Voigt et al. (2026) and is licensed under CC-BY-4.0.

2.2.2. CONTRAIL LIFECYCLE

The lifecycle of a persistent contrail can be split into four phases (Gerz et al., 1998). In the *jet phase* (first second after emission), the exhaust expanding behind the engine is caught by the vortex sheet shed by the wings, which rolls up into a pair of counter-rotating vortices. Soot and other particles are activated into water droplets and freeze into ice crystals, as described in the previous section. In the following *vortex phase* (first few minutes), the vortex sheet splits into a primary wake which begins to descend and a secondary wake that remains at altitude (Paoli and Shariff, 2016). Ice crystals in the primary wake begin to sublimate due to adiabatic warming, whereas those in the secondary, upper wake continue to grow in the ice supersaturated ambient air (Kärcher, 2018). After a few minutes, the vortices begin to collapse (*dissipation phase*). Ice crystals in the upper wake tend to persist longer due to the lower ambient temperature. Finally, in the *diffusion phase*, the contrail spreads due to atmospheric turbulence and wind shear.

Most contrails quickly dissipate in the usually dry ambient air and have a negligible impact on the climate. However, if the ambient conditions are supersaturated with respect to ice, contrails can persist for many hours (Haywood et al., 2009; Schumann and Heymsfield, 2017; Gierens and Vázquez-Navarro, 2018). Note that while contrail formation is well constrained by the SAC, ice supersaturated regions (ISSRs) remain difficult to forecast (Gierens et al., 2020; Hofer et al., 2024b; see also the discussion in Section 4.2.4). Over time, the initially linear structure is lost and the contrail transitions into contrail-cirrus, which can merge with natural cirrus and be advected over large distances, including into regions

where formation criteria are not met (Kärcher, 2018).

Contrail-cirrus lifetime is constrained by a microphysical pathway, where ice crystals are sedimented into lower, drier layers, and by synoptic pathways, where ice crystals are blown out of an ISSR by the wind or the air containing the contrail becomes subsaturated due to large-scale subsidence (Bier et al., 2017; Hofer and Gierens, 2025). The former pathway is particularly relevant for the introduction of alternative aviation fuels such as SAF and particularly hydrogen, since the use of these fuels result in fewer but larger ice crystals that sediment faster (Bier et al., 2024). The lifetime of contrail-cirrus produced by aircraft using these fuels is thus expected to be shorter, reducing their radiative impact (Lottermoser and Unterstrasser, 2026).

2.2.3. CONTRAIL MEASUREMENTS

The properties of contrails and contrail-cirrus can be analysed using in-situ measurements and remote sensing from satellites, lidar and ground-based instrumentation. In-situ measurements aid in our understanding of microphysics, particle composition and ice crystal numbers, whereas remote sensing provides data on contrail optical depth, coverage, lifetime and radiative forcing.

In-situ measurements

In-situ measurements are useful for determining the microphysical properties of individual contrails and for understanding the difference between contrail and natural cirrus. They are generally performed by flying an instrumented chase aircraft into a contrail produced by another aircraft, either in the near-field (order of hundreds of metres) or far-field (order of tens of kilometres). The first in-flight measurements investigated the fundamental properties of contrails (e.g. Knollenberg, 1972; Heymsfield et al., 1998) and the differences between contrails produced by aircraft of various sizes (Voigt et al., 2010).

Recent measurement campaigns have focused on the use of alternative aviation fuels and their effect on contrail properties. Since emitted soot particles act as the primary nuclei for contrail ice crystals (Kleine et al., 2018; see also Section 2.2.1), it was assumed that the use of SAFs, which tend to contain fewer aromatic compounds than conventional kerosene, would reduce the contrail ice crystal number. This was first demonstrated by the ACCESS campaign (2013–2014), which used a 50:50 biofuel blend (Moore et al., 2017), and later by the ECLIF1 (2015) and ECLIF2/ND-MAX (2018) campaigns (Voigt et al., 2021; Bräuer et al., 2021). More recently, the ECLIF3 (2021) campaign investigated contrail properties from 100 % SAF. Märkl et al. (2024), probing an Airbus A350, found a 35 % reduction in soot particle number and a 56 % reduction in ice particle number from HEFA-SPK compared to conventional kerosene. Dischl et al. (2025) demonstrated the importance of the fuel sulphur content on volatile particle and contrail ice numbers in the low-soot regime.

The VOLCAN campaign (2023) was the first to investigate contrails produced at very low soot emission levels, by chasing an Airbus A321neo with LEAP-1A engines in lean-burn mode (Voigt et al., 2026). Substantial ice crystal numbers were found even though the engines emitted three orders of magnitude less soot in lean-burn compared to forced rich-burn mode. This clearly highlights the importance of volatile particles in the absence of soot, notably volatile sulphate as well as organic and lubrication oil particles (Yu et al., 2012; Ungeheuer et al., 2022). The role of these particles will become even more important for future aircraft powered by hydrogen, where no soot particles will be released (Bier et al., 2024; Zink et al., 2025). The first in-situ measurements of contrails produced by hydrogen combustion were conducted only very recently during the Blue Condor project[1].

Remote sensing

Remote sensing of contrails and contrail-cirrus is useful for quantifying the distribution, optical properties and radiative effects over extended spatial and temporal scales. Most observational studies of contrails and contrail-cirrus rely on passive satellite imagery, which primarily retrieves cloud-top properties and allows for the analysis of contrail coverage, optical thickness and radiative effects. Active remote sensing using lidar or radar can provide vertically resolved information and also probe the internal structure of cloud columns, enabling the detection of optically thin contrails and contrail-cirrus embedded within natural cirrus.

Inherent in passive satellite-based contrail observational studies is a trade-off between spatial and temporal resolution. Early studies used imagers on Low Earth Orbit (LEO) satellites (e.g. Bakan et al., 1994; Mannstein et al., 1999; Spangenberg et al., 2013) to estimate contrail coverage and radiative forcing. These satellites provide high spatial resolution but only infrequent overpasses with a narrow swath path, limiting their ability to capture the temporal evolution of individual contrails. As a result, tracking contrails over their full lifecycle required data from multiple satellites to be combined (e.g. Duda et al., 2019). More recent work has shifted towards geostationary (GEO) satellites such as GOES[2] and Meteosat, which provide continuous observations at high temporal resolution, thereby enabling the tracking of contrails throughout their full lifecycles. However, this comes at the expense of coarser spatial resolution, constraining the detectability of narrow and optically thin contrails.

This highlights a central challenge for passive remote sensing. Young contrails are initially only tens to hundreds of metres wide, expanding to widths of only several kilometres as they evolve (Iwabuchi et al., 2012; Duda et al., 2013). As a result, young contrails may remain below the resolution of satellite imagers

[1]https://www.dlr.de/en/latest/news/2025/world-first-in-flight-measurements-of-contrails-from-hydrogen-propulsion [Accessed: 11/02/2026]
[2]Geostationary Operational Environmental Satellite

for several minutes after formation: recent studies have found mean times to observation in geostationary imagery ranging between 10 and 90 minutes, depending in particular on the resolution of the instrument used Gierens and Vázquez-Navarro (2018); Chevallier et al. (2023); Geraedts et al. (2024); Gryspeerdt et al. (2024). Later, the contrail or contrail-cirrus may become too optically thin or may not have enough contrast to be distinguished from the background. Consequently, Gierens and Vázquez-Navarro (2018) estimate that total contrail lifetimes could easily be three times as large as those observed by satellites. Furthermore, Driver et al. (2025) determine that only around half of contrails are detectable, although a majority of their radiative forcing is captured because optically thicker contrails are more readily observed. This introduces a sampling bias towards the most radiatively important contrails, which could have consequences since the detectability of contrails produced by novel aviation fuels has been shown to be significantly lower.

As contrails age, they can be advected, spread and deform (see Section 2.2.2). Once the characteristic linear structure of a contrail is lost – generally within one or two hours after formation (Mannstein et al., 1999) – it can no longer be reliably distinguished from natural cirrus without temporal context. Consequently, a key focus of contemporary research is on methods that attribute a detected contrail to the aircraft that formed it, for example by coupling weather data, contrail modelling and ADS-B flight trajectory data (Chevallier et al., 2023; Geraedts et al., 2024; Sarna et al., 2025). Various computer vision and machine learning methods have been proposed to improve detection and tracking performance (Mannstein et al., 1999; Vázquez-Navarro et al., 2015; Meijer et al., 2022; Ng et al., 2023; Santos Gabriel et al., 2026).

A limited number of studies have investigated contrails and contrail-cirrus using active spaceborne lidar and radar on the polar Low-Earth Orbit (LEO) satellites CALIPSO (Winker et al., 2009) and CloudSat (Stephens et al., 2002, 2018) respectively. Iwabuchi et al. (2012) explore the geographical distribution and optical properties of persistent contrails. More recently, the impact of contrails forming within existing cirrus clouds, so-called embedded contrails, has been explored (Tesche et al., 2016; Marjani et al., 2022). Seelig et al. (2025) in particular show that embedded contrails are likely responsible for an additional radiative forcing corresponding to around 10 % of that from line-shaped contrails.

A comprehensive understanding of contrail impacts therefore requires the integration of multiple data sources with modelling approaches. Such an integrated contrail monitoring framework is particularly relevant in the context of monitoring and verification of aviation non-CO_2 effects, where robust and scalable observational capabilities will be essential.

2.2.4. CONTRAIL CLIMATE IMPACTS

Contrails and contrail-cirrus influence the Earth's radiation budget through their interaction with both shortwave and longwave radiation. Ice crystals scatter incoming shortwave radiation back into space during the day (cooling effect) and absorb outgoing longwave radiation and re-emit it at lower temperatures at all times (warming effect). The effectiveness with which clouds absorb and scatter radiation is often expressed in terms of optical thickness (Kärcher, 2018). The net radiative effect is diurnal in nature and dependent on multiple factors, including air traffic density, time of day, solar zenith angle and location (Meerkötter et al., 1999; Markowicz and Witek, 2011; Forster et al., 2012; Schumann and Heymsfield, 2017). In aggregate, the warming effect of contrails has been shown to dominate (e.g. Grewe et al., 2017b; Lee et al., 2021).

Initial assessments on the global climate impact of contrails only considered persistent, linear contrails. IPCC (1999) estimated persistent contrail RF at $20\ (5, 60)\ \mathrm{mW\,m^{-2}}$ for air traffic in the year 1992. The uncertainty range was reduced by subsequent studies (e.g. Kärcher et al., 2010; Chen and Gettelman, 2013; Spangenberg et al., 2013), which together estimate $3 - 16\ \mathrm{mW\,m^{-2}}$ for air traffic between 2002 and 2006 (see Figure 7 of Kärcher et al., 2018). The first combined contrail and contrail-cirrus RF estimate of $38\ \mathrm{mW\,m^{-2}}$ was determined by Burkhardt and Kärcher (2011) using ECHAM4-CCMod (see Section 3.2). The combined best estimate of $111.4\ (33, 189)\ \mathrm{mW\,m^{-2}}$ (RF; Lee et al., 2021) for global air traffic in 2018 (see Section 2.1.2) is based on studies by Burkhardt and Kärcher (2011); Chen and Gettelman (2013); Schumann et al. (2015); Bock and Burkhardt (2016), although this best estimate was likely an overestimation due to their scaling methodology (see Section 3.3 and the discussion in Appendix 3.A).

Estimating the magnitude of contrail-cirrus radiative forcing is associated with a high degree of uncertainty (Zhang et al., 2025). A key source of uncertainty is the interaction between contrail-cirrus and natural cirrus clouds. For example, a recent study showed that persistent contrails tend to form in regions already containing subvisible or visible cirrus, resulting in an uncertain climate impact (Petzold et al., 2025). Both cloud types compete for available water vapour, which can partially offset the climate impact attributable to contrails (Burkhardt and Kärcher, 2009; Bickel, 2023). The introduction of new engine concepts and aviation fuels has also resulted in unanswered questions regarding the role of volatile particles and ambient aerosols in ice nucleation (see Section 2.2.1).

The efficacy of line-shaped contrails under the RF framework is substantially less than unity (Ponater, 2005; Rap et al., 2010). This means that for the same unit of radiative forcing, line-shaped contrails produce a smaller change in global mean surface temperature than CO_2 (see Section 2.1.1). Recent studies (Bickel et al., 2020; Ponater et al., 2021; Bickel et al., 2025) have focused on determining efficacy values also for contrail-cirrus. Bickel et al. (2025) estimate 0.208 ± 0.106 and 0.380 ± 0.257 within the RF and ERF frameworks respectively. Note that Lee et al. (2021, see Figure 2.2) used the ERF/RF ratio to determine ERF from an RF

estimate, which Bickel (2023) note is only valid inter alia if the efficacy of contrail-cirrus within the ERF framework is close to unity, which it is not. This clearly demonstrates the continued need to consider efficacy within future assessments, even when using the ERF.

2.2.5. CONTRAIL MITIGATION

The climate impact of contrail-cirrus can be tackled from both an operational and technological perspective (Kärcher, 2018). In terms of operations, recent studies have shown that a small number of flights can have an outsize contribution to the total warming from contrail-cirrus (e.g. Grewe et al., 2014; Teoh et al., 2020a, 2022a). Avoiding contrail formation, in particular the so-called "big hits", is a topic of ongoing research (e.g. Gierens et al., 2008; Filippone, 2015; Rosenow and Fricke, 2019). The first operational contrail avoidance trials are ongoing at the time of writing (e.g. D-KULT; Matthes et al., 2026) or have recently concluded, such as the EUROCONTROL MUAC trial of 2021 (Sausen et al., 2024). Several open questions should be addressed before contrail avoidance is routinely used in daily operations (Grewe et al., 2017c). Possibly the most important open question is related to the problem that although contrail formation can be reliably forecasted, persistence currently cannot (Gierens et al., 2020; Wilhelm et al., 2022; Hofer et al., 2024b).

The technological perspective considers changes to aircraft design and the use of alternative fuels. SAFs tend to have a higher hydrogen-to-carbon ratio and lower proportion of aromatics compared to conventional kerosene. This results in a lower soot and ice crystal number concentration (Moore et al., 2017; Bräuer et al., 2021; Voigt et al., 2021), which in turn reduces the optical depth and climate impact of contrails (Burkhardt et al., 2018). However, the higher hydrogen-to-carbon ratio also results in increased water vapour emissions and thus to the more frequent formation of persistent contrails (Rojo et al., 2015; Caiazzo et al., 2017; Teoh et al., 2022b; Hofer et al., 2024a, see also Chapter 4).

In the longer term, another promising technology is hydrogen, either combusted in a jet engine or used in a fuel cell. Unlike conventional jet fuels, it is not expected to produce any soot or particulate emissions, although the formation of ultrafine volatile particles from lubricant oil vapours has been observed in laboratory combustion tests (Ungeheuer et al., 2022). It is expected that contrails produced by hydrogen-powered aircraft will have significantly fewer, larger ice crystals, thus resulting in a lower optical thickness and radiative forcing (Marquart et al., 2005; Bier et al., 2024; Lottermoser and Unterstrasser, 2026). However, due to the large variability in the properties and concentration of the ambient aerosols (e.g. Brock et al., 2021; Voigt et al., 2022), the resulting ice crystal numbers and radiative effect are still highly uncertain.

The use of H_2 in a jet engine will also increase water vapour emissions, from $1.25\,\mathrm{kg\,kg^{-1}}$ (kerosene) to around $8.94\,\mathrm{kg\,kg^{-1}}$(hydrogen). Taking into account that

H_2 has a larger gravimetric energy density than kerosene – 120.9 compared to $43.6\,\mathrm{MJ\,kg^{-1}}$ – the slope of the SAC mixing line is around 2.6 times larger for H_2 combustion than for kerosene for the same overall propulsion system efficiency. Given the low exhaust temperature, that factor is even higher for H_2 fuel cells (see also Section 4.2.1), depending on the operating voltage of the fuel cell (Gierens, 2021; Richardson, 2025; Hillenbrand and Unterstrasser, 2026). We can, therefore, expect a significant increase in contrail formation from H_2 aircraft (e.g. Grewe et al., 2017a; Kaufmann et al., 2024). However, recent studies (Wolf et al., 2023; Sanogo et al., 2024) show that contrail formation frequency does not scale linearly with this factor. Kaufmann et al. (2024) in particular show that contrail formation from hydrogen-powered aircraft is strongly dependent on season, altitude and latitude. This suggests that the ambient atmospheric conditions and processes, rather than the aircraft design, mostly limit persistent contrail formation.

Other technologies reduce the slope of the mixing line, promising less frequent contrail formation. Notable examples are hybrid-electric aircraft and the Water-Enhanced Turbofan (WET) concept. Hybrid-electric aircraft are promising in that they could be flown such that only electric power is used within regions of potential persistent contrail formation. Even when electric power is combined with conventional fuel during continuous use, the mixing line slope of the combined system is lower, resulting in fewer contrails forming (Yin et al., 2020). However, hybrid-electric aircraft have a limited use case due to their low speed and service ceiling. Another possibility for reducing the mixing line slope is by condensing, storing and releasing water in areas in which the ambient conditions are not conducive to persistent contrail formation. A notable example of this is the WET concept (Schmitz et al., 2021; Pouzolz et al., 2021; Kaiser et al., 2022). The benefit of such a system is that it can be integrated into a wider range of aircraft and is not limited by speed and service ceiling.

2.3. CLIMATE METRICS

Aviation CO_2 and non-CO_2 climate effects occur on a wide range of timescales, ranging from hours to centuries (see Section 2.1.2). To introduce the full climate impact of aviation into policy, it is necessary to express all climate effects on a common scale. This is done using a climate metric, which relates non-CO_2 emissions to their consequences on the climate and/or on society (Fuglestvedt et al., 2003, 2010; Wuebbles et al., 2010; Tanaka et al., 2010). However, establishing an adequate equivalence across different species and effects is not trivial, especially when there are large differences in atmospheric lifetimes and efficacies (Ponater et al., 2006) or dependence on the emission time, altitude or location (Lund et al., 2017; Frömming et al., 2021).

This section provides an overview of the purpose and design of climate met-

rics (Section 2.3.1) and the calculation methods for each climate metric considered in this work (Section 2.3.2).

2.3.1. DESIGN OF CLIMATE METRICS

Climate metrics provide a means by which non-experts, notably policymakers both in government and industry, can compare different results, scenarios or strategies. The climate metric itself essentially provides a shortcut between the output of a potentially highly complex climate model or scenario and an impact to either the climate or society. Nevertheless, to ensure that decisions are based on current scientific understanding, climate metrics must accurately reflect the response to an emission (Niklaß et al., 2019).

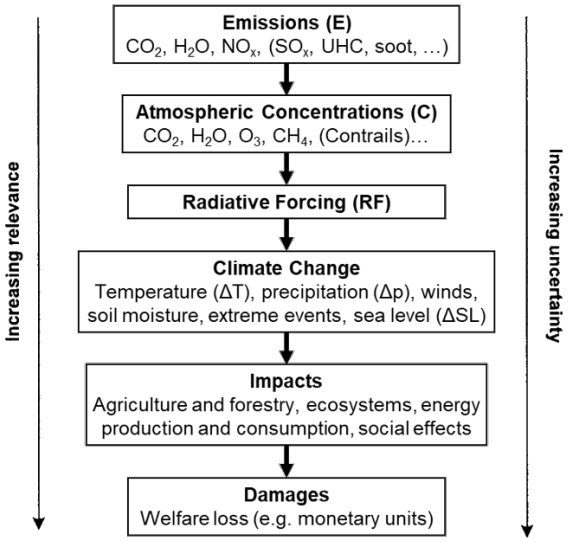


Figure 2.5: Cause-effect chain from emissions to damages. Climate metrics further down the chain are more relevant to society, but include a larger number of assumptions and uncertainties in their underlying climate models. The figure is adapted from Fuglestvedt et al. (2003) and reproduced with permission from *Springer Nature*.

To identify different options in climate metric design, Fuglestvedt et al. (2003) developed a cause-effect chain from emissions to damages. This is adapted to aviation emissions in Figure 2.5. Fuglestvedt et al. (1999) argue that an ideal climate metric, at least from the perspective of a policymaker, would be at the bottom of the chain. Using such a climate metric, one would be able to directly compare the cost of mitigation against the (monetary) damage an emission would cause to the environment and to society. However, the further down the chain a climate metric is, the more assumptions it contains and the larger the uncertainties are (Fuglestvedt et al., 2003; Shine et al., 2007; Fuglestvedt et al., 2010; Dallara et al., 2011). This becomes particularly problematic once economic

models are included. The choice of climate metric is thus always a compromise between its relevance to society and the level of uncertainty in the underlying model(s). To provide a point of comparison, the most commonly used climate metrics are only on the third (e.g. GWP) and fourth (e.g. GTP, ATR) links of the chain.

In this work, we only consider physical climate metrics, i.e. climate metrics that do not contain any economic models or assumptions. Specifically, we investigate the following conventional climate metrics: Radiative Forcing (RF), Global Warming Potential (GWP), Global Temperature Change Potential (GTP), Integrated GTP (iGTP) and Average Temperature Response (ATR). We also consider the recently proposed, unconventional method, denoted GWP*, which relates changes in emission rates of short-lived species to pulses of CO_2. Finally, we create derivates of the GWP and GWP* that are weighted by the efficacy, which we denote the Efficacy-weighted Global Warming Potential (EGWP) and EGWP* respectively. The calculation methods for all climate metrics are provided in the next section.

2.3.2. CLIMATE METRIC CALCULATIONS

The calculation methods for all seven climate metrics are given in Table 2.1. These methods require a time-series of radiative forcing (RF) or resulting temperature change ΔT. Note that in this work, we add an A to denote an absolute climate metric (i.e. AGWP, AEGWP, AGTP, iAGTP) and use rATR to denote the relative ATR (to CO_2). The GWP* and EGWP* do not have absolute and relative forms.

Table 2.1: Calculation methods for all climate metrics used in this research, where t_0 is the start of an emission series and, therefore, also the year for which a climate metric is to be calculated; H the time horizon; r the efficacy; and i a single species. The warming-equivalent emission variable $E_{CO_2\text{-we}}$ is explained in the calculation description of the GWP*. Note that these methods all require the time-series of radiative forcing (RF) or temperature change ΔT at least from t_0 until $t_0 + H$, which requires the use of a separate climate model. The GWP* and EGWP* require the time-series of RF at least from $t_0 - 20$ until $t_0 + H$.

Climate Metric	Calculation Method
RF	$\mathrm{RF}_H = \mathrm{RF}(t_0 + H)$
GWP	$\mathrm{AGWP}_H = \int_{t_0}^{t_0+H} \mathrm{RF}(t)\,\mathrm{d}t$
EGWP	$\mathrm{AEGWP}_{\mathrm{i},H} = r_\mathrm{i} \int_{t_0}^{t_0+H} \mathrm{RF}_\mathrm{i}(t)\,\mathrm{d}t$
GTP	$\mathrm{AGTP}_H = \Delta T(t_0 + H)$
iGTP	$\mathrm{iAGTP}_H = \int_{t_0}^{t_0+H} \Delta T(t)\,\mathrm{d}t$
ATR	$\mathrm{ATR}_H = \frac{1}{H}\int_{t_0}^{t_0+H} \Delta T(t)\,\mathrm{d}t = \frac{1}{H}\mathrm{iAGTP}_H$
GWP*	$E_{\mathrm{CO_2-we}}(t) = g(s)\cdot\left[(1-s)\frac{\Delta\mathrm{RF}(t)}{\Delta t}\frac{H}{\mathrm{AGWP}_{H(\mathrm{CO_2})}} + s\cdot\frac{\overline{\mathrm{RF}}(t)}{\mathrm{AGWP}_{H(\mathrm{CO_2})}}\right]$
EGWP*	Same as GWP* except replacing RF_i with $\mathrm{RF}_\mathrm{i}\cdot r_\mathrm{i}$

RF

Radiative Forcing (RF) is the globally averaged net change in the planetary energy balance caused by a perturbation. In this work, "RF" corresponds to the stratospheric-adjusted RF (see Section 2.1.1 for more detail). The RF is generally used as the basis for climate metrics such as the GWP. However, the RF can itself also be used as a climate metric, simply denoting the radiative forcing at a time horizon H. Since it considers only a single point in time, it is referred to as an endpoint climate metric.

EF

The concept of Energy Forcing (EF) was introduced by Schumann et al. (2011) as a means of determining the cumulative effect that a single contrail has on the climate in terms of energy over its lifetime. The EF [J] is calculated for a contrail using,

$$EF = \int_{\text{lifetime}} RF_{\text{net}}(t) \cdot L(t) \cdot W(t)\, \mathrm{d}t \tag{2.5}$$

where $RF_{\text{net}} = RF_{\text{LW}} + RF_{\text{SW}}$ [$\mathrm{W\,m^{-2}}$] is the "local net contrail radiative forcing"[3] (the wording varies by publication), L [m] the contrail length and W [m] the contrail width. Since a contrail lifetime is much smaller than a year, the annual mean RF [$\mathrm{W\,m^{-2}}$] is equivalent to the EF [J] divided by the Earth's surface area [$\mathrm{m^2}$] and seconds in the year [s] (see e.g. Teoh et al., 2024).

The EF is limited in its utility as a climate metric. Since each species has a different lifetime, the EF effectively integrates over an infinite time (see the Supplement of Irvine et al., 2014). For (very) short-lived species or effects, such as contrails, this is not a factor. However, the integration time presents a major problem for species that induce changes in other species with varying atmospheric lifetimes, such as NO_x emissions (see Section 2.1.3). The infinite integration time is also clearly not appropriate for (very) long-lived species such as CO_2, since their EF values would become comparatively very large. Previous studies (e.g. Teoh et al., 2020b) thus introduced a time horizon and use the AGWP (see below) to determine an EF for CO_2. Recognising that the EF can be easily converted to an annual mean RF and, therefore, to an AGWP (see also the Supplement of Irvine et al., 2014), and noting the limitations in its use for other aviation emission species, the EF is not further considered in this work.

[3] Arguably, there cannot be a "local radiative forcing", because radiative forcing is by definition a global value. Perhaps a more accurate description of this variable would be "local radiative effect". However, we use the original term here for consistency with previous studies.

GWP

The Global Warming Potential (GWP) was introduced by Rodhe (1990) and was included in the first assessment report of the IPCC (IPCC, 1990), over time becoming one of the most commonly used climate policy in (inter)national climate policymaking. The temporal integration makes the GWP less dependent on the time horizon than the simple RF, but since it does not correspond to a specific time in the future, there is no obvious choice for the time horizon (Allen et al., 2016). Nevertheless, Tanaka et al. (2021) show that the GWP_{100} is a good approximator of cost-effective climate metrics and is a good choice for the implementation of the Paris Agreement. Using the GWP for aviation would maximise compatibility with other sectors. However, studies considering suitable climate metrics for international climate policy have generally not considered aviation-specific non-CO_2 effects.

EGWP

The Efficacy-weighted Global Warming Potential (EGWP) was developed by Megill et al. (2024) as a derivative of the GWP. It aims to introduce the efficacy (see Section 2.1.1) of non-CO_2 emissions into the GWP method, such that the results obtained by the GWP more closely match those of temperature-based climate metrics. The EGWP for a single species i is then the GWP of that species multiplied by its efficacy r_i. We note that this calculation method is still quite uncertain, in particular for contrail-cirrus (Ponater et al., 2021), although it is not expected to affect the results of this study. Another potential approach to calculate the EGWP would be to use the Effective Radiative Forcing (ERF, see Section 2.1.1) and corresponding efficacies r'_i. Further work is required to develop better estimates of the efficacies for aviation emissions.

GTP

The Global Temperature-Change Potential (GTP) was first proposed by Shine et al. (2005). Like the RF, the GTP is an endpoint climate metric: the AGTP is simply the temperature change at a given time horizon H.

ATR and iGTP

The Average Temperature Response (ATR) and Integrated Global Temperature-Change Potential (iGTP) were developed independently by Dallara et al. (2011) and Peters et al. (2011) respectively. The ATR initially included a weighting function and used an infinite time horizon H. However, the infinite time horizon in particular made it inappropriate for global fuel scenarios. Since its inception, therefore, the ATR has been repurposed and is now generally used as the average temperature change over a given time horizon, as shown in Table 2.1. The weighting function is also no longer used. The relative ATR is denoted rATR in

this research for clarity. The iGTP is simply the integral of the GTP over the time horizon H. Note that therefore $\mathrm{rATR}_H = \mathrm{iGTP}_H$.

2

GWP* and EGWP*

Whilst radiative forcing due to long-lived emission species such as CO_2 scales with the cumulative integral of emissions, radiative forcing from short-lived emission species (SLCPs) depends both on the emission rate and atmospheric lifetime of the species. The GWP* methodology was initially proposed by Allen et al. (2018) to improve equivalence between these two responses by equating step changes in SLCP emission rates to CO_2 pulses, averaged over time. Since emission rates are meaningless for NO_x-induced aviation effects and for contrails, for use in aviation, the GWP* methodology must instead use radiative forcing. An equivalent calculation based on radiative forcing was proposed by Allen et al. (2018) and for this study modified using the improvements suggested by Cain et al. (2019) and Smith et al. (2021) to obtain:

$$E_{\mathrm{CO_2-we}}(t) = g(s) \cdot \left[(1-s) \cdot \frac{\Delta \mathrm{RF}(t)}{\Delta t} \cdot \frac{H}{\mathrm{AGWP}_{H(\mathrm{CO_2})}} + s \cdot \frac{\overline{\mathrm{RF}}(t)}{\mathrm{AGWP}_{H(\mathrm{CO_2})}} \right] \tag{2.6}$$

where $E_{\mathrm{CO_2-we}}(t)$ are CO_2-warming equivalent emissions as a function of time, $\Delta\mathrm{RF}$ the change in radiative forcing over the previous Δt = 20 years, $\overline{\mathrm{RF}}$ the running average of RF and $\mathrm{AGWP}_{H(\mathrm{CO_2})}$ the AGWP of a CO_2 pulse at a time horizon of H years. The above equation differs to the one used by Lee et al. (2021) only by the multiplication by $g(s)$,

$$g(s) = \frac{1 - \exp(-s/(1-s))}{s} \tag{2.7}$$

which was introduced in the same year by Smith et al. (2021) to improve consistency with the linear models used for climate metric calculations. In Chapter 7, we use s = 0.75 to be consistent with Smith et al. (2021). However, we note that this value was calculated for methane and thus may not be optimal for other aviation non-CO_2 emissions and effects.

The EGWP* was developed by Megill et al. (2024) as a derivative of the GWP*. Similarly to the EGWP, it makes use of the efficacy r_i to more closely match the results obtained by temperature-based climate metrics. The GWP* methodology is adapted by replacing RF_i with $\mathrm{RF}_\mathrm{i} \cdot r_\mathrm{i}$.

The GWP* and EGWP* differ from the other climate metrics considered in this study in that they are flow-based climate metrics: The GWP* method does not provide a single value over a specific time horizon. Instead, it provides a

CO_2-eq value as a function of time. This makes compatibility with existing policy challenging, as discussed in Section 7.3.3.

REFERENCES

Allen, M. R., Fuglestvedt, J. S., Shine, K. P., Reisinger, A., Pierrehumbert, R. T., and Forster, P. M.: New use of global warming potentials to compare cumulative and short-lived climate pollutants, Nature Climate Change, 6, 773–776, doi: 10.1038/nclimate2998, 2016.

Allen, M. R., Shine, K. P., Fuglestvedt, J. S., Millar, R. J., Cain, M., Frame, D. J., and Macey, A. H.: A solution to the misrepresentations of CO2-equivalent emissions of short-lived climate pollutants under ambitious mitigation, npj Climate and Atmospheric Science, 1, doi: 10.1038/s41612-018-0026-8, 2018.

Appleman, H.: The formation of exhaust condensation trails by jet aircraft, Bulletin of the American Meteorological Society, 34, 14–20, doi: 10.1175/1520-0477-34.1.14, 1953.

Bakan, S., Betancor, M., Gayler, V., and Graßl, H.: Contrail frequency over Europe from NOAA-satellite images, Annales Geophysicae, 12, 962–968, doi: 10.1007/s00585-994-0962-y, 1994.

Bickel, M.: Climate Impact of Contrail Cirrus, Ph.D. thesis, LMU München, München, doi: 10.57676/MZMG-R403, 2023.

Bickel, M., Ponater, M., Bock, L., Burkhardt, U., and Reineke, S.: Estimating the effective radiative forcing of contrail cirrus, Journal of Climate, 33, 1991–2005, doi: 10.1175/JCLI-D-19-0467.1, 2020.

Bickel, M., Ponater, M., Burkhardt, U., Righi, M., Hendricks, J., and Jöckel, P.: Contrail cirrus climate impact: from radiative forcing to surface temperature change, Journal of Climate, 38, 1895–1912, doi: 10.1175/JCLI-D-24-0245.1, 2025.

Bier, A., Burkhardt, U., and Bock, L.: Synoptic control of contrail cirrus life cycles and their modification due to reduced soot number emissions: contrail cirrus life cycles, Journal of Geophysical Research: Atmospheres, 122, 11,584–11,603, doi: 10.1002/2017JD027011, 2017.

Bier, A., Unterstrasser, S., Zink, J., Hillenbrand, D., Jurkat-Witschas, T., and Lottermoser, A.: Contrail formation on ambient aerosol particles for aircraft with hydrogen combustion: a box model trajectory study, Atmospheric Chemistry and Physics, 24, 2319–2344, doi: 10.5194/acp-24-2319-2024, 2024.

Bock, L. and Burkhardt, U.: Reassessing properties and radiative forcing of contrail cirrus using a climate model, Journal of Geophysical Research: Atmospheres, 121, 9717–9736, doi: 10.1002/2016JD025112, 2016.

Boucher, O. and Reddy, M.: Climate trade-off between black carbon and carbon dioxide emissions, Energy Policy, 36, 193–200, doi: 10.1016/j.enpol.2007.08.039, 2008.

Brock, C. A., Froyd, K. D., Dollner, M., Williamson, C. J., Schill, G., Murphy, D. M., Wagner, N. J., Kupc, A., Jimenez, J. L., Campuzano-Jost, P., Nault, B. A., Schroder, J. C., Day, D. A., Price, D. J., Weinzierl, B., Schwarz, J. P., Katich, J. M., Wang, S., Zeng, L., Weber, R., Dibb, J., Scheuer, E., Diskin, G. S., DiGangi, J. P., Bui, T., Dean-Day, J. M., Thompson, C. R., Peischl, J., Ryerson, T. B., Bourgeois, I., Daube, B. C., Commane, R., and Wofsy, S. C.: Ambient aerosol properties in the remote atmosphere from global-scale in situ measurements, Atmospheric Chemistry and Physics, 21, 15 023–15 063, doi: 10.5194/acp-21-15023-2021, 2021.

Bräuer, T., Voigt, C., Sauer, D., Kaufmann, S., Hahn, V., Scheibe, M., Schlager, H., Huber, F., Le Clercq, P., Moore, R. H., and Anderson, B. E.: Reduced ice number concentrations in contrails from low-aromatic biofuel blends, Atmospheric Chemistry and Physics, 21, 16 817–16 826, doi: 10.5194/acp-21-16817-2021, 2021.

Burkhardt, U. and Kärcher, B.: Process-based simulation of contrail cirrus in a global climate model, Journal of Geophysical Research, 114, D16 201, doi: 10.1029/2008JD011491, 2009.

Burkhardt, U. and Kärcher, B.: Global radiative forcing from contrail cirrus, Nature Climate Change, 1, 54–58, doi: 10.1038/nclimate1068, 2011.

Burkhardt, U., Bock, L., and Bier, A.: Mitigating the contrail cirrus climate impact by reducing aircraft soot number emissions, npj Climate and Atmospheric Science, 1, 37, doi: 10.1038/s41612-018-0046-4, 2018.

Caiazzo, F., Agarwal, A., Speth, R. L., and Barrett, S. R. H.: Impact of biofuels on contrail warming,

Environmental Research Letters, 12, 114 013, doi: 10.1088/1748-9326/aa893b, 2017.

Cain, M., Lynch, J., Allen, M. R., Fuglestvedt, J. S., Frame, D. J., and Macey, A. H.: Improved calculation of warming-equivalent emissions for short-lived climate pollutants, npj Climate and Atmospheric Science, 2, 29, doi: 10.1038/s41612-019-0086-4, 2019.

Chen, C.-C. and Gettelman, A.: Simulated radiative forcing from contrails and contrail cirrus, Atmospheric Chemistry and Physics, 13, 12 525–12 536, doi: 10.5194/acp-13-12525-2013, 2013.

Chevallier, R., Shapiro, M., Engberg, Z., Soler, M., and Delahaye, D.: Linear contrails detection, tracking and matching with aircraft using geostationary satellite and air traffic data, Aerospace, 10, 578, doi: 10.3390/aerospace10070578, 2023.

Cohen, Y., Hauglustaine, D., Staniaszek, Z., Lund, M. T., Dedoussi, I., Matthes, S., Quadros, F., Righi, M., Skowron, A., and Thor, R.: Impact of present aircraft NO_x and aerosol emissions on atmospheric composition and climate: results from a model intercomparison, EGUsphere [preprint], doi: 10.5194/egusphere-2025-4273, 2025.

Dallara, E. S., Kroo, I. M., and Waitz, I. A.: Metric for comparing lifetime average climate impact of aircraft, AIAA Journal, 49, 1600–1613, doi: 10.2514/1.J050763, 2011.

Dischl, R., Märkl, R., Sauer, D., Voigt, C., Harlaß, T., Scheibe, M., Hahn, V., Kaufmann, S., Marsing, A., Dörnbrack, A., Roiger, A., Yu, F., Gauthier, M., Renard, C., Swann, P., Johnson, M., Ahrens, D., Sallinen, R., Eckel, G., and Le Clercq, P.: Fuel sulfur content can modulate contrail ice crystal numbers, Communications Earth & Environment, 6, 902, doi: 10.1038/s43247-025-02951-5, 2025.

Driver, O. G. A., Stettler, M. E. J., and Gryspeerdt, E.: Factors limiting contrail detection in satellite imagery, Atmospheric Measurement Techniques, 18, 1115–1134, doi: 10.5194/amt-18-1115-2025, 2025.

Duda, D. P., Minnis, P., Khlopenkov, K., Chee, T. L., and Boeke, R.: Estimation of 2006 Northern Hemisphere contrail coverage using MODIS data, Geophysical Research Letters, 40, 612–617, doi: 10.1002/grl.50097, 2013.

Duda, D. P., Bedka, S. T., Minnis, P., Spangenberg, D., Khlopenkov, K., Chee, T., and Smith Jr., W. L.: Northern Hemisphere contrail properties derived from Terra and Aqua MODIS data for 2006 and 2012, Atmospheric Chemistry and Physics, 19, 5313–5330, doi: 10.5194/acp-19-5313-2019, 2019.

Etminan, M., Myhre, G., Highwood, E. J., and Shine, K. P.: Radiative forcing of carbon dioxide, methane, and nitrous oxide: A significant revision of the methane radiative forcing, Geophysical Research Letters, 43, doi: 10.1002/2016gl071930, 2016.

Filippone, A.: Assessment of aircraft contrail avoidance strategies, Journal of Aircraft, 52, 872–877, doi: 10.2514/1.C033176, 2015.

Finney, D. L., Doherty, R. M., Wild, O., Young, P. J., and Butler, A.: Response of lightning NOx emissions and ozone production to climate change: Insights from the Atmospheric Chemistry and Climate Model Intercomparison Project, Geophysical Research Letters, 43, 5492–5500, doi: 10.1002/2016GL068825, 2016.

Forster, L., Emde, C., Mayer, B., and Unterstrasser, S.: Effects of three-dimensional photon transport on the radiative forcing of realistic contrails, Journal of the Atmospheric Sciences, 69, 2243–2255, doi: 10.1175/JAS-D-11-0206.1, 2012.

Frömming, C., Ponater, M., Dahlmann, K., Grewe, V., Lee, D. S., and Sausen, R.: Aviation-induced radiative forcing and surface temperature change in dependency of the emission altitude, Journal of Geophysical Research: Atmospheres, 117, doi: 10.1029/2012JD018204, 2012.

Frömming, C., Grewe, V., Brinkop, S., Jöckel, P., Haslerud, A. S., Rosanka, S., van Manen, J., and Matthes, S.: Influence of weather situation on non-CO2 aviation climate effects: the REACT4C climate change functions, Atmospheric Chemistry and Physics, 21, 9151–9172, doi: 10.5194/acp-21-9151-2021, 2021.

Fuglestvedt, J., Berntsen, T. K., Isaksen, I. S., Mao, H., Liang, X.-Z., and Wang, W.-C.: Climatic forcing of nitrogen oxides through changes in tropospheric ozone and methane; global 3D model studies, Atmospheric Environment, 33, 961–977, doi: 10.1016/S1352-2310(98)00217-9, 1999.

Fuglestvedt, J., Shine, K., Berntsen, T., Cook, J., Lee, D., Stenke, A., Skeie, R., Velders, G., and Waitz, I.: Transport impacts on atmosphere and climate: Metrics, Atmospheric Environment, 44, 4648–

4677, doi: 10.1016/j.atmosenv.2009.04.044, 2010.

Fuglestvedt, J. S., Berntsen, T. K., Godal, O., Sausen, R., Shine, K. P., and Skodvin, T.: Metrics of climate change: assessing radiative forcing and emission indices, Climatic Change, 58, 267–331, doi: 10.1023/A:1023905326842, 2003.

Fushimi, A., Saitoh, K., Fujitani, Y., and Takegawa, N.: Identification of jet lubrication oil as a major component of aircraft exhaust nanoparticles, Atmospheric Chemistry and Physics, 19, 6389–6399, doi: 10.5194/acp-19-6389-2019, 2019.

Geraedts, S., Brand, E., Dean, T. R., Eastham, S., Elkin, C., Engberg, Z., Hager, U., Langmore, I., McCloskey, K., Yue-Hei Ng, J., Platt, J. C., Sankar, T., Sarna, A., Shapiro, M., and Goyal, N.: A scalable system to measure contrail formation on a per-flight basis, Environmental Research Communications, 6, 015 008, doi: 10.1088/2515-7620/ad11ab, 2024.

Gerz, T., Dürbeck, T., and Konopka, P.: Transport and effective diffusion of aircraft emissions, Journal of Geophysical Research: Atmospheres, 103, 25 905–25 913, doi: 10.1029/98JD02282, 1998.

Gierens, K.: Theory of contrail formation for fuel cells, Aerospace, 8, 164, doi: 10.3390/aerospace8060164, 2021.

Gierens, K. and Vázquez-Navarro, M.: Statistical analysis of contrail lifetimes from a satellite perspective, Meteorologische Zeitschrift, 27, 88 472, doi: 10.1127/metz/2018/0888, 2018.

Gierens, K., Lim, L., and Eleftheratos, K.: A review of various strategies for contrail avoidance, The Open Atmospheric Science Journal, 2, 1–7, doi: 10.2174/1874282300802010001, 2008.

Gierens, K., Matthes, S., Rohs, S., and Susanne Rohs: How well can persistent contrails be predicted, Aerospace, 7, 169, doi: 10.3390/aerospace7120169, 2020.

Grewe, V. and Stenke, A.: AirClim: An efficient tool for climate evaluation of aircraft technology, Atmospheric Chemistry and Physics, 8, 4621–4639, doi: 10.5194/acp-8-4621-2008, 2008.

Grewe, V., Dameris, M., Fichter, C., and Sausen, R.: Impact of aircraft NOx emissions. Part 1: Interactively coupled climate-chemistry simulations and sensitivities to climate-chemistry feedback, lightning and model resolution, Meteorologische Zeitschrift, 11, 177–186, doi: 10.1127/0941-2948/2002/0011-0177, 2002.

Grewe, V., Champougny, T., Matthes, S., Frömming, C., Brinkop, S., Søvde, O. A., Irvine, E. A., and Halscheidt, L.: Reduction of the air traffic's contribution to climate change: A REACT4C case study, Atmospheric Environment, 94, 616–625, doi: 10.1016/j.atmosenv.2014.05.059, 2014.

Grewe, V., Bock, L., Burkhardt, U., Dahlmann, K., Gierens, K., Hüttenhofer, L., Unterstrasser, S., Gangoli Rao, A., Bhat, A., Yin, F., Reichel, T. G., Paschereit, O., and Levy, Y.: Assessing the climate impact of the AHEAD multi-fuel blended wing body, Meteorologische Zeitschrift, 26, 711–725, doi: 10.1127/metz/2016/0758, 2017a.

Grewe, V., Dahlmann, K., Flink, J., Frömming, C., Ghosh, R., Gierens, K., Heller, R., Hendricks, J., Jöckel, P., Kaufmann, S., Kölker, K., Linke, F., Luchkova, T., Lührs, B., Van Manen, J., Matthes, S., Minikin, A., Niklaß, M., Plohr, M., Righi, M., Rosanka, S., Schmitt, A., Schumann, U., Terekhov, I., Unterstrasser, S., Vázquez-Navarro, M., Voigt, C., Wicke, K., Yamashita, H., Zahn, A., and Ziereis, H.: Mitigating the climate impact from aviation: achievements and results of the DLR WeCare project, Aerospace, 4, 34, doi: 10.3390/aerospace4030034, 2017b.

Grewe, V., Matthes, S., Frömming, C., Brinkop, S., Jöckel, P., Gierens, K., Champougny, T., Fuglestvedt, J., Haslerud, A., Irvine, E., and Shine, K.: Feasibility of climate-optimized air traffic routing for trans-Atlantic flights, Environmental Research Letters, 12, 034 003, doi: 10.1088/1748-9326/aa5ba0, 2017c.

Grewe, V., Matthes, S., and Dahlmann, K.: The contribution of aviation NOx emissions to climate change: are we ignoring methodological flaws?, Environmental Research Letters, 14, 121 003, doi: 10.1088/1748-9326/ab5dd7, 2019.

Grewe, V., Niklaß, M., Dahlmann, K., Eichinger, R., Matthes, S., Lau, A., Scheelhaase, J., Linke, F., and Plohr, M.: Pathways for including non-carbon dioxide aviation climate effects in the European Emission Trading System, Communications Earth & Environment, 7, 243, doi: 10.1038/s43247-026-03265-w, 2026.

Grimonprez, S., Faccinetto, A., Batut, S., Wu, J., Desgroux, P., and Petitprez, D.: Cloud condensation

nuclei from the activation with ozone of soot particles sampled from a kerosene diffusion flame, Aerosol Science and Technology, 52, 814–827, doi: 10.1080/02786826.2018.1472367, 2018.

Gryspeerdt, E., Stettler, M. E. J., Teoh, R., Burkhardt, U., Delovski, T., Driver, O. G. A., and Painemal, D.: Operational differences lead to longer lifetimes of satellite detectable contrails from more fuel efficient aircraft, Environmental Research Letters, 19, 084 059, doi: 10.1088/1748-9326/ad5b78, 2024.

Hansen, J., Sato, M., Ruedy, R., Nazarenko, L., Lacis, A., Schmidt, G. A., Russell, G., Aleinov, I., Bauer, M., Bauer, S., Bell, N., Cairns, B., Canuto, V., Chandler, M., Cheng, Y., Del Genio, A., Faluvegi, G., Fleming, E., Friend, A., Hall, T., Jackman, C., Kelley, M., Kiang, N., Koch, D., Lean, J., Lerner, J., Lo, K., Menon, S., Miller, R., Minnis, P., Novakov, T., Oinas, V., Perlwitz, J., Perlwitz, J., Rind, D., Romanou, A., Shindell, D., Stone, P., Sun, S., Tausnev, N., Thresher, D., Wielicki, B., Wong, T., Yao, M., and Zhang, S.: Efficacy of climate forcings, Journal of Geophysical Research, 110, D18 104, doi: 10.1029/2005JD005776, 2005.

Hasselmann, K., Sausen, R., Maier-Reimer, E., and Voss, R.: On the cold start problem in transient simulations with coupled atmosphere-ocean models, Climate Dynamics, 9, 53–61, doi: 10.1007/BF00210008, 1993.

Haywood, J. M., Allan, R. P., Bornemann, J., Forster, P. M., Francis, P. N., Milton, S., Rädel, G., Rap, A., Shine, K. P., and Thorpe, R.: A case study of the radiative forcing of persistent contrails evolving into contrail-induced cirrus, Journal of Geophysical Research: Atmospheres, 114, 2009JD012 650, doi: 10.1029/2009JD012650, 2009.

Hendricks, J., Righi, M., Brinkop, S., Dahlmann, K., Mertens, M., Beer, C. G., Grewe, V., Kaiser, C. J., and Ponater, M.: Large present-day and future climate forcing due to non-CO2 emissions from global transport, npj Climate and Atmospheric Science, 9, doi: 10.1038/s41612-026-01383-y, 2026.

Heymsfield, A. J., Lawson, R. P., and Sachse, G. W.: Growth of ice crystals in a precipitating contrail, Geophysical Research Letters, 25, 1335–1338, doi: 10.1029/98GL00189, 1998.

Hillenbrand, D. and Unterstrasser, S.: Contrail formation: generalised theory and a mitigation proposition for fuel-cell-propelled aircraft, The Aeronautical Journal, pp. 1–26, doi: 10.1017/aer.2026.10185, 2026.

Hofer, S., Gierens, K., and Rohs, S.: Contrail formation and persistence conditions for alternative fuels, Meteorologische Zeitschrift, 33, 43–49, doi: 10.1127/metz/2024/1178, 2024a.

Hofer, S., Gierens, K., and Rohs, S.: How well can persistent contrails be predicted? An update, Atmospheric Chemistry and Physics, 24, 7911–7925, doi: 10.5194/acp-24-7911-2024, 2024b.

Hofer, S. M. and Gierens, K. M.: Synoptic and microphysical lifetime constraints for contrails, Atmospheric Chemistry and Physics, 25, 9235–9247, doi: 10.5194/acp-25-9235-2025, 2025.

IPCC: Climate Change: The IPCC Scientific Assessment, Cambridge University Press, Cambridge, United Kingdom and New York, NY, USA, ISBN 978-0-521-40360-3, 1990.

IPCC: Aviation and the Global Atmosphere, Cambridge University Press, Cambridge, United Kingdom and New York, NY, USA, 1999.

IPCC: Climate Change 2001: The Scientific Basis. Contribution of Working Group I to the Third Assessment Report of the Intergovernmental Panel on Climate Change, Cambridge University Press, Cambridge, United Kingdom and New York, NY, USA, ISBN 0-521-80767-0, 2001.

IPCC: Climate Change 2013: The Physical Science Basis. Contribution of Working Group I to the Fifth Assessment Report of the Intergovernmental Panel on Climate Change, Cambridge University Press, Cambridge, United Kingdom and New York, NY, USA, ISBN 978-1-107-66182-0, 2013.

IPCC: Climate Change 2021 – The Physical Science Basis: Working Group I Contribution to the Sixth Assessment Report of the Intergovernmental Panel on Climate Change, Cambridge University Press, Cambridge, United Kingdom and New York, NY, USA, ISBN 978-1-009-15789-6, doi: 10.1017/9781009157896, 2023.

Irvine, E. A., Hoskins, B. J., and Shine, K. P.: A simple framework for assessing the trade-off between the climate impact of aviation carbon dioxide emissions and contrails for a single flight, Environmental Research Letters, 9, 064 021, doi: 10.1088/1748-9326/9/6/064021, 2014.

Iwabuchi, H., Yang, P., Liou, K. N., and Minnis, P.: Physical and optical properties of persistent

contrails: Climatology and interpretation, Journal of Geophysical Research: Atmospheres, 117, 2011JD017 020, doi: 10.1029/2011JD017020, 2012.

Jones, S. and Miake-Lye, R.: Contrail modeling of ECLIF2/ND-MAX flights: Effects of nvPM particle numbers and fuel sulfur content, Meteorologische Zeitschrift, 33, 35–41, doi: 10.1127/metz/2023/1180, 2024.

Kaiser, S., Schmitz, O., Ziegler, P., and Klingels, H.: The Water-Enhanced Turbofan as enabler for climatenNeutral aviation, Applied Sciences, 12, 12 431, doi: 10.3390/app122312431, 2022.

Kaufmann, S., Dischl, R., and Voigt, C.: Regional and seasonal impact of hydrogen propulsion systems on potential contrail cirrus cover, Atmospheric Environment: X, 24, 100 298, doi: 10.1016/j.aeaoa.2024.100298, 2024.

Kleine, J., Voigt, C., Sauer, D., Schlager, H., Scheibe, M., Jurkat-Witschas, T., Kaufmann, S., Kärcher, B., and Anderson, B. E.: In situ observations of ice particle losses in a young persistent contrail, Geophysical Research Letters, 45, doi: 10.1029/2018GL079390, 2018.

Knollenberg, R. G.: Measurements of the growth of the ice budget in a persisting contrail, Journal of the Atmospheric Sciences, 29, 1367–1374, doi: 10.1175/1520-0469(1972)029<1367:MOTGOT>2.0.CO;2, 1972.

Kärcher, B.: Formation and radiative forcing of contrail cirrus, Nature Communications, 9, 1824–1824, doi: 10.1038/s41467-018-04068-0, 2018.

Kärcher, B. and Yu, F.: Role of aircraft soot emissions in contrail formation, Geophysical Research Letters, 36, L01 804, doi: 10.1029/2008GL036649, 2009.

Kärcher, B., Peter, T., Biermann, U. M., and Schumann, U.: The initial composition of jet condensation trails, Journal of the Atmospheric Sciences, 53, 3066–3083, doi: 10.1175/1520-0469(1996)053<3066:TICOJC>2.0.CO;2, 1996.

Kärcher, B., Burkhardt, U., Ponater, M., and Frömming, C.: Importance of representing optical depth variability for estimates of global line-shaped contrail radiative forcing, Proceedings of the National Academy of Sciences, 107, 19 181–19 184, doi: 10.1073/pnas.1005555107, 2010.

Kärcher, B., Burkhardt, U., Bier, A., Bock, L., and Ford, I. J.: The microphysical pathway to contrail formation, Journal of Geophysical Research: Atmospheres, 120, 7893–7927, doi: 10.1002/2015JD023491, 2015.

Kärcher, B., Kleine, J., Sauer, D., and Voigt, C.: Contrail formation: Analysis of sublimation mechanisms, Geophysical Research Letters, 45, doi: 10.1029/2018gl079391, 2018.

Lee, D., Pitari, G., Grewe, V., Gierens, K., Penner, J., Petzold, A., Prather, M., Schumann, U., Bais, A., and Berntsen, T.: Transport impacts on atmosphere and climate: Aviation, Atmospheric Environment, 44, 4678–4734, doi: 10.1016/j.atmosenv.2009.06.005, 2010.

Lee, D., Fahey, D., Skowron, A., Allen, M., Burkhardt, U., Chen, Q., Doherty, S., Freeman, S., Forster, P., Fuglestvedt, J., Gettelman, A., De León, R., Lim, L., Lund, M., Millar, R., Owen, B., Penner, J., Pitari, G., Prather, M., Sausen, R., and Wilcox, L.: The contribution of global aviation to anthropogenic climate forcing for 2000 to 2018, Atmospheric Environment, 244, 117 834, doi: 10.1016/j.atmosenv.2020.117834, 2021.

Lewellen, D. C.: Persistent contrails and contrail cirrus. Part II: Full lifetime behavior, Journal of the Atmospheric Sciences, 71, 4420–4438, doi: 10.1175/JAS-D-13-0317.1, 2014.

Lottermoser, A. and Unterstrasser, S.: Modeling the impact of alternative fuels and hydrogen propulsion on contrail-cirrus: A parameter study, Journal of Geophysical Research: Atmospheres, 131, e2025JD044 604, doi: 10.1029/2025JD044604, 2026.

Lund, M. T., Aamaas, B., Berntsen, T., Bock, L., Burkhardt, U., Fuglestvedt, J. S., and Shine, K. P.: Emission metrics for quantifying regional climate impacts of aviation, Earth System Dynamics, 8, 547–563, doi: 10.5194/esd-8-547-2017, 2017.

Mannstein, H., Meyer, R., and Wendling, P.: Operational detection of contrails from NOAA-AVHRR-data, International Journal of Remote Sensing, 20, 1641–1660, doi: 10.1080/014311699212650, 1999.

Marjani, S., Tesche, M., Bräuer, P., Sourdeval, O., and Quaas, J.: Satellite observations of the impact

of individual aircraft on ice crystal number in thin cirrus clouds, Geophysical Research Letters, 49, doi: 10.1029/2021GL096173, 2022.

Markowicz, K. M. and Witek, M.: Sensitivity study of global contrail radiative forcing due to particle shape, Journal of Geophysical Research: Atmospheres, 116, n/a–n/a, doi: 10.1029/2011JD016345, 2011.

Marquart, S., Ponater, M., Ström, L., and Gierens, K.: An upgraded estimate of the radiative forcing of cryoplane contrails, Meteorologische Zeitschrift, 14, 573–582, doi: 10.1127/0941-2948/2005/0057, 2005.

Matthes, S., Gierens, K., Beckmann, B., Bugliaro, L., Dietmüller, S., Frömming, C., Hanst, M., Hofer, S., Jene, J., Kirschler, S., Köhler, C. G., Lau, A., Leemüller, R., Liedtke, A., Mendiguchia Meuser, M., Peter, P., Santos Gabriel, V., Köhler, I., Saueressig, G., Schlemmer, L., Sperling, J., Schlobach, S., Schultz, R., Von Sack, K., and Waltenberg, N.: D-KULT: data and tools for routine eco-efficient flight operations, J. Env. Com. Air Transp. Sys. Discuss. [preprint], doi: 10.5194/jecats-2026-3, 2026.

Meerkötter, R., Schumann, U., Doelling, D. R., Minnis, P., Nakajima, T., and Tsushima, Y.: Radiative forcing by contrails, Annales Geophysicae, 17, 1080–1094, doi: 10.1007/s00585-999-1080-7, 1999.

Megill, L., Deck, K., and Grewe, V.: Alternative climate metrics to the Global Warming Potential are more suitable for assessing aviation non-CO2 effects, Communications Earth & Environment, 5, 249, doi: 10.1038/s43247-024-01423-6, 2024.

Meijer, V. R., Kulik, L., Eastham, S. D., Allroggen, F., Speth, R. L., Karaman, S., and Barrett, S. R. H.: Contrail coverage over the united states before and during the COVID-19 pandemic, Environmental Research Letters, 17, 034 039, doi: 10.1088/1748-9326/ac26f0, 2022.

Moore, R. H., Thornhill, K. L., Weinzierl, B., Sauer, D., D'Ascoli, E., Kim, J., Lichtenstern, M., Scheibe, M., Beaton, B., Beyersdorf, A. J., Barrick, J., Bulzan, D., Corr, C. A., Crosbie, E., Jurkat, T., Martin, R., Riddick, D., Shook, M., Slover, G., Voigt, C., White, R., Winstead, E., Yasky, R., Ziemba, L. D., Brown, A., Schlager, H., and Anderson, B. E.: Biofuel blending reduces particle emissions from aircraft engines at cruise conditions, Nature, 543, 411–415, doi: 10.1038/nature21420, 2017.

Myhre, G., Nilsen, J. S., Gulstad, L., Shine, K. P., Rognerud, B., and Isaksen, I. S. A.: Radiative forcing due to stratospheric water vapour from CH4 oxidation, Geophysical Research Letters, 34, 2006GL027 472, doi: 10.1029/2006GL027472, 2007.

Myhre, G., Shine, K., Rädel, G., Gauss, M., Isaksen, I., Tang, Q., Prather, M., Williams, J., van Velthoven, P., Dessens, O., Koffi, B., Szopa, S., Hoor, P., Grewe, V., Borken-Kleefeld, J., Berntsen, T., and Fuglestvedt, J.: Radiative forcing due to changes in ozone and methane caused by the transport sector, Atmospheric Environment, 45, 387–394, doi: 10.1016/j.atmosenv.2010.10.001, 2011.

Myhre, G., Shindell, D., Bréon, F.-M., Collins, W., Fuglestvedt, J., Huang, J., Koch, D., Lamarque, J.-F., Lee, D., Mendoza, B., Nakajima, T., Robock, A., Stephens, G., and Zhang, H.: Anthropogenic and Natural Radiative Forcing, in: Climate Change 2013: The Physical Science Basis. Contribution of Working Group I to the Fifth Assessment Report of the Intergovernmental Panel on Climate Change, Cambridge University Press, Cambridge, United Kingdom and New York, NY, USA, 2013.

Märkl, R. S., Voigt, C., Sauer, D., Dischl, R. K., Kaufmann, S., Harlaß, T., Hahn, V., Roiger, A., Weiß-Rehm, C., Burkhardt, U., Schumann, U., Marsing, A., Scheibe, M., Dörnbrack, A., Renard, C., Gauthier, M., Swann, P., Madden, P., Luff, D., Sallinen, R., Schripp, T., and Le Clercq, P.: Powering aircraft with 100% sustainable aviation fuel reduces ice crystals in contrails, Atmospheric Chemistry and Physics, 24, 3813–3837, doi: 10.5194/acp-24-3813-2024, 2024.

Ng, J. Y.-H., McCloskey, K., Cui, J., Meijer, V. R., Brand, E., Sarna, A., Goyal, N., Van Arsdale, C., and Geraedts, S.: Contrail detection on GOES-16 ABI with the OpenContrails dataset, IEEE Transactions on Geoscience and Remote Sensing, doi: https://doi.org/10.1109/TGRS.2023.3345226, 2023.

Niklaß, M., Dahlmann, K., Grewe, V., Maertens, S., Plohr, M., Janina Scheelhaase, Jonathan Schwieger, Urs Brodmann, Claudia Kurzböck, Mischa Repmann, Nadin Schweizer, and Moritz von Unger: Integration of non-CO2 effects of aviation in the EU ETS and under CORSIA - Final Report, Tech. rep., Umweltbundesamt Deutschland, 2019.

Paoli, R. and Shariff, K.: Contrail modeling and simulation, Annual Review of Fluid Mechanics, 48, 393–427, doi: 10.1146/annurev-fluid-010814-013619, 2016.

Peters, G. P., Aamaas, B., Berntsen, T., and Fuglestvedt, J. S.: The integrated global temperature change potential (iGTP) and relationships between emission metrics, Environmental Research Letters, 6, 044 021, doi: 10.1088/1748-9326/6/4/044021, 2011.

Petzold, A., Gysel, M., Vancassel, X., Hitzenberger, R., Puxbaum, H., Vrochticky, S., Weingartner, E., Baltensperger, U., and Mirabel, P.: On the effects of organic matter and sulphur-containing compounds on the CCN activation of combustion particles, Atmospheric Chemistry and Physics, 5, 3187–3203, doi: 10.5194/acp-5-3187-2005, 2005.

Petzold, A., Khan, N. F., Li, Y., Spichtinger, P., Rohs, S., Crewell, S., Wahner, A., and Krämer, M.: Most long-lived contrails form within cirrus clouds with uncertain climate impact, Nature Communications, 16, 9695, doi: 10.1038/s41467-025-65532-2, 2025.

Pletzer, J.: The climate impact of hypersonic transport, Ph.D. thesis, Delft University of Technology, Delft, doi: 10.4233/UUID:39ACCA9A-53BA-4B9C-B9C0-B6C99F552E25, 2024.

Pletzer, J. and Grewe, V.: Sensitivities of atmospheric composition and climate to altitude and latitude of hypersonic aircraft emissions, Atmospheric Chemistry and Physics, 24, 1743–1775, doi: 10.5194/acp-24-1743-2024, 2024.

Pletzer, J., Hauglustaine, D., Cohen, Y., Jöckel, P., and Grewe, V.: The climate impact of hydrogen-powered hypersonic transport, Atmospheric Chemistry and Physics, 22, 14 323–14 354, doi: 10.5194/acp-22-14323-2022, 2022.

Ponater, M.: On contrail climate sensitivity, Geophysical Research Letters, 32, L10 706, doi: 10.1029/2005GL022580, 2005.

Ponater, M., Pechtl, S., Sausen, R., Schumann, U., and Hüttig, G.: Potential of the cryoplane technology to reduce aircraft climate impact: A state-of-the-art assessment, Atmospheric Environment, 40, 6928–6944, doi: 10.1016/j.atmosenv.2006.06.036, 2006.

Ponater, M., Bickel, M., Bock, L., and Burkhardt, U.: Towards determining the contrail cirrus efficacy, Aerospace, 8, 42, doi: 10.3390/aerospace8020042, 2021.

Ponsonby, J., King, L., Murray, B. J., and Stettler, M. E. J.: Jet aircraft lubrication oil droplets as contrail ice-forming particles, Atmospheric Chemistry and Physics, 24, 2045–2058, doi: 10.5194/acp-24-2045-2024, 2024.

Popovicheva, O., Persiantseva, N. M., Shonija, N. K., DeMott, P., Koehler, K., Petters, M., Kreidenweis, S., Tishkova, V., Demirdjian, B., and Suzanne, J.: Water interaction with hydrophobic and hydrophilic soot particles, Physical Chemistry Chemical Physics, 10, 2332, doi: 10.1039/b718944n, 2008.

Pouzolz, R., Schmitz, O., and Klingels, H.: Evaluation of the climate impact reduction potential of the Water-Enhanced Turbofan (WET) concept, Aerospace, 8, 59, doi: 10.3390/aerospace8030059, 2021.

Rap, A., Forster, P. M., Jones, A., Jones, A., Boucher, O., Haywood, J., Bellouin, N., and De León, R.: Parameterization of contrails in the UK Met Office Climate Model, Journal of Geophysical Research, 115, doi: 10.1029/2009jd012443, 2010.

Richardson, E. S.: Contrail Formation Criterion for Assessment of Alternative Propulsion Technologies, Journal of Propulsion and Power, 41, 264–276, doi: 10.2514/1.B39430, 2025.

Righi, M., Hendricks, J., and Brinkop, S.: The global impact of the transport sectors on aerosol and climate under the Shared Socioeconomic Pathways (SSPs), Earth System Dynamics Discussions, doi: 10.5194/esd-2022-52, 2023.

Righi, M., Testa, B., Beer, C. G., Hendricks, J., and Kanji, Z. A.: Aviation soot interactions with natural cirrus clouds are unlikely to have a significant impact on global climate, Atmospheric Chemistry and Physics, 25, 18 341–18 353, doi: 10.5194/acp-25-18341-2025, 2025.

Rodhe, H.: A comparison of the contribution of various gases to the greenhouse effect, Science, 248, 1217–1219, doi: 10.1126/science.248.4960.1217, 1990.

Rojo, C., Vancassel, X., Mirabel, P., Ponche, J.-L., and Garnier, F.: Impact of alternative jet fuels on aircraft-induced aerosols, Fuel, 144, 335–341, doi: 10.1016/j.fuel.2014.12.021, 2015.

Rosenow, J. and Fricke, H.: Individual condensation trails in aircraft trajectory optimization, Sustainability, 11, 6082, doi: 10.3390/su11216082, 2019.

Sanogo, S., Boucher, O., Bellouin, N., Borella, A., Wolf, K., and Rohs, S.: Variability in the properties of the distribution of the relative humidity with respect to ice: implications for contrail formation, Atmospheric Chemistry and Physics, 24, 5495–5511, doi: 10.5194/acp-24-5495-2024, 2024.

Santos Gabriel, V., Bugliaro, L., Piontek, D., Ries, S., and Voigt, C.: An adaptive segmentation approach for contrail detection in Meteosat Second Generation satellite imagery, EGUsphere [preprint], doi: 10.5194/egusphere-2025-6275, 2026.

Sarna, A., Meijer, V., Chevallier, R., Duncan, A., McConnaughay, K., Geraedts, S., and McCloskey, K.: Benchmarking and improving algorithms for attributing satellite-observed contrails to flights, Atmospheric Measurement Techniques, 18, 3495–3532, doi: 10.5194/amt-18-3495-2025, 2025.

Sausen, R. and Schumann, U.: Estimates of the climate response to aircraft CO2 and NOx emissions scenarios, Climatic Change, 44, 27–58, doi: 10.1023/A:1005579306109, 2000.

Sausen, R., Hofer, S., Gierens, K., Bugliaro, L., Ehrmanntraut, R., Sitova, I., Walczak, K., Burridge-Diesing, A., Bowman, M., and Miller, N.: Can we successfully avoid persistent contrails by small altitude adjustments of flights in the real world?, Meteorologische Zeitschrift, 33, 83–98, doi: 10.1127/metz/2023/1157, 2024.

Schmidt, E.: Die Entstehung von Eisnebel aus den Auspuffgasen von Flugmotoren, Schriften der Deutschen Akademie der Luftfahrtforschung, 5, 1–22, 1941.

Schmitz, O., Klingels, H., and Kufner, P.: Aero engine concepts beyond 2030: Part 1—The steam injecting and recovering aero engine, Journal of Engineering for Gas Turbines and Power, 143, 021 001, doi: 10.1115/1.4048985, 2021.

Schumann, U.: On conditions for contrail formation from aircraft exhausts, Meteorologische Zeitschrift, 5, 4–23, doi: 10.1127/metz/5/1996/4, 1996.

Schumann, U. and Heymsfield, A. J.: On the life cycle of individual contrails and contrail cirrus, Meteorological Monographs, 58, 3.1–3.24, doi: 10.1175/AMSMONOGRAPHS-D-16-0005.1, 2017.

Schumann, U., Graf, K., and Mannstein, H.: Potential to reduce the climate impact of aviation by flight level changes, in: 3rd AIAA Atmospheric Space Environments Conference, American Institute of Aeronautics and Astronautics, Honolulu, Hawaii, ISBN 978-1-62410-143-4, doi: 10.2514/6.2011-3376, 2011.

Schumann, U., Penner, J. E., Chen, Y., Zhou, C., and Graf, K.: Dehydration effects from contrails in a coupled contrail–climate model, Atmospheric Chemistry and Physics, 15, 11 179–11 199, doi: 10.5194/acp-15-11179-2015, 2015.

Seelig, T., Wolf, K., Bellouin, N., and Tesche, M.: Quantification of the radiative forcing of contrails embedded in cirrus clouds, Nature Communications, 16, 10 703, doi: 10.1038/s41467-025-66231-8, 2025.

Seinfeld, J. H. and Pandis, S. N.: Atmospheric chemistry and physics: From air pollution to climate change, John Wiley & Sons, Inc, Hoboken, New Jersey, USA, third edn., ISBN 978-1-118-94740-1, 2016.

Shine, K. P., Fuglestvedt, J. S., Hailemariam, K., and Stuber, N.: Alternatives to the Global Warming Potential for comparing climate impacts of emissions of greenhouse gases, Climatic Change, 68, 281–302, doi: 10.1007/s10584-005-1146-9, 2005.

Shine, K. P., Berntsen, T. K., Fuglestvedt, J. S., Skeie, R. B., and Stuber, N.: Comparing the climate effect of emissions of short- and long-lived climate agents, Philosophical Transactions of the Royal Society A: Mathematical, Physical and Engineering Sciences, 365, 1903–1914, doi: 10.1098/rsta.2007.2050, 2007.

Smith, M. A., Cain, M., and Allen, M. R.: Further improvement of warming-equivalent emissions calculation, npj Climate and Atmospheric Science, 4, 19, doi: 10.1038/s41612-021-00169-8, 2021.

Spangenberg, D. A., Minnis, P., Bedka, S. T., Palikonda, R., Duda, D. P., and Rose, F. G.: Contrail radiative forcing over the Northern Hemisphere from 2006 Aqua MODIS data, Geophysical Research Letters, 40, 595–600, doi: 10.1002/grl.50168, 2013.

Stephens, G., Winker, D., Pelon, J., Trepte, C., Vane, D., Yuhas, C., L'Ecuyer, T., and Lebsock, M.: CloudSat and CALIPSO within the A-Train: Ten years of actively observing the Earth system, Bulletin of the American Meteorological Society, 99, 569–581, doi: 10.1175/BAMS-D-16-0324.1, 2018.

Stephens, G. L., Vane, D. G., Boain, R. J., Mace, G. G., Sassen, K., Wang, Z., Illingworth, A. J., O'connor, E. J., Rossow, W. B., Durden, S. L., Miller, S. D., Austin, R. T., Benedetti, A., Mitrescu, C., and the CloudSat Science Team: THE CLOUDSAT MISSION AND THE A-TRAIN: A New Dimension of Space-Based Observations of Clouds and Precipitation, Bulletin of the American Meteorological Society, 83, 1771–1790, doi: 10.1175/BAMS-83-12-1771, 2002.

Stevenson, D. S., Doherty, R. M., Sanderson, M. G., Collins, W. J., Johnson, C. E., and Derwent, R. G.: Radiative forcing from aircraft NOx emissions: mechanisms and seasonal dependence, Journal of Geophysical Research, 109, D17 307, doi: 10.1029/2004JD004759, 2004.

Tanaka, K., Peters, G. P., and Fuglestvedt, J. S.: Policy Update: Multicomponent climate policy: why do emission metrics matter?, Carbon Management, 1, 191–197, doi: 10.4155/cmt.10.28, 2010.

Tanaka, K., Boucher, O., Ciais, P., Johansson, D. J. A., and Morfeldt, J.: Cost-effective implementation of the Paris Agreement using flexible greenhouse gas metrics, Science Advances, 7, eabf9020, doi: 10.1126/sciadv.abf9020, 2021.

Teoh, R., Schumann, U., Majumdar, A., and Stettler, M. E. J.: Mitigating the climate forcing of aircraft contrails by small-scale diversions and technology adoption, Environmental Science & Technology, 54, 2941–2950, doi: 10.1021/acs.est.9b05608, 2020a.

Teoh, R., Schumann, U., and Stettler, M. E. J.: Beyond contrail avoidance: Efficacy of flight altitude changes to minimise contrail climate forcing, Aerospace, 7, 121, doi: 10.3390/aerospace7090121, 2020b.

Teoh, R., Schumann, U., Gryspeerdt, E., Shapiro, M., Molloy, J., Koudis, G., Voigt, C., and Stettler, M. E. J.: Aviation contrail climate effects in the North Atlantic from 2016 to 2021, Atmospheric Chemistry and Physics, 22, 10 919–10 935, doi: 10.5194/acp-22-10919-2022, 2022a.

Teoh, R., Schumann, U., Voigt, C., Schripp, T., Shapiro, M., Engberg, Z., Molloy, J., Koudis, G., and Stettler, M. E. J.: Targeted use of sustainable aviation fuel to maximize climate benefits, Environmental Science & Technology, 56, 17 246–17 255, doi: 10.1021/acs.est.2c05781, 2022b.

Teoh, R., Engberg, Z., Schumann, U., Voigt, C., Shapiro, M., Rohs, S., and Stettler, M. E. J.: Global aviation contrail climate effects from 2019 to 2021, Atmospheric Chemistry and Physics, 24, 6071–6093, doi: 10.5194/acp-24-6071-2024, 2024.

Tesche, M., Achtert, P., Glantz, P., and Noone, K. J.: Aviation effects on already-existing cirrus clouds, Nature Communications, 7, 12 016, doi: 10.1038/ncomms12016, 2016.

Ungeheuer, F., Caudillo, L., Ditas, F., Simon, M., Van Pinxteren, D., Kılıç, D., Rose, D., Jacobi, S., Kürten, A., Curtius, J., and Vogel, A. L.: Nucleation of jet engine oil vapours is a large source of aviation-related ultrafine particles, Communications Earth & Environment, 3, 319, doi: 10.1038/s43247-022-00653-w, 2022.

Voigt, C., Schumann, U., Jurkat, T., Schäuble, D., Schlager, H., Petzold, A., Gayet, J.-F., Krämer, M., Schneider, J., Borrmann, S., Schmale, J., Jessberger, P., Hamburger, T., Lichtenstern, M., Scheibe, M., Gourbeyre, C., Meyer, J., Kübbeler, M., Frey, W., Kalesse, H., Butler, T., Lawrence, M. G., Holzäpfel, F., Arnold, F., Wendisch, M., Döpelheuer, A., Gottschaldt, K., Baumann, R., Zöger, M., Sölch, I., Rautenhaus, M., and Dörnbrack, A.: In-situ observations of young contrails – overview and selected results from the CONCERT campaign, Atmospheric Chemistry and Physics, 10, 9039–9056, doi: 10.5194/acp-10-9039-2010, 2010.

Voigt, C., Kleine, J., Sauer, D., Moore, R. H., Bräuer, T., Le Clercq, P., Kaufmann, S., Scheibe, M., Jurkat-Witschas, T., Aigner, M., Bauder, U., Boose, Y., Borrmann, S., Crosbie, E., Diskin, G. S., DiGangi, J., Hahn, V., Heckl, C., Huber, F., Nowak, J. B., Rapp, M., Rauch, B., Robinson, C., Schripp, T., Shook, M., Winstead, E., Ziemba, L., Schlager, H., and Anderson, B. E.: Cleaner burning aviation fuels can reduce contrail cloudiness, Communications Earth & Environment, 2, 114, doi: 10.1038/s43247-021-00174-y, 2021.

Voigt, C., Lelieveld, J., Schlager, H., Schneider, J., Curtius, J., Meerkötter, R., Sauer, D., Bugliaro, L., Bohn, B., Crowley, J. N., Erbertseder, T., Groß, S., Hahn, V., Li, Q., Mertens, M., Pöhlker, M. L., Pozzer, A., Schumann, U., Tomsche, L., Williams, J., Zahn, A., Andreae, M., Borrmann, S., Bräuer, T., Dörich, R., Dörnbrack, A., Edtbauer, A., Ernle, L., Fischer, H., Giez, A., Granzin, M., Grewe, V., Harder, H., Heinritzi, M., Holanda, B. A., Jöckel, P., Kaiser, K., Krüger, O. O., Lucke, J., Marsing, A., Martin, A., Matthes, S., Pöhlker, C., Pöschl, U., Reifenberg, S., Ringsdorf, A., Scheibe, M., Tadic, I., Zauner-

Wieczorek, M., Henke, R., and Rapp, M.: Cleaner skies during the COVID-19 lockdown, Bulletin of the American Meteorological Society, 103, E1796–E1827, doi: 10.1175/BAMS-D-21-0012.1, 2022.

Voigt, C., Märkl, R., Sauer, D., Dischl, R., Renard, C., Seeliger, K., Yu, F., Kaufmann, S., Bräuer, T., Jurkat-Witschas, T., Le Chenadec, G., Moreau, J., Requena-Esteban, E., Bonne, N., Vals, M., Roche, A., Zelina, J., Dörnbrack, A., Eirenschmalz, L., Heckl, C., Horst, E., Lichtenstern, M., Marsing, A., Neumann, G., Roiger, A., Scheibe, M., Stock, P., Giez, A., Eckel, G., and Le Clercq, P.: Substantial aircraft contrail formation at low soot emission levels, Nature, 652, 112–118, doi: 10.1038/s41586-026-10286-0, 2026.

Vázquez-Navarro, M., Mannstein, H., and Kox, S.: Contrail life cycle and properties from 1 year of MSG/SEVIRI rapid-scan images, Atmospheric Chemistry and Physics, 15, 8739–8749, doi: 10.5194/acp-15-8739-2015, 2015.

Wilhelm, L., Gierens, K., and Rohs, S.: Meteorological conditions that promote persistent contrails, Applied Sciences, 12, 4450, doi: 10.3390/app12094450, 2022.

Winker, D. M., Vaughan, M. A., Omar, A., Hu, Y., Powell, K. A., Liu, Z., Hunt, W. H., and Young, S. A.: Overview of the CALIPSO mission and CALIOP data processing algorithms, Journal of Atmospheric and Oceanic Technology, 26, 2310–2323, doi: 10.1175/2009JTECHA1281.1, 2009.

Wolf, K., Bellouin, N., and Boucher, O.: Long-term upper-troposphere climatology of potential contrail occurrence over the Paris area derived from radiosonde observations, Atmospheric Chemistry and Physics, 23, 287–309, doi: 10.5194/acp-23-287-2023, 2023.

Wong, H.-W. and Miake-Lye, R. C.: Parametric studies of contrail ice particle formation in jet regime using microphysical parcel modeling, Atmospheric Chemistry and Physics, 10, 3261–3272, doi: 10.5194/acp-10-3261-2010, 2010.

Wuebbles, D., Forster, P., Rogers, H., and Herman, R.: Issues and uncertainties affecting metrics for aviation impacts on climate, Bulletin of the American Meteorological Society, 91, 491–496, doi: 10.1175/2009BAMS2840.1, 2010.

Yin, F., Grewe, V., and Gierens, K.: Impact of hybrid-electric aircraft on contrail coverage, Aerospace, 7, 147, doi: 10.3390/aerospace7100147, number: 10, 2020.

Yu, F. and Turco, R. P.: The role of ions in the formation and evolution of particles in aircraft plumes, Geophysical Research Letters, 24, 1927–1930, doi: 10.1029/97GL01822, 1997.

Yu, Z., Herndon, S. C., Ziemba, L. D., Timko, M. T., Liscinsky, D. S., Anderson, B. E., and Miake-Lye, R. C.: Identification of lubrication oil in the particulate matter emissions from engine exhaust of in-service commercial aircraft, Environmental Science & Technology, 46, 9630–9637, doi: 10.1021/es301692t, 2012.

Zhang, W., Van Weverberg, K., Morcrette, C. J., Feng, W., Furtado, K., Field, P. R., Chen, C.-C., Gettelman, A., Forster, P. M., Marsh, D. R., and Rap, A.: Impact of host climate model on contrail cirrus effective radiative forcing estimates, Atmospheric Chemistry and Physics, 25, 473–489, doi: 10.5194/acp-25-473-2025, 2025.

Zink, J., Unterstrasser, S., and Jurkat-Witschas, T.: On the potential role of lubrication oil particles in contrail formation for kerosene and hydrogen combustion, Journal of Geophysical Research: Atmospheres, 130, doi: 10.1029/2025jd043487, 2025.

Buzz, silenced.

I wonder,
as we debug the world,
will we miss them?

— LM

3

MODELLING

The first climate models were developed in the 1950s as extensions of numerical weather prediction models, adapted to represent climatic processes on much longer timescales. Since then, climate modelling has evolved from highly idealised one- or two-dimensional representations to increasingly comprehensive frameworks that couple the atmosphere and ocean in three dimensions and time, commonly referred to as General Circulation Models (GCMs). Subsequent developments incorporated additional components and feedbacks, including aerosol dynamics, atmospheric chemistry, land processes and the carbon cycle. The current state of the art is represented by Earth System Models (ESMs), which explicitly simulate a wide range of interacting physical, chemical and biological processes. These models are vital for advancing our understanding of the Earth system response to anthropogenic perturbations and form the backbone of coordinated multi-model efforts such as the Coupled Model Intercomparison Projects (CMIP, Dunne et al., 2025) to project future climate pathways.

Despite their importance, ESMs are computationally highly intensive, which severely constrains the number of scenarios, sensitivities or uncertainty ranges that can be explored. This limitation motivates the use of models with reduced complexity for applications that require large ensembles or fast scenario evaluations. Such models are valid at the global or regional level and parameterise many processes and are commonly referred to as Simple Climate Models (SCMs). In general terms, SCMs represent the causal chain: emissions → concentration change → radiative forcing → temperature change. There are a wide variety of SCMs, which differ in scope, complexity and intended application (see e.g. Nicholls et al., 2020). Notable examples include MAGICC (Meinshausen et al., 2011), FaIR (Smith et al., 2018; Leach et al., 2021), OSCAR (Gasser et al., 2017) and CICERO-SCM (Sandstad et al., 2024). While these models are well suited for global, multi-sector assessments, they are typically not sufficiently tailored to capture the specific characteristics of aviation emissions and effects, in particular the strong dependence on emission location.

A range of modelling approaches have been developed specifically to assess the climate impact of aviation emissions. Generally, these models can be categorised into weather-dependent and climatological or response models. Weather-dependent models are generally applicable to operational strategies and include the Contrail-Cirrus Prediction tool (CoCiP, see Section 3.2) and the algorithmic Climate Change Functions (aCCFs; Van Manen and Grewe, 2019; Dietmüller et al., 2023; Yin et al., 2023). The aCCFs were developed from comprehensive chemistry-climate model simulations using regressions to enable the rapid estimation of the CO_2 and non-CO_2 climate effects of specific flights in expected weather conditions, thereby allowing integration into trajectory optimisation and daily flight planning (Simorgh et al., 2024; Castino et al., 2024). On the other hand, climatological or response models are useful for simulating long-term aviation industry scenarios. This work focuses on AirClim (Grewe and Stenke, 2008; Dahlmann et al., 2016) and its successor OpenAirClim (Völk et al., 2025), which are described in more detail in the following section, but other models such as

LEEA (Köhler et al., 2008; Rädel and Shine, 2008) also exist.

This chapter explores existing modelling and attribution approaches for aviation emissions and climate impacts. The next section describes the response models AirClim and OpenAirClim. Section 3.2 explores contrail modelling approaches and provides a detailed overview of the AirClim contrail module. Emission inventories and global aviation scenarios are compared in Section 3.3. Finally, an overview of attribution methods is provided in Section 3.4.

3.1. RESPONSE MODELLING WITH (OPEN)AIRCLIM

The climate impact of air traffic has traditionally been assessed using comprehensive chemistry–climate models (CCMs), which explicitly resolve relevant physical and chemical processes in the atmosphere. While these models provide a high level of process fidelity, the simulation of multi-year aviation scenarios is computationally expensive and can, depending on model complexity and experimental design, require weeks of compute time on high-performance computing systems. Such approaches are therefore well suited to detailed process studies, but are impractical for the systematic evaluation of large numbers of technology options, operational strategies, or scenario ensembles.

Response models, such as AirClim and its successor OpenAirClim, adopt a fundamentally different methodology. Instead of explicitly simulating atmospheric processes, they rely on pre-computed climate responses and statistical relationships derived from targeted simulations with comprehensive climate models. These responses are typically formulated as functions of emission location (altitude, latitude, longitude) and are interpolated over idealised emission regions to estimate globally averaged radiative forcing or near-surface temperature change. As a result, a single multi-year aviation scenario can be evaluated within seconds to minutes on a standard desktop or laptop computer. This high computational efficiency enables the systematic comparison of a large number of scenarios and facilitates sensitivity analyses and uncertainty assessments that would be infeasible using CCMs.

AirClim is a non-linear climate-chemistry response model developed at the DLR for estimating the radiative forcing and temperature change due to emissions of aviation CO_2, NO_x and H_2O as well as the formation of contrails. The model was initially developed for the climate impact analysis of supersonic aircraft (Grewe and Stenke, 2008), but has since been extended to include subsonic flight levels (Fichter, 2009), contrail-cirrus (Dahlmann, 2011) and an internal Monte Carlo simulation to quantify uncertainties (Dahlmann et al., 2016). AirClim combines emission and scenario inputs with pre-calculated data and regressions obtained from simulations using more complex climate models. The methodology differs per species. As a response model, AirClim is very fast and efficient, making it ideal for the assessment of future aviation scenarios (e.g. Grewe et al.,

2021), operational strategies and changes (e.g. Matthes et al., 2021; Zengerling et al., 2025) and multidisciplinary optimisation schemes and aircraft design (e.g. Grewe et al., 2010, 2017a).

OpenAirClim[1] (Völk et al., 2025) is a new response model based on the original AirClim concept, but includes a large number of enhancements. The full OpenAirClim framework is open-source and designed for close and transparent collaboration across research, industry and policy. The model is under development by an international consortium led by the DLR Institute of Atmospheric Physics (DLR-PA), which includes Delft University of Technology (TU Delft), the Royal Netherlands Aerospace Centre (NLR) and Chalmers University of Technology. Compared to its predecessor, OpenAirClim can:

- handle multiple emission inventories over time (4D dependence);
- attribute the climate impact to specific aircraft;
- apply a tagging methodology for atmospheric chemistry;
- calculate the contrail climate impact of novel aviation fuels; and
- provide uncertainty and robustness metrics.

The main OpenAirClim paper is in preparation at the time of writing. A core software output of this dissertation is the OpenAirClim contrail module (oac.cont, described in Chapter 5). In addition, the development of an emission inventory generator (GEDAI) is at the time of writing in early development, but not described in this dissertation. Its objective is to create OpenAirClim-compatible emission inventories from ADS-B data or from expected routes, enabling reproducible, transparent and flexible aviation emissions modelling.

3.2. CONTRAIL MODELLING

A wide range of contrail modelling approaches has been developed to investigate contrail formation, evolution and climate impact. These approaches span several levels of abstraction. They differ in their representation of plume dynamics, microphysics, atmospheric variability and radiative processes, as well as in their computational costs and intended application.

3.2.1. PHYSICAL CONTRAIL MODELS

At the most idealised level, zero-dimensional (0D) box models (e.g. Kärcher and Yu, 2009; Wong and Miake-Lye, 2010) simulate contrail formation and early microphysical evolution. These models typically represent an average mixing state across the exhaust plume cross-section and simplify plume dynamics through

[1]See https://openairclim.org [Last accessed: 01/04/2026].

parameterised or plume-averaged mixing. They allow detailed treatment of microphysics and chemistry and relatively low computational cost and have been used to investigate ice nucleation pathways, particle activation and sensitivity to the exhaust composition. However, the strong spatial variability within the turbulent plume – the result of the hot exhaust mixing with the ambient air – is generally not resolved. These models thus cannot capture the full heterogeneity of temperature, humidity and particle concentrations, which influence ice crystal formation.

The dominant turbulent motions and spatial variation of the plume are generally captured by three-dimensional (3D) Large-Eddy Simulations (LES). LES models simulate the formation and evolution of contrails in an idealised atmospheric environment with high spatial and temporal resolution, providing detailed insights into jet/vortex interaction (Paoli et al., 2013), ice crystal activation (Lewellen, 2020) and the transition of contrails into contrail-cirrus (Unterstrasser and Gierens, 2010a,b).

A widely used framework for such studies is the EULAG-LCM model system, which couples the non-hydrostatic fluid solver EULAG (Smolarkiewicz and Grell, 1992) with a Lagrangian Cloud Module (LCM) for representing microphysical processes (Sölch and Kärcher, 2010). Using this model, Unterstrasser (2014) demonstrated that the microphysical and geometric properties of contrails in the vortex phase are strongly controlled by both meteorological and aircraft-dependent parameters. Subsequent simulations of the dispersion phase indicated that aged contrail-cirrus becomes increasingly difficult to distinguish from natural cirrus based on microphysical properties alone (Unterstrasser et al., 2017). More recent LES studies have extended this framework to assess the impact of novel aviation fuels and propulsion technologies. For example, Lottermoser and Unterstrasser (2026) demonstrate that reduced initial ice crystal numbers, expected for low-soot fuels and hydrogen, lead to shorter-lived contrail-cirrus and thus lower radiative impact.

Early global studies investigated the radiative impact of line-shaped contrails by combining an air traffic inventory with reanalysis data (e.g. Sausen et al., 1998; Duda et al., 2005; Rädel and Shine, 2008). This was followed by the introduction of line-shaped contrails (e.g. Ponater et al., 2002) and later contrail-cirrus (Burkhardt and Kärcher, 2009) into General Circulation Models (GCMs). GCMs are used to investigate the properties and radiative influence of contrails at a regional to global scale. They incorporate contrail processes through parameterisations derived from dedicated LES simulations and can be tuned to more closely match measurements and historical climate data. Due to their coarse spatial resolution, GCMs do not simulate individual contrails, but instead model contrail formation and spreading within grid boxes, often treating ensembles or clusters of contrails collectively. This dissertation uses the results of simulations using the GCM ECHAM5 (Roeckner et al., 2003, 2006) extended by the Hamburg Aerosol Module (HAM, Stier et al., 2005). The integrated contrail-cirrus module

(CCMod) was initially developed for ECHAM4 by Burkhardt and Kärcher (2009), who introduced a separate cloud class for contrail-cirrus that enabled competition with simulated natural cirrus clouds for water vapour. The model setup is described in more detail in Section 5.2.

A spectrum of further simplified models exist, designed for specific use cases. This includes CERM (Caiazzo et al., 2017) and the Contrail-Cirrus Prediction model (CoCiP; Schumann, 2012). CoCiP is a Lagrangian model that simulates the life cycle of contrails using simplified physical parameterisations. An open-source implementation of CoCiP is available as pycontrails (Shapiro et al., 2025). CoCiP simulates the development of contrail segments along individual flight trajectories using ambient atmospheric conditions defined by NWP data. Contrail segments are initiated if the conditions at two consecutive waypoints satisfy the Schmidt-Appleman criterion. The model then tracks the evolution of each segment over time, allowing the resulting contrail-cirrus to persist until the contrail ice crystal number, optical depth or lifetime exceed predefined thresholds (Schumann, 2012). For each contrail segment, CoCiP calculates an Energy Forcing (EF, see Section 2.3.2). CoCiP is also available in gridded mode and has recently been coupled with the global Icosahedral Non-hydrostatic numerical weather prediction model ICON (Zängl et al., 2015), which allows simulated contrails to interact with the background atmosphere (Schumann and Seifert, 2025).

At a higher level of abstraction are algorithmic and climatological models, which rely on pre-computed responses from comprehensive LES, GCM or ESM simulations to estimate contrail radiative forcing. These include the previously mentioned (algorithmic) Climate Change Functions and the response models AirClim and OpenAirClim. These reduced-complexity approaches allow for the rapid analysis of multi-year and multi-fuel scenarios whilst retaining the key sensitivities of their parent models. The contrail implementation in AirClim is described in the following section; the new OpenAirClim contrail module is a focus of this dissertation and is developed in Chapter 5.

3.2.2. CONTRAIL RESPONSE MODELLING WITH AIRCLIM

The AirClim contrail module was developed by Dahlmann (2011) and subsequently reported and improved by Hüttenhofer (2013); Dahlmann et al. (2016); Grewe et al. (2017a, 2021). This section describes the module integrated into AirClim 2.1. The module aims to calculate the changes in the contrail-induced annual global average stratospheric-adjusted radiative forcing due to an emission inventory and scenario. The methodology can be represented as: flown distance → contrail formation → contrail-cirrus coverage → radiative forcing.

Three aircraft-dependent parameters are required for the calculation of the contrail climate impact:

- G – slope of the Schmidt-Appleman mixing line slope [$\mathrm{Pa\,K^{-1}}$]. Valid range: $1.62–4.80\,\mathrm{Pa\,K^{-1}}$;
- η_{fac} – overall propulsion efficiency η compared to the reference efficiency ($\eta = 0.333$);
- PM_{rel} – soot number emission index compared to the reference value $1 \times 10^{15}\,\mathrm{kg^{-1}}$ (note the difference to OpenAirClim; see Chapter 5). Valid range: ≥ 0.1 (corresponding to $\geq 1 \times 10^{14}\,\mathrm{kg^{-1}}$).

Contrail formation

Contrail formation is classified by the Schmidt-Appleman Criterion (SAC, see Section 2.2.1) and ice supersaturation (see Section 2.2.2). AirClim introduced the concept of Contrail Flight Distance Density (CFDD), which is the flown distance weighted by the probability of persistent contrail formation. It is calculated using,

$$\mathrm{CFDD}(i,j) = \sum_k \left(\frac{d(i,j,k)}{A(i,j)} \cdot p_{\mathrm{SAC}}(G,i,j,k) \right) \tag{3.1}$$

where $d(i,j,k)$ is the distance flown [km] in each grid box (latitude i, longitude j, pressure level k), $A(i,j)$ is the area [$\mathrm{km^2}$] of each grid box as viewed from above and $p_{\mathrm{SAC}}(G,i,j,k)$ is the climatological probability of a persistent contrail formation at that location for an aircraft with slope G. This latter variable is determined by linearly interpolating between three pre-calculated values, corresponding to aircraft powered by conventional kerosene, liquid natural gas (LNG) and hydrogen combustion (Grewe et al., 2017a). The sum over pressure level approximates a maximum random overlap.

Contrail-cirrus coverage

The contrail-cirrus coverage cccov is determined using a function fitted from results of simulations using ECHAM4-CCMod (Dahlmann, 2011),

$$\mathrm{cccov}(i,j) = 0.128 \cdot \mathrm{ISS}(i,j) \cdot \arctan\left(97.7\ [\mathrm{km^2\ km^{-1}}] \cdot \frac{\mathrm{CFDD}(i,j)}{\mathrm{ISS}(i,j)} \right) \tag{3.2}$$

where $\mathrm{ISS}(i,j)$ is the vertically-overlapped proportion of each grid cell (i,j,k) that is supersaturated with respect to ice. The contrail-cirrus coverage is further multiplied by three weighting functions w_1 to w_3, developed by Hüttenhofer (2013) to refine the AirClim response functions to more closely match the ECHAM4-CCMod results. The weighting functions were reported by Grewe et al. (2017a) and are defined as,

$$w_1 = 0.863 \cdot \cos\left(lat \cdot \frac{\pi}{50}\right) \tag{3.3}$$

$$w_2 = 1.0 + 15.0 \cdot \left|0.045 \cdot \cos\left(0.045 \cdot lat\right) + 0.045\right| \cdot (\eta_{fac} - 1.0) \tag{3.4}$$

$$w_3 = 1.0 + 0.24 \cdot \cos\left(lat \cdot \frac{\pi}{23}\right) \tag{3.5}$$

where lat is the latitude (corresponding to index i). A global contrail-cirrus coverage $\overline{\text{cccov}}$ is obtained by area-weighting cccov.

Radiative forcing

A linear relationship between the global contrail-cirrus coverage $\overline{\text{cccov}}$ was found by Dahlmann (2011) using results of simulations with ECHAM4-CCMod,

$$\text{RF} = 14.9\ [\text{W m}^{-2}] \cdot \overline{\text{cccov}} \cdot PM_{\text{fac}} \tag{3.6}$$

where PM_{fac} is a parameterisation of the relationship between soot emissions and radiative forcing found by Burkhardt et al. (2018). It is defined for $PM_{\text{rel}} \geq 0.1$ as (Grewe et al., 2021),

$$PM_{\text{fac}} = \frac{\arctan\left(1.9 \cdot PM_{\text{rel}}^{0.74}\right)}{\arctan(1.9)} \tag{3.7}$$

Validation

AirClim 2.0 was able to replicate the RF of ECHAM4-CCMod simulations using the same emission inventory to within 10 % (Dahlmann, 2011; Dahlmann et al., 2016). Including the corrections introduced by Hüttenhofer (2013) (as reported by Grewe et al., 2017a), this was reduced in AirClim 2.1 to within 0.8 % for conventional kerosene and 4.2 % for hydrogen combustion. Dahlmann et al. (2016) further showed good agreement between AirClim and ECHAM4-CCMod for changes in cruise altitude. In general, Bruder et al. (2026) find that the AirClim contrail RF values are well within the confidence interval provided by Lee et al. (2021).

3.3. EMISSION INVENTORIES AND SCENARIOS

Many aviation scenarios and emission inventories exist, using various top-down or bottom-up approaches. The majority of these focus on fuel use and CO_2

emissions over time, but to calculate the contrail climate impact the flown distance is required. Figure 3.1 shows the scenarios and emission inventories considered in this study. The lines correspond to scenarios; markers to discrete emission inventories that I have access to. The impact of COVID-19 can be clearly identified, which was considered by contemporary studies.

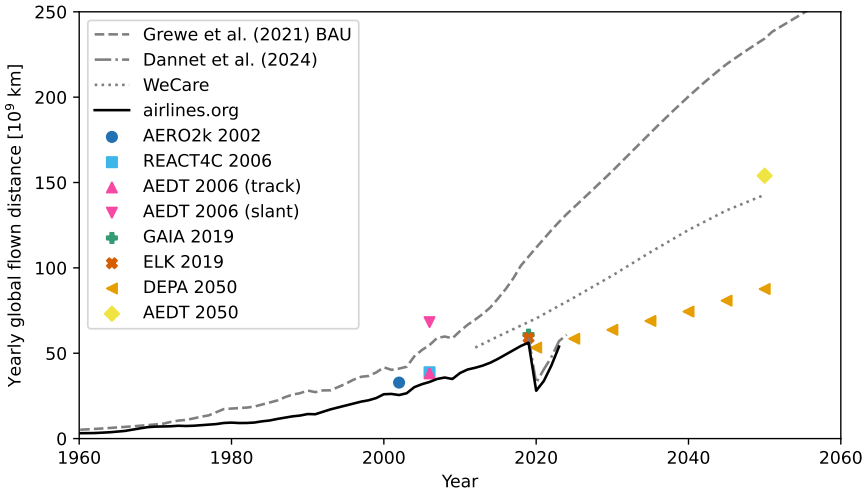


Figure 3.1: Aviation scenarios and emission inventories considered in this study. Shown are studies and inventories that determine a yearly global flown distance. The lines correspond to scenarios; markers to discrete, 3D emission inventories.

Teoh et al. (2024) find a pre-COVID flown distance of $6.09 \times 10^{10}\,\mathrm{km}$ in 2019 using ADS-B data. This is corroborated by the results of the DLR EmissionsLandKarte project (ELK; Weder et al., 2025; Righi et al., 2026), who find $5.89 \times 10^{10}\,\mathrm{km}$ in 2019 and Dannet et al. (2024), who find $5.92 \times 10^{10}\,\mathrm{km}$ also in 2019. The DLR project DEPA 2050 (Leipold et al., 2021) assume a slightly lower value, at $5.33 \times 10^{10}\,\mathrm{km}$ in 2020 (not including COVID-19 effects). The WeCare study (Grewe et al., 2017b) assumes generally higher values, but as an earlier study of course could not foresee the effects of COVID-19. The Grewe et al. (2021) scenarios are clearly outliers, estimating $10.1 \times 10^{10}\,\mathrm{km}$ in 2018. In that study, the flown distance is calculated from the Revenue Passenger Kilometres (RPK) using an assumption on the number of passengers per flight, assumed to linearly increase from 40 in 1940 to 82 in 2018 (from the WeCare project, see Grewe et al., 2017b). It is likely that the flown kilometres are highly dependent on this assumption, which led to the high estimate of flown distance.

The AERO2k 2002 (Eyers et al., 2004) and AEDT 2006 (Wilkerson et al., 2010; Chen et al., 2012) emission inventories have often been used for contrail studies. The REACT4C 2006 inventory was developed for a European project with the same name (see e.g. Grewe et al., 2014). The AEDT 2050 inventory was developed by Bock and Burkhardt (2019) from AEDT 2006 based on a demand forecast

from 1998 and thus could also not foresee the effect of COVID-19. However, should the growth of global aviation flown distance continue at a similar rate to the few years before 2019, this increase until 2050 is not unreasonable. The DEPA 2050 study seems to be fairly pessimistic in comparison.

The vertical and latitudinal profiles of the emission inventories are shown in Figure 3.2. For simplicity, the inventories are binned by pressure level and latitude, which results in a few artefacts (particularly for the REACT4C inventory). Nevertheless, this analysis provides a good idea of the distribution of air traffic in each inventory. The REACT4C inventory has generally more air traffic at higher pressure levels (lower altitude), whereas the ELK inventory has significantly more air traffic at lower pressure levels (higher altitude). Since the probability of persistent contrail formation reduces with decreasing altitude (see Chapter 4), we can expect a lower contrail RF using REACT4C and a higher contrail RF using ELK. The newer emission inventories, ELK (for 2019) and DEPA 2050 (for 2020) show a clear increase in air traffic in the tropics compared to the inventories in 2002 and 2006. This is due to particularly high growth in the Asia Pacific region[2].

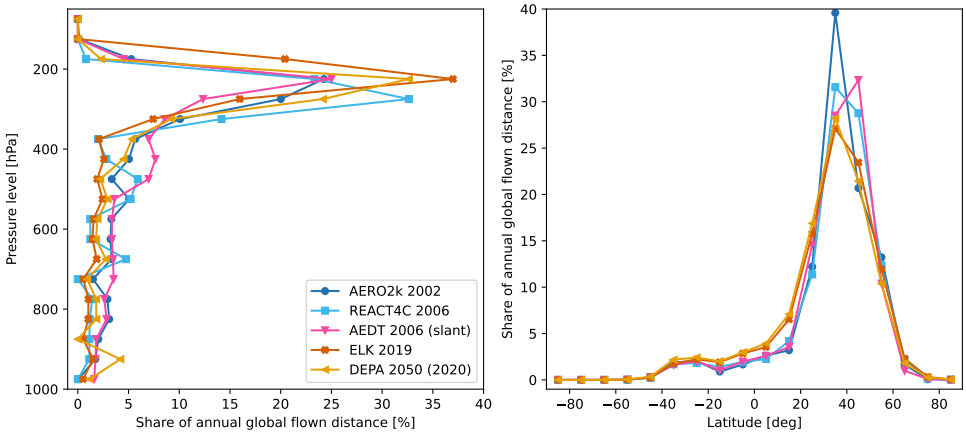


Figure 3.2: Vertical and latitudinal profiles of various emission inventories.

Contrail studies using the AEDT 2006 inventory differentiate between the ground-projected 2D "track" and the 3D flight path "slant" distance. Considering slant rather than track distance increases the global flight distance by a factor of 1.8 (Bock and Burkhardt, 2016). As described in Appendix 3.A, it is unclear how such a large difference could be found and it is thus likely that best estimates using the slant distance overestimate the contrail radiative forcing. The OpenAirClim contrail module (described in Chapter 5) tries to overcome the issues described in the Appendix by scaling the emission inventories before calculating the climate impact.

[2]https://www.iata.org/en/iata-repository/publications/economic-reports/airline-industry-outlook-update---mid-year-2019/ [Last accessed: 26/11/2025]

3.4. ATTRIBUTION METHODS

The process of attribution refers to the extent to which individual causal factors contribute to an observed change in a system. In the context of climate science, this typically involves determining how emissions from a given source – such as a country, sector or technology – contribute to changes in anthropogenic radiative forcing or temperature change. This is not a straightforward process because many non-linearities are present in the climate system (e.g. Clappier et al., 2017). Different methods have different advantages and disadvantages, rely on different assumptions and thus yield different results. As a result, attribution is politically salient. It plays a central role in climate negotiations because it can be used to allocate responsibility for anthropogenic climate change. A prominent example is the "Brazilian Proposal", which suggested distributing mitigation obligations among countries according to their historical greenhouse gas emissions (Enting, 1998; Trudinger and Enting, 2005; Höhne and Blok, 2005).

Attribution methods can be additive or non-additive (Trudinger and Enting, 2005). If a method is non-additive, the contribution of a group of sources differs depending on whether they are quantified together or separately. In other words, using a non-additive method, $y_{\mathrm{A}}(t) + y_{\mathrm{B}}(t) \neq y_{\mathrm{A+B}}(t)$. This can limit the applicability of these methods, because sources cannot be arbitrarily combinable. In the following, we introduce four common attribution methods, which have been integrated into OpenAirClim. We make use of the notation applied by Boucher et al. (2021).

NON-ADDITIVE METHODS

A commonly used method is the *residual attribution method (R)*, otherwise referred to as the "all-but-one" method. The effect (e.g. radiative forcing) attributed to a given source s at time t is the difference between two simulations: one with all anthropogenic activities ($x(t)$) and the other excluding the source in question ($x(t) - x_{\mathrm{s}}(t)$). This can be written as,

$$y_{\mathrm{s}}^{R}(t) = f(x(t)) - f(x(t) - x_{\mathrm{s}}(t)) \tag{3.8}$$

where f is the relationship between the source and effect. For small perturbations, this method is equivalent to the *marginal attribution method (M)*, which determines the contribution "at the margin" and can be written as,

$$y_{\mathrm{s}}^{M}(t) = \left.\frac{\mathrm{d}f}{\mathrm{d}x}\right|_{x(t)} \cdot x_{\mathrm{s}}(t) \tag{3.9}$$

Since this method requires the derivative of the function f, it may not be univer-

sally applicable. As Boucher et al. (2021) note, the point at which the derivative is calculated also matters and is hardly ever justified.

ADDITIVE METHODS

The simplest additive method is the *proportional attribution method (P)*, which can be written as,

$$y_{\mathrm{s}}^{P}(t) = \frac{x_{\mathrm{s}}(t)}{x(t)} \cdot f(x(t)) \tag{3.10}$$

For single-variable systems, i.e. $A \rightarrow B$, the proportional attribution method is functionally equivalent to the tagging method (Grewe, 2013). This includes, for example, the attribution of the CO_2 radiative forcing resulting from CO_2 concentrations from various sources; or the attribution of the contrail-cirrus coverage resulting from contrail formation from multiple aircraft (see Section 5.6 for attribution within the OpenAirClim contrail module).

The *differential attribution method (D)* uses the differential of the effect with respect to the source and can be written as,

$$y_{\mathrm{s}}^{D}(t) = \int_0^t \left.\frac{\mathrm{d}f}{\mathrm{d}x}\right|_{x(t')} \frac{\mathrm{d}x_{\mathrm{s}}(t')}{\mathrm{d}t'} \mathrm{d}t' \tag{3.11}$$

and can be extended to the *time-sliced attribution method (TS)*,

$$y_{\mathrm{s}}^{TS}(t) = \int_0^t \left.\frac{\mathrm{d}f}{\mathrm{d}x}\right|_{x(t,t')} \frac{\partial x_{\mathrm{s}}(t,t')}{\partial t'} \mathrm{d}t' \tag{3.12}$$

where $x_{\mathrm{s}}(t,t')$ and $x(t,t')$ correspond to the input (e.g. CO_2 concentration) to be attributed at time t due to emissions up to time t' from only the source s and all anthropogenic activities respectively. This last approach enables the differentiation between the impacts of early and late emissions, as demonstrated by Boucher et al. (2021). However, it is significantly more difficult to integrate and not available as an option for OpenAirClim.

INFLUENCE OF THE METHOD CHOICE

The choice of attribution method influences the relative contribution of a given source to the resulting effect. Boucher et al. (2021) apply the above attribution methods to investigate the contribution of global aviation operations to CO_2 radiative forcing. They find that using the conventional non-additive residual

method, which is functionally equivalent to the marginal method for small perturbations, results in the smallest estimate of CO_2 RF attributable to aviation. Using the alternative methods proportional, differential and time-sliced increases this estimate by 20, 13 and 12 % respectively (see their Figure 4).

Substantially larger differences are observable for NO_x chemistry. Emmons et al. (2012) find that using a tagging rather than perturbation approach increases the contribution of ozone by 2–4 times. Similar differences have been identified by Maruhashi (2025) (mean factor 1.83) for quantifying the contributions of transport NO_x emissions to ozone and methane.

The choice of attribution method is thus a consequential decision for accurately estimating the relative importance of different sources or emission species. This is particularly important given the recent shift to the use of ERF rather than RF (see Section 2.1.1), which is generally calculated as the difference between two simulations: a form of residual attribution. For non-linear responses, the ERF values determined for different sources in this manner are not additive and may be underestimated. It is thus important to ensure that the attribution method selected properly aligns with the research question.

3.A. APPENDIX: CRITICAL ANALYSIS OF TRACK AND SLANT DISTANCES IN EMISSION INVENTORIES

Contrail studies using the AEDT 2006 inventory (see Section 3.3) differentiate between the ground-projected 2D "track" and the 3D flight path "slant" distance. The first reference to this difference in scientific literature is Chen et al. (2012). Bock and Burkhardt (2016) compare the AEDT 2006 inventory with both track and slant distance (their Figure 1)[3]. They find that considering slant rather than track distance increases global flight distance by a factor of 1.8 – from $3.82 \times 10^{10}\,\mathrm{km}$ to $6.82 \times 10^{10}\,\mathrm{km}$. They note that the track and slant distances notably differ at lower levels, attributing this difference to the ascent and descent of aircraft. Note, however, that care must be taken with reading their Figure 1 – there is still a significant difference between track and slant in the cruise levels, even if this is not obvious at a casual glance. A marked increase in normalised flown distance at lower altitude is also not clearly identifiable in Figure 3.2 in comparison to other inventories such as AERO2k. However, accepting that there is a larger proportion of flown distance in the lower altitudes compared to the track, then we can expect the difference in RF to be relatively small, since the probability of persistent contrail formation is significantly lower at lower altitudes. And indeed, Bock and Burkhardt (2016) find $56\,\mathrm{mW\,m^{-2}}$ for slant rather than $49\,\mathrm{mW\,m^{-2}}$ for track, a 14 % increase even though the total distance increased by 80 %.

Nevertheless, an increase in flight distance of this magnitude is simply unrealistic. Converting between a 2D, ground-projected track distance to a 3D flight path distance means considering two factors. The first is that the distance travelled is larger due to being further away from the Earth's core. Assuming the Earth to be a perfect sphere, the flown distance is increased by a factor $(R_\mathrm{E} + h)/R_\mathrm{E}$, where $R_\mathrm{E} = 6371\,\mathrm{km}$. For a typical cruise altitude h of 10 km, this results in an essentially negligible difference of 0.2 %. The second factor considers ascent and descent. Assuming a climb angle $\theta = 9°$, the actual flight path is approximately 1.2 % larger than the ground-projected path – 63.9 km rather than 63.1 km to reach 10 km. Typical descent angles are even lower. The climb and descent phases are only a small part of any given flight. Assuming they constitute 10 % of any given flight, we can expect a global difference between a 2D and 3D distance of 0.1 % – again, essentially negligible.

It is therefore unclear how such a large difference could be found between the track and slant distances in the AEDT 2006 inventory. There is no mention of a different method (e.g. great-circle assumption) being used for one distance compared to the other. In fact, there is no mention of a "slant" or "flight path distance" in the AEDT technical and user guides[4]. The only reference to "slant" refers to the slant range, which is used for noise level interpolation.

[3] I was not able to obtain access to the track version of the AEDT 2006 inventory and could thus not include it in this study.

[4] https://aedt.faa.gov/ [Last accessed: 25/11/2025]

The result of this is that a number of previous studies are likely overestimating the contrail-cirrus RF for a given year. Lee et al. (2021), for example, use the "RF that would be expected in 2006 when using slant distance from the AEDT inventory" as the reference (see their Supplementary Material). The results of the AERO2k inventory, using results from the older Burkhardt and Kärcher (2011) study with ECHAM4-CCMod, are scaled by a factor $S_1 = 1.4$ to get a value for 2006 and by a factor $S_2 = 1.14$ to convert from a track to slant distance. It is not clear how the first of these two values was determined (the second is assumed to be the 14 % difference found above), and the validity of this method is highly questionable: it is not obvious why the same scaling factors should be valid for a different emission inventory and model. Furthermore, in the supplement, the authors attribute the result of the slant distance ($56\,\mathrm{mW\,m^{-2}}$) to the track distance, which is then used to calculate a distance-dependent RF ($1.45 \times 10^{-9}\,\mathrm{mW\,m^{-2}\,km^{-1}}$). This is clearly not consistent. Finally, to determine results in the years 2005, 2006, 2011 and 2018, the distance-dependent RF is linearly scaled according to the global flight distance in those years determined by ICAO. The authors do not demonstrate why such a linear method should be valid for contrail-cirrus RF, which numerous previous studies have shown to be highly non-linear. As a result, the 2018 best-estimate value presented by Lee et al. (2021) is a significant overestimation. Of course, a more consistent value would still likely fit within their large uncertainty range, even if the methodological issues noted here are not related to the uncertainty.

This work tries to overcome these issues by scaling the emission inventory before calculating the climate impact (see Section 5.4). Application of this strategy would remove the need for a fair number of the scaling factors described above and would provide consistent results across the models.

REFERENCES

Bock, L. and Burkhardt, U.: Reassessing properties and radiative forcing of contrail cirrus using a climate model, Journal of Geophysical Research: Atmospheres, 121, 9717–9736, doi: 10.1002/2016JD025112, 2016.

Bock, L. and Burkhardt, U.: Contrail cirrus radiative forcing for future air traffic, Atmospheric Chemistry and Physics, 19, 8163–8174, doi: 10.5194/acp-19-8163-2019, 2019.

Boucher, O., Borella, A., Gasser, T., and Hauglustaine, D.: On the contribution of global aviation to the CO2 radiative forcing of climate, Atmospheric Environment, 267, 118 762, doi: 10.1016/j.atmosenv.2021.118762, 2021.

Bruder, H., Thor, R. N., Niklaß, M., Dahlmann, K., Eichinger, R., Linke, F., Grewe, V., Matthes, S., and Unterstrasser, S.: The DLR CO2-equivalent estimator FlightClim v1.0: an easy-to-use estimation of per flight CO2 and non-CO2 climate effects, Geoscientific Model Development, 19, 3551–3567, doi: 10.5194/gmd-19-3551-2026, 2026.

Burkhardt, U. and Kärcher, B.: Process-based simulation of contrail cirrus in a global climate model, Journal of Geophysical Research, 114, D16 201, doi: 10.1029/2008JD011491, 2009.

Burkhardt, U. and Kärcher, B.: Global radiative forcing from contrail cirrus, Nature Climate Change, 1, 54–58, doi: 10.1038/nclimate1068, 2011.

Burkhardt, U., Bock, L., and Bier, A.: Mitigating the contrail cirrus climate impact by reducing aircraft soot number emissions, npj Climate and Atmospheric Science, 1, 37, doi: 10.1038/s41612-018-0046-4, 2018.

Caiazzo, F., Agarwal, A., Speth, R. L., and Barrett, S. R. H.: Impact of biofuels on contrail warming, Environmental Research Letters, 12, 114 013, doi: 10.1088/1748-9326/aa893b, 2017.

Castino, F., Yin, F., Grewe, V., Yamashita, H., Matthes, S., Dietmüller, S., Baumann, S., Soler, M., Simorgh, A., Mendiguchia Meuser, M., Linke, F., and Lührs, B.: Decision-making strategies implemented in SolFinder 1.0 to identify eco-efficient aircraft trajectories: application study in AirTraf 3.0, Geoscientific Model Development, 17, 4031–4052, doi: 10.5194/gmd-17-4031-2024, 2024.

Chen, C., Gettelman, A., Craig, C., Minnis, P., and Duda, D. P.: Global contrail coverage simulated by CAM5 with the inventory of 2006 global aircraft emissions, Journal of Advances in Modeling Earth Systems, 4, 2011MS000 105, doi: 10.1029/2011MS000105, 2012.

Clappier, A., Belis, C. A., Pernigotti, D., and Thunis, P.: Source apportionment and sensitivity analysis: two methodologies with two different purposes, Geoscientific Model Development, 10, 4245–4256, doi: 10.5194/gmd-10-4245-2017, 2017.

Dahlmann, K.: Eine Methode zur effizienten Bewertung von Maßnahmen zur Klimaoptimierung des Luftverkehrs, Ph.D. thesis, Ludwig-Maximilians-Universität München, München, doi: 10.5282/edoc.14199, 2011.

Dahlmann, K., Grewe, V., Frömming, C., and Burkhardt, U.: Can we reliably assess climate mitigation options for air traffic scenarios despite large uncertainties in atmospheric processes?, Transportation Research Part D: Transport and Environment, 46, 40–55, doi: 10.1016/j.trd.2016.03.006, 2016.

Dannet, G., Boucher, O., and Bellouin, N.: Features and evolution of civil aviation CO2 emissions based on ADS-B data for the period between 2019–2024, Metascience in Aerospace, 1, 346–370, doi: 10.3934/mina.2024016, 2024.

Dietmüller, S., Matthes, S., Dahlmann, K., Yamashita, H., Simorgh, A., Soler, M., Linke, F., Lührs, B., Meuser, M. M., Weder, C., Grewe, V., Yin, F., and Castino, F.: A Python library for computing individual and merged non-CO_2 algorithmic climate change functions: CLIMaCCF V1.0, Geoscientific Model Development, 16, 4405–4425, doi: 10.5194/gmd-16-4405-2023, 2023.

Duda, D. P., Minnis, P., and Palikonda, R.: Estimated contrail frequency and coverage over the contiguous United States from numerical weather prediction analyses and flight track data, Meteorologische Zeitschrift, 14, 537–548, doi: 10.1127/0941-2948/2005/0050, 2005.

Dunne, J. P., Hewitt, H. T., Arblaster, J. M., Bonou, F., Boucher, O., Cavazos, T., Dingley, B., Durack, P. J., Hassler, B., Juckes, M., Miyakawa, T., Mizielinski, M., Naik, V., Nicholls, Z., O'Rourke, E., Pincus,

R., Sanderson, B. M., Simpson, I. R., and Taylor, K. E.: An evolving Coupled Model Intercomparison Project phase 7 (CMIP7) and Fast Track in support of future climate assessment, Geoscientific Model Development, 18, 6671–6700, doi: 10.5194/gmd-18-6671-2025, 2025.

Emmons, L. K., Hess, P., Lamarque, J.-F., and Pfister, G.: Tagged ozone mechanism for MOZART-4, CAM-chem and other chemical transport models, Geoscientific Model Development, 5, 1531–1542, doi: 10.5194/gmd-5-1531-2012, 2012.

Enting, I. G.: Attribution of greenhouse gas emissions, concentrations and radiative forcing, Tech. Rep. 38, CSIRO Atmospheric Research, Aspendale, Australia, ISBN 978-0-643-06344-0, 1998.

Eyers, C. J., Norman, P., Middel, J., Plohr, M., Michot, S., Atkinson, K., and Christou, R. A.: AERO2K global aviation emissions inventories for 2002 and 2025, Tech. Rep. QINETIQ/04/01113, QinetiQ Ltd, Farnborough, U.K., 2004.

Fichter, C.: Climate Impact of Air Traffic Emissions in Dependency of the Emission Location and Altitude, Ph.D. thesis, Manchester Metropolitan University, 2009.

Gasser, T., Ciais, P., Boucher, O., Quilcaille, Y., Tortora, M., Bopp, L., and Hauglustaine, D.: The compact Earth system model OSCAR v2. 2: description and first results, Geoscientific Model Development, 10, 271–319, doi: https://doi.org/10.5194/gmd-10-271-2017, 2017.

Grewe, V.: A generalized tagging method, Geoscientific Model Development, 6, 247–253, doi: 10.5194/gmd-6-247-2013, 2013.

Grewe, V. and Stenke, A.: AirClim: An efficient tool for climate evaluation of aircraft technology, Atmospheric Chemistry and Physics, 8, 4621–4639, doi: 10.5194/acp-8-4621-2008, 2008.

Grewe, V., Stenke, A., Plohr, M., and Korovkin, V. D.: Climate functions for the use in multi-disciplinary optimisation in the pre-design of supersonic business jet, The Aeronautical Journal, 114, 259–269, doi: 10.1017/S0001924000003705, 2010.

Grewe, V., Frömming, C., Matthes, S., Brinkop, S., Ponater, M., Dietmüller, S., Jöckel, P., Garny, H., Tsati, E., Dahlmann, K., Søvde, O. A., Fuglestvedt, J., Berntsen, T. K., Shine, K. P., Irvine, E. A., Champougny, T., and Hullah, P.: Aircraft routing with minimal climate impact: the REACT4C climate cost function modelling approach (V1.0), Geoscientific Model Development, 7, 175–201, doi: 10.5194/gmd-7-175-2014, 2014.

Grewe, V., Bock, L., Burkhardt, U., Dahlmann, K., Gierens, K., Hüttenhofer, L., Unterstrasser, S., Gangoli Rao, A., Bhat, A., Yin, F., Reichel, T. G., Paschereit, O., and Levy, Y.: Assessing the climate impact of the AHEAD multi-fuel blended wing body, Meteorologische Zeitschrift, 26, 711–725, doi: 10.1127/metz/2016/0758, 2017a.

Grewe, V., Dahlmann, K., Flink, J., Frömming, C., Ghosh, R., Gierens, K., Heller, R., Hendricks, J., Jöckel, P., Kaufmann, S., Kölker, K., Linke, F., Luchkova, T., Lührs, B., Van Manen, J., Matthes, S., Minikin, A., Niklaß, M., Plohr, M., Righi, M., Rosanka, S., Schmitt, A., Schumann, U., Terekhov, I., Unterstrasser, S., Vázquez-Navarro, M., Voigt, C., Wicke, K., Yamashita, H., Zahn, A., and Ziereis, H.: Mitigating the climate impact from aviation: achievements and results of the DLR WeCare project, Aerospace, 4, 34, doi: 10.3390/aerospace4030034, 2017b.

Grewe, V., Gangoli Rao, A., Grönstedt, T., Xisto, C., Linke, F., Melkert, J., Middel, J., Ohlenforst, B., Blakey, S., Christie, S., Matthes, S., and Dahlmann, K.: Evaluating the climate impact of aviation emission scenarios towards the Paris agreement including COVID-19 effects, Nature Communications, 12, 3841, doi: 10.1038/s41467-021-24091-y, 2021.

Höhne, N. and Blok, K.: Calculating historical contributions to climate change – discussing the 'Brazilian proposal', Climatic Change, 71, 141–173, doi: 10.1007/s10584-005-5929-9, 2005.

Hüttenhofer, L.: Parametrisierung von Kondensstreifenzirren für AirClim 2.0, Bachelor's thesis, Ludwig-Maximilians-Universität München, München, 2013.

Kärcher, B. and Yu, F.: Role of aircraft soot emissions in contrail formation, Geophysical Research Letters, 36, L01 804, doi: 10.1029/2008GL036649, 2009.

Köhler, M. O., Rädel, G., Dessens, O., Shine, K. P., Rogers, H. L., Wild, O., and Pyle, J. A.: Impact of perturbations to nitrogen oxide emissions from global aviation, Journal of Geophysical Research: Atmospheres, 113, 2007JD009 140, doi: 10.1029/2007JD009140, 2008.

Leach, N. J., Jenkins, S., Nicholls, Z., Smith, C. J., Lynch, J., Cain, M., Walsh, T., Wu, B., Tsutsui, J., and

Allen, M. R.: FaIRv2.0.0: a generalized impulse response model for climate uncertainty and future scenario exploration, Geoscientific Model Development, 14, 3007–3036, doi: 10.5194/gmd-14-3007-2021, 2021.

Lee, D., Fahey, D., Skowron, A., Allen, M., Burkhardt, U., Chen, Q., Doherty, S., Freeman, S., Forster, P., Fuglestvedt, J., Gettelman, A., De León, R., Lim, L., Lund, M., Millar, R., Owen, B., Penner, J., Pitari, G., Prather, M., Sausen, R., and Wilcox, L.: The contribution of global aviation to anthropogenic climate forcing for 2000 to 2018, Atmospheric Environment, 244, 117 834, doi: 10.1016/j.atmosenv.2020.117834, 2021.

Leipold, A., Aptsiauri, G., Ayazkhani, A., Bauder, U., Becker, R.-G., Berghof, R., Claßen, A., Dadashi, A., Dahlmann, K., Dzikus, N., Flüthmann, N., Grewe, V., Göhlich, L., Grimme, W., Günther, Y., Jaksche, R., Jung, M., Knabe, F., Kutne, P., Le Clercq, P., Pabst, H., Poggel, S., Staggat, M., Wicke, K., Wolters, F., Zanger, J., and Zill, T.: DEPA 2050 – Development Pathways for Aviation up to 2050 (Final Report), Tech. rep., DLR, Köln, https://elib.dlr.de/142185/, 2021.

Lewellen, D. C.: A Large-Eddy Simulation study of contrail ice number formation, Journal of the Atmospheric Sciences, 77, 2585–2604, doi: 10.1175/JAS-D-19-0322.1, 2020.

Lottermoser, A. and Unterstrasser, S.: Modeling the impact of alternative fuels and hydrogen propulsion on contrail-cirrus: A parameter study, Journal of Geophysical Research: Atmospheres, 131, e2025JD044 604, doi: 10.1029/2025JD044604, 2026.

Maruhashi, J.: Characterizing the transport patterns and climate effects of aviation emissions using a novel Lagrangian tagging method, Ph.D. thesis, Delft University of Technology, Delft, doi: 10.4233/UUID:177577F9-D99C-4D57-A7A2-5142CCE8C03D, 2025.

Matthes, S., Lim, L., Burkhardt, U., Dahlmann, K., Dietmüller, S., Grewe, V., Haslerud, A. S., Hendricks, J., Owen, B., Pitari, G., Righi, M., and Skowron, A.: Mitigation of non-CO2 aviation's climate impact by changing cruise altitudes, Aerospace, 8, 36, doi: 10.3390/aerospace8020036, 2021.

Meinshausen, M., Raper, S. C. B., and Wigley, T. M. L.: Emulating coupled atmosphere-ocean and carbon cycle models with a simpler model, MAGICC6 – Part 1: Model description and calibration, Atmospheric Chemistry and Physics, 11, 1417–1456, doi: 10.5194/acp-11-1417-2011, 2011.

Nicholls, Z. R. J., Meinshausen, M., Lewis, J., Gieseke, R., Dommenget, D., Dorheim, K., Fan, C.-S., Fuglestvedt, J. S., Gasser, T., Golüke, U., Goodwin, P., Hartin, C., Hope, A. P., Kriegler, E., Leach, N. J., Marchegiani, D., McBride, L. A., Quilcaille, Y., Rogelj, J., Salawitch, R. J., Samset, B. H., Sandstad, M., Shiklomanov, A. N., Skeie, R. B., Smith, C. J., Smith, S., Tanaka, K., Tsutsui, J., and Xie, Z.: Reduced Complexity Model Intercomparison Project Phase 1: introduction and evaluation of global-mean temperature response, Geoscientific Model Development, 13, 5175–5190, doi: 10.5194/gmd-13-5175-2020, 2020.

Paoli, R., Nybelen, L., Picot, J., and Cariolle, D.: Effects of jet/vortex interaction on contrail formation in supersaturated conditions, Physics of Fluids, 25, 053 305, doi: 10.1063/1.4807063, 2013.

Ponater, M., Marquart, S., and Sausen, R.: Contrails in a comprehensive global climate model: Parameterization and radiative forcing results, Journal of Geophysical Research: Atmospheres, 107, doi: 10.1029/2001JD000429, 2002.

Righi, M., Ehrenberger, S., Brinkop, S., Hendricks, J., Hellekes, J., Banyś, P., Dasgupta, I., Draheim, P., Fitz, A., Löber, M., Pregger, T., Scholz, Y., Schulz, A., Suhr, B., Thomsen, N., Weder, C. M., Berster, P., Clococeanu, M., Gelhausen, M., Lau, A., Linke, F., Matthes, S., and Zengerling, Z. L.: The ELK global emission inventory for the transport sectors, Earth System Science Data, 18, 1619–1664, doi: 10.5194/essd-18-1619-2026, 2026.

Roeckner, E., Bäuml, G., Bonaventura, L., Brokopf, R., Esch, M., Giorgetta, M., Hagemann, S., Kirchner, I., Kornblueh, L., Manzini, E., Rhodin, A., Schlese, U., Schulzweida, U., and Tompkins: The atmospheric general circulation model ECHAM5. Part 1: Model description, Tech. Rep. 349, Max-Planck-Institut für Meteorologie, Hamburg, ISSN 0937-1060, 2003.

Roeckner, E., Brokopf, R., Esch, M., Giorgetta, M., Hagemann, S., Kornblueh, L., Manzini, E., Schlese, U., and Schulzweida, U.: Sensitivity of simulated climate to horizontal and vertical resolution in the ECHAM5 atmosphere model, Journal of Climate, 19, 3771–3791, 2006.

Rädel, G. and Shine, K. P.: Radiative forcing by persistent contrails and its dependence on cruise altitudes, Journal of Geophysical Research: Atmospheres, 113, 2007JD009 117, doi:

10.1029/2007JD009117, 2008.

Sandstad, M., Aamaas, B., Johansen, A. N., Lund, M. T., Peters, G. P., Samset, B. H., Sanderson, B. M., and Skeie, R. B.: CICERO Simple Climate Model (CICERO-SCM v1.1.1) – an improved simple climate model with a parameter calibration tool, Geoscientific Model Development, 17, 6589–6625, doi: 10.5194/gmd-17-6589-2024, 2024.

Sausen, R., Gierens, K., Ponater, M., and Schumann, U.: A diagnostic study of the global distribution of contrails part I: Present day climate, Theoretical and Applied Climatology, 61, 127–141, doi: 10.1007/s007040050058, 1998.

Schumann, U.: A contrail cirrus prediction model, Geoscientific Model Development, 5, 543–580, doi: 10.5194/gmd-5-543-2012, 2012.

Schumann, U. and Seifert, A.: On the weather impact of contrails: new insights from coupled ICON–CoCiP simulations, Atmospheric Chemistry and Physics, 25, 18 571–18 597, doi: 10.5194/acp-25-18571-2025, 2025.

Shapiro, M., Engberg, Z., Teoh, R., Stettler, M., Dean, T., and Abbott, T.: pycontrails: Python library for modeling aviation climate impacts, Zenodo [software], doi: 10.5281/zenodo.7775435, 2025.

Simorgh, A., Soler, M., Dietmüller, S., Matthes, S., Yamashita, H., Castino, F., and Yin, F.: Robust 4D climate-optimal aircraft trajectory planning under weather-induced uncertainties: Free-routing airspace, Transportation Research Part D: Transport and Environment, 131, 104 196, doi: 10.1016/j.trd.2024.104196, 2024.

Smith, C. J., Forster, P. M., Allen, M., Leach, N., Millar, R. J., Passerello, G. A., and Regayre, L. A.: FAIR v1.3: a simple emissions-based impulse response and carbon cycle model, Geoscientific Model Development, 11, 2273–2297, doi: 10.5194/gmd-11-2273-2018, 2018.

Smolarkiewicz, P. K. and Grell, G. A.: A class of monotone interpolation schemes, Journal of Computational Physics, 101, 431–440, doi: 10.1016/0021-9991(92)90018-T, 1992.

Stier, P., Feichter, J., Kinne, S., Kloster, S., Vignati, E., Wilson, J., Ganzeveld, L., Tegen, I., Werner, M., Balkanski, Y., Schulz, M., Boucher, O., Minikin, A., and Petzold, A.: The aerosol-climate model ECHAM5-HAM, Atmospheric Chemistry and Physics, 5, 1125–1156, doi: 10.5194/acp-5-1125-2005, 2005.

Sölch, I. and Kärcher, B.: A large-eddy model for cirrus clouds with explicit aerosol and ice microphysics and Lagrangian ice particle tracking, Quarterly Journal of the Royal Meteorological Society, 136, 2074–2093, doi: 10.1002/qj.689, 2010.

Teoh, R., Engberg, Z., Shapiro, M., Dray, L., and Stettler, M. E. J.: The high-resolution Global Aviation emissions Inventory based on ADS-B (GAIA) for 2019–2021, Atmospheric Chemistry and Physics, 24, 725–744, doi: 10.5194/acp-24-725-2024, 2024.

Trudinger, C. and Enting, I.: Comparison of formalisms for attributing responsibility for climate change: Non-linearities in the Brazilian Proposal approach, Climatic Change, 68, 67–99, doi: 10.1007/s10584-005-6012-2, 2005.

Unterstrasser, S.: Large-eddy simulation study of contrail microphysics and geometry during the vortex phase and consequences on contrail-to-cirrus transition, Journal of Geophysical Research: Atmospheres, 119, 7537–7555, doi: 10.1002/2013JD021418, 2014.

Unterstrasser, S. and Gierens, K.: Numerical simulations of contrail-to-cirrus transition – Part 1: An extensive parametric study, Atmospheric Chemistry and Physics, 10, 2017–2036, doi: 10.5194/acp-10-2017-2010, 2010a.

Unterstrasser, S. and Gierens, K.: Numerical simulations of contrail-to-cirrus transition – Part 2: Impact of initial ice crystal number, radiation, stratification, secondary nucleation and layer depth, Atmospheric Chemistry and Physics, 10, 2037–2051, doi: 10.5194/acp-10-2037-2010, 2010b.

Unterstrasser, S., Gierens, K., Sölch, I., and Lainer, M.: Numerical simulations of homogeneously nucleated natural cirrus and contrail-cirrus. Part 1: How different are they?, Meteorologische Zeitschrift, 26, 621–642, doi: 10.1127/metz/2016/0777, 2017.

Van Manen, J. and Grewe, V.: Algorithmic climate change functions for the use in eco-efficient flight planning, Transportation Research Part D: Transport and Environment, 67, 388–405, doi: 10.1016/j.trd.2018.12.016, 2019.

Völk, S., Yamashita, H., Megill, L., Dahlmann, K., and Grewe, V.: OpenAirClim, Zenodo [software], doi: 10.5281/ZENODO.13682728, 2025.

Weder, C. M., Berster, P., Clococeanu, M., Gelhausen, M., Lau, A., Linke, F., Matthes, S., Zengerling, Z. L., Brinkop, S., Hendricks, J., Schulz, A., and Righi, M.: ELK - Global Emission Inventory - Aviation Sector, 2019, DLR [dataset], doi: 10.15489/86S8UWPXIK95, 2025.

Wilkerson, J. T., Jacobson, M. Z., Malwitz, A., Balasubramanian, S., Wayson, R., Fleming, G., Naiman, A. D., and Lele, S. K.: Analysis of emission data from global commercial aviation: 2004 and 2006, Atmospheric Chemistry and Physics, 10, 6391–6408, doi: 10.5194/acp-10-6391-2010, 2010.

Wong, H.-W. and Miake-Lye, R. C.: Parametric studies of contrail ice particle formation in jet regime using microphysical parcel modeling, Atmospheric Chemistry and Physics, 10, 3261–3272, doi: 10.5194/acp-10-3261-2010, 2010.

Yin, F., Grewe, V., Castino, F., Rao, P., Matthes, S., Dahlmann, K., Dietmüller, S., Frömming, C., Yamashita, H., Peter, P., Klingaman, E., Shine, K. P., Lührs, B., and Linke, F.: Predicting the climate impact of aviation for en-route emissions: the algorithmic climate change function submodel ACCF 1.0 of EMAC 2.53, Geoscientific Model Development, 16, 3313–3334, doi: 10.5194/gmd-16-3313-2023, 2023.

Zengerling, Z. L., Kumpa, S., Clococeanu, M., Mendiguchía Meuser, M., Solzer, J., and Dahlmann, K.: Assessing climate effects resulting from airspace closures following the Ukrainian crisis, Journal of Open Aviation Science, 2, doi: 10.59490/joas.2024.8152, 2025.

Zängl, G., Reinert, D., Rípodas, P., and Baldauf, M.: The ICON (ICOsahedral Non-hydrostatic) modelling framework of DWD and MPI-M: Description of the non-hydrostatic dynamical core, Quarterly Journal of the Royal Meteorological Society, 141, 563–579, doi: 10.1002/qj.2378, 2015.

Persistence.

morning sky,
thin white lines lingering,
more grey hairs today.

— LM

4

LIMITING FACTORS OF PERSISTENT CONTRAIL FORMATION

This chapter has been published as:

Megill, L. and Grewe, V.: Investigating the limiting aircraft-design-dependent and environmental factors of persistent contrail formation, Atmospheric Chemistry & Physics, 25, 7, doi: 10.5194/acp-25-4131-2025, 2025.

Data and code available at:

Megill, L. and Grewe, V.: Data and code underlying the publication "Investigating the limiting aircraft-design-dependent and environmental factors of persistent contrail formation", 4TU.ResearchData, doi: 10.4121/cdb4e3bb-d6f4-4422-a715-b6187098a314, 2025.

ABSTRACT

Mounting evidence has highlighted the role of aviation non-CO_2 emissions in contributing to anthropogenic climate change. Of particular importance is the impact of contrails, which recent studies attribute to over one third of the total effective radiative forcing from aircraft operations. However, the relative importance of the aircraft design-dependent and environmental factors that influence the formation of persistent contrails is not yet well understood. In this paper, we use ERA5 data from the 2010 decade to better understand the interplay between the factors on a climatological timescale. We identify ice supersaturation as the most limiting factor for all considered aircraft designs, underscoring the importance of accurately estimating ice supersaturated regions. We also develop climatological relationships that describe potential persistent contrail formation as a function of the pressure level and Schmidt-Appleman mixing line slope. We find that the influence of aircraft design on persistent contrail formation reduces with increasing altitude. Compared to a state-of-the-art conventional aircraft with an overall propulsion system efficiency of 0.37, envisioned water vapour extraction technologies have the potential to reduce the formation of persistent contrails by up to 85.1 %. On the other hand, compared to the same reference, hydrogen combustion and fuel cell aircraft could increase globally-averaged persistent contrail formation by 46.5 and 54.7 % respectively. Due to differing contrail properties, further work is required to translate these changes into climate impacts. This study is a step towards the development of a new, computationally inexpensive method to analyse the contrail climate impact of novel aviation fuels and propulsion technologies.

4.1. INTRODUCTION

Aviation contributes to anthropogenic climate change through carbon dioxide (CO_2) emissions and non-CO_2 emissions and effects. Of particular importance is the formation of condensation trails, or contrails, which can form behind aircraft. Contrails form when the hot and humid exhaust gases mix with the cold ambient air. If the plume becomes supersaturated with respect to liquid water, condensation nuclei in the exhaust, primarily soot, activate (Kärcher and Yu, 2009; Kärcher et al., 2015). At sufficiently low ambient temperatures, the droplets freeze into ice crystals, producing a visible contrail. These thermodynamic requirements are described by the Schmidt–Appleman Criterion (Schumann, 1996).

While most contrails dissipate rapidly and have a negligible impact on the climate, if the ambient conditions are supersaturated with respect to ice, contrails can persist and spread to form contrail-cirrus (Haywood et al., 2009; Schumann and Heymsfield, 2017). Current best estimates indicate that contrails and the associated aircraft-induced cloudiness may account for around half of the total anthropogenic effective radiative forcing attributed to aviation in 2018 from operations between 1940 and 2018 (Lee et al., 2021), although uncertainties remain substantial (Burkhardt and Kärcher, 2011; Kärcher, 2018; Lee et al., 2021).

In this chapter, we aim to better understand the interplay between aircraft-dependent and -independent factors which limit persistent contrail formation on a climatological timescale. Persistent contrail formation can be limited by three main factors: droplet formation, droplet freezing and persistence. Our objectives are 1) to identify which factor(s) is/are generally responsible for the boundaries of persistent contrail formation regions; 2) determine the altitude-, latitude- and seasonal dependence of these factors and of persistent contrail formation regions; and 3) explore possibilities for the targeted introduction of future aircraft designs to reduce persistent contrail formation. This study also considers how the introduction of novel aviation fuels and propulsion technologies (see Section 2.2.5) could affect persistent contrail formation and is thus a prerequisite for the development of the OpenAirClim contrail module, described in Chapter 5.

In the following section, we describe the methodology and data used in this study. The resulting limiting factors of climatological persistent contrail formation are analysed, discussed and compared to one another in Section 4.3. We conclude the study in Section 4.4.

4.2. DATA AND METHODS

This section outlines the data and methods used to calculate the limiting factors of persistent contrail formation on a climatological basis. Section 4.2.1 describes the thermodynamic contrail formation and persistence criteria and provides the calculation methods for the mixing line slopes of various propulsion systems. We cover the full range of possible mixing line slopes, but also specify certain aircraft designs for easier comparison between different technologies, which are described in Section 4.2.2. We provide an overview of our air traffic scenario in Section 4.2.3. In Section 4.2.4, we present the reanalysis dataset and the corresponding humidity corrections used in this study. Finally, the limiting factors and maximum slope analyses are described in Sections 4.2.5 and 4.2.7 respectively.

4.2.1. CONTRAIL FORMATION AND PERSISTENCE

As described in the Section 2.2, contrails form as the hot and moist aircraft engine exhaust plume mixes with the cold and dry ambient air. The mixing process is ap-

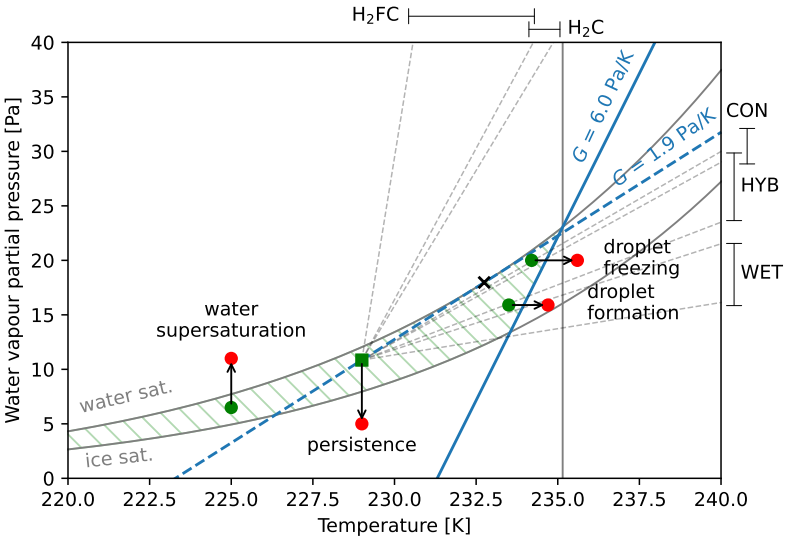


Figure 4.1: Ambient temperature vs. water vapour partial pressure diagram for an example aircraft mixing line. A persistent contrail would form behind an aircraft with $G = 6\,\mathrm{Pa\,K^{-1}}$ (blue line), if the ambient conditions are within the green hashed area. Four limiting factors can be identified that define this area, represented by the arrows from green (persistent contrail forms) to red (persistent contrail does not form) points. Ranges of mixing line slopes for each aircraft type at $250\,\mathrm{hPa}$ (FL340) are shown with dotted lines. The dashed blue line $G = 1.9\,\mathrm{Pa\,K^{-1}}$ is the threshold mixing line for the ambient condition defined by the green square. The point at which this mixing line is tangential to the water saturation curve (T_{max}, see main text) is shown by a black cross.

proximated by Schmidt-Appleman theory (Schumann, 1996) as isobaric mixing, resulting in a straight mixing line on a temperature vs. water vapour partial pressure diagram (e.g. the dashed lines in Figure 4.1). This does not correspond to the actual mixing pathway once droplets form (see e.g. Kärcher et al., 2015), but since the formation and persistence criteria are unaffected, the thermodynamic approximation is sufficient for this analysis. The slope G of the mixing line is a function of the ambient pressure as well as aircraft engine and fuel-dependent properties. For conventional kerosene (CON), the slope can be calculated using the following equation (Schumann, 1996),

$$G_{\mathrm{CON}} = \frac{c_p p_a}{\epsilon} \frac{\mathrm{EI}_{H_2O}}{(1-\eta)\,Q} \tag{4.1}$$

where $c_p = 1004\,\mathrm{J\,kg^{-1}\,K^{-1}}$ is the isobaric heat capacity of air, p_a the ambient pressure [Pa], $\epsilon = 0.622$ the molar mass ratio of water vapour and dry air, EI_{H_2O} the emission index of water vapour [$\mathrm{kg\,kg^{-1}(fuel)}$], η the overall propulsion system efficiency and Q the lower heating value of the fuel [$\mathrm{MJ\,kg^{-1}}$].

This definition was adapted by Yin et al. (2020) to parallel hybrid battery-electric aircraft by introducing a ratio R, where $R = 1$ is pure liquid fuel operation and $R = 0$ is pure electric operation. The quasi-electric energy content Q_E^0 is defined as $Q\,(\eta_K/\eta_E)$, where K refers to liquid fuel (kerosene) and E to the electric system.

$$G_{\mathrm{HYB}} = \frac{c_p p_a}{\epsilon} \frac{R \cdot \mathrm{EI}_{H_2O}}{R(1-\eta_K)Q + (1-R)(1-\eta_E)Q_E^0} \tag{4.2}$$

The definition was further modified for hydrogen combustion (H_2C) and fuel cell (H_2FC) aircraft by Gierens (2021). Eq. (4.3) is very similar to the standard definition and is used for hydrogen combustion, where the lower heating value $|\Delta h| = 120.9\,\mathrm{MJ\,kg^{-1}}$.

$$G_{\mathrm{H_2C}} = \frac{c_p p_a}{\epsilon} \frac{\mathrm{EI}_{H_2O}}{(1-\eta)|\Delta h|} \tag{4.3}$$

The calculation for fuel cells is more complex. Fuel cells operate in conjunction with electric motors, which fully decouples the exhaust from the propulsion. The exhaust could be modified to recover heat, separate and store water or achieve a desired ice crystal size. The properties of contrails produced by fuel cell powered aircraft thus depend on the design of the fuel cell system to a much larger degree than for traditional gas turbine engines. Moreover, due to the potentially very high supersaturations reached in the plume, homogeneous droplet nucleation could also take place even without the presence of aerosols (e.g. Hillenbrand and Unterstrasser, 2026).

In this study, we have used the simplified modification of Gierens (2021), shown in Eq. (4.4). We make use of the mol-based heat capacity of the exhaust gases $\overline{c_p}$, which Gierens (2021) showed not to be a constant (see their Eq. (15)). Nevertheless, we assume it to be $30.6\,\mathrm{J\,mol^{-1}\,K^{-1}}$ for all pressure levels for simplicity. This is possible because the variability of the heat capacity is low. We further define the electric efficiency η_E, the basic efficiency η_0 and the formation enthalpy of water vapour Δh_m. For simplicity we combine the two efficiencies into a single efficiency η, as in Table 4.1.

$$G_{\mathrm{H_2FC}} = \frac{\overline{c_p} p_a}{(1-\eta_E\eta_0)|\Delta h_m|} \tag{4.4}$$

We note that since publication of the article underlying this chapter (Megill and Grewe, 2025), a separate study was published that investigated the Schmidt-Appleman theory for alternative propulsion technologies, including fuel cells: Richardson (2025) shows that the theory developed by Gierens (2021) applies to uncooled fuel cells with high operating temperatures such as Solid Oxide

fuel cells (SOFCs), but not to low-temperature Proton Exchange Membrane fuel cells (PEMFCs), which will likely make up the first generation of hydrogen fuel cell aircraft. Richardson (2025) differentiates between PEMFC systems with external (exhaust heat is radiated into the ambient outside of the propeller wash) and internal cooling (exhaust heat is radiated into the propeller wash). The latter system has G values somewhat larger than for hydrogen combustion, whereas the former system has G values an order of magnitude larger, at $250\,\mathrm{hPa}$ up to nearly $60\,\mathrm{Pa\,K^{-1}}$ (cf. Table 4.1). Our results are still valid for the Richardson (2025) method: only the corresponding G value would need to be updated.

To determine whether a persistent contrail forms at a given location, we check the following three conditions, which we define as *limiting factors*:

1) *droplet formation* - ambient temperature less than the threshold temperature (see below) and ambient water vapour partial pressure above the threshold mixing line;
2) *droplet freezing* - ambient temperature less than the homogeneous freezing temperature ($235.15\,\mathrm{K}$);
3) *persistence* - ambient water vapour partial pressure above the ice saturation curve.

If these three conditions are all met, a contrail forms and persists. For completeness, a fourth boundary, water supersaturation, can also be defined. However, for the pressure levels of interest in this article, the occurrence of these conditions is insignificant (Krämer et al., 2009). The limiting factors are shown in Figure 4.1 (arrows between green and red dots).

To aid in determining droplet formation, we can define two threshold temperatures T_{min} and T_{max}. Consider first the ambient conditions represented by the green square marker ($229\,\mathrm{K}$, $10.9\,\mathrm{Pa}$) and the corresponding dashed blue mixing line for $G = 1.9\,\mathrm{Pa\,K^{-1}}$ in Figure 4.1. For these ambient conditions, an aircraft with a mixing line slope less than $G = 1.9\ \mathrm{Pa\,K^{-1}}$ would not produce a contrail since the mixture never becomes supersaturated with respect to water. The temperature T_{max}, or sometimes Θ (e.g. Kärcher et al., 2015), thus traditionally refers to the temperature at which the threshold mixing line ($G = 1.9\,\mathrm{Pa\,K^{-1}}$) is tangent to the water saturation curve, in this case around $232.7\,\mathrm{K}$ (black cross marker). The temperature T_{min} refers to the temperature at which the threshold mixing line has a water vapour partial pressure of $0\,\mathrm{Pa}$, in this case around $223.2\,\mathrm{K}$.

However, we argue that this definition of T_{max} is insufficient for aircraft with higher mixing line slopes. In order for a contrail to form, droplet formation and droplet freezing must occur concurrently. If, using the standard definition, T_{max} is found to be larger than $235.15\,\mathrm{K}$ (which occurs for $G > 2.38\,\mathrm{Pa\,K^{-1}}$), it is possible that the plume becomes subsaturated with respect to water again before it cools below $235.15\,\mathrm{K}$. There is thus insufficient time in the plume for ice crystals to form before the water droplets evaporate (see e.g. Figure 3 of Bier et al.,

2024). This effect has been described as a reduction in the "effective freezing temperature" because ice crystal numbers reduce as the ambient temperature approaches 235.15 K (Kärcher, 2018; Bier et al., 2022, 2024).

To counter this problem, for aircraft with $G > 2.38\,\mathrm{Pa\,K^{-1}}$, we set the threshold mixing line to intersect with the point of water saturation at the homogeneous freezing temperature - see the blue threshold mixing line for $G = 6\,\mathrm{Pa\,K^{-1}}$ in Figure 4.1. By doing so, we ensure that all possible mixing lines for the ambient conditions within the green hatched area are at some point concurrently supersaturated with respect to water and colder than the homogeneous freezing temperature. Using this method, we are able to closely replicate the ambient temperatures at which Bier et al. (2022) and Bier et al. (2024) find final ice crystal numbers of zero (their Figures 5(c) and 4 respectively) - see Figure 4.A.1. In this study, we therefore extend the original approximation of $T_{\max}$ by Schumann (1996) and the amendment for higher temperatures by Gierens (2021) to,

$$T_{\max} = \begin{cases} 226.69 + 9.43 \ln(G - 0.053) + 0.72 (\ln(G - 0.053))^2 & \text{for } T < 233\,\mathrm{K} \text{ or } G \leq 2\,\mathrm{Pa\,K^{-1}} \\ 226.03 + 10.22 \ln G + 0.335 (\ln G)^2 + 0.0642 (\ln G)^3 & \text{for } 2.38\,\mathrm{Pa\,K^{-1}} \geq G > 2\,\mathrm{Pa\,K^{-1}} \\ 235.15 & \text{for } G > 2.38\,\mathrm{Pa\,K^{-1}} \end{cases} \quad (4.5)$$

For an alternative approach that considers the role of volatile plume particles in the activation process, see the *extended K15 method* developed by Ponsonby et al. (2025). They show that the Schmidt-Appleman threshold becomes more stringent when particle properties are included, which they suggest can be modelled by shifting $T_{\max}$ (see their Figure 3). Their approach is not directly compatible with the one presented here. A dedicated comparison is thus recommended for subsequent work.

4.2.2. AIRCRAFT DEFINITIONS

For the limiting factors analysis, we define a range of aircraft, representative of different propulsion technologies. This is necessary to limit required computational resources, but nevertheless allows for a good comparison between the technologies. We select ten aircraft-fuel combinations that span a range of G from 0.48 to $15.8\,\mathrm{Pa\,K^{-1}}$ at 250 hPa (Table 4.1).

We define four conventional, kerosene-powered aircraft as CON-XX, where XX is the overall propulsion system efficiency η in percent: 30 % for the previous generation, 37 % for the current state-of-the-art, 40 % for the next generation and 43 % for the future generation. We note that there are a wide range of conventional aircraft currently operating and that the overall propulsion system efficiency varies with the operating condition, altitude and a multitude of other factors. Assuming a single value for comparison is thus not optimal, but necessary for this analysis. Unless otherwise stated, we use CON-37 as the reference

Table 4.1: Definition of aircraft-engine-fuel combinations used in this study, representative of different current and future propulsion technologies. See text for the description of the variables. The units are as follows: $[c_p] = \mathrm{J\,mol^{-1}\,K^{-1}}$ for H_2FC and $\mathrm{J\,kg^{-1}\,K^{-1}}$ otherwise; $[\mathrm{EI}_{H_2O}] = \mathrm{kg\,kg^{-1}}$; $[\Delta h] = \mathrm{kJ\,mol^{-1}}$ for H_2FC and $[Q] = \mathrm{MJ\,kg^{-1}}$ otherwise; $[G_{250}] = \mathrm{Pa\,K^{-1}}$. The results for the aircraft IDs in brackets are available at the linked data source, but have not been presented in this study's results for the sake of brevity.

Aircraft ID	Description	Eq.	c_p	EI_{H_2O}	Q or Δh	η	G (250 hPa)
WET-75	-75% EI_{H_2O}	(4.1)	1004	0.31	43.6	0.40	0.48
(WET-50)	-50% EI_{H_2O}	(4.1)	1004	0.63	43.6	0.40	0.97
HYB-80	80% hybrid-electric	(4.2)	1004	1.25	43.6	0.4 (K), 0.8 (E)	1.15
CON-30	Prev. gen. CON	(4.1)	1004	1.25	43.6	0.30	1.65
CON-37	Current gen. CON	(4.1)	1004	1.25	43.6	0.37	1.84
CON-40	Next gen. CON	(4.1)	1004	1.25	43.6	0.40	1.93
(CON-43)	Future gen. CON	(4.1)	1004	1.25	43.6	0.43	2.03
H2C-40	H_2C	(4.3)	1004	8.94	120.9	0.40	4.97
(H2FC-LV)	H_2FC ~0.5 V	(4.4)	30.6	-	-241.82	0.40	5.27
H2FC-HV	H_2FC ~1.0 V	(4.4)	30.6	-	-241.82	0.80	15.8

aircraft in this study.

We further define an 80 % parallel hybrid-electric aircraft HYB-80. We use a high degree of electrification to differentiate it from the conventional aircraft - a 60 % hybrid-electric aircraft would have approximately the same mixing line slope as CON-30. We further include two potential aircraft designs that reduce the effective emission index of water vapour EI_{H_2O} using the Water-Enhanced Turbofan (WET) concept. In this study, we assume for simplicity a reduction in EI_{H_2O} of 50 % (WET-50) and 75 % (WET-75). We ignore the impact of any potential emissions of stored, liquid water that is released outside of ice supersaturated regions (ISSRs). We also define three different hydrogen-powered aircraft: H2C-40 is a hydrogen combustion (H_2C) aircraft, which assumes $\eta = 0.4$; H2FC-LV and H2FC-HV are hydrogen fuel cell (H_2FC) aircraft which have operating voltages of 0.5 and $1.0\,\mathrm{V}$ respectively. The operating voltage has a very large influence on the slope of the mixing line, as Gierens (2021) showed.

4.2.3. AIR TRAFFIC DATA

We use a representative future air traffic scenario to weight our results and identify areas of particular interest. In this study, we use the progressive scenario of the DLR internal project *Development Pathways for Aviation up to 2050* (DEPA 2050, Leipold et al., 2021). A key objective of this project was to define and assess the development of the aviation industry until the year 2050 from multiple angles, including climate, economics and society. It also studied the potential entry into service of various novel aviation fuels and technologies. This scenario was selected for this research since it is representative of a future multi-fuel global fleet and because there are no restrictions on its publication. We use the forecasted aggregate yearly fuel and distance flown by the global fleet of aircraft in

the year 2050 from the DEPA 2050 progressive scenario, which is available with a 1° latitude resolution. The emission inventory is included in the linked data and is shown graphically in Figure 4.A.2.

4.2.4. ERA5 DATA AND CORRECTIONS

To calculate regions of potential persistent contrail formation we use the European Centre for Medium-Range Weather Forecasts' (ECMWF) fifth generation reanalysis dataset (ERA5, Hersbach et al., 2020) stored on the German Climate Computing Center's (DKRZ) supercomputer Levante. Specifically, we use the ambient temperature and relative humidity at pressure levels 350, 300, 250, 225, 200, 175 and 150 hPa within the 2010 decade (December 2009 to November 2019 inclusive). In this study, we use RHi to denote relative humidity with respect to ice and RHw to denote relative humidity with respect to water. We further define the seasons as DJF, MAM, JJA and SON respectively. To avoid autocorrelation and reduce the computational time, whilst still obtaining a climatological response, we randomly select 2160 hours per season over the 10-year time frame - this corresponds to 10 % of all hourly values within the 2010 decade. We use *numpy.random.choice* with seed 42 without replacement to determine which hours to choose per season for repeatability. Figure 4.A.3 shows the hours that were selected.

The ERA5 HRES temperature and relative humidity values are archived on a reduced Gaussian grid with a resolution of N320. The pre-interpolated data is available on DKRZ Levante as daily GRIB files. We decided to use the irregular N320 grid for our analysis, rather than interpolated data, to avoid any artefacts of interpolation in the relative humidity data in particular. However, this complicates the definition of cell neighbours and the calculation of the limiting factors, as described in the next section.

Numerous authors have shown the difficulty of estimating ice supersaturated regions (ISSRs) and hence contrail persistence with reanalysis data. For example, Agarwal et al. (2022) found that ERA5 could overestimate ISSR coverage when compared to radiosonde measurements, whereas Reutter et al. (2020) found an underestimation in comparison to in situ IAGOS measurements (Petzold et al., 2015). Gierens et al. (2020), comparing ERA5 with MOZAIC data (Marenco et al., 1998), found that although contrail formation can be predicted reliably, persistence cannot. In a follow-up study, Hofer et al. (2024b) found that even using variables other than the relative humidity, ISSR prediction cannot yet be significantly improved.

There have been many suggestions on how to correct ERA5 data to more accurately estimate ISSRs, both at a regional (Teoh et al., 2022; Wang et al., 2024) and global scale (Wolf et al., 2023b; Hofer et al., 2024b; Teoh et al., 2024). In this study, we enhance the ERA5 humidity by applying a correcting factor of $1/\mathrm{RHi}_{\mathrm{cor}}$ for $\mathrm{RHi}_{\mathrm{cor}} \in \{1.0, 0.98, 0.95, 0.90\}$, as in previous studies (e.g. Schumann, 2012;

Teoh et al., 2020; Reutter et al., 2020; Schumann et al., 2021). We note that this approach does not consider a latitude-dependence of the ERA5 RHi error (Teoh et al., 2024). However, modifying the cumulative distribution function found for ERA5 by Hofer et al. (2024b, their Figure 4) to include the RHi enhancements, we find that $RHi_C = 0.95$ provides a good fit against MOZAIC/IAGOS data for $RHi \leq 1.0$ (Figure 4.A.4), which is of relevance for this study. We further discuss the regional implications of this method in Section 4.3.6.

4.2.5. LIMITING FACTORS ANALYSIS

The objective of the limiting factors analysis is to understand the aircraft design-, altitude-, latitude- and seasonal dependence of the factors responsible for persistent contrail formation. This helps us identify regions where the introduction of aircraft using novel propulsion systems and fuels with substantially higher mixing line slopes, e.g. hydrogen combustion, would lead to increased persistent contrail formation. Or, where the use of aircraft with substantially lower mixing line slopes, such as hybrid-electric or WET aircraft, could be particularly beneficial.

We first consider the probability of persistent contrail formation p_{pcf} for each aircraft design. This is calculated by creating a boolean mask for persistent contrail formation using the three limiting factors for all 3D grid cells, time steps and aircraft designs. The boolean values for each grid cell are averaged and saved per month. Since the underlying ERA5 grid is irregular, when reporting and analysing a global p_{pcf}, we use an area- and level-weighting. We calculate the area of all grid cells as viewed from above using the *calculate_areas* method of the Python library *scipy.spatial.SphericalVoronoi* with an assumed spherical Earth radius of 6371 km and assume the cell areas to be constant with altitude. Since ERA5 also has irregular spacing in altitude, we use the difference (in hPa) between pressure levels to level-weight the results.

We then consider each limiting factor individually. For each aircraft design, time step and grid cell, we determine which of the limiting factors prevent a persistent contrail from forming. By summing the number of times each factor was limiting and normalising by the number of time steps, we obtain the probability of each limiting factor preventing persistent contrail formation. The results are saved per season-year (e.g. 2010 DJF) to limit memory usage. We then investigate the dependence of each limiting factor on altitude, latitude and season. When reporting global results, we perform area- and level-weighting as before.

4.2.6. ANALYSIS OF PERSISTENT CONTRAIL FORMATION REGION BOUNDARIES

We now consider again Figure 4.1: If an aircraft is flying with the mixing line slope G shown by the blue line in ambient conditions within the green hatched area, a persistent contrail will form. If the ambient conditions are subsequently no longer within the green hatched area, due to changes in the ambient temperature, rela-

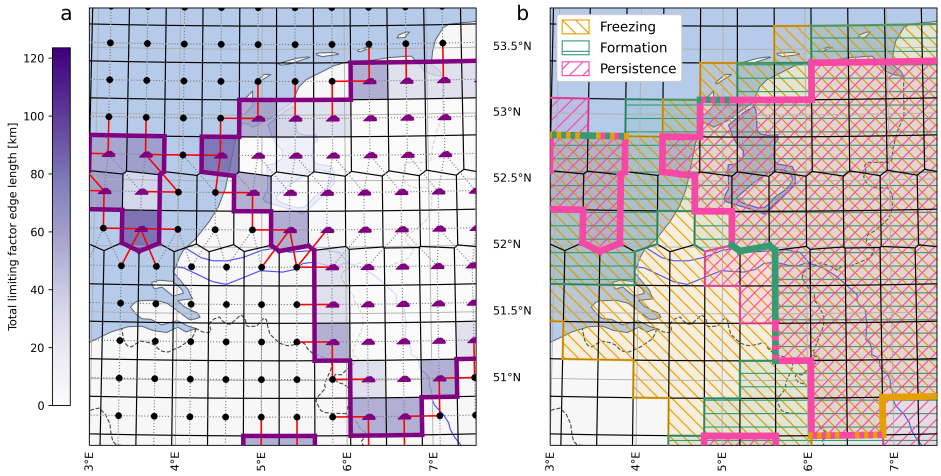


Figure 4.2: Example of the horizontal limiting factors analysis for H2C-40 using fictional data at a single pressure level over the Netherlands. **(a)** Analysis of the total limiting factor - persistent contrails would form at all grid points with a purple cloud icon. The red lines correspond to all possible boundary crossings into the potential persistent contrail formation regions; the purple shading to the length of the boundary around each grid cell. **(b)** Droplet freezing (yellow hatching), droplet formation (green hatching) and persistence (pink hatching) limiting factors. The thick coloured lines represent which limiting factor is responsible for the boundary. If multiple factors are responsible, the line is dashed. For the analysis of each limiting factor individually, only the correspondingly coloured boundaries are considered in the edge length around each grid cell.

tive humidity, altitude or in aircraft performance, the aircraft will stop producing a persistent contrail, thus defining the boundary of a persistent contrail formation region. One or more of the limiting factors will have been responsible for that boundary.

The objective of this analysis is to understand the relative importance of the limiting factors in defining the horizontal and vertical boundaries of persistent contrail formation regions. In the horizontal direction, we begin by calculating the total perimeter of all persistent contrail formation regions. Then, we compare the length of the boundary caused by each limiting factor to the total perimeter. The boundary lengths for each limiting factor are thus subsets of the total. But since multiple factors can be simultaneously limiting, the sum of all limiting factor boundary lengths is greater than the total. A large boundary length for a given limiting factor means that that factor was often responsible for persistent contrails forming.

We demonstrate this analysis graphically in an example shown in Figure 4.2 for H2C-40 using fictional data on the ERA5 grid for a single time and pressure level over the Netherlands. We calculate the borders between grid cells (black lines) using the *scipy.spatial. SphericalVoronoi* method and find cell neighbours (gray dotted lines) by determining which cells share a pair of edge vertices. The

combination of persistence, droplet freezing and droplet formation (coloured hatching) results in potential persistent contrail formation regions (purple cloud icons). We are interested in the boundaries of persistent contrail formation regions, therefore we need to identify neighbouring cells with different icons (red lines). These cells i and j share a border d_{ij} (thick purple line), which we calculate using the Haversine formula assuming an Earth radius of 6371 km. The colour gradient bar indicates the length of the persistent contrail formation region border around each grid cell: a darker purple corresponds to a longer boundary, a lighter purple to a shorter boundary. By globally summing all d_{ij}, we obtain the total perimeter of all persistent contrail formation regions. This is repeated for the boundaries caused by individual limiting factors (thick yellow, green and pink lines).

Programmatically, for each aircraft design and time step, we create four 3D boolean masks: one for potential persistent contrail formation and one per limiting factor. For each aircraft design, time step, pressure level and limiting factor, we create a global, symmetric adjacency matrix A of size $n \times n$, where $n = 542080$ is the number of grid points in the ERA5 grid. For any two adjacent cells i and j, $A_{ij} = d_{ij}$ (shared border length, thick purple line) if the persistent contrail formation boolean at i is TRUE (persistent contrail forms, purple cloud icon) and the limiting factor boolean at j is FALSE (the limiting factor has prevented persistent contrail formation, black point), else $A_{ij} = 0$. To obtain the total perimeter, we set $A_{ij} = d_{ij}$ if *any* limiting factor boolean at j is FALSE. We then obtain the vector of size n of boundary lengths around each grid cell (cell colour gradient) by summing the columns of the adjacency matrix. This procedure is repeated for each time step and the monthly summed values for each aircraft design, grid cell, pressure level and limiting factor are saved. We repeat the full analysis for all RHi enhancements.

We perform a similar analysis in the vertical direction to analyse the impact of changing altitude and thus mixing line slope G. For simplicity, we neglect the changes in aircraft operating conditions during climb or descent to a new altitude. Vertically adjacent cells can be found easily because the latitude-longitude location of the cells is constant with altitude. Since there are no clearly defined edge lengths in the vertical direction, we calculate the boundaries of persistent contrail formation regions by summing the cell areas as viewed from above.

4.2.7. MAXIMUM SLOPE ANALYSIS

In the limiting factors analysis, fixed aircraft designs with specific values of G are used. The objective of this second analysis is to explore the dependence of persistent contrail formation p_{pcf} on G in more detail and determine whether there is a climatological relationship between the two. We analyse the results at the global level as well as on three latitude-dependent scales: the northern extratropics (latitude > 30°N), the tropics (30°S ≤ latitude ≤ 30°N) and the southern extratropics (latitude < 30°S).

For each cell where the ambient conditions are sufficient for persistent contrail formation, we use the Newton method to find the slope where the mixing line is tangent to the water saturation curve. If the temperature at which this mixing line is tangential to the water saturation curve (T_{max}) is greater than the homogeneous freezing temperature (235.15 K), we set T_{max} to 235.15 K (see Section 4.2.1). The slope of the line that connects the ambient conditions to the water supersaturated conditions for T_{max} is thus the maximum mixing line slope for which a persistent contrail would not form. We define this threshold mixing line G_{max}. For example, for the ambient conditions shown by a green square in Figure 4.1, the corresponding maximum slope is $G_{\mathrm{max}} = 1.9\,\mathrm{Pa\,K^{-1}}$ (blue dashed line). For each region, altitude and time step, we use a histogram with a bin size of $0.2\,\mathrm{Pa\,K^{-1}}$ to determine the distribution of G_{max}. By taking the cumulative sum of the histograms, we obtain p_{pcf} as a function of G.

4.3. RESULTS AND DISCUSSION

This section presents and discusses the results of the limiting factors analyses. Sections 4.3.1 and 4.3.2 analyse the limiting factors within each grid cell and at the boundaries of persistent contrail formation regions. The altitude- and latitude-dependence of these regions and the changes in global potential persistent contrail formation p_{pcf} are presented in Section 4.3.3. In Section 4.3.4, we develop climatological relationships between the mixing line slope and the p_{pcf}. Finally, we discuss the interplay and competition between the limiting factors in Section 4.3.5 and the limitations and uncertainties of our study in Section 4.3.6.

4.3.1. LIMITING FACTORS OF PERSISTENT CONTRAIL FORMATION

The global area- and level-weighted potential persistent contrail formation (p_{pcf}, left side of Figure 4.3) is dependent on aircraft design. Enhancing the area of ice supersaturation by lowering the relative humidity threshold as a means of correcting ERA5 relative humidity (see Sect. 4.2.4) increases p_{pcf}, proportionally more for aircraft with higher G (markers). This suggests that persistent contrail formation is primarily limited by ice supersaturation (persistence limiting factor), and indeed this is also found by comparing the number of times each of the three factors prevented persistent contrails from forming (right side of Figure 4.3): Of the grid cells investigated, 92.3 % were not supersaturated with respect to ice. Enhancing humidity by lowering the threshold for ice supersaturation naturally reduces how limiting the persistence limiting factor is. Droplet formation is highly dependent on the slope of the mixing line G, varying between 19.2 % (H2FC-HV) and 89.5 % (WET-75). It does not have a significant dependence on humidity enhancements. Droplet freezing is independent of aircraft design, only limiting 18.2 % of the time and by definition unaffected by humidity enhancements.

The altitude- and latitude-dependence of the limiting factors is shown in Fig-

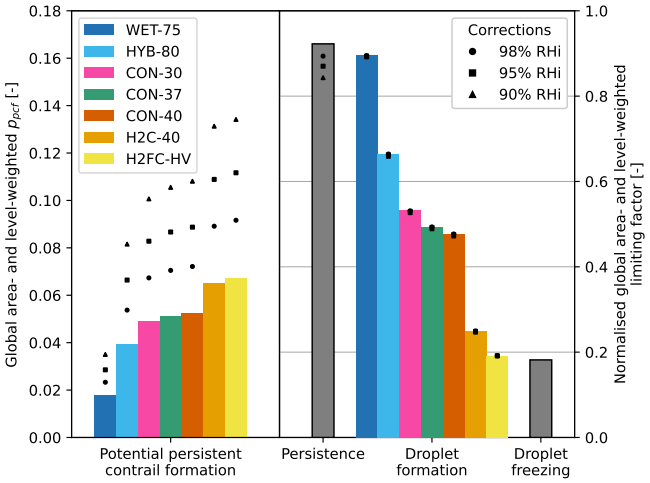


Figure 4.3: Global area- and level-weighted potential persistent contrail formation during the 2010 decade (left) and the normalised frequency that each limiting factor prevented a persistent contrail from forming (right). A normalised frequency of 0 would mean that the factor never limited persistent contrail formation; 1 that it always does. Dependence on aircraft design is shown by the different colours - the persistence and droplet freezing limiting factors are independent of aircraft design and thus only have single values. The RHi enhancements are shown as scatter points - note the difference in the y-scale.

ure 4.4. The persistence limiting factor is less limiting in the extratropics at lower altitudes (350 to 250 hPa) and in the tropics at higher altitudes (225 to 150 hPa). On the other hand, droplet freezing is generally only limiting in the tropics at altitudes below FL300 (pressure levels $\geq$ 300 hPa). It is by definition unaffected by humidity enhancements.

Interesting to note is that the results of the H2FC-HV droplet formation limiting factor closely follow those of the aircraft design-independent droplet freezing limiting factor. This is due to our definition of $T_{\max}$ at high mixing line slopes (see Section 4.2.1): The higher the aircraft mixing line slope, the steeper the threshold mixing line slope and thus the closer it resembles the vertical droplet freezing limit at 235.15 K.

4.3.2. BOUNDARIES OF PERSISTENT CONTRAIL FORMATION REGIONS

Persistence is also found to be more limiting compared to the other factors at the region boundaries. Figure 4.5 shows the sum over all pressure levels of the horizontal (a) and vertical (b) boundary lengths/areas of potential persistent contrail formation regions as a function of the limiting factor and aircraft design. We show the total in absolute terms and the individual limiting factors relative to the total for ease of comparison. Because more than one limiting factor may simul-

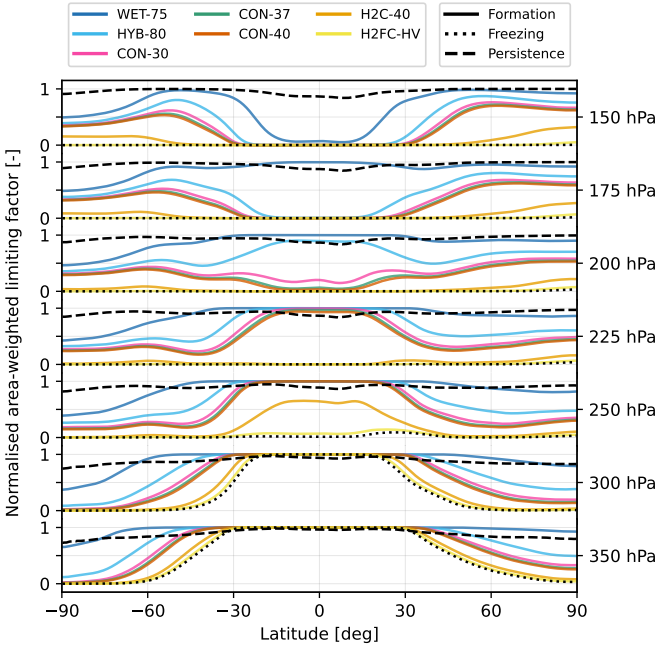


Figure 4.4: Normalised and area-weighted global limiting factors of the 2010 decade as a function of latitude (x-axis) and altitude (secondary y-axis). A normalised frequency of 0 would mean that the factor never limits persistent contrail formation; 1 that it always does. Droplet freezing (dotted lines) and persistence (dashed lines) are independent of aircraft design. Droplet formation is dependent on aircraft design and shown for the different designs (colours).

taneously be responsible for a boundary, the sum of the individual limiting factors may be larger than 100 %. Since the horizontal and vertical directions cannot be directly compared, we have visually aligned the y-axes for the CON-37 total limiting factor such that at least the shapes of the responses can be compared. In both cases, the persistence limiting factor dominates for all aircraft designs and increases with increasing G. This is because as G increases, contrail formation can occur in a larger number of coherent regions, increasing the total region boundary length ("total" in the plots), but which are nevertheless still bounded by ice supersaturation – see also Section 4.3.5.

Droplet formation can be limiting when the ambient conditions would be sufficient for persistent contrail formation, but G is sufficiently low that the exhaust does not become supersaturated with respect to water. The droplet formation limiting factor thus becomes less relevant as G increases. Since G changes with altitude for the same aircraft, droplet formation is responsible for a significantly larger proportion of the persistent contrail formation region boundaries in the vertical direction compared to the horizontal. It is particularly limiting for very low G aircraft such as the WET-75.

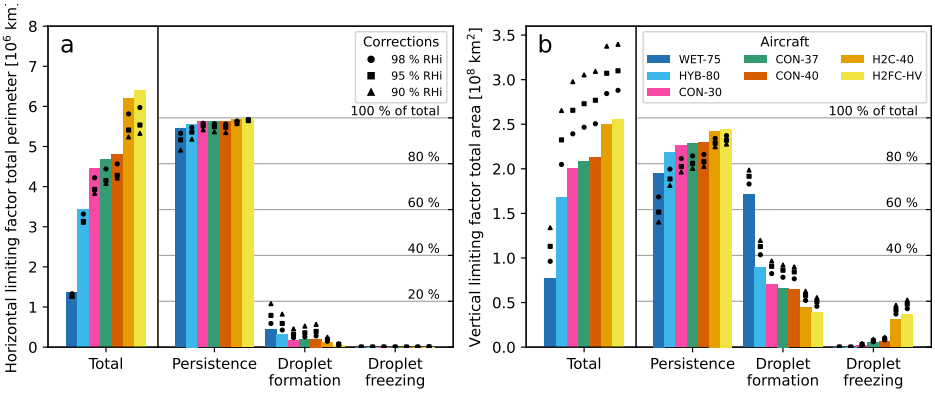


Figure 4.5: Horizontal (a) and vertical (b) total limiting factor results. The "total" limiting factors are shown in absolute values, visually aligned for CON-37 such that the shapes of the responses can be compared; the individual limiting factors are shown relative to the corresponding total value and are given in percent. Because more than one factor may simultaneously be limiting, the sum of the individual percentages may be larger than 1 (see text). The RHi enhancements (see Section 4.2.4) are shown as scatter points.

In comparison, the droplet freezing limiting factor becomes more important with increasing G. Low mixing line slopes prevent contrails from forming near the freezing boundary. Therefore, droplet freezing is only relevant for aircraft with a high G, in particular hydrogen-powered aircraft. Again due to the changing G with altitude and larger change in ambient temperature in the vertical compared to the horizontal direction, the droplet freezing limiting factor is also more relevant in the vertical direction.

The RHi correction does not influence which factor is most limiting, with the single exception of WET-75 in the vertical direction. It also does not, on a climatological timescale, influence in which areas persistent contrails form: As the humidity is enhanced, the probability that a persistent contrail forms increases where the probability was already greater than zero (see Figure 4.A.5). However, the persistence results show that many ambient conditions in ERA5 are close to being saturated with respect to ice. Our results thus only add to the consensus that improving ISSR forecasting is vital for estimating persistent contrail formation (Gierens et al., 2020; Hofer et al., 2024b).

In the horizontal direction, enhancing humidity seems to reduce the total edge length, even though the potential persistent contrail formation regions are larger. A significant reduction in edge length can be identified by enhancing humidity by only 2 %, in particular for hydrogen-powered aircraft. This suggests that the potential persistent contrail formation regions, predominantly described by ice supersaturation, grow and coalesce with enhancing humidity, reducing the total length of their boundaries. Further work would be required to prove this theory. In the horizontal direction, the RHi correction has a virtually no in-

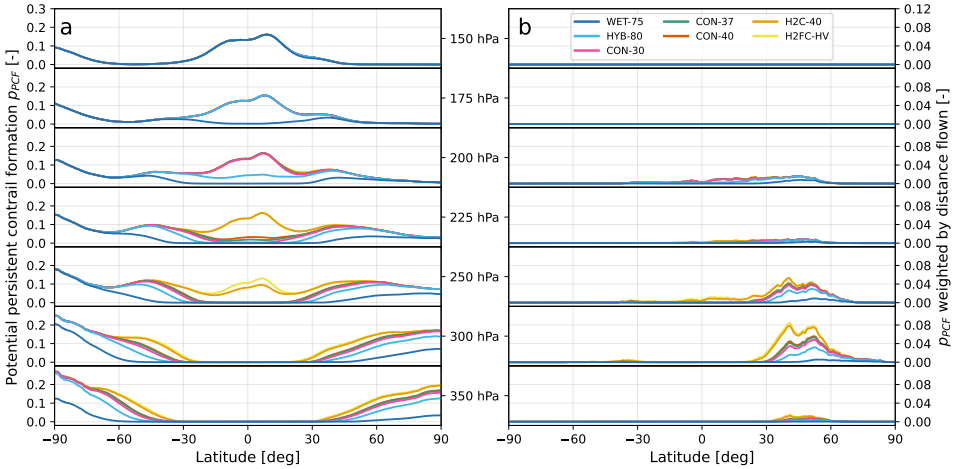


Figure 4.6: Potential persistent contrail formation as a function of latitude (x-axis) and altitude (secondary y-axis). (a) unweighted p_{pcf}; (b) p_{pcf} weighted by the distance flown in the DEPA 2050 air traffic scenario in the year 2050 to identify important areas for persistent contrail formation.

fluence on the droplet freezing, but a major influence on the droplet formation limiting factor. In both cases, however, the perimeter remains two orders of magnitude smaller than that of the persistence limiting factor. In the vertical direction, enhancing humidity increases the boundary area significantly for the total. Seemingly, the boundary between different pressure levels is emphasised by the enhanced humidity, notably for the droplet formation limiting factor.

4.3.3. SPATIAL VARIABILITY OF PERSISTENT CONTRAIL FORMATION

The summation of the region edges does not provide any information about where persistent contrails form. Therefore, we now explore the altitude-, latitude- and aircraft-dependence of persistent contrail formation regions. Figure 4.6(a) shows that aircraft design is only ever limiting at lower altitudes: Except for aircraft with very low mixing line slopes (HYB-80, WET-75), whether a contrail forms and persists for pressure levels < $200\,\mathrm{hPa}$ (altitudes above FL385) depends solely on the ambient conditions.

It has been widely assumed that the introduction of hydrogen-powered aircraft would result in a significant increase in the formation of persistent contrails. Our results show that hydrogen-powered aircraft could indeed form many more persistent contrails than existing conventional aircraft. Comparing H2C-40 ($G = 5.27\,\mathrm{Pa\,K^{-1}}$) and H2FC-HV ($G = 15.8\,\mathrm{Pa\,K^{-1}}$) with CON-37 ($G = 1.84\,\mathrm{Pa\,K^{-1}}$), our results match those of Kaufmann et al. (2024, the right side of their Figure 5): At low altitude (350 to $300\,\mathrm{hPa}$), a large difference in persistent contrail formation (Kaufmann et al. (2024) call this "potential contrail-cirrus cover") can be seen be-

tween 30 to 60°S and 30 to 60°N, incidentally coinciding with significant air traffic over Europe and the US. In total, across all latitudes and considered altitudes, hydrogen-powered aircraft have the potential to produce between 18.3 % (H2C) and 20.8 % (H2FC) more persistent contrails than conventional aircraft (CON-37, see Table 4.A.1).

Since these results do not consider where aircraft actually fly, we have also used the DEPA 2050 air traffic scenario to weight the results, as shown in Figure 4.6(b). DEPA 2050 is only available with a 1° latitude resolution, so we conservatively regrid the limiting factors results to match this resolution (conserving the total sum of distance flown). The tropical increase in persistent contrail formation at 250 to 225 hPa is now less pronounced because there are few aircraft flying in this region. Instead, of particular importance are the northern extratropics between 300 and 250 hPa (FL300 to FL340), which are the lower cruise altitudes for typical airliners. In total, our simple distance-weighted proxy shows a globally-averaged increase of 46.5 % to 54.7 % for hydrogen-powered aircraft (H2C and H2FC respectively) compared to conventional aircraft (CON-37, see Table 4.A.1). This indicates that replacing existing aircraft along existing and expected flight routes with hydrogen-powered designs would significantly increase persistent contrail formation - on a climatological timescale whilst ignoring any real-time avoidance strategies.

Significant reductions in persistent contrail formation could be gained by reducing the water vapour emission index: globally, WET-50 ($G = 0.97\,\mathrm{Pa\,K^{-1}}$) achieves a 26.0 % reduction; WET-75 ($G = 0.48\,\mathrm{Pa\,K^{-1}}$) a 56.6 % reduction. Along the DEPA 2050 flight routes, this further improves to 51.7 % and 85.1 % respectively. There is also clearly potential for the targeted introduction of aircraft with very low mixing line slopes, in particular at higher altitudes (225 to 200 hPa, FL360 - FL385) in the tropics. Here, the WET aircraft considered would produce little to no persistent contrails at all, with unweighted reductions of 83.2 - 91.4 % (WET-50) and 99.5 - 99.96 % (WET-75).

For all aircraft designs, persistent contrail formation increases with altitude in the tropics and decreases in the extratropics, in line with previous studies (e.g. Matthes et al., 2021). Among others, Barton et al. (2023) suggest designing hydrogen-powered aircraft capable of flying at higher altitudes in the extratropics - around 14 km (140 hPa) - to avoid forming persistent contrails. We find that very few persistent contrails are formed at 150 hPa north of 30°N and between 30°S and 60°S (very few flight tracks extend south of 60°S). Since this is due to a lack of ice supersaturation in these regions (see Figure 4.4), this concept does not need to be limited to hydrogen-powered aircraft. However, these altitudes are above the local tropopause and releasing significant amounts of water vapour and NO_x into the stratosphere can result in a significant increase in climate impact (Grewe et al., 2010; van 't Hoff et al., 2025). We therefore stress that these results should not be used in isolation to determine a possible optimum cruise altitude. Rather, the full climate impact of a given design must be considered.

4.3.4. CLIMATOLOGICAL POTENTIAL PERSISTENT CONTRAIL FORMATION

We now aim to determine whether there is a climatological relationship between the mixing line slope G and the potential persistent contrail formation p_{pcf}. Figure 4.7 shows p_{pcf} as a function of G for each pressure level and for all data together, without RHi enhancement. The results for all RHi enhancements are shown in Figure 4.A.6. The supremum value for each pressure level and time can be determined by ignoring the droplet formation limiting factor, since it resembles the droplet freezing limiting factor as $G \to \infty$. For many pressure levels, 99 % of that supremum value is achieved at much lower mixing line slopes ($G_{99\%sup}$ in Table 4.2 and black circular markers in Figure 4.7). Generally, the higher the altitude, the earlier the results asymptote and the less influence the aircraft design has. This also matches the results found in Figure 4.6.

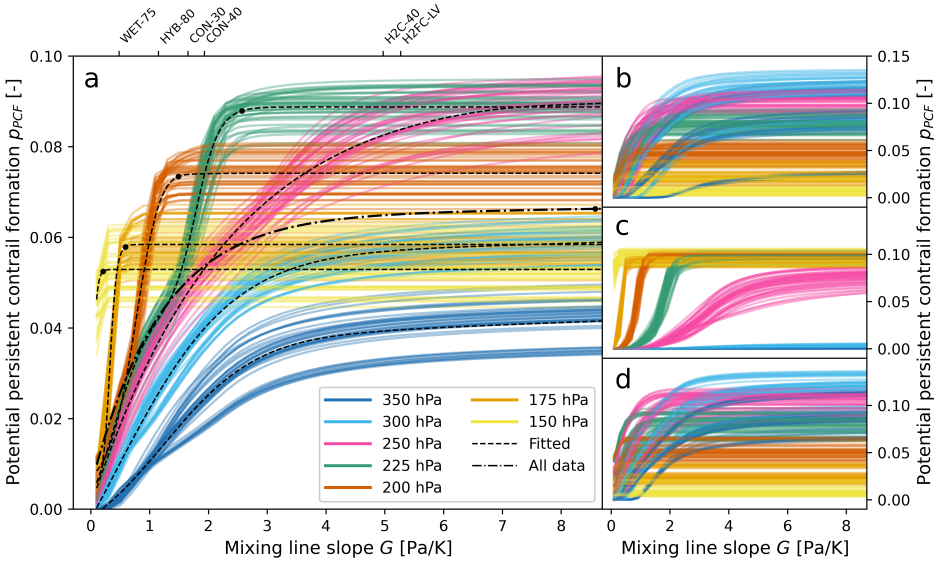


Figure 4.7: Potential persistent contrail formation p_{pcf} as a function of the mixing line slope G on a climatological timescale for pressure levels 350 to 150 hPa **(a)** at a global scale and for **(b)** the northern extratropics, **(c)** the tropics and **(d)** the southern extratropics. Each coloured line corresponds to a single season within the 2010 decade. The dashed lines are the fitted responses using the modified logistic function in Eq. (4.6) and parameters as defined in Table 4.2, for each pressure level individually ("fitted") and for all pressure levels together ("all data"). The markers show at which value of G the corresponding p_{pcf} reaches within 1 % of the supremum. The mixing line slopes of the different aircraft designs are shown for the pressure level 250 hPa for reference.

For very low G, persistent contrails form only at very high altitude. As G increases, more persistent contrails are formed at lower altitudes (higher pressure levels). The pressure levels with the highest p_{pcf} is likely between 250 and 225 hPa (FL340 - FL360) at $G > 7\,\mathrm{Pa\,K^{-1}}$. For these two pressure levels in particular, the results seem to be the addition of two different responses. We find that the initial

slope is the extratropical response (both northern and southern) and the second slope the tropical response (right side of Figure 4.7). Given the higher tropopause and ambient temperature in the tropics, persistent contrails generally form at higher values of G compared to the extratropics.

We fit the responses using the sum of two logistic functions, one representing the response from the tropics and the other from the extratropics. A conventional logistic function includes the supremum L, the growth rate k and the midpoint of the growth x_0, with limits 0 for $x \to -\infty$ and L for $x \to +\infty$. We have allowed the extratropical logistic function to be shifted vertically by d for a better fit, noting that the fitting function is only valid for $G > 0\,\mathrm{Pa\,K^{-1}}$ $G > 0\,\mathrm{Pa\,K^{-1}}$. To find the optimal parameters, we consider the tropical logistic function to be an addition to the extratropical function. Therefore, we split the data into two at a certain value of G: We use the values of G up until this split to create the extratropical response and the values after the split to create the tropical response. We subsequently use a minimisation function to determine the best value for the split.

$$f(x) = \frac{L_1}{1 + \mathrm{e}^{-k_1(x - x_{0,1})}} + \frac{L_2}{1 + \mathrm{e}^{-k_2(x - x_{0,2})}} + d \tag{4.6}$$

The result is that the value of the maximum for the full equation can be read as $L_1 + L_2 + d$. For the pressure levels 175 and $150\,\mathrm{hPa}$, we find that there is no need to use a second logistic function because persistent contrails do not form at these pressures in the extratropics. For these pressure levels, therefore, the value of the asymptote is simply $L + d$.

The parameters found by the minimisation function are shown in Table 4.2. We generally find a good fit and a high coefficient of determination (R^2), except for $150\,\mathrm{hPa}$ and all level data together. At $150\,\mathrm{hPa}$, the seasonal responses reach an asymptote at a very low G, such that the response is essentially horizontal and thus by definition cannot have a good R^2 value. By considering all level data together, the differentiation between the extratropical and tropical responses are essentially no longer visible. The R^2 value is thus not high, clearly showing that including level information is beneficial in determining p_{pcf}. We note that the "all data" response in Figure 4.7 has a similar shape to the gentle sloping curve in Figure 2 of Hofer et al. (2024a), who consider persistent contrail formation from potential SAF aircraft using IAGOS/MOZAIC data, irrespective of the altitude.

As Figure 4.3 demonstrated, p_{pcf} increases with enhanced relative humidity because more ambient conditions, in particular closer to the freezing temperature limit, are conducive to persistent contrail formation. The same analysis as above is conducted for all RHi enhancements and shown in Figure 4.A.6. The fitted results are stretched to higher p_{pcf} but maintain the same general shape, including the marked difference in the extratropical and tropical responses. This again suggests that, on a climatological timescale, as relative humidity is enhanced, the probability that a persistent contrail forms increases where the prob-

Table 4.2: Optimal parameters for potential persistent contrail formation as a function of the mixing line slope G (Eq. 4.6) on a climatological timescale for pressure levels 350 to 150 hPa and for all pressure levels together ("all data"). The supremum value of the function $L + d$ is shown as a percentage. For each pressure level, the top values of L, k and x_0 are for the first logistic function (extratropical response) and the bottom values for the second logistic function (tropical response). The pressure levels 175 and 150 hPa are primarily driven by the tropical response (see Figure 4.7) and thus did not benefit from the second logistic function. The variable $G_{99\%sup}$ corresponds to the lowest value of G for which the corresponding p_{pcf} is within 1 % of the supremum $L + d$.

Level	L	k	x_0	d	$L+d$ [%]	R^2	$G_{99\%sup}$ [Pa K^{-1}]
All data	9.001 0.001	0.84 0.51	-5.92 8.12	-8.936	6.70	0.253	8.58
350 hPa	0.049 0.004	1.24 0.48	1.24 7.07	-0.011	4.28	0.846	11.63
300 hPa	0.100 0.003	1.00 0.53	0.39 8.60	-0.043	6.02	0.946	10.94
250 hPa	2.072 -0.002	0.45 1.87	-6.86 7.76	-1.979	9.13	0.958	10.40
225 hPa	0.055 0.044	3.17 5.13	0.38 1.80	-0.010	8.88	0.954	2.57
200 hPa	0.077 -0.007	4.32 5.14	0.78 1.38	0.005	7.41	0.891	1.49
175 hPa	0.054	17.3	0.32	0.005	5.84	0.680	0.59
150 hPa	0.237	24.5	-0.04	-0.185	5.29	0.018	0.21

ability was already greater than zero (see Figure 4.A.5).

4.3.5. COMPETITION BETWEEN LIMITING FACTORS

We find that for all aircraft designs, persistence is the most limiting factor and most responsible for the boundaries of persistent contrail formation regions (Figures 4.3 and 4.5 respectively). At first glance, this seems counterintuitive: Persistence is independent of aircraft design, but the size of the potential persistent contrail formation regions do depend on the aircraft design and vary significantly.

On the one hand, we can view the persistence and droplet freezing limiting factors as together creating an upper bound to the potential persistent contrail formation region size. In this case, the droplet formation limiting factor controls what proportion of this region is available for persistent contrails to form. Figure 4.7 shows that the level of control varies with latitude and altitude: at high altitudes, aircraft design has barely any influence. This, however, does not explain why persistence is most limiting for all aircraft designs.

Consider instead an upper bound created by droplet formation and droplet freezing. This corresponds to the total region where contrails are expected to form, but not necessarily persist. Since most region boundaries are defined by the persistence limiting factor, the results suggest that there are horizontally contiguous ice supersaturated structures in which, for a specific G, contrails either form or do not form across the full domain. In other words, an aircraft with a low

G may fly through an ice supersaturated area but not form a contrail because the larger region is not conducive to droplet formation, whereas an aircraft with a high G flying on the same trajectory may instead form a non-persistent contrail outside of the same ice supersaturated area and a persistent contrail within it.

How should the competition between the persistence and droplet formation limiting factors then be viewed? Persistence is responsible for the majority of boundary crossings because ERA5 grid cells are only ever slightly supersaturated with respect to ice and the relative humidity field is more heterogeneous than the temperature field. Small changes in relative humidity may thus cause a neighbouring grid cell to no longer be supersaturated with respect to ice, but remain conducive to droplet formation. However, droplet formation is more important than the boundary analysis would suggest. In the case of the low-G aircraft, droplet formation was clearly most limiting, but this is not recognised by our boundary analysis because no persistent contrail formation occurred. Its relevance reduces as G increases, where the limiting Schmidt-Appleman slope acts much like a vertical boundary. Indeed, the droplet freezing and H2FC-HV droplet formation limiting factors show very similar results (see Figures 4.3 and 4.4).

4.3.6. UNCERTAINTIES AND LIMITATIONS

As with all climatological analyses and models, there are a number of limitations in the usage of our results. For example, consider the latitude-dependent results in Figure 4.7. In theory, more information could be gained by including two distinct extratropical and tropical responses. No persistent contrails are produced in the tropics at $350\,\mathrm{hPa}$ and essentially none are produced at $300\,\mathrm{hPa}$, but if the globally averaged fits were to be used, persistent contrails would be assumed to form in these regions. However, the results in the individual latitude bands also have a higher seasonal dependence (notably in the tropics at $250\,\mathrm{hPa}$). There is thus a trade-off in the level of detail that can be included if persistent contrail formation is to be climatologically modelled. Clearly, it would be inappropriate to analyse the climate impact of an aviation scenario that only considers aircraft flying in one latitude region using the globally fitted responses. Similarly, it would also be inappropriate to use the fits to analyse aircraft flying only in a single season. Instead, our results are useful for global aviation or aircraft-specific scenarios with a time step of at least one year.

It is also important to underline the difference between persistent contrail formation and the resulting contrail-cirrus coverage and climate impact. The results presented in this study are valid only for static persistent contrail formation, i.e. do not consider contrail spreading or temporal changes in the local ambient conditions: We assume a contrail to be persistent if the ambient conditions are supersaturated with respect to ice at the time of formation. However, since the water vapour field is highly heterogeneous and can vary rapidly with time, the contrail may not actually persist and hence result only in a low or even negligible climate impact.

It is also possible that persistent contrails formed in one grid cell spread to neighbouring cells due to mixing. Particularly interesting are neighbouring cells that are limited by the droplet formation limiting factor, i.e. are themselves not conducive for persistent contrail formation, but are supersaturated with respect to ice and are below the homogeneous freezing temperature. In a previous study (Wolf et al., 2023a), these regions were defined as "reservoirs" for persistent contrails. As contrails spread vertically and/or horizontally over time, they may persist in grid cells that our analysis identified as limited by droplet formation. Such spreading is certainly important for the calculation of a contrail-cirrus coverage, but since it is a secondary, dynamic effect we have not included it in this study.

Care should also be taken when using our results to inform aircraft design or flight trajectories. For example, we show that replacing kerosene with hydrogen along assumed future flight trajectories could result in around 50 % more persistent contrails (see Table 4.A.1) on a climatological timescale without considering contrail avoidance strategies. This does not, however, translate to a 50 % larger radiative forcing or temperature change due to differing contrail properties. For example, Rap et al. (2023) find a 70 % increase in contrail coverage from hydrogen-powered aircraft compared to conventional aircraft, but also find a 25 % reduction in contrail-cirrus Effective Radiative Forcing (ERF). Similar results were found by Grewe et al. (2017). Persistent contrail formation should thus not be used as a direct proxy for climate impact and more research is required into contrail properties from novel aviation fuels and propulsion technologies. We also reiterate that contrails are only part of the equation and that the full climate impact, including other non-CO_2 effects, should be used to inform aircraft design or flight trajectories.

The globally averaged, climatological results presented in this study are not expected to change significantly due to a changing climate. Our results show that persistence is the most limiting factor for all aircraft designs. Therefore, the probability of persistent contrail formation should vary in tandem with the frequency and location of ISSRs. Climate models predict a generally warmer upper troposphere and generally cooler lower stratosphere, leading to a decrease in relative humidity in the tropics and an increase towards the poles (Irvine and Shine, 2015; Benetatos et al., 2024). This is reflected in the results of both Chen and Gettelman (2016) and Bock and Burkhardt (2019), who find for a future atmosphere a decrease in the probability of persistent contrail formation (here p_{pcf}) in the tropics and an increase in the northern extratropics. Chen and Gettelman (2016) find a net reduction in contrail-cirrus radiative forcing, whereas Bock and Burkhardt (2019) expect the radiative forcing to approximately even out.

If the global p_{pcf} remains approximately the same, then the limiting factor results (Figure 4.5) and the competition between the limiting factors should also remain unchanged. However, the regional differences in ISSR location may modify the shape of the responses in Figure 4.7, lowering the maximum p_{pcf} values in the tropics and raising them in the extratropics. For the pressure levels 250 to $200\,\mathrm{hPa}$,

which are driven by both a tropical and extratropical response, the global result will likely have a steeper initial slope and a shallower secondary slope, shifted slightly to higher mixing line slopes. The maximum values and the general shape of the responses are not expected to change significantly.

Finally, we do not expect the choice of global aviation scenario to have significantly affected the weighted results. In this study, we used the DEPA 2050 progressive scenario for the year 2050 since it is representative of a future multi-fuel global fleet and due to its ease of publication. By changing the aircraft design and slope G, we implicitly assume flight altitude and routing remains constant, even though this may not be the case, particularly for novel aviation fuels and technologies such as fuel cell and hybrid-electric propulsion setups. Changing the global scenario may produce slightly different weighted results, but the focus is nevertheless expected to remain on the northern extratropics at $300-250\,\mathrm{hPa}$.

4.4. CONCLUSION

Persistent contrail formation is limited by three main factors: droplet formation, droplet freezing and persistence. Our investigation using ERA5 data in the 2010 decade finds persistence (ice supersaturation) to be the most limiting factor. Of the considered grid cells, 92.3 % are not supersaturated with respect to ice and thus not conducive to persistent contrail formation. Droplet freezing is found to be limiting 18.2 % of the time and droplet formation between 19.2 % (high voltage hydrogen fuel cell) and 89.5 % (Water Enhanced Turbofan with 75 % water vapour reduction). The boundaries of persistent contrail formation regions are also generally defined by the persistence limiting factor, regardless of aircraft design. In other words, should an aircraft – without changing its operating condition – start producing a persistent contrail, generally it is because the air mass it has entered is supersaturated with respect to ice. Our results thus underscore the importance of accurately estimating ice supersaturated regions (Gierens et al., 2020; Hofer et al., 2024b).

We demonstrate the feasibility of developing high-quality climatological relationships between the mixing line slope G and the potential persistent contrail formation p_{pcf} for individual pressure levels. We create these relationships using the sum of two modified logistic functions, one representing the response from the tropics and the other from the extratropics. The combination of the persistence and droplet freezing limiting factors create an upper bound for the size of persistent contrail formation regions, which varies by latitude, altitude and season. We find that, due to the distribution of ice supersaturation with altitude, aircraft design becomes less limiting with increasing altitude (decreasing pressure level). For very low G, persistent contrails form only at very high altitude. As G increases, more persistent contrails are also formed at lower altitudes. These climatological relationships are the first step in the development of a compu-

tationally inexpensive method to analyse the contrail climate impact of novel aviation fuels and propulsion technologies on a climatological timescale.

Novel aviation fuels and propulsion technologies will have a major impact on persistent contrail formation. Across all considered flight levels, improving overall propulsion efficiency from 0.30 to 0.40 increases persistent contrail formation by 13.6 % along representative flight trajectories; from 0.37 to 0.40 by 4.0 %. A significant reduction in persistent contrail formation could be achieved using a water vapour emission reduction system such as the Water Enhanced Turbofan concept - up to 85.1 % by reducing the water vapour emission index by 75 % compared to a reference conventional aircraft with an overall propulsion system efficiency of 0.37. On the other hand, compared to the same reference aircraft, hydrogen combustion or fuel cell aircraft could result in a 46.5 to 54.7 % increase respectively. It is, however, important to keep in mind which aircraft is taken as reference - an overall propulsion system efficiency of 0.37 is representative of current state-of-the-art, but likely higher than the global average. Compared to the global average, the increase may be even higher.

Persistent contrail formation, as analysed here, is not synonymous with contrail climate impact. Contrails produced by aircraft using alternative fuels such as hydrogen are expected to have very different optical and radiative properties. Although such aircraft may produce significantly more persistent contrails, their overall contrail climate impact may in fact be lower than conventional aircraft – this is explored in more detail in Chapter 5. Nonetheless, the results of this analysis point to a clear potential for the targeted introduction of aircraft with low mixing line slopes to significantly reduce persistent contrail formation.

4.A. APPENDIX

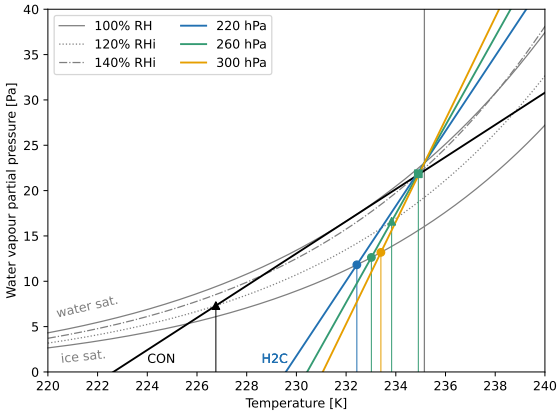


Figure 4.A.1: Ambient temperature vs. water vapour partial pressure diagram with threshold mixing lines for a conventional, kerosene-powered aircraft (CON, black line for $240\,\mathrm{hPa}$) and a hydrogen combustion aircraft (H2C, coloured lines for different pressure levels). The ice and water saturation curves are shown for 100 % (gray lines), as well as the curve for ice supersaturations of 120 % (dotted gray line) and 140 % (dash-dotted gray line). The intersection of the threshold mixing lines with these curves are marked for comparison with Bier et al. (2022) and Bier et al. (2024) - see main text.

Table 4.A.1: Potential persistent contrail formation p_{pcf} and DEPA 2050 distance-weighted p_{pcf} for the pressure levels 300 and $250\,\mathrm{hPa}$ and all considered pressure levels, averaged over four latitude bands: the southern extratropics (xtropS), tropics (trop), nothern extratropics (xtropN) and all latitudes. Percentage changes are provided for the globally-averaged values for simple comparison. The full data is available within the linked dataset.

Aircraft	Pressure level	p_{pcf}				Distance-weighted p_{pcf}			
		xtropS	trop	xtropN	all	xtropS	trop	xtropN	all
WET-75	300 hPa	0.057	0.000	0.028	0.028 (37.1 %)	0.000	0.000	0.002	0.001 (10.1 %)
	250 hPa	0.061	0.000	0.030	0.031 (45.4 %)	0.000	0.000	0.003	0.001 (16.2 %)
	all	0.044	0.015	0.019	0.026 (43.4 %)	0.000	0.000	0.001	0.000 (14.9 %)
WET-50	300 hPa	0.096	0.000	0.064	0.053 (69.6 %)	0.000	0.000	0.008	0.003 (40.6 %)
	250 hPa	0.086	0.000	0.064	0.050 (74.7 %)	0.000	0.000	0.009	0.003 (53.1 %)
	all	0.065	0.029	0.040	0.044 (74.0 %)	0.000	0.000	0.004	0.001 (48.3 %)
HYB-80	300 hPa	0.104	0.000	0.075	0.060 (78.3 %)	0.000	0.000	0.011	0.004 (53.8 %)
	250 hPa	0.093	0.000	0.073	0.055 (82.6 %)	0.000	0.000	0.011	0.004 (66.3 %)
	all	0.069	0.033	0.045	0.049 (81.7 %)	0.000	0.000	0.004	0.002 (61.7 %)
CON-30	300 hPa	0.119	0.000	0.100	0.073 (95.3 %)	0.000	0.000	0.017	0.006 (88.0 %)
	250 hPa	0.104	0.004	0.086	0.065 (96.3 %)	0.000	0.001	0.015	0.005 (92.6 %)
	all	0.076	0.043	0.055	0.058 (96.5 %)	0.000	0.001	0.006	0.002 (91.5 %)
CON-37	300 hPa	0.124	0.000	0.105	0.076 (100.0 %)	0.000	0.000	0.020	0.007 (100.0 %)
	250 hPa	0.106	0.007	0.089	0.067 (100.0 %)	0.000	0.001	0.016	0.006 (100.0 %)
	all	0.078	0.045	0.057	0.060 (100.0 %)	0.000	0.001	0.007	0.003 (100.0 %)
CON-40	300 hPa	0.126	0.000	0.108	0.078 (102.1 %)	0.000	0.000	0.021	0.007 (105.9 %)
	250 hPa	0.107	0.008	0.090	0.068 (101.7 %)	0.000	0.001	0.016	0.006 (103.3 %)
	all	0.079	0.047	0.058	0.061 (101.7 %)	0.000	0.001	0.007	0.003 (104.0 %)
H2C-40	300 hPa	0.142	0.003	0.128	0.091 (119.3 %)	0.001	0.001	0.032	0.011 (164.8 %)
	250 hPa	0.111	0.063	0.098	0.091 (134.8 %)	0.001	0.006	0.019	0.009 (149.0 %)
	all	0.084	0.064	0.065	0.071 (118.3 %)	0.000	0.002	0.009	0.004 (146.5 %)
H2FC-HV	300 hPa	0.145	0.004	0.131	0.093 (122.4 %)	0.001	0.002	0.034	0.012 (177.2 %)
	250 hPa	0.111	0.078	0.099	0.096 (142.8 %)	0.001	0.007	0.019	0.009 (157.5 %)
	all	0.085	0.066	0.067	0.073 (120.8 %)	0.000	0.003	0.009	0.004 (154.7 %)

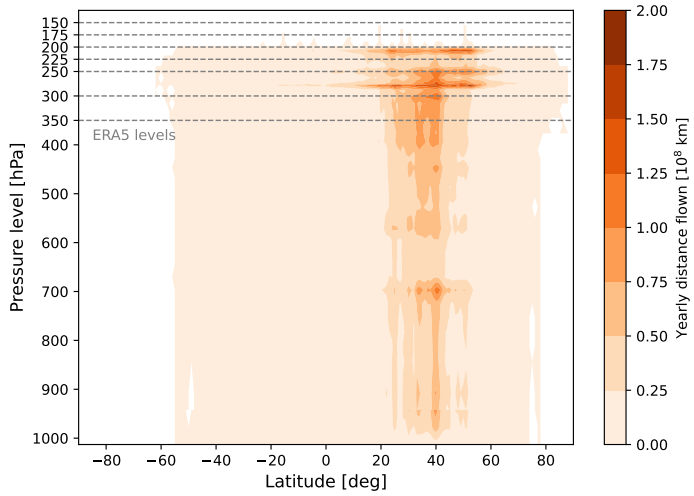


Figure 4.A.2: DEPA 2050 progressive scenario for the year 2050 used to weight the potential persistent contrail formation. Also shown are the ERA5 pressure levels considered in the study.

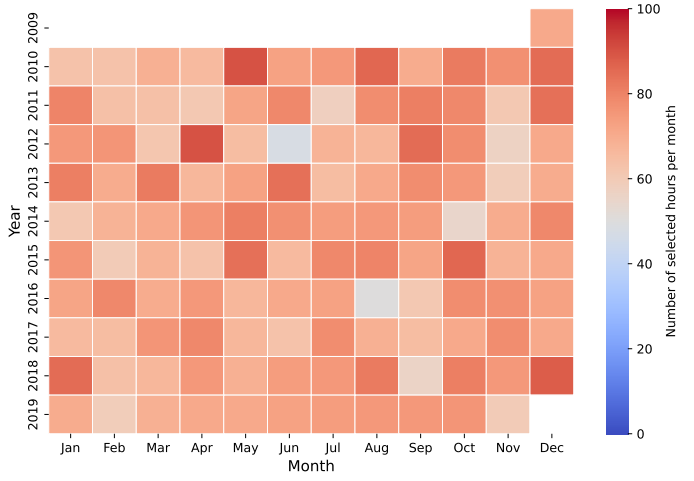


Figure 4.A.3: Number of hours randomly selected in ERA5 within the 2010 decade.

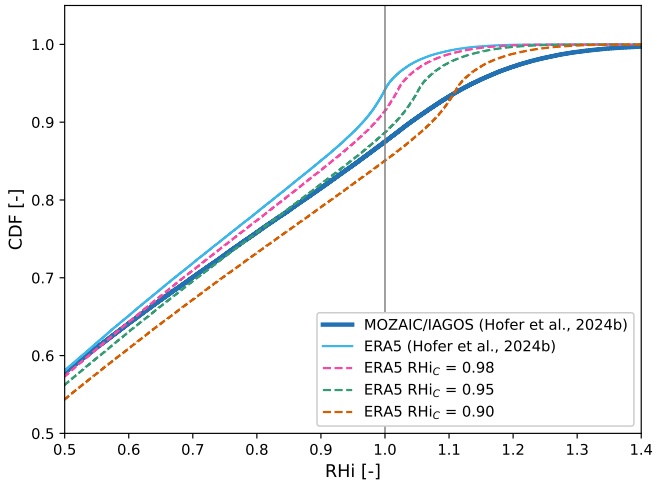


Figure 4.A.4: Comparison of the cumulative distribution functions of ERA5 and MOZAIC/IAGOS from (Hofer et al., 2024b). We enhance the ERA5 relative humidity by applying simple factors and find that RHi$_C$ = 0.95 provides a good fit against MOZAIC/IAGOS data for RHi $\leq$ 1.0.

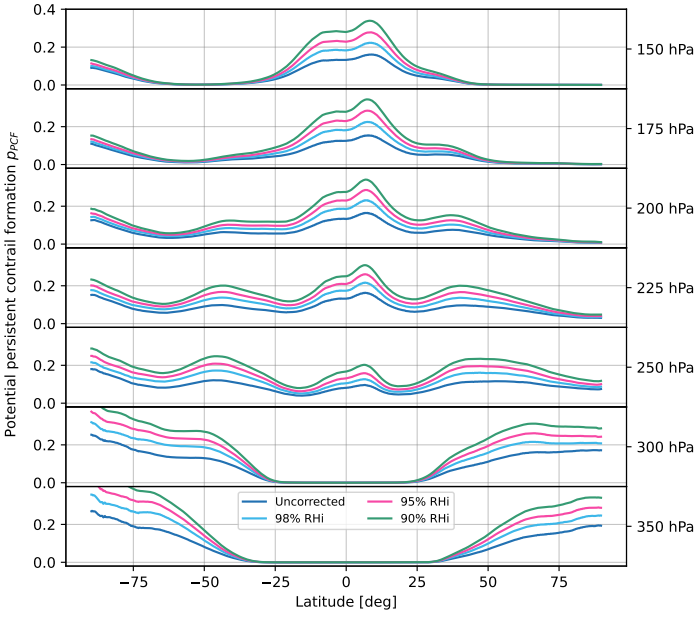


Figure 4.A.5: Potential persistent contrail formation as a function of latitude (x-axis) and altitude (secondary y-axis) for different relative humidity enhancements.

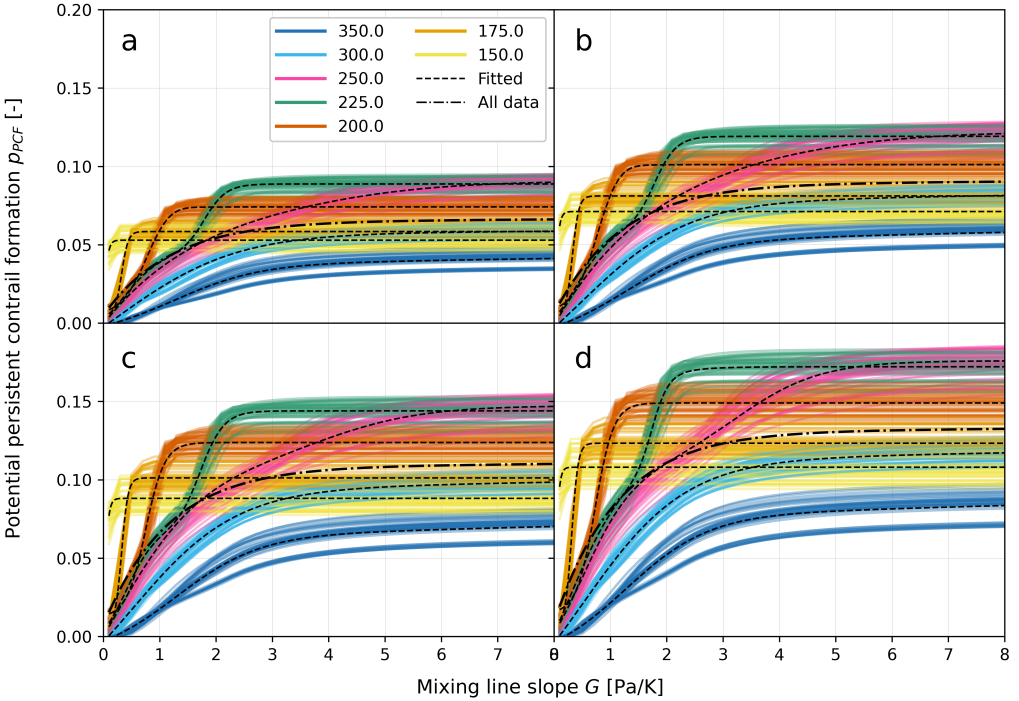


Figure 4.A.6: Potential persistent contrail formation p_{pcf} as a function of the mixing line slope G on a climatological timescale for pressure levels 350 to $150\,\mathrm{hPa}$. We enhance the relative humidity by applying simple factors 1/RHi$_C$: **(a)** no correction, **(b)** RHi$_C$ = 98 %, **(c)** RHi$_C$ = 95 %, **(d)** RHi$_C$ = 90 %. Each coloured line corresponds to a single season within the 2010 decade. The dashed lines are the fitted responses using a modified logistic function, for each pressure level individually ("fitted") and for all pressure levels together ("all data").

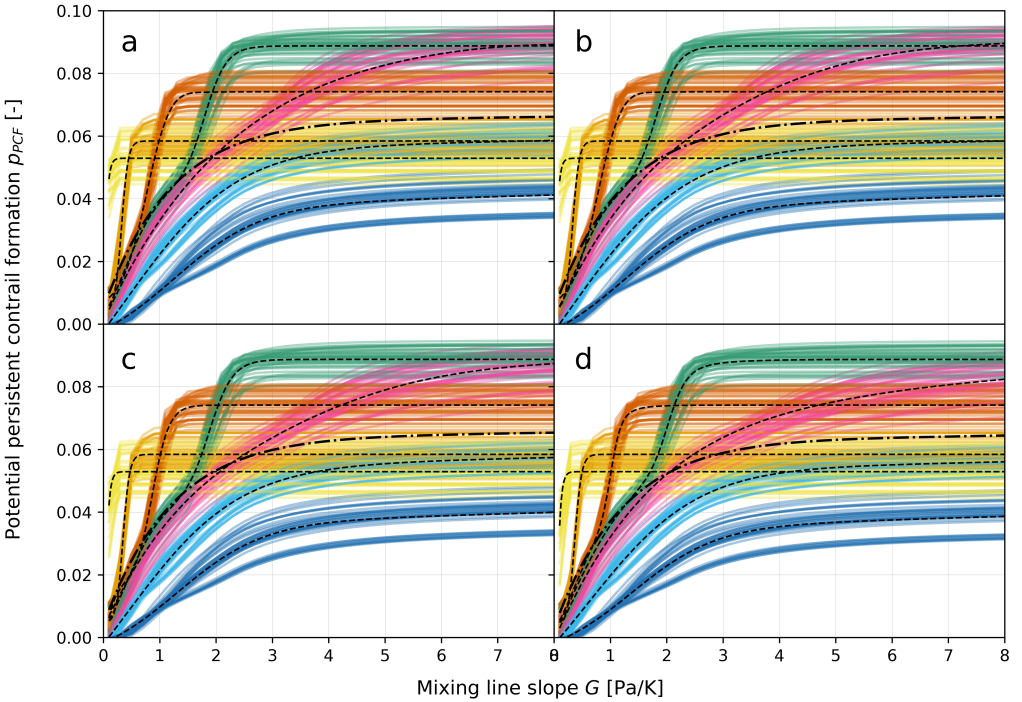


Figure 4.A.7: Potential persistent contrail formation p_{pcf} as a function of the mixing line slope G on a climatological timescale for pressure levels 350 to $150\,\mathrm{hPa}$. We increase all ambient temperatures by **(a)** $0\,\mathrm{K}$, **(b)** $0.1\,\mathrm{K}$, **(c)** $0.5\,\mathrm{K}$, **(d)** $1.0\,\mathrm{K}$. Each coloured line corresponds to a single season within the 2010 decade. The dashed lines are the fitted responses using a modified logistic function, for each pressure level individually ("fitted") and for all pressure levels together ("all data"). There is very little discernible difference between the uncorrected and corrected results. Most notable is the slight reduction in p_{pcf} at $250\,\mathrm{hPa}$ at high G.

REFERENCES

Agarwal, A., Meijer, V. R., Eastham, S. D., Speth, R. L., and Barrett, S. R. H.: Reanalysis-driven simulations may overestimate persistent contrail formation by 100%–250%, Environmental Research Letters, 17, 014 045, doi: 10.1088/1748-9326/ac38d9, 2022.

Barton, D. I., Hall, C. A., and Oldfield, M. K.: Design of a hydrogen aircraft for zero persistent contrails, Aerospace, 10, 688, doi: 10.3390/aerospace10080688, 2023.

Benetatos, C., Eleftheratos, K., Gierens, K., and Zerefos, C.: A statistically significant increase in ice supersaturation in the atmosphere in the past 40 years, Scientific Reports, 14, 24 760, doi: 10.1038/s41598-024-75756-9, 2024.

Bier, A., Unterstrasser, S., and Vancassel, X.: Box model trajectory studies of contrail formation using a particle-based cloud microphysics scheme, Atmospheric Chemistry and Physics, 22, 823–845, doi: 10.5194/acp-22-823-2022, 2022.

Bier, A., Unterstrasser, S., Zink, J., Hillenbrand, D., Jurkat-Witschas, T., and Lottermoser, A.: Contrail formation on ambient aerosol particles for aircraft with hydrogen combustion: a box model trajectory study, Atmospheric Chemistry and Physics, 24, 2319–2344, doi: 10.5194/acp-24-2319-2024, 2024.

Bock, L. and Burkhardt, U.: Contrail cirrus radiative forcing for future air traffic, Atmospheric Chemistry and Physics, 19, 8163–8174, doi: 10.5194/acp-19-8163-2019, 2019.

Burkhardt, U. and Kärcher, B.: Global radiative forcing from contrail cirrus, Nature Climate Change, 1, 54–58, doi: 10.1038/nclimate1068, 2011.

Chen, C.-C. and Gettelman, A.: Simulated 2050 aviation radiative forcing from contrails and aerosols, Atmospheric Chemistry and Physics, 16, 7317–7333, doi: 10.5194/acp-16-7317-2016, 2016.

Gierens, K.: Theory of contrail formation for fuel cells, Aerospace, 8, 164, doi: 10.3390/aerospace8060164, 2021.

Gierens, K., Matthes, S., Rohs, S., and Susanne Rohs: How well can persistent contrails be predicted, Aerospace, 7, 169, doi: 10.3390/aerospace7120169, 2020.

Grewe, V., Plohr, M., Cerino, G., Muzio, M. D., Deremaux, Y., Galerneau, M., Martin, P. d. S., Chaika, T., Hasselrot, A., Tengzelius, U., and Korovkin, V. D.: Estimates of the climate impact of future small-scale supersonic transport aircraft – results from the HISAC EU-project, The Aeronautical Journal, 114, 199–206, doi: 10.1017/S000192400000364X, 2010.

Grewe, V., Bock, L., Burkhardt, U., Dahlmann, K., Gierens, K., Hüttenhofer, L., Unterstrasser, S., Gangoli Rao, A., Bhat, A., Yin, F., Reichel, T. G., Paschereit, O., and Levy, Y.: Assessing the climate impact of the AHEAD multi-fuel blended wing body, Meteorologische Zeitschrift, 26, 711–725, doi: 10.1127/metz/2016/0758, 2017.

Haywood, J. M., Allan, R. P., Bornemann, J., Forster, P. M., Francis, P. N., Milton, S., Rädel, G., Rap, A., Shine, K. P., and Thorpe, R.: A case study of the radiative forcing of persistent contrails evolving into contrail-induced cirrus, Journal of Geophysical Research: Atmospheres, 114, 2009JD012 650, doi: 10.1029/2009JD012650, 2009.

Hersbach, H., Bell, B., Berrisford, P., Hirahara, S., Horányi, A., Muñoz-Sabater, J., Nicolas, J., Peubey, C., Radu, R., Schepers, D., Simmons, A., Soci, C., Abdalla, S., Abellan, X., Balsamo, G., Bechtold, P., Biavati, G., Bidlot, J., Bonavita, M., De Chiara, G., Dahlgren, P., Dee, D., Diamantakis, M., Dragani, R., Flemming, J., Forbes, R., Fuentes, M., Geer, A., Haimberger, L., Healy, S., Hogan, R. J., Hólm, E., Janisková, M., Keeley, S., Laloyaux, P., Lopez, P., Lupu, C., Radnoti, G., De Rosnay, P., Rozum, I., Vamborg, F., Villaume, S., and Thépaut, J.: The ERA5 global reanalysis, Quarterly Journal of the Royal Meteorological Society, 146, 1999–2049, doi: 10.1002/qj.3803, 2020.

Hillenbrand, D. and Unterstrasser, S.: Contrail formation: generalised theory and a mitigation proposition for fuel-cell-propelled aircraft, The Aeronautical Journal, pp. 1–26, doi: 10.1017/aer.2026.10185, 2026.

Hofer, S., Gierens, K., and Rohs, S.: Contrail formation and persistence conditions for alternative fuels, Meteorologische Zeitschrift, 33, 43–49, doi: 10.1127/metz/2024/1178, 2024a.

Hofer, S., Gierens, K., and Rohs, S.: How well can persistent contrails be predicted? An update, Atmospheric Chemistry and Physics, 24, 7911–7925, doi: 10.5194/acp-24-7911-2024, 2024b.

Irvine, E. A. and Shine, K. P.: Ice supersaturation and the potential for contrail formation in a changing climate, Earth System Dynamics, 6, 555–568, doi: 10.5194/esd-6-555-2015, 2015.

Kaufmann, S., Dischl, R., and Voigt, C.: Regional and seasonal impact of hydrogen propulsion systems on potential contrail cirrus cover, Atmospheric Environment: X, 24, 100 298, doi: 10.1016/j.aeaoa.2024.100298, 2024.

Krämer, M., Schiller, C., Afchine, A., Bauer, R., Gensch, I., Mangold, A., Schlicht, S., Spelten, N., Sitnikov, N., Borrmann, S., De Reus, M., and Spichtinger, P.: Ice supersaturations and cirrus cloud crystal numbers, Atmospheric Chemistry and Physics, 9, 3505–3522, doi: 10.5194/acp-9-3505-2009, 2009.

Kärcher, B.: Formation and radiative forcing of contrail cirrus, Nature Communications, 9, 1824–1824, doi: 10.1038/s41467-018-04068-0, 2018.

Kärcher, B. and Yu, F.: Role of aircraft soot emissions in contrail formation, Geophysical Research Letters, 36, L01 804, doi: 10.1029/2008GL036649, 2009.

Kärcher, B., Burkhardt, U., Bier, A., Bock, L., and Ford, I. J.: The microphysical pathway to contrail formation, Journal of Geophysical Research: Atmospheres, 120, 7893–7927, doi: 10.1002/2015JD023491, 2015.

Lee, D., Fahey, D., Skowron, A., Allen, M., Burkhardt, U., Chen, Q., Doherty, S., Freeman, S., Forster, P., Fuglestvedt, J., Gettelman, A., De León, R., Lim, L., Lund, M., Millar, R., Owen, B., Penner, J., Pitari, G., Prather, M., Sausen, R., and Wilcox, L.: The contribution of global aviation to anthropogenic climate forcing for 2000 to 2018, Atmospheric Environment, 244, 117 834, doi: 10.1016/j.atmosenv.2020.117834, 2021.

Leipold, A., Aptsiauri, G., Ayazkhani, A., Bauder, U., Becker, R.-G., Berghof, R., Claßen, A., Dadashi, A., Dahlmann, K., Dzikus, N., Flüthmann, N., Grewe, V., Göhlich, L., Grimme, W., Günther, Y., Jaksche, R., Jung, M., Knabe, F., Kutne, P., Le Clercq, P., Pabst, H., Poggel, S., Staggat, M., Wicke, K., Wolters, F., Zanger, J., and Zill, T.: DEPA 2050 – Development Pathways for Aviation up to 2050 (Final Report), Tech. rep., DLR, Köln, https://elib.dlr.de/142185/, 2021.

Marenco, A., Thouret, V., Nédélec, P., Smit, H., Helten, M., Kley, D., Karcher, F., Simon, P., Law, K., Pyle, J., Poschmann, G., von Wrede, R., Hume, C., and Cook, T.: Measurement of ozone and water vapor by Airbus in-service aircraft: The MOZAIC airborne program, an overview, Journal of Geophysical Research: Atmospheres, 103, 25 631–25 642, doi: 10.1029/98JD00977, 1998.

Matthes, S., Lim, L., Burkhardt, U., Dahlmann, K., Dietmüller, S., Grewe, V., Haslerud, A. S., Hendricks, J., Owen, B., Pitari, G., Righi, M., and Skowron, A.: Mitigation of non-CO2 aviation's climate impact by changing cruise altitudes, Aerospace, 8, 36, doi: 10.3390/aerospace8020036, 2021.

Megill, L. and Grewe, V.: Investigating the limiting aircraft-design-dependent and environmental factors of persistent contrail formation, Atmos. Chem. Phys., 25, 4131–4149, doi: 10.5194/acp-25-4131-2025, 2025.

Petzold, A., Thouret, V., Gerbig, C., Zahn, A., Brenninkmeijer, C. A. M., Gallagher, M., Hermann, M., Pontaud, M., Ziereis, H., Boulanger, D., Marshall, J., Nédélec, P., Smit, H. G. J., Friess, U., Flaud, J.-M., Wahner, A., Cammas, J.-P., Volz-Thomas, A., and Team, I.: Global-scale atmosphere monitoring by in-service aircraft – current achievements and future prospects of the European Research Infrastructure IAGOS, Tellus B: Chemical and Physical Meteorology, 67, 28 452, doi: 10.3402/tellusb.v67.28452, 2015.

Ponsonby, J., Teoh, R., Kärcher, B., and Stettler, M. E. J.: An updated microphysical model for particle activation in contrails: the role of volatile plume particles, Atmospheric Chemistry and Physics, 25, 18 617–18 637, doi: 10.5194/acp-25-18617-2025, 2025.

Rap, A., Feng, W., Forster, P., Marsh, D., and Murray, B.: The climate impact of contrails from hydrogen combustion and fuel cell aircraft, in: EGU General Assembly 2023, Vienna, Austria, doi: 10.5194/egusphere-egu23-5520, 2023.

Reutter, P., Neis, P., Rohs, S., and Sauvage, B.: Ice supersaturated regions: properties and validation of ERA-Interim reanalysis with IAGOS in situ water vapour measurements, Atmospheric Chemistry

and Physics, 20, 787–804, doi: 10.5194/acp-20-787-2020, 2020.

Richardson, E. S.: Contrail Formation Criterion for Assessment of Alternative Propulsion Technologies, Journal of Propulsion and Power, 41, 264–276, doi: 10.2514/1.B39430, 2025.

Schumann, U.: On conditions for contrail formation from aircraft exhausts, Meteorologische Zeitschrift, 5, 4–23, doi: 10.1127/metz/5/1996/4, 1996.

Schumann, U.: A contrail cirrus prediction model, Geoscientific Model Development, 5, 543–580, doi: 10.5194/gmd-5-543-2012, 2012.

Schumann, U. and Heymsfield, A. J.: On the life cycle of individual contrails and contrail cirrus, Meteorological Monographs, 58, 3.1–3.24, doi: 10.1175/AMSMONOGRAPHS-D-16-0005.1, 2017.

Schumann, U., Poll, I., Teoh, R., Koelle, R., Spinielli, E., Molloy, J., Koudis, G. S., Baumann, R., Bugliaro, L., Stettler, M., and Voigt, C.: Air traffic and contrail changes over Europe during COVID-19: a model study, Atmospheric Chemistry and Physics, 21, 7429–7450, doi: 10.5194/acp-21-7429-2021, 2021.

Teoh, R., Schumann, U., Majumdar, A., and Stettler, M. E. J.: Mitigating the climate forcing of aircraft contrails by small-scale diversions and technology adoption, Environmental Science & Technology, 54, 2941–2950, doi: 10.1021/acs.est.9b05608, 2020.

Teoh, R., Schumann, U., Gryspeerdt, E., Shapiro, M., Molloy, J., Koudis, G., Voigt, C., and Stettler, M. E. J.: Aviation contrail climate effects in the North Atlantic from 2016 to 2021, Atmospheric Chemistry and Physics, 22, 10 919–10 935, doi: 10.5194/acp-22-10919-2022, 2022.

Teoh, R., Engberg, Z., Schumann, U., Voigt, C., Shapiro, M., Rohs, S., and Stettler, M. E. J.: Global aviation contrail climate effects from 2019 to 2021, Atmospheric Chemistry and Physics, 24, 6071–6093, doi: 10.5194/acp-24-6071-2024, 2024.

van 't Hoff, J. A., Hauglustaine, D., Pletzer, J., Skowron, A., Grewe, V., Matthes, S., Meuser, M. M., Thor, R. N., and Dedoussi, I. C.: Multi-model assessment of the atmospheric and radiative effects of supersonic transport aircraft, Atmospheric Chemistry and Physics, 25, 2515–2550, doi: 10.5194/acp-25-2515-2025, 2025.

Wang, Z., Bugliaro, L., Gierens, K., Hegglin, M. I., Rohs, S., Petzold, A., Kaufmann, S., and Voigt, C.: Machine learning for improvement of upper tropospheric relative humidity in ERA5 weather model data, EGUsphere [preprint], doi: 10.5194/egusphere-2024-2012, 2024.

Wolf, K., Bellouin, N., and Boucher, O.: Long-term upper-troposphere climatology of potential contrail occurrence over the Paris area derived from radiosonde observations, Atmospheric Chemistry and Physics, 23, 287–309, doi: 10.5194/acp-23-287-2023, 2023a.

Wolf, K., Bellouin, N., Boucher, O., Rohs, S., and Li, Y.: Correction of temperature and relative humidity biases in ERA5 by bivariate quantile mapping: Implications for contrail classification, EGUsphere [preprint], doi: 10.5194/egusphere-2023-2356, 2023b.

Yin, F., Grewe, V., and Gierens, K.: Impact of hybrid-electric aircraft on contrail coverage, Aerospace, 7, 147, doi: 10.3390/aerospace7100147, number: 10, 2020.

Cloud cover.

chasing the summer,
white lines across the sky,
tomorrow's heat.

— LM

5

DEVELOPMENT OF THE OPENAIRCLIM CONTRAIL MODULE

Data and code available at:

Megill, L., Weiß-Rehm, C., Bickel, M., Burkhardt, U. and Grewe, V.: Data and code underlying the development of the OpenAirClim Contrail Module, 4TU.ResearchData, doi: 10.4121/bf6b471a-3dbb-4ba5-b703-518599d51a7f, 2026.

ABSTRACT

Contrail-cirrus is widely recognised as the dominant contributor to anthropogenic radiative forcing from aviation operations. The development and assessment of new fuels, propulsion systems and operational concepts aimed at mitigating the contrail climate impact require transparent, flexible and computationally efficient tools, capable of simulating a wide range of scenarios. This chapter presents a new climatological contrail module for the open-source response model OpenAirClim, developed using simulations from the ECHAM5-CCMod general circulation model. The module calculates contrail-induced changes in global mean radiative forcing based on user-defined emission inventories and aviation scenarios. It supports a broad range of fuels as well as multiple aircraft types within a single inventory, enabling the analysis of multi-fuel and mixed-fleet scenarios. A comparison with literature demonstrates its ability to capture the sensitivity of contrail climate effects to variations in soot emissions and to reproduce saturation behaviour under very high future air traffic scenarios.

5.1. INTRODUCTION

The aviation industry is a significant and growing contributor to anthropogenic climate change, currently responsible for around 3.7 % of anthropogenic Effective Radiative Forcing (Lee et al., 2021, see also Section 2.1). The climate impacts of aviation operations have traditionally been assessed using comprehensive climate models that explicitly resolve physical and chemical processes in the atmosphere. While these models provide a high level of detail, their application is often limited by their high computational intensity (see Chapter 3). As novel fuels, propulsion systems and operational concepts are developed and introduced, there is a need for standardised, open and efficient tools to quantify their influence, independently and within global aviation scenarios.

OpenAirClim is an open-source response model currently under development by an international consortium led by the Institute of Atmospheric Physics at the German Aerospace Center (DLR-PA). It has its roots in the climatological methodology employed by its predecessor AirClim (Grewe and Stenke, 2008; Dahlmann et al., 2016): Rather than simulating physical processes, OpenAirClim uses regressions from the results of more comprehensive climate models and is thus computationally fast and efficient, allowing it to be used in optimisation studies. A general overview of OpenAirClim and its predecessor is provided in Section 3.1.

In this chapter, we introduce a new contrail module for OpenAirClim[1]. The objective of the module is to calculate the changes in the contrail-induced global mean stratospheric-adjusted radiative forcing and surface temperature change due to an input emission inventory and scenario. The challenge in the development of this module is that, unlike AirClim (see Section 3.2.2), it will allow the simulation of inventories and scenarios that include aircraft with varying fuels and propulsion technologies. Such simulations are highly complex due to the impact of emission location (see Chapter 4), saturation effects and the differing optical and radiative properties of contrails produced by alternative fuels.

This chapter continues with a short description of the ECHAM5-CCMod model setup and the simulations that underlie the development of the contrail module (Section 5.2). The development of the module is described in Section 5.3 and subsequently validated against literature in Section 5.4. The sensitivity of the module to various design parameters is explored in Section 5.5, followed by a discussion on the best-suited attribution methodology for contrails (Section 5.6). The results are discussed in Section 5.7 and the chapter concluded in Section 5.8. A concise and abridged overview of the module and its underlying functions is provided in Appendix A.

5.2. ECHAM5-CCMOD MODEL SETUP

The OpenAirClim contrail module is based on simulations using the atmospheric General Circulation Model ECHAM5 (Roeckner et al., 2003, 2006) extended by the Hamburg Aerosol Module (HAM, Stier et al., 2005). The contrail-cirrus parameterisation (CCMod) was initially developed for ECHAM4 by Burkhardt and Kärcher (2009). It introduced a separate cloud class for contrail-cirrus, in addition to naturally occurring cirrus clouds. In CCMod, contrail formation is governed by the Schmidt-Appleman Criterion (see Section 4.2.1); persistence is assumed in cloud-free, ice-supersaturated model grid boxes.

The contrail-cirrus parameterisation has been extended a number of times. Particularly important for the development of the OpenAirClim contrail module, in comparison to its predecessor AirClim (based on Burkhardt and Kärcher, 2009, 2011, see also Section 3.2.2), are the introduction of 1) a microphysical two-moment scheme (Bock and Burkhardt, 2016b); and 2) parameterisations for contrail ice nucleation (Kärcher et al., 2015) and ice crystal survival in the vortex phase (Unterstrasser, 2016; Bier and Burkhardt, 2019, 2022). These improve-

[1]The module is based on ECHAM5-CCMod simulations (see Section 5.2) that, at the time of writing, are not yet publicly available. Section 5.2 thus provides initial context on what simulations were done – for further detail, the reader is directed to the dedicated publications in preparation by Cornelius Weiß-Rehm and Ulrike Burkhardt. The OpenAirClim contrail module, as described in this chapter, will also only be fully integrated into the public repository following these publications. Until then, a reduced-capability version of the module will be available, which uses the methodology described in this section but cannot simulate the low soot regime (see Section 5.3.5).

ments allow the new OpenAirClim module to better describe the impact of soot on the radiative properties of contrail-cirrus.

As described in the following sections, the OpenAirClim contrail module is developed using the results of a series of ECHAM5-CCMod simulations. The simulations are initialised using an estimate of the 2050 atmosphere following SSP2-4.5. The multi-model mean surface temperature and sea ice cover for the year 2050 are taken from CMIP6 model simulations and the CO_2 concentration is increased accordingly. A custom tropopause is introduced, which is based on ERA5 reanalysis data from 1980–2010 and vertically shifted to account for expansion of the troposphere with increasing global temperature. This tropopause definition is used to reduce the cold bias and avoid contrail-cirrus in the stratosphere. A T63 resolution is used, corresponding to 1.875° (latitude) by 1.875° (longitude), with 41 vertical hybrid pressure levels[2].

Two different 3D emission inventories are simulated with CCMod (Figure 5.1): regional only (R) and regional plus short-/medium-range aircraft (R&SMR). The inventories are subsets of the DLR TraK emission inventory in the year 2050 (personal communication Christian Weder), except that the regional aircraft are shifted to slightly higher altitudes following feedback from Airbus. However, only the R&SMR results were ultimately used to develop the OpenAirClim contrail module, because the signal from the regional-only simulations was found to be too weak. The regional simulations are, however, used for validation of the module. The regional aircraft are assumed to have an average wingspan of 27.5 m; R&SMR 35.0 m.

Three fuels are considered: conventional kerosene (hereafter KER), Sustainable Aviation Fuel (SAF) and hydrogen (H_2). Hydrogen can be both combusted (H_2C) and used with a fuel cell (H_2FC). For the sake of simplicity, we refer to the resulting four propulsion system options as "fuels". The specifications of each fuel are given in Table 5.1. The hydrogen fuel cell was not simulated with the R&SMR inventory and was thus not used for the development of the module – only for validation.

Table 5.1: Fuels used in the ECHAM5-CCMod simulations.

Fuel	Inventories	EI_{H_2O}	Q or Δh	η	EI_s
KER	R, R&SMR	$1.24\,kg\,kg^{-1}$	$43.2\,MJ\,kg^{-1}$	0.40	$7.5 \times 10^{14}\,kg^{-1}$
SAF	R, R&SMR	$1.37\,kg\,kg^{-1}$	$44.1\,MJ\,kg^{-1}$	0.40	$2 \times 10^{14}\,kg^{-1}$
H_2C	R, R&SMR	$8.94\,kg\,kg^{-1}$	$120\,MJ\,kg^{-1}$	0.41	$0.0\,kg^{-1}$
H_2FC	R	-	$-241.82\,kJ\,mol^{-1}$	0.40	$0.0\,kg^{-1}$

The response functions developed in this chapter are assumed to be highly non-linear. To obtain a wide range of results to aid in fitting, a series of multipliers (0.3, 0.6, 1, 3, 5) are used on the flown distance in the R and R&SMR inventories.

[2]More detail on this approach will be provided by the upcoming, dedicated publications.

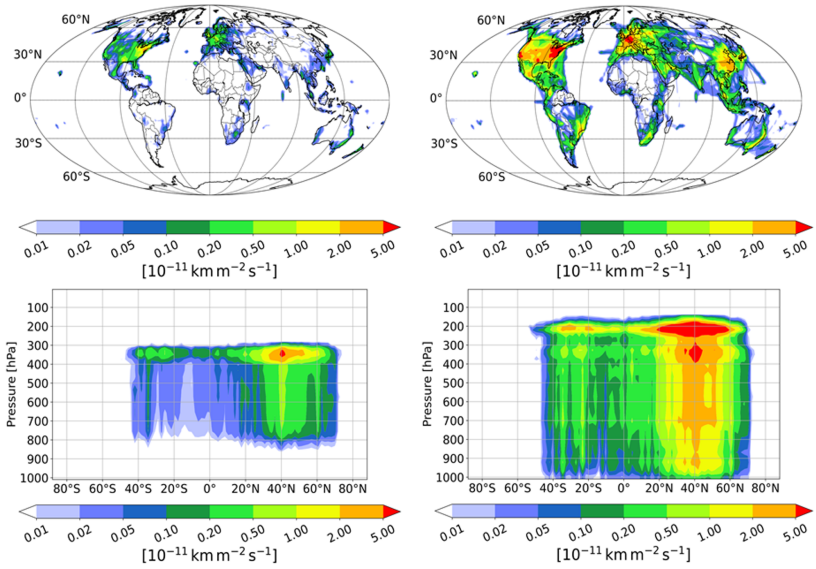


Figure 5.1: Subsets of the DLR TraK inventory used in the ECHAM5-CCMod simulations for the development of the OpenAirClim contrail module. Left: regional aircraft only; right: regional and short-/medium-range aircraft. Plots courtesy of Marius Bickel.

From the 2050 inventories, the multiplier 0.3 approximately corresponds to the year 2000; 0.6 to 2020. Saturation effects were clearly present in the relationship between formation and contrail-cirrus coverage in AirClim (see Figure A.3 of Dahlmann et al., 2016) using the original ECHAM4-CCMod simulations, which used the 2006 atmosphere as a baseline. It is thus expected that the 2050 atmosphere will also show significant saturation and the multiplier 3 and 5 are selected to help describe this effect, as well as further increased air traffic beyond 2050.

The R and R&SMR simulations are not sufficient on their own for the development of the contrail module: Because long-range aircraft are not considered, large areas of high air traffic such as the North Atlantic are not included (Figure 5.1). Due to computational and time limitations, it was not possible to perform dedicated simulations for long-range air traffic. Therefore, the simulations described in this section were complemented by a single, previous simulation with similar initialisation but assuming a 2006 climate and using the global AEDT 2006 inventory (see also Section 3.3). The aircraft definition used for this simulation is identical to KER in Table 5.1, except with $\mathrm{EI_s} = 1.5 \times 10^{15}\,\mathrm{kg^{-1}}$. The AEDT 2006 simulation is used to ensure the RF model is valid also for long-range air traffic (Section 5.3.6; specifically, the results of this simulation are included in Figure 5.9). It is assumed that the difference in climatic conditions is negligible. This setup is, of course, not ideal, even if no discrepancies were found. It is highly recommended for future development of the OpenAirClim contrail module to perform dedicated simulations with global air traffic, including long-range aircraft.

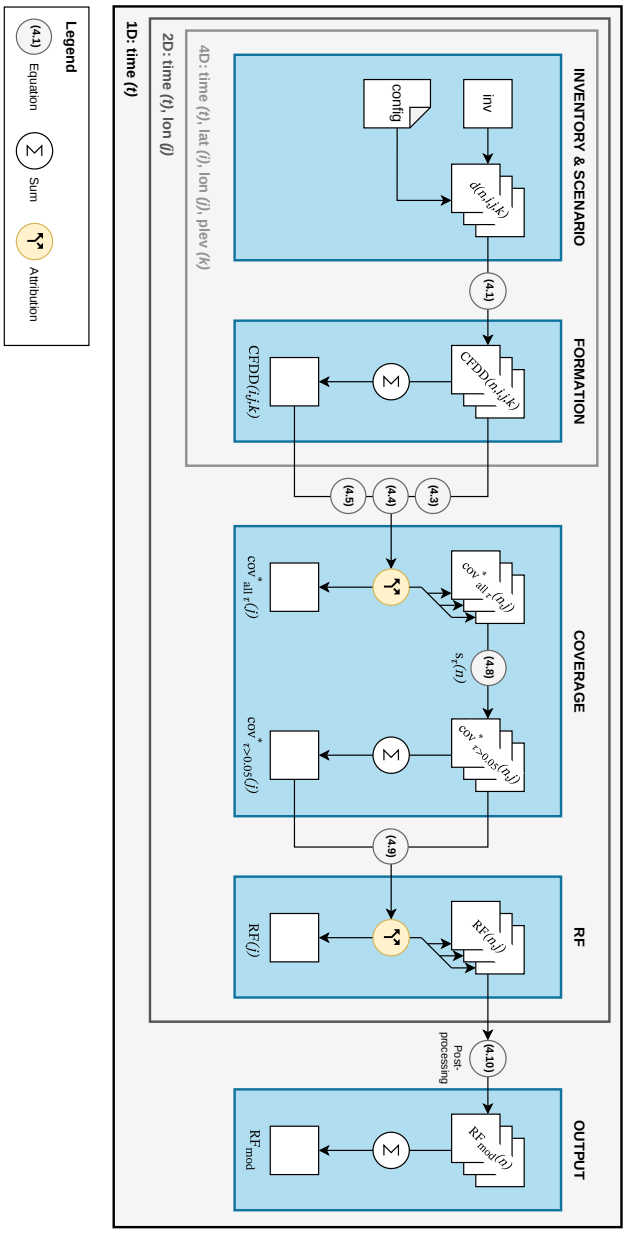


Figure 5.2: Overview of the OpenAirClim Contrail Module.

5.3. MODULE DEVELOPMENT

The objective of the OpenAirClim Contrail Module (oac.cont) is to calculate the changes in the contrail-induced global annual mean stratospheric-adjusted radiative forcing due to an input emission inventory and scenario. The high-level setup is in line with AirClim 2.1 (Dahlmann et al., 2016; Grewe et al., 2017, see also Section 3.2.2) and can be represented as: emission inventory → contrail formation → contrail-cirrus coverage → radiative forcing. A more detailed overview is provided by Figure 5.2.

The section continues with an overview of the development process and philosophy. The four core calculation steps are then described: emission inventory (Section 5.3.2), contrail formation (Section 5.3.3), contrail-cirrus coverage (Section 5.3.4) and contrail RF (Section 5.3.6). We also describe the influence of nvPM emissions (Section 5.3.5) and aircraft size (Section 5.3.7).

5.3.1. DEVELOPMENT PROCESS & STRATEGY

Since OpenAirClim is a response model, it does not aim to independently simulate each physical stage of contrail evolution. The primary objective of the development process is to reproduce the contrail radiative forcing (RF) simulated by ECHAM5-CCMod, as well as its spatial sensitivities, as accurately as possible. The development strategy therefore prioritises consistency with CCMod RF over the independent accuracy of intermediate variables such as contrail formation and contrail-cirrus coverage. These intermediate variables are required to preserve a physically interpretable modelling chain. However, their primary role is to support an accurate and internally consistent estimate of RF, rather than to exactly reproduce CCMod values at each intermediate step.

Figure 5.3 illustrates how this strategy guided the development process. The figure shows the order in which relationships were established during development, not the order of calculations within the operational module (for this, see Figure 5.2). The purple dotted boxes represent inputs (emission inventories) and outputs from the ECHAM5-CCMod simulations. White boxes represent quantities calculated within oac.cont. Development proceeds from both ends of the modelling chain, starting from the emission inventory on one side and the radiative forcing on the other. The intermediate relationships are then constructed in order of the associated labels.

First, ① the climatological relationships identified in Chapter 4 are extended to additional pressure levels and are used to determine the Contrail Flight Distance Density (CFDD), a proxy for contrail formation (see Section 5.3.3). Next, ② analysis of the CCMod simulations (see Section 5.3.6) reveals a robust, fuel-independent relationship between optically thick contrail-cirrus coverage ($\mathrm{cov}_{\tau>0.05}$) and RF. However, the CFDD does not distinguish between the formation of op-

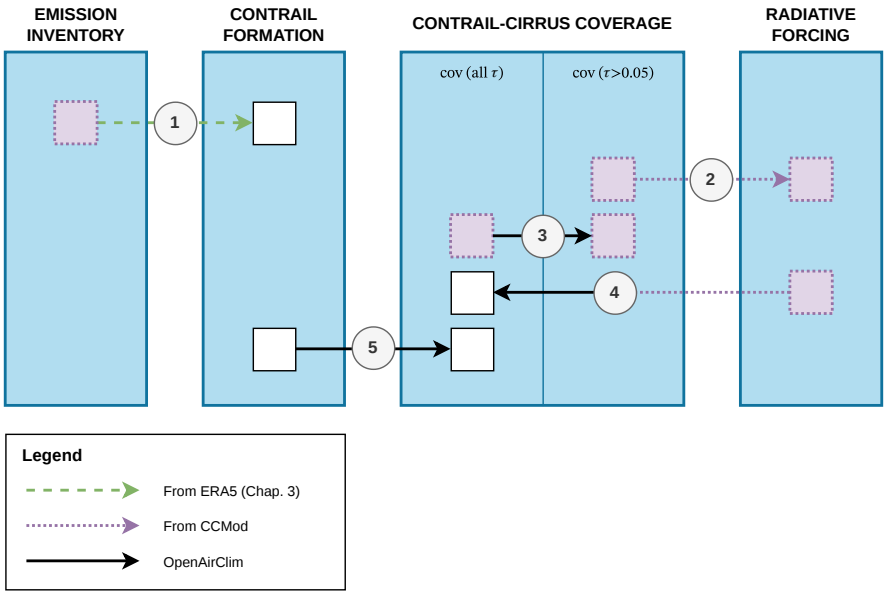


Figure 5.3: Development Process for the OpenAirClim Contrail Module. The purple dotted boxes represent inputs and outputs from the ECHAM5-CCMod simulations; the white boxes quantities calculated by the contrail module. Model development proceeded in order of the labels (circles).

tically thin and optically thick contrails and therefore cannot directly provide $\mathrm{cov}_{\tau>0.05}$. To address this, ③ a relationship is introduced that links total contrail-cirrus coverage (all optical depths, $\mathrm{cov}_{\mathrm{all}\ \tau}$) to $\mathrm{cov}_{\tau>0.05}$ as a function of the soot number emission index (see Section 5.3.5). This relationship is derived from the CCMod simulations and supporting literature.

At this stage, the only remaining unknown relationship is between CFDD and $\mathrm{cov}_{\mathrm{all}\ \tau}$. Rather than determining this relationship independently, which would risk introducing inconsistencies with the RF response, the development proceeds by working backwards from the CCMod RF results. Specifically, ④ the relationships established in steps ② and ③ are inverted and applied to the CCMod RF to derive a fully consistent (hereafter referred to "RF-anchored") estimate of $\mathrm{cov}_{\mathrm{all}\ \tau}$ (white rather than purple dotted box in the figure). This step anchors the intermediate variables directly to the RF response. In this work, the RF-anchored coverage values are denoted with an asterisk (i.e. $\mathrm{cov}^{*}_{\mathrm{all}\ \tau}$ and $\mathrm{cov}^{*}_{\tau>0.05}$). Finally, ⑤ CFDD is linked to the RF-anchored $\mathrm{cov}^{*}_{\mathrm{all}\ \tau}$ (see Section 5.3.4), completing the modelling chain.

This development strategy ensures that the final RF calculated by oac.cont faithfully reproduces the RF response simulated by CCMod. By anchoring the intermediate relationships to the RF response, rather than fitting each step inde-

pendently, the module avoids the propagation of errors through the modelling chain. This approach thus provides a robust, internally consistent and computationally efficient representation of contrail RF.

5.3.2. EMISSION INVENTORY AND SIMULATION CONFIGURATION

The OpenAirClim emission inventory files are in netCDF format and consist of yearly aggregated emission data for each species and corresponding emission locations (latitude, longitude, pressure level). The emission inventories are thus highly flexible: emission data may be provided on either regular or irregular grids. Emission inventories can be provided for multiple different years. OpenAirClim either interpolates between the input emission inventories, or scales the results following a time evolution defined by the user. See the OpenAirClim documentation[3] and the upcoming main OpenAirClim publication for more detail.

For the calculation of the contrail climate impact, the yearly aggregated, 3D-resolved distance flown is required. If multiple aircraft are present within the emission inventory, each entry in the inventory must be accompanied by an identifier (variable `ac` in the netCDF file). The user is free to choose appropriate labels for the inventory in question. For example, the labels could correspond to the aircraft type (e.g. `A320` or `B737`) or to the propulsion technology (e.g. `SAF` or `H2C`). Important is only that all identifiers in the input emission inventories are defined in the simulation configuration – the OpenAirClim documentation provides more detail on how to do this. To calculate a contrail climate impact, the following contrail-relevant parameters must be defined for each identifier:

- G_{250}: Slope of the mixing line G at 250 hPa in Pa K^{-1}. Valid range: ≥ 0.48 Pa K^{-1}. Alternatively, the necessary parameters to calculate the slope can be provided, using equations (1) to (4) in Megill and Grewe (2025). See Section 5.3.3;
- $\mathrm{EI_s}$: Soot number emission index in kg^{-1}. Valid range[4]: ≥ 0.0 kg^{-1}. See Section 5.3.5;
- b: Wing span in m. Valid range (high soot regime only): [20 m, 80 m] (defaults to 35 m). See Section 5.3.7.

Further parameters, such as the fuel sulphur content, could be added in future updates.

5.3.3. CONTRAIL FORMATION

In OpenAirClim, as in AirClim, contrail formation potential is represented using the Contrail Flight Distance Density (CFDD; Dahlmann et al., 2016, see Sec-

[3]Documentation is available at: https://openairclim.org

[4]Until publication of the underlying ECHAM5-CCMod simulation data, the publicly available valid range is limited to $\geq 1.5 \times 10^{14}$ kg^{-1}

tion 3.2.2). However, unlike AirClim, the CFDD is calculated for each fleet n in the emission inventory and in all three spatial dimensions,

$$\mathrm{CFDD}(n,i,j,k) = \frac{d(n,i,j,k)}{A(i,j)} \cdot p_{\mathrm{pcf}}(G_{250}(n),i,j,k) \tag{5.1}$$

where $d(n,i,j,k)$ is the slant (3D) distance flown (km) in each grid box (aircraft, latitude, longitude, pressure level); $A(i,j)$ is the horizontal area of each grid column (km^2); and $p_{\mathrm{pcf}}(G_{250}(n),i,j,k)$ (denoted p_{SAC} in AirClim 2.1) is the probability of persistent contrail formation in each grid box ($\in [0,1]$) for an aircraft n with a Schmidt-Appleman mixing line slope G_{250} at 250 hPa. The pressure level 250 hPa, corresponding to Flight Level 340, or 34000 ft in the International Standard Atmosphere, is chosen as the reference pressure level.

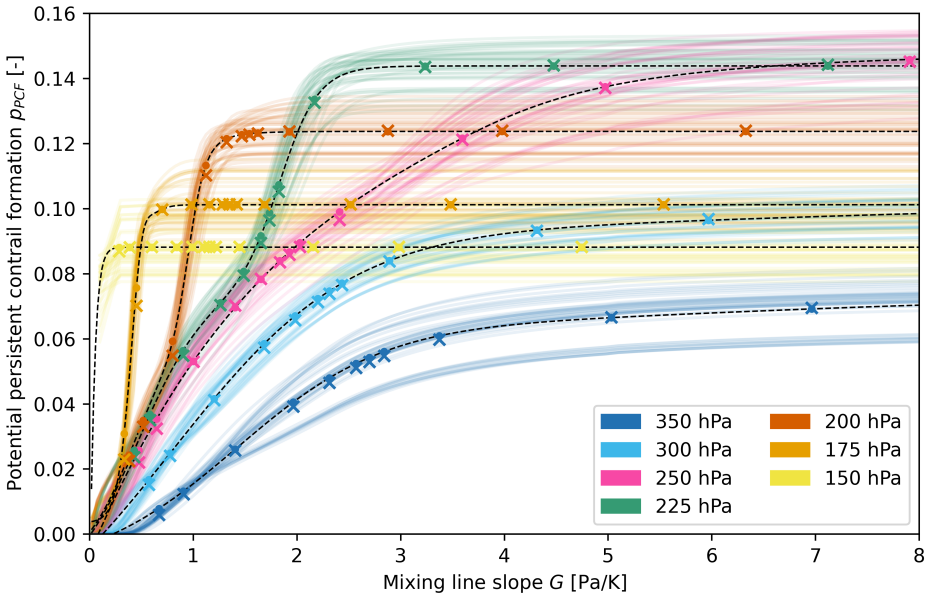


Figure 5.4: Potential persistent contrail formation p_{pcf} as a function of the mixing line slope G on a climatological timescale for pressure levels 350 to 150 hPa. Each coloured line corresponds to the results of a single season within the 2010s, calculated following the Megill and Grewe (2025) method. The logistic fits are shown for each pressure level with dashed, black lines. The markers represent the 3D-resolved p_{pcf} values for each of the 13 aircraft designs, globally averaged: crosses the initial p_{pcf}; dots after scaling to match the fits to enable interpolation.

The p_{pcf} is pre-calculated for 13 aircraft designs with G_{250} values between 0.48 and $15.82\,\mathrm{Pa\,K^{-1}}$. Following the Megill and Grewe (2025) methodology (Chapter 4), the European Centre for Medium-Range Weather Forecasts' (ECMWF) fifth-generation reanalysis dataset (ERA5, Hersbach et al., 2020) is used for this purpose. Specifically, the ambient temperature and relative humidity at 18 pressure

levels between 1000 and 70 hPa in the 2010s (December 2009 to November 2019, inclusive) are considered. The relative humidity is enhanced by a factor $1/0.95$ such that the ERA5 data more closely resembles IAGOS (Petzold et al., 2015) and MOZAIC (Marenco et al., 1998) measurements (see Figure 4.A.4).

Between the pre-calculated values, the 3D-resolved p_{pcf} is interpolated along modified logistic functions of the form,

$$\overline{p_{\mathrm{pcf}}}(G) = \frac{L_1}{1 + \mathrm{e}^{-k_1(G-G_{0,1})}} + \frac{L_2}{1 + \mathrm{e}^{-k_2(G-G_{0,2})}} + d \tag{5.2}$$

where $\overline{p_{\mathrm{pcf}}}$ is the global, area-weighted average p_{pcf}. The fits are shown for select pressure levels in Figure 5.4. All 3D-resolved p_{pcf} values are scaled to fit exactly onto the fit (circular vs. cross markers in Figure 5.4) to enable interpolation. Unlike in Megill and Grewe (2025, see Section 4.3.4), the full function is used for all pressure levels to simplify the methodology. This has very limited effect on the fits compared to that study, because in cases where originally only one logistic function was used, the other logistic function tends towards zero.

In Figure 5.5, we compare the p_{pcf} developed using ERA5 to that found by the underlying ECHAM5-CCMod simulations and the ECHAM4-CCMod (Dahlmann et al., 2016, used in AirClim 2.1) simulations. We note that the ERA5 results make use of a contemporary atmosphere (2010s), whereas the CCMod simulations assumed atmospheric conditions in 2050. Since Megill and Grewe (2025) found that the most limiting factor for all aircraft designs is persistence, p_{pcf} should vary proportionally to the frequency and location of ice supersaturated regions (ISSRs). Previous studies (e.g. Irvine and Shine, 2015; Benetatos et al., 2024) predict future atmospheres to have a generally warmer upper troposphere and generally cooler lower stratosphere. This, in turn, should lead to a decrease in relative humidity – and thus also p_{pcf} – in the tropics and an increase towards the poles. However, this affect is assumed to be small (see e.g. Bock and Burkhardt, 2019).

In general, the results are highly consistent, but there are a few notable differences. In the tropics at high altitudes (200 to 175 hPa), ERA5 predicts a significantly higher potential for persistent contrail formation for all fuels than ECHAM5-CCMod; at 250 to 225 hPa, this is limited to H_2C aircraft. A difference between the ECHAM4-CCMod and ECHAM5-CCMod results can be identified in the extratropics, particularly at pressure levels below 250 hPa. This is because the new ECHAM5-CCMod simulations used a tropopause cut-off (see Section 5.2), assuming that no contrails form in the stratosphere, which was not done in the ECHAM4-CCMod simulations. That AirClim thus overestimated persistent contrail formation in the extratropics was identified by Grewe et al. (2017), who introduced a latitude-dependent correction to the contrail-cirrus coverage.

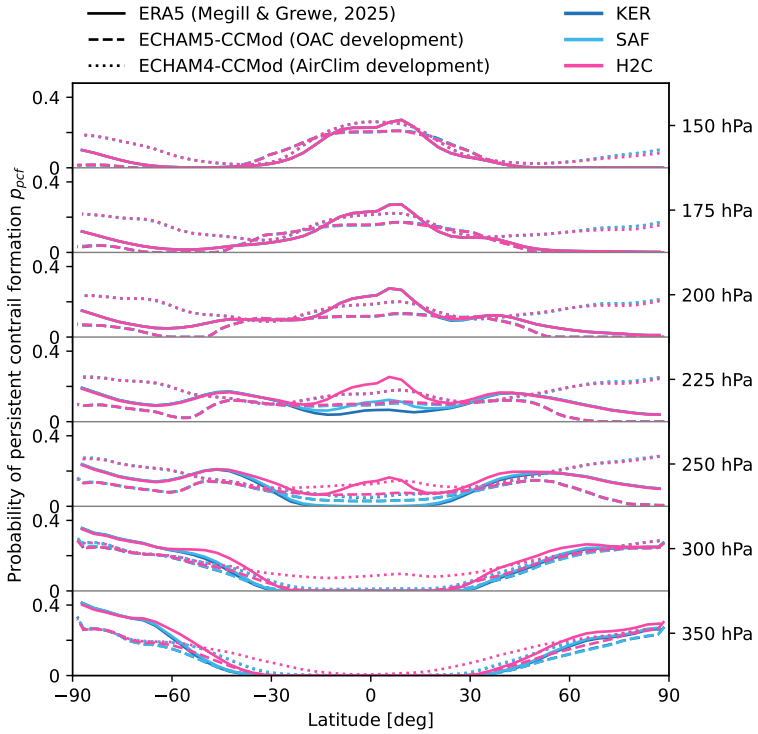


Figure 5.5: Comparison of potential persistent contrail formation determined using ERA5 (solid line), ECHAM5-CCMod (dashed line) and ECHAM4-CCMod (used in AirClim 2.1, dotted line) for the fuels kerosene (KER, dark blue), SAF (light blue) and hydrogen combustion (H2C, pink). Select pressure levels between 350 and 150 hPa are shown for reference.

5.3.4. CONTRAIL-CIRRUS COVERAGE

The relationship between persistent contrail formation and contrail-cirrus coverage is highly complex. Two key challenges arise: first, contrail-cirrus coverage exhibits strongly non-linear saturation behaviour with increasing air traffic; and second, contrails formed by different fuels and propulsion technologies differ substantially in their physical and optical properties. Note that this section follows the physical pathway from emissions to RF, but that the development strategy (see Section 5.3.1) requires references to later sections to motivate certain modelling decisions.

The ECHAM5-CCMod simulations provide three measures of contrail-cirrus coverage: total coverage across all optical depths ($\mathrm{cov}_{\mathrm{all}\ \tau}$), moderate optical depth coverage ($\mathrm{cov}_{\tau>0.02}$) and optically thick coverage ($\mathrm{cov}_{\tau>0.05}$). The optical depth is defined with respect to $550\,\mathrm{nm}$. As discussed in Section 5.3.6, $\mathrm{cov}_{\tau>0.05}$ exhibits the most robust and direct relationship with radiative forcing and therefore

serves as the intermediate variable linking contrail-cirrus coverage to RF within oac.cont. However, the CFDD represents only the climatological potential for persistent contrail formation and does not contain information about the resulting distribution of optical depth. It is therefore not possible to derive $\mathrm{cov}_{\tau>0.05}$ directly from CFDD without introducing an explicit parameterisation of optical depth (see Section 5.3.5).

As outlined in the development strategy (Section 5.3.1), oac.cont is constructed such that intermediate variables support an RF estimate that is internally consistent with the CCMod response ("RF-anchored"). To achieve this, we work backwards from the RF, inverting the relationship between $\mathrm{cov}_{\tau>0.05}$ and RF (Section 5.3.6) and dividing by the soot-dependent scaling factor for optical depth s_τ (Section 5.3.5). This yields an estimate for the total contrail-cirrus coverage across all optical depths, denoted here as $\mathrm{cov}^*_{\mathrm{all}\ \tau}$. The benefit of this approach is that it preserves physical interpretability whilst maintaining consistency for the RF. Figure 5.A.1 compares the RF-anchored coverage values to those from CCMod.

In order to find the best fit function between CFDD and $\mathrm{cov}^*_{\mathrm{all}\ \tau}$, a set of candidate saturation-type base functions are identified (Table 5.A.2). For each candidate function, optimal parameters are found by minimising the sum of squared residuals, using uniform weighting and the Nelder-Mead minimisation algorithm in `scipy`. The best-performing candidate function is defined as the one with the lowest total sum of squared residuals across all fuels. This is found to be Function 30, which uses a hyperbolic tangent of the form,

$$\mathrm{cov}^*_{\mathrm{all}\ \tau}(n,i,j,k) = a \cdot \tanh\left(b \cdot \mathrm{CFDD}(n,i,j,k)\right) \tag{5.3}$$

where parameter $a = 0.0772$ controls the asymptotic maximum coverage and $b = 132.3\,\mathrm{km}$ the sensitivity to the CFDD. The coverage is then combined vertically using a random overlap assumption, i.e. assuming statistical independence between vertical layers k,

$$\mathrm{cov}^*_{\mathrm{all}\ \tau}(n,i,j) = 1 - \prod_k \left(1 - \mathrm{cov}^*_{\mathrm{all}\ \tau}(n,i,j,k)\right) \tag{5.4}$$

and then area-weighted over the latitude i,

$$\mathrm{cov}^*_{\mathrm{all}\ \tau}(n,j) = \frac{\sum_i \mathrm{cov}^*_{\mathrm{all}\ \tau}(n,i,j) \cdot A(i,j)}{\sum_i A(i,j)} \tag{5.5}$$

The predicted and RF-anchored contrail-cirrus coverage are compared for Function 30 in Figure 5.6. The fit yields a high coefficient of determination ($R^2 = 0.8746$) with a standard deviation of $\sigma = 0.22\,\%$ (of area-weighted $\mathrm{cov}^*_{\mathrm{all}\ \tau}$), indicating that the model captures the saturation response well. The gray region in the

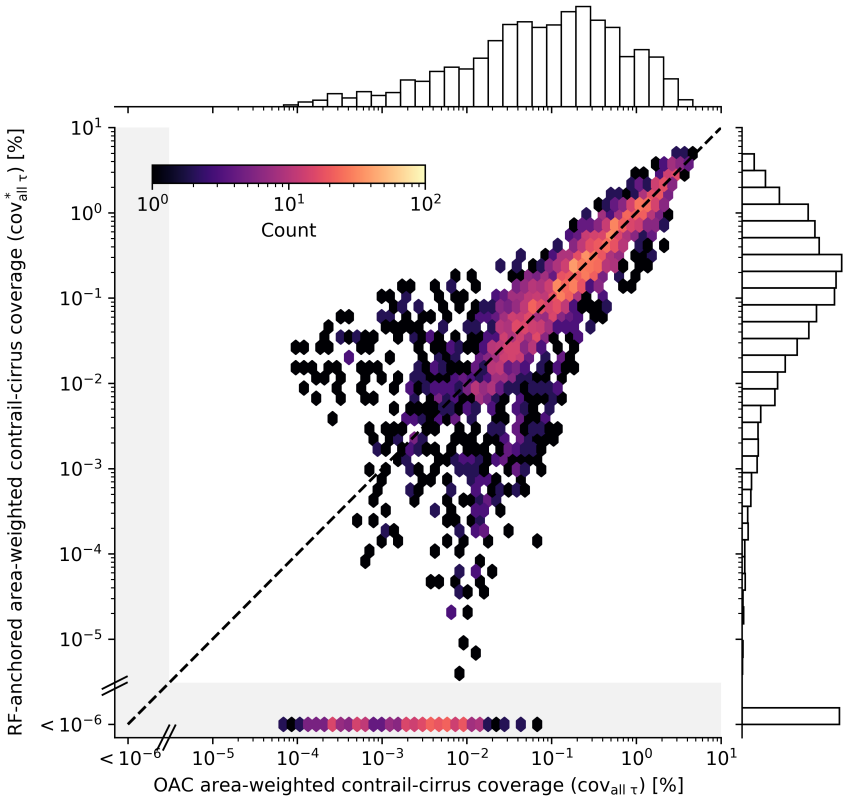


Figure 5.6: Performance of contrail-cirrus coverage function 30. The area-weighted contrail-cirrus coverage (all τ) calculated by Function 30 (x-axis) for all fuels compared to CCMod (y-axis). The gray area corresponds to values below 10^{-6} %. The values in the lower part of the plot are where the model calculates a contrail-cirrus coverage that was not present in the CCMod results.

figure corresponds to values below 10^{-6} %. In a small number of cases, the model predicts non-zero coverage where CCMod expected zero coverage. This likely results from difference in p_{pcf} between OpenAirClim and CCMod, in particular the stratosphere cut-off assumption applied in the the CCMod simulations (see Section 5.2). These spurious coverages are typically below 0.02 % and therefore have a negligible influence on RF.

5.3.5. INFLUENCE OF PARTICLE EMISSIONS

The number and size of contrail ice crystals play a central role in determining the optical and radiative properties of contrail-cirrus. For conventional, rich-quench-lean (RQL) engines, soot particles dominate contrail ice nucleation (Kleine et al., 2018). However, as low-soot technologies such as lean burn engines

(Voigt et al., 2026) and alternative aviation fuels such as SAF (Voigt et al., 2021; Märkl et al., 2024; Dischl et al., 2025) and hydrogen (Bier et al., 2024; Zink et al., 2025) are introduced, the relative importance of other aerosols within the exhaust plume increases. Further background is provided in Section 2.2.

Previous studies (e.g. Burkhardt et al., 2018; Bier and Burkhardt, 2022; Märkl et al., 2024; Rubin-Zuzic et al., 2025) demonstrate a strongly non-linear dependence between soot number emissions and contrail radiative forcing. To account for this, an "RF reduction factor" was introduced to AirClim 2.1 (Grewe et al., 2021) that was based on the relationship identified by Burkhardt et al. (2018, their Figure 1f),

$$\Delta RF^{\mathrm{contr}} = \frac{\arctan\left(1.9 \cdot x^{0.74}\right)}{\arctan(1.9)} \tag{5.6}$$

where x denotes the soot number emission index relative to the reference value $1.5 \times 10^{15}\,\mathrm{kg}^{-1}$. A lower bound of $x = 0.1$ was imposed, corresponding to the approximate limit of the soot-rich regime (Grewe et al., 2021). However, these earlier simulations did not explicitly model contrail ice nucleation and survival in the vortex phase. Instead, the contrail ice number concentration and plume cross sectional area were prescribed based on measurements. Subsequent work by Bier and Burkhardt (2022) found that this approach likely overestimates ice crystal number concentrations compared to simulations that explicitly represent microphysical processes.

As shown in Section 5.3.6 (see in particular Figure 5.8), the relationship between optically thick contrail-cirrus coverage $\mathrm{cov}_{\tau>0.05}$ and RF is largely independent of fuel type. Instead, reduced soot emissions primarily influence the optical depth distribution of contrail-cirrus, resulting in a smaller fraction of optically thick coverage. This motivates the introduction of a scaling factor s_τ, which represents the fraction of total contrail-cirrus coverage that is optically thick. This factor enables the conversion between the total coverage $\mathrm{cov}_{\mathrm{all}\ \tau}$ and optically thick coverage $\mathrm{cov}_{\tau>0.05}$ as a function of soot emissions.

We distinguish between the high- and low-soot regimes. In the high-soot regime ($x \geq x_0$, where $x_0 = 0.1$), a single empirical fit with a similar form to AirClim is derived from literature. In the low-soot regime ($0 < x < x_0$), the relationship is uncertain. To capture a range of plausible behaviours, we introduce a composite logistic-beta function with three low-soot cases that smoothly connects the low- and high-soot regimes at x_0. The function is shown in Figure 5.7 against the CCMod results and literature. Mathematically, it is defined as[5],

[5]For clarity, the argument (x) is omitted from u.

$$s_\tau(x) = \begin{cases} 0.91 \cdot \arctan\left(1.96 \cdot x^{0.58}\right) & \text{for } x \geq 0.1 \\ c_0 + (y_0 - c_0) \cdot w(x) - d \cdot h(x) & \text{for } 0 < x < 0.1 \\ 0.385 & \text{for } x = 0 \end{cases}$$

$$w(x) = \frac{2\,u^k}{1 + u^k}, \quad \text{where } u = \frac{x}{x_0} \tag{5.7}$$

$$h(x) = u^p \cdot (1 - u)$$

$$d = x_0 \left(y_0' - \frac{1}{2}(y_0 - c_0) \cdot \frac{k}{x_0} \right)$$

where $c_0 = \lim_{x \to 0^+} s_\tau(x)$ is the value as x approaches 0 for a given case, $y_0 = s_\tau(x_0)$ is the value of the high-soot fit at the transition point and y_0' is its derivative (also at x_0).

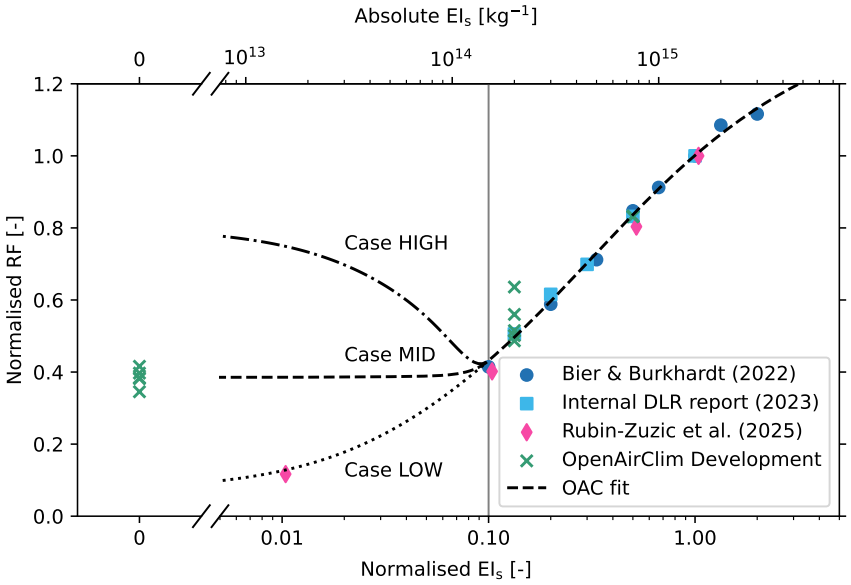


Figure 5.7: Normalised RF as a function of the soot number emission index. The high-soot regime is modelled using a single fit; the low-soot regime with three different cases. Case MID is used by default in OpenAirClim. At zero soot emissions (hydrogen), a single normalised RF is assumed, as described in the text.

The function is constructed such that both the value and gradient are continuous at the transition point x_0, ensuring a smooth attachment between the low- and high-soot regimes. At exactly $x = 0$, corresponding to hydrogen combustion with zero soot emissions, $s_\tau = 0.385$ based on the CCMod simulation results. The parameter c_0 therefore describes the limiting behaviour as $x \to 0^+$, while the

discrete value at $x = 0$ is imposed independently.

The transition function w controls the monotonic transition between the limiting value c_0 and the transition point y_0, while the term involving h introduces a local curvature adjustment near x_0, allowing the gradient of the composite function to match that of the high-soot fit. The parameters k and p control the steepness of the transition and the shape of the curvature adjustment, respectively.

Three sets of parameters are implemented at the time of writing, shown in Table 5.2. Case MID aligns with the hydrogen simulations as $x \to 0$ and is currently used by default by oac.cont. Cases LOW and HIGH are designed to define lower and upper boundaries, following Rubin-Zuzic et al. (2025) and Voigt et al. (2026) respectively. Further work is required to better constrain the low-soot regime. Once in-situ measurement and dedicated modelling data are available, the cases can easily be adapted accordingly.

Table 5.2: Parameters for the low-soot regime modelling cases.

	c_0	k	p
Case MID	0.385	2.0	2.5
Case LOW	0.08	1.0	0.3
Case HIGH	0.8	3.5	1.2

Finally, for a given aircraft n, the RF-anchored total contrail-cirrus coverage $\mathrm{cov}^*_{\mathrm{all}\ \tau}$ is converted to optically thick coverage $\mathrm{cov}^*_{\tau>0.05}$ using the scaling factor,

$$\mathrm{cov}^*_{\tau>0.05}(n, j) = \mathrm{cov}^*_{\mathrm{all}\ \tau}(n, j) \cdot s_\tau(n) \tag{5.8}$$

5.3.6. RADIATIVE FORCING

The relationship between contrail-cirrus coverage and radiative forcing (RF) and its dependence on fuel type is shown in Figure 5.8. Consistent with previous studies (Bock and Burkhardt, 2019), the total coverage $\mathrm{cov}_{\mathrm{all}\ \tau}$ varies only weakly between fuels, but the effect on RF is high due to differences in optical depth. Comparing the top and bottom panels shows that hydrogen-powered aircraft tend to produce contrails with smaller optical depths. This is likely coupled with a shorter lifetime (e.g. Lottermoser and Unterstrasser, 2026), but this cannot be deduced from these results. The RF is thus lower for hydrogen-powered aircraft than for those powered by kerosene and SAF.

The relationship between coverage and RF becomes both more linear and less dependent on fuel type when considering optically thick coverage alone (bottom panel of Figure 5.8). Therefore, $\mathrm{cov}_{\tau>0.05}$ provides the most robust predictor of RF within the modelling framework. The relationship between $\mathrm{cov}_{\tau>0.05}$ and RF is shown in more detail in Figure 5.9. For reference, the globally area-weighted re-

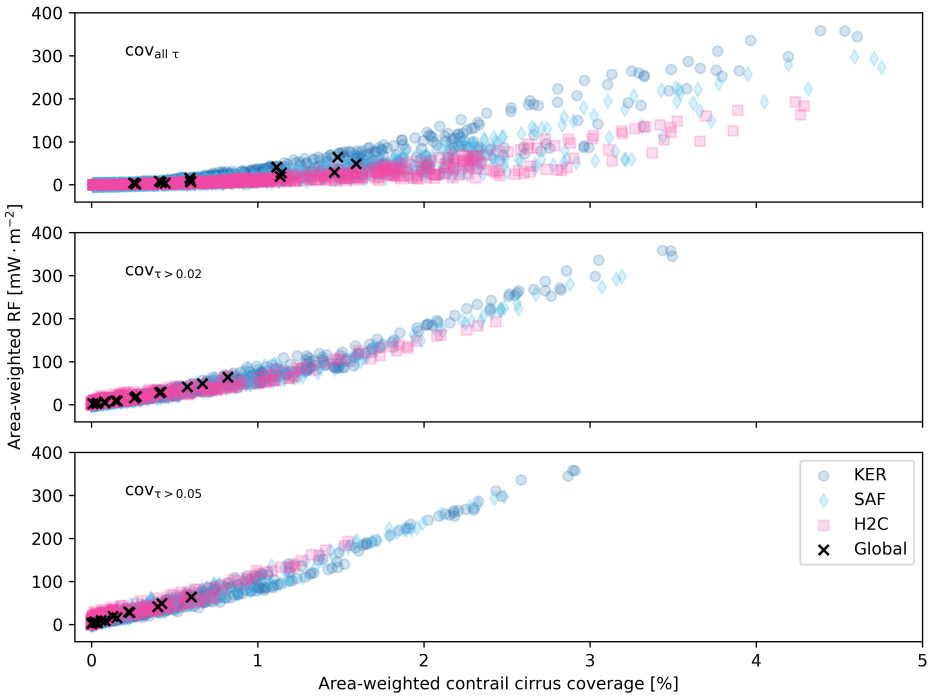


Figure 5.8: Relationship between contrail-cirrus coverage and RF from the ECHAM5-CCMod simulations. $cov_{all\ \tau}$ (3D) is defined also in pressure level; the remaining coverages are randomly overlapped. As only optically thicker contrails are considered, the relationship between the contrail-cirrus coverage and radiative forcing becomes less fuel-dependent.

sults are shown for each fuel and multiplier (crosses) alongside results from previous global studies (circles). Because the regional and short-/medium-range inventories do not represent long-range air traffic, the CCMod data is supplemented with results from a global simulation using the AEDT 2006 emission inventory (see Section 5.2).

A clear regional dependence is observed. For a given coverage, contrails formed over North America generally produce a larger RF than those formed over Europe or Asia. Consequently, although the global fit (dashed line) has a high degree of accuracy, it is dominated by regions with higher coverage and RF. This could become relevant for scenario analyses restricted to specific geographic regions.

To account for this regional dependence, separate relationships are derived between $cov_{\tau>0.05}$ and RF for four regions defined by longitude (see also Supplementary Figure 5.A.2): Americas (235, 330]; Europe, Middle-East and Africa (330, 60]; Asia and Australia (60, 160]; and Pacific (160, 235]. Within each region, RF is determined using a power-law relationship of the form,

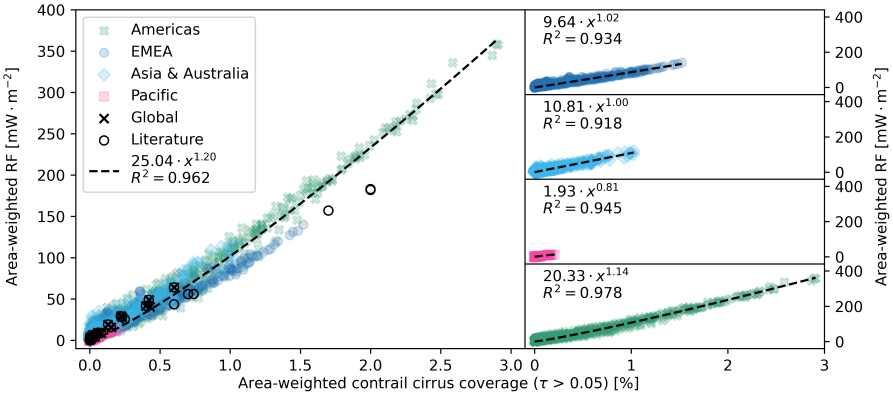


Figure 5.9: Area-weighted (latitude) contrail-cirrus coverage vs. Radiative Forcing. The results from Bock and Burkhardt (2016a, 2019); Bier and Burkhardt (2022) are shown for comparison ("Literature").

$$\mathrm{RF}(j) = c_j \cdot \mathrm{cov}^*_{\tau>0.05}(j)^{\gamma_j} \tag{5.9}$$

where $\mathrm{cov}^*_{\tau>0.05}(j)$ is the area-weighted optically thick RF-anchored contrail-cirrus coverage (see Section 5.3.1) for longitude band j, and c_j and γ_j are region-specific fit parameters (derived using the CCMod simulation results). These fits achieve high coefficients of determination (R^2), but the range of validity differs depending on the region due to data availability (see the right side of Figure 5.9). OpenAirClim therefore checks whether input coverage values fall outside the fitted range and issues a warning if extrapolation occurs. The Pacific region in particular (pink squares) would benefit from additional, dedicated simulations to improve fit robustness.

By default, OpenAirClim applies these regional parameterisations. Because the model grid uses equal longitudinal spacing, each band contributes equally to the global mean RF. The global RF is thus simply the mean of $\mathrm{RF}(j)$. Finally, the global RF is attributed to each fleet n in the emission inventory. This procedure is described in Section 5.6.

5.3.7. DEPENDENCE ON AIRCRAFT SIZE

The ice crystal number and thus contrail optical depth depends on the fuel flow and properties of the wake vortex, which in turn depends on the aircraft type and size. Large aircraft tend to produce contrails with a higher number of ice crystals, resulting in overall deeper contrails (Unterstrasser and Görsch, 2014). To account for this, we apply a simple post-processing on the RF presented by Bruder et al.

(2026, see their Supplementary Section S1),

$$\mathrm{RF}_{\mathrm{mod}}(n) = \mathrm{RF}(n) \cdot \frac{\upsilon + w \cdot b(n)}{\upsilon + w \cdot b_{\mathrm{ref}}} \tag{5.10}$$

where $b(n) \in [20\ \mathrm{m}, 80\ \mathrm{m}]$ is the wingspan of fleet n. Since the ECHAM5-CCMod simulations for TraK-SMR assume a wingspan b of 35 m, we use this value as the reference wingspan b_{ref}, rather than 38 m used by Bruder et al. (2026). We keep $w = 0.0287\ \mathrm{m}^{-1}$ the same and thus update υ to $0.43 \cdot {}^{35}/_{38} \approx 0.396$. If no wingspan is given, OpenAirClim defaults to $b_{\mathrm{ref}} = 35\ \mathrm{m}$.

This dependence has a number of caveats. The post-processing is based on a very limited number of LES simulations: Only three different atmospheric scenarios were studied for aircraft using conventional kerosene – the soot number emission index was not varied. For hydrogen-powered aircraft with fewer contrail ice crystals, the response may differ significantly. Therefore, the correction is not applied in the low-soot regime ($b(n)$ is assumed to be equal to b_{ref}). The dependence also assumes a single relationship between the fuel flow and wingspan, which is not necessarily representative of all aircraft.

Future work should focus on performing LES and GCM studies for different initial contrails, in additional atmospheric scenarios and for a wider range of aircraft design parameters, covering all sizes and fuels. It should also be investigated whether such a correction can be applied at an earlier stage – rather than a post-processing of RF – since ideally, the change in optical depth should be accounted for in the contrail-cirrus coverage.

5.4. VALIDATION

This section validates the OpenAirClim contrail module against published estimates of global annual-mean contrail RF across a range of emission inventories and traffic levels. Consistent with the development strategy (Section 5.3.1), the validation focuses on global (and where available, regional) mean RF. The studies used for comparison with the OpenAirClim contrail module are compiled in Table 5.A.1 with the relevant input parameters for OpenAirClim. A detailed overview of the data, including the assumptions made where data was missing or not reported, is available as an Excel spreadsheet in the linked dataset.

To place published studies on a comparable scale, we introduce a modified soot number emission index $EI_{\mathrm{s,mod}}$. Earlier CCMod studies (notably Bock and Burkhardt, 2016a; Burkhardt et al., 2018; Bock and Burkhardt, 2019) prescribed the initial contrail ice number concentration n_{co} and contrail cross sectional area A_{co} from observations, rather than resolving variability in the jet and vortex phases. This led to substantially higher post-vortex ice crystal numbers

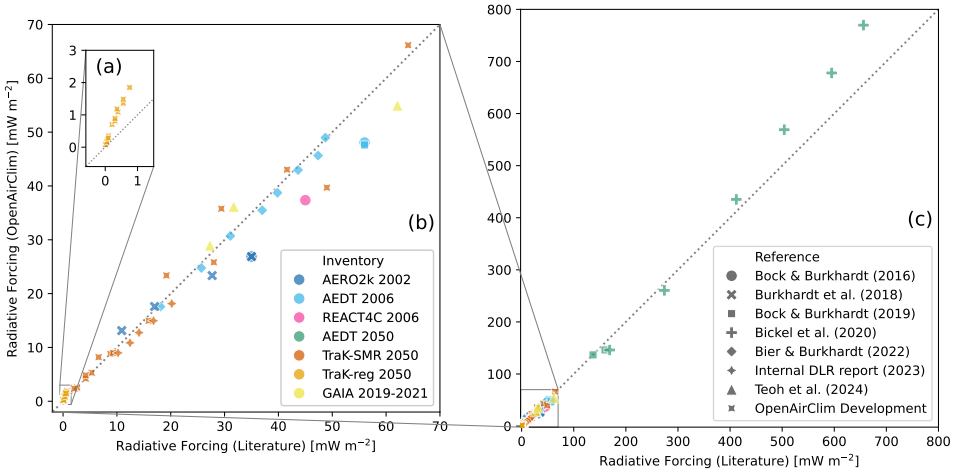


Figure 5.10: Comparison of global RF from literature and calculated using the OpenAirClim contrail module. The colours correspond to the emission inventories used, the marker shapes to the reference. "OpenAirClim Development" refers to the ECHAM5-CCMod simulations underlying the contrail module.

5

N_{ice} than in newer CCMod configurations. For these earlier studies, we therefore adjust the reported $\mathrm{EI_s}$ to an effective value $EI_{\mathrm{s,mod}}$ using a linear relationship between $\mathrm{EI_s}$ and N_{ice} derived from Bier and Burkhardt (2022). This adjustment is applied only in the high-soot regime, where it is expected to be adequate (see also Section 5.3.5). We note that this procedure is an approximation intended to improve cross-study comparability, it is not generally valid and should not be used in lieu of updated microphysics.

Figure 5.10 compares published global annual-mean contrail RF to the RF computed by the OpenAirClim contrail module for the corresponding inventory and input parameter assumptions. Panel (a) shows regional air traffic; (b) present-day air traffic and the range of the CCMod simulations that were used to develop the contrail module ($< 64.1\,\mathrm{mW\,m^{-2}}$); and (c) increased, future air traffic.

Overall, the module shows good agreement with the literature. The module reflects simulations with the inventory that was used to develop it very well (TraK-SMR 2050). It also shows good agreement against Bier and Burkhardt (2022) using the AEDT 2006 (slant distance) inventory. Agreement is weaker for older CCMod studies (Bock and Burkhardt, 2016a; Burkhardt et al., 2018; Bock and Burkhardt, 2019), which likely reflects differences in the treatment of the initial conditions and the approximate nature of the $EI_{\mathrm{s,mod}}$ adjustment. Comparisons to non-CCMod studies are currently limited by a lack of openly available inventory data. Nevertheless, the comparison to Teoh et al. (2024) (pycontrails and GAIA inventory, see Sections 3.2 and 3.3) suggests broadly consistent global mean RF magnitudes. A more in-depth comparison between OpenAirClim and

pycontrails at the yearly-aggregated or climatological level would be a useful and interesting next research step.

In Figure 5.10(c), we test the performance of the contrail module at (very) high levels of air traffic using the AEDT 2050 inventory. Because the wingspan of this inventory is not reported, we assume $b = 50\,\mathrm{m}$ for consistency with AEDT 2006. Bock and Burkhardt (2019) estimate $160\,\mathrm{mW\,m^{-2}}$ for air traffic in the year 2050. Bickel et al. (2020) then scale this emission inventory by up to 12 times to better understand saturation effects. Since not much information is available about their simulation setup, we assume an identical simulation setup to Bock and Burkhardt (2019). OpenAirClim seems to capture the RF response well until 4 times the AEDT 2050 air traffic (around $400\,\mathrm{mW\,m^{-2}}$); for larger multipliers, the module overestimates RF relative to CCMod, suggesting that saturation behaviour is not fully captured by the current parameterisations at this level of air traffic.

For regional-only air traffic inventories (TraK-reg 2050), the module reproduces the general response seen in the ECHAM5-CCMod simulations, but tends to estimate larger RF values (Figure 5.10(a)). In fact, the module is highly sensitive to these inventories, as Figure 5.11 shows. Here, the various emission inventories are modified by increasing or decreasing all emission altitudes by 2000 ft. The RF values are normalised with respect to the RF of the original, unmodified inventory. The pink points correspond to the ECHAM4-CCMod response using the REACT4C inventory, reported by Matthes et al. (2021): OpenAirClim has similar, if somewhat higher, sensitivity to the cruise altitude. At regional cruise altitudes and below, the sensitivity of the module is substantially higher, demonstrated by the larger slope. This behaviour is expected, since the p_{pcf} substantially reduces with reducing altitude (increasing pressure level).

OpenAirClim estimates lower contrail RF than its predecessor AirClim, as demonstrated in Figure 5.12(a). This is expected behaviour, because AirClim was based on simulations with ECHAM4-CCMod (Dahlmann et al., 2016) and OpenAirClim on a recent version of ECHAM5-CCMod which parametrises microphysical processes in the jet and vortex phase (Bier and Burkhardt, 2022). As discussed in Section 5.3.5, this latter study showed that previous CCMod simulations likely significantly overestimated the ice crystal number, leading to an overestimation of the RF for the same $\mathrm{EI_s}$.

The relative RF as a function of $\mathrm{EI_s}$ is compared in Figure 5.12(b) for both AirClim and OpenAirClim. Note that $1 \times 10^{15}\,\mathrm{kg^{-1}}$ is used as the reference, which corresponds to the reference used for AirClim (see Burkhardt et al., 2018; Grewe et al., 2021) – OpenAirClim uses the reference value $1.5 \times 10^{15}\,\mathrm{kg^{-1}}$ to align with the CCMod simulations with which it is built. The responses are generally similar, but OpenAirClim's response is less steep as the soot number reduces. The low soot regime begins at $1.5 \times 10^{14}\,\mathrm{kg^{-1}}$, below which AirClim is not defined and OpenAirClim uses three cases, as described in Section 5.3.5 – this regime can thus not be compared.

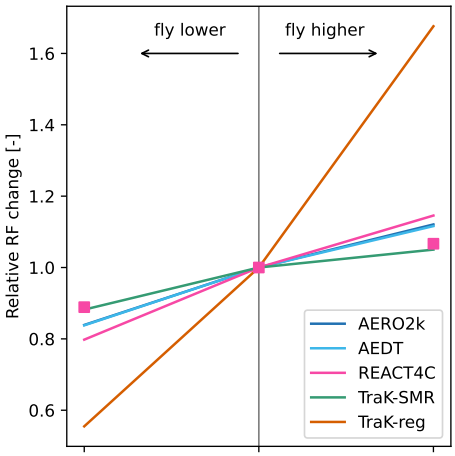


Figure 5.11: Sensitivity of OpenAirClim to changes in cruise altitude. Shown is the change in normalised RF when the aircraft in each emission inventory are assumed to fly 2000 ft higher or lower. The pink squares correspond to the ECHAM4-CCMod response to the REACT4C inventory, as found by Matthes et al. (2021).

To compare the contrail module to other modelling results, we calculate a best estimate for the global mean contrail RF for 2018. The widely cited estimate of $111.4\ (33, 189)\ \mathrm{mW\,m^{-2}}$ from Lee et al. (2021) relies on the AEDT 2006 inventory and a linear scaling approach (see Sections 3.3 and 5.4) that is simplified and uncertain. Here, we instead uniformly scale the AERO2k 2002, REACT4C 2006, ELK 2019 and DEPA 2050 (2020) emission inventories to the 2018 global flown distance of $5.26\times10^{10}\ \mathrm{km}$ reported by Lee et al. (2021). We assume $G_{250} = 1.84$ (overall propulsion efficiency of 0.37), $\mathrm{EI_s} = 1.5 \times 10^{15}\ \mathrm{kg^{-1}}$ and wingspan $b = 50\ \mathrm{m}$ to be representative of current air traffic. OpenAirClim estimates 42.3, 48.4, 58.7 and $45.4\ \mathrm{mW\,m^{-2}}$ for each emission inventory respectively, on average $48.7\ \mathrm{mW\,m^{-2}}$. This is substantially lower than the central estimate in Lee et al. (2021), but consistent with other recent assessments that suggest lower contrail RF values (e.g. Teoh et al., 2024). As expected (see Section 3.3), the ELK inventory produces a greater RF value since it has a larger proportion of air traffic at higher altitudes, where the likelihood of persistent contrail formation is larger.

5.5. SENSITIVITY TO DESIGN PARAMETERS

To assess the response of the contrail module to key aircraft design parameters, we evaluate its sensitivity to variations in the Schmidt-Appleman mixing line slope G_{250} and soot number emission index $\mathrm{EI_s}$. Figure 5.13 shows the global RF calculated using the 2020 emission inventory from DEPA 2050 for a range of G_{250} and $\mathrm{EI_s}$ values. The black cross indicates a representative, contempo-

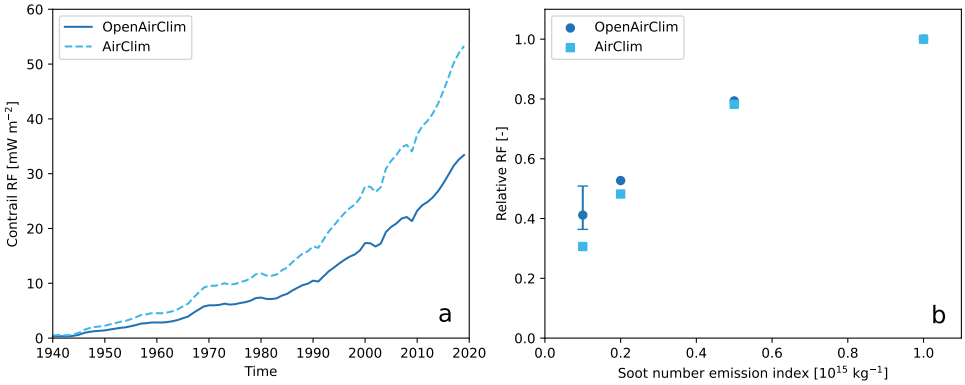


Figure 5.12: Comparison between the AirClim and OpenAirClim contrail modules. (a) RF over time following a historical scenario with the AERO2k emission inventory for a conventional, kerosene-powered aircraft with $\eta = 0.3$, $\mathrm{EI_s} = 1 \times 10^{15}\,\mathrm{kg^{-1}}$ and $b = 50\,\mathrm{m}$; (b) Relative RF in the year 2019 as a function of $\mathrm{EI_s}$. OpenAirClim has an error bar corresponding to the values for the three low soot cases.

5

rary kerosene-powered aircraft ($\eta = 0.37$, $\mathrm{EI_s} = 1.5 \times 10^{15}\,\mathrm{kg^{-1}}$). The upper axis shows the G_{250} values of selected aircraft designs (Table 4.1) for reference. The dashed line demarcates the boundary between the high- and low-soot regimes, following Figure 5.7.

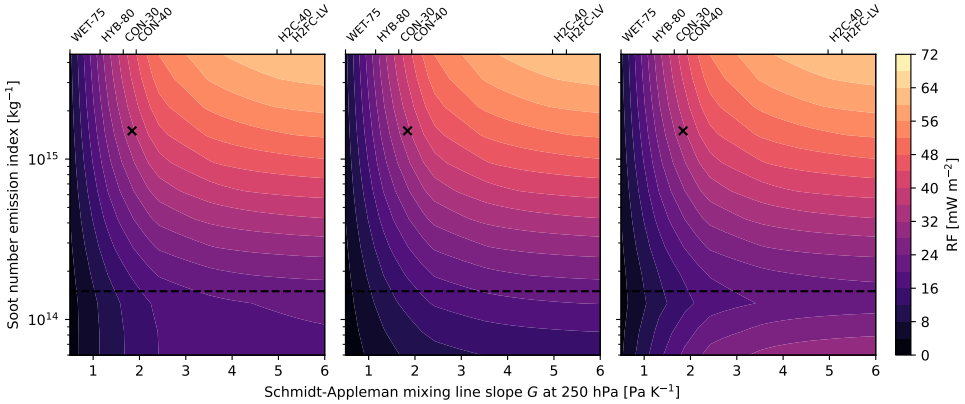


Figure 5.13: Sensitivity of the OpenAirClim contrail module to two aircraft design parameters. From left to right: low-soot regime cases MID, LOW, HIGH. The black cross represents a typical contemporary conventional kerosene-powered aircraft (see text). The dashed line demarcates the boundary between the high- and low-soot regimes.

The results show a strong sensitivity to G_{250} at present-day values (black cross). Reducing G, for example by introducing hybrid-electric propulsion systems or by actively reducing the water vapour emission index (WET concept), is highly effective at lowering expected RF. The opposite is also true: raising G, for example by

increasing η, results in higher RF. Reducing $\mathrm{EI_s}$ is effective at reducing RF within the high-soot regime, but its behaviour in the low-soot regime is uncertain (see Section 5.3.5). These behaviours are consistent with the underlying CCMod simulations and confirm that the module reproduces the expected physical sensitivities to aircraft propulsion efficiency and soot emissions.

5.6. CONTRAIL ATTRIBUTION

A key capability of OpenAirClim is the simulation of emission inventories and scenarios containing multiple aircraft types and aviation fuels. Because the relationships between contrail formation, contrail-cirrus coverage and radiative forcing are non-linear, determining the relative contribution of each aircraft or fuel at each step is not trivial. Quantifying the relative contributions thus requires the use of an attribution method. A more detailed background on attribution is provided in Section 3.4. An overview of the attribution methods currently implemented into OpenAirClim is available in the online documentation[6].

The full module setup is shown in Figure 5.2. OpenAirClim allows emission inventories containing multiple so-called aircraft identifiers, representing different aircraft designs, fuels or fleet categories. The Contrail Flight Distance Density (CFDD) is first calculated for each identifier based on the corresponding distance flown and aircraft-specific parameters (Section 5.3.2). These contributions are then summed to obtain the total CFDD, from which the total contrail-cirrus coverage $\mathrm{cov_{all\ \tau}}$ is calculated. Attribution is subsequently applied to determine the contribution of each identifier to $\mathrm{cov_{all\ \tau}}$. After the soot-dependent correction s_τ is applied, the resulting optically thick contrail-cirrus coverage $\mathrm{cov_{\tau>0.05}}$ is again summed across all identifiers and used to calculate the RF. Finally, the contribution of each identifier to the RF is determined. Attribution is thus performed twice: for contrail-cirrus coverage and for RF.

Attribution methods can be broadly classified as additive or non-additive. Additive methods satisfy the condition that a total value is equal to the sum of the contributions from each aircraft identifier, for example

$$\mathrm{RF}(j) = \sum_n \mathrm{RF(n,j)} \tag{5.11}$$

whereas non-additive methods do not preserve this property. Therefore, the implementation of non-additive methods into the contrail module would require additional global simulations in which different combinations of aircraft identifiers are evaluated in order to isolate interaction effects. Furthermore, additive attribution provides a consistent and flexible framework that allows aircraft iden-

[6]https://openairclim.org/background/attribution.html [Last accessed: 26/11/2025]

tifiers to be arbitrarily added or removed, without affecting the values of other aircraft. For these reasons, the contrail module currently supports only additive attribution methods.

The contrail module implements proportional attribution, consistent with the tagging-based approach used in other OpenAirClim modules (see the upcoming main OpenAirClim paper). In proportional attribution, the contribution of each aircraft identifier to the output variable is determined from its fractional contribution to the input variable. Specifically, the contribution of identifier n to $\mathrm{cov}_{\mathrm{all}\ \tau}$ is determined from its relative contribution to CFDD, and the contribution to RF is determined from its relative contribution to $\mathrm{cov}_{\tau>0.05}$.

This attribution framework enables the quantification of the relative climate impact of different aircraft types, fuels or even operational concepts within a shared scenario context. This capability is demonstrated in Chapter 6 for the complex and highly integrated ICAO scenarios. Future updates of the contrail module may incorporate additional attribution methods, for example following scientific advancements.

5.7. DISCUSSION

This section discusses the validity range and limitations of the OpenAirClim contrail module. Specifically, we compare the module to a simplified, linearised approach, address the applicability of the module to different emission inventories and scenarios and discuss the robustness of the underlying parameterisations.

The validity of the contrail module compared to comprehensive contrail climate models is demonstrated in Section 5.4. To gauge its utility, it is instructive to further compare it to a simple distance-based RF method, as used for example by Lee et al. (2021, see their Appendix E and supplementary data) to obtain a best estimate for contrail RF in 2018. To do this, we briefly describe the method and then compare it to the results of the comprehensive contrail climate models, mirroring the approach of Figure 5.10.

The simple distance-based method uses the RF value obtained by a reference simulation and divides it by the flown distance in the underlying emission inventory to obtain a distance-dependent RF value. Using the Bier and Burkhardt (2022) simulation for AEDT 2006 and $\mathrm{EI_s} = 1.5 \times 10^{15}\,\mathrm{kg^{-1}}$ as reference, we determine the distance-dependent RF values of $6.4 \times 10^{-10}\,\mathrm{mW\,m^{-2}\,km^{-1}}$ (slant distance) and $1.1 \times 10^{-9}\,\mathrm{mW\,m^{-2}\,km^{-1}}$ (track distance)[7]. Applying these values to other emission inventories allows RF to be estimated from the flown distance (either track of slant). Additionally, we apply the correction factor s_τ (Eq. 5.7) to

[7] As we discuss in Appendix 3.A, it is unclear how there can be such a big difference between the track and slant distances. Nevertheless, we apply the values consistently, depending on how the respective emission inventory is defined.

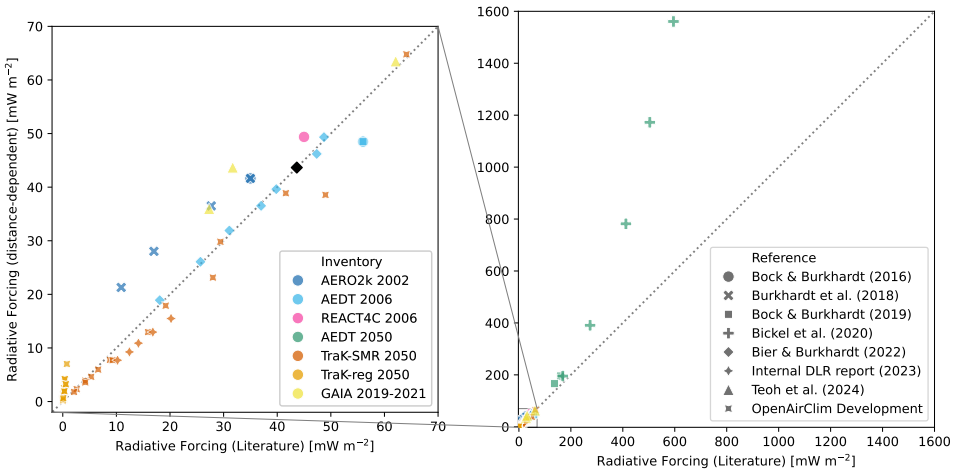


Figure 5.14: Comparison of global RF from literature and calculated using a simple distance-dependent model based on Bier and Burkhardt (2022). The colours correspond to the emission inventories used, the marker shapes to the reference. The black diamond is the simulation used to calculate the distance-dependent RF value, both for track and slant distance. The OpenAirClim s_τ correction is applied to account for changes in the soot emission. "OpenAirClim Development" refers to the ECHAM5-CCMod simulations underlying the contrail module.

account for changes in soot emissions (this was not considered by Lee et al., 2021).

As shown in Figure 5.14, this simple method (with the soot correction) exhibits good agreement with simulations that closely resemble the reference, i.e. using the Bier and Burkhardt (2022) setup or a derivative thereof (TraK-SMR 2020 inventory simulations). In these cases, the spatial distribution of air traffic, altitude profiles and contrail formation conditions remain similar, such that the RF scales approximately linearly with total flown distance. This suggests that linearised approaches may be sufficient for certain applications, particularly when incremental changes to existing air traffic are analysed.

However, the simple model struggles to capture changes in RF for emission inventories and scenarios with substantially different characteristics. This is evident for the regional-only inventory (TraK-reg 2050) and for scenarios with strongly increased air traffic (multipliers of AEDT 2050), where saturation effects become important. In these cases, non-linearities in contrail formation, contrail-cirrus coverage and radiative forcing result in the total RF no longer scaling linearly with flown distance. This behaviour is, however, captured by the OpenAirClim contrail module (see Figure 5.10), demonstrating its utility across a wide range of scenarios.

Nevertheless, the results also highlight the importance of ensuring that emission inventories and scenarios fall within the validity range of the OpenAirClim

contrail module's underlying parameterisations. The module is based on simulations for regional and short-/medium-range air traffic, supplemented by a simulation with a global emission inventory. Validation against literature shows that the module captures RF behaviour well across a wide range of conditions, including high-traffic scenarios. However, comprehensive contrail modelling for high air traffic scenarios and for novel fuels such as SAF and hydrogen remains limited. A comparison with dedicated climate simulations addressing this shortcoming would further strengthen confidence in the module.

Similarly, it may be interesting to investigate how to improve the module's ability to simulate inventories that cover a limited geographical area or a single aircraft type (e.g. only regional aircraft). As the validation showed, the module currently tends to overestimate the RF of regional-only inventories compared to ECHAM5-CCMod. This is expected behaviour, because isolating individual aircraft types or fleets without accounting for the broader aviation context generally leads to overestimations. To obtain a realistic estimation of the climate impact of regional aircraft, the remaining, background air traffic also needs to be simulated. Therefore, the question remains whether the aforementioned ability is actually useful for OpenAirClim. A more accurate approach would instead be to tag the desired air traffic using an identifier (see Section 5.3.2) and then obtain its relative contribution within the global context.

5.8. SUMMARY AND OUTLOOK

This chapter presented the development and validation of a new contrail module for OpenAirClim. The module provides a computationally efficient representation of contrail formation, contrail-cirrus coverage and radiative forcing, based on parameterisations derived from ECHAM5-CCMod simulations. The development strategy ensured internal consistency by anchoring intermediate relationships to the radiative forcing response of the underlying climate model. The module is underpinned by meteorological reanalysis data (based on Chapter 4) and captures key non-linear relationships, such as saturation behaviour for high, future air traffic volumes and the dependence of contrail optical thickness on soot emissions. Validation against published studies demonstrated the capability of the module to reproduce contrail RF across a wide range of emission inventories, aircraft types, fuels and air traffic levels.

Several areas for further improvement remain. The current correction for aircraft size was developed using only a limited set of simulations and should be extended to cover a wider range of atmospheric scenarios and aircraft designs. However, highest on the list should be the parameterisation of the low-soot regime, which would benefit from further investigation through both in-situ measurements and dedicated microphysical simulations. This is particularly important for novel aviation fuels such as SAF and hydrogen, but would also al-

low the module to better represent present-day air traffic which already contains low-soot technologies such as lean burn. The influence of additional fuel-dependent factors such as the fuel sulphur content should also be investigated and incorporated into future model versions.

A dedicated investigation into model uncertainties is highly recommended. The OpenAirClim contrail module inherits uncertainties from the models underlying it, namely ERA5 and ECHAM5-CCMod, and introduces modelling uncertainties at each parameterisation step. Quantifying the overall uncertainty is challenging since many of these uncertainties are linked or dependent on one another. Lee et al. (2021) estimate the uncertainty of their contrail-cirrus RF at 70 % due to uncertainties associated with the radiative response to contrail-cirrus and with the upper-tropospheric water budget and contrail cirrus scheme. The uncertainties are assumed to be independent and are partially based on expert judgement. Further research should focus on understanding and reducing the uncertainties in the contrail climate impact. Further OpenAirClim development should focus on the introduction of an integrated Monte Carlo framework and dedicated uncertainty quantification module.

Further validation using dedicated simulations with other contrail models, in particular for high air traffic, would strengthen confidence in the module. Furthermore, it should be investigated whether a model other than ECHAM5-CCMod can be used to perform similar simulations to those underlying the development shown in this chapter, such that the OpenAirClim contrail module becomes less dependent on a single, closed-source climate model. This would also be in the spirit of the open-source philosophy underpinning the development of OpenAirClim.

Overall, despite these current limitations, the OpenAirClim contrail module provides a substantial improvement over simple, distance-dependent approaches, whilst maintaining computational efficiency. This enables the efficient and flexible simulation of a wide range of aviation scenarios, including those involving new propulsion technologies and alternative fuels. As a result, it provides a robust and flexible framework for assessing the climate impact of aviation and is well suited to support future research and scenario analyses.

5.A. APPENDIX

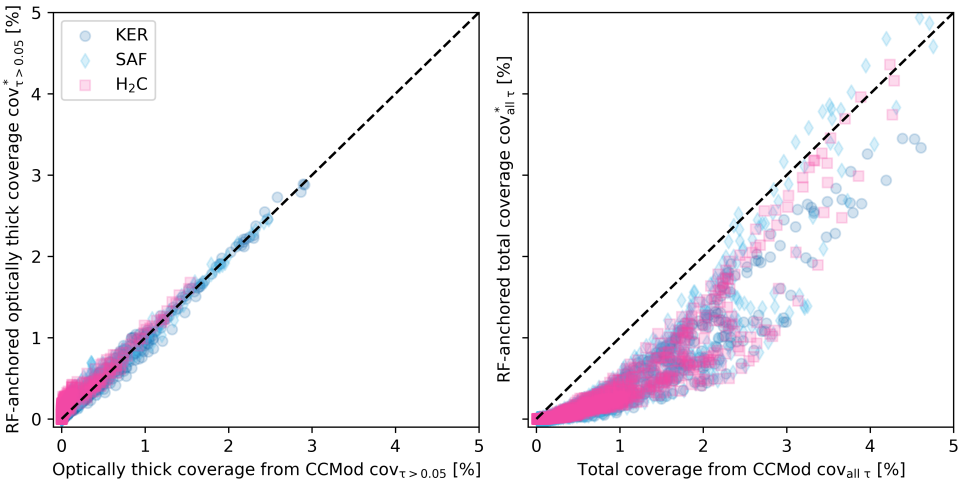


Figure 5.A.1: RF-anchored reconstruction of contrail-cirrus coverage. Comparison between total (all τ) and optically thick ($\tau > 0.05$) contrail-cirrus coverage from ECHAM5-CCMod and the corresponding coverages inferred from CCMod RF values using the relationships developed in Sections 5.3.5 and 5.3.6. The dashed line indicates the 1:1 relationship. The benefit of the approach is clear: The fuel-dependence has been mostly eliminated from $\mathrm{cov}^*_{\mathrm{all}\ \tau}$, thereby enabling a single fit for all fuels between CFDD and $\mathrm{cov}^*_{\mathrm{all}\ \tau}$. The fuel dependence is instead included in s_τ (see Section 5.3.5).

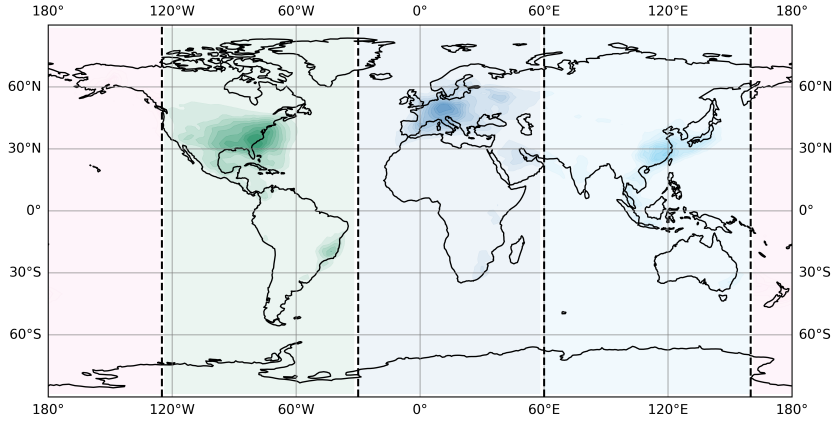


Figure 5.A.2: Regions of the Radiative Forcing model. The regions are EMEA (dark blue), Asia and Australia (light blue), Pacific (pink) and Americas (green). The colour gradient corresponds to the fuel use of the TraK-SMR (2050) inventory.

Table 5.A.1: Literature used for validation of the OpenAirClim contrail module. N_{sims} refers to the number of simulations, b the (assumed) wingspan, G_{250} the Schmidt-Appleman slope at 250 hPa, $EI_{\text{s,mod}}$ the modified soot number emission index (see the main text). For multiple simulations, ranges for various parameters are provided. A detailed overview of the data, including the assumptions made where data was missing or not reported, is available in the linked dataset.

Model	Inventory	Type	N_{sims}	b [m]	G_{250} [Pa K^{-1}]	$EI_{\text{s,mod}}$ [$\times 10^{15}$ kg^{-1}]	RF [mW m^{-2}]	Reference
ECHAM5-CCMod	AERO2k 2002	track	1	50.0	1.65	2.67	35.0	Bock and Burkhardt (2016a)
ECHAM5-CCMod	AEDT 2006	slant	1	50.0	1.67	2.67	56.0	Bock and Burkhardt (2016a)
ECHAM4-CCMod	REACT4C 2006	track	1	50.0	1.67	2.67	45.0	Bock and Burkhardt (2016a)
ECHAM5-CCMod	AERO2k 2002	track	4	50.0	1.65	0.267 – 2.67	10.9 – 35.0	Burkhardt et al. (2018)
ECHAM5-CCMod	AEDT 2006	slant	1	50.0	1.65	2.67	56.0	Bier and Burkhardt (2019)
ECHAM5-CCMod	AEDT 2050	slant	1	50.0	1.65	2.67	160.0	Bier and Burkhardt (2019)
ECHAM5-CCMod	AEDT 2050	slant	1	50.0	1.99	1.17	137.0	Bier and Burkhardt (2019)
ECHAM5-CCMod	AEDT 2050	track	7	50.0	1.65	2.67	169.0 – 701.0	Bickel et al. (2020)
ECHAM5-CCMod	AEDT 2006	slant	8	50.0	1.67	0.15 – 3.0	18.09 – 48.72	Bier and Burkhardt (2022)
ECHAM5-CCMod	Trak-SMR 2050	slant	5	35.0	1.93 – 2.09	0.2 – 1.5	10.2 – 20.2	Internal DLR report (2023)
pycontrails v0.30.0	GAIA 2019	track	1	50.0	1.66	1.02	62.1	Teoh et al. (2024)
pycontrails v0.30.0	GAIA 2020	track	1	50.0	1.66	1.02	27.3	Teoh et al. (2024)
pycontrails v0.30.0	GAIA 2021	track	1	50.0	1.66	1.02	31.7	Teoh et al. (2024)
ECHAM5-CCMod	TraK-SMR	slant	15	35.0	1.93 – 5.1	0.0 – 0.75	2.1 – 64.1	OpenAirClim Development
ECHAM5-CCMod	Trak-reg	slant	20	27.5	1.93 – 15.8	0.0 – 0.75	0.012 – 0.76	OpenAirClim Development

Table 5.A.2: Contrail-cirrus coverage functions. The numbering groups models into families with the same underlying form. Shown are only the most promising models for clarity.

ID	Model	Description
0	$a \cdot \mathrm{ISS} \cdot \arctan\left(b \cdot \mathrm{CFDD} \cdot \mathrm{ISS}^{-1}\right)$	AirClim 2.1 function
10	$a \cdot \mathrm{CFDD}^{\gamma}$	
20	$a \cdot \arctan(b \cdot \mathrm{CFDD})$	
21	$a \cdot \arctan(b \cdot \mathrm{CFDD})^{\gamma}$	
22	$a \cdot \arctan(b \cdot \mathrm{CFDD}^{\gamma})$	
23	$a \cdot \mathrm{ISS} \cdot \arctan\left(b \cdot \mathrm{CFDD} \cdot \mathrm{ISS}^{-1}\right)^{\gamma}$	
24	$a \cdot \mathrm{ISS} \cdot \arctan\left(b \cdot \mathrm{CFDD}^{\gamma} \cdot \mathrm{ISS}^{-1}\right)$	
25	$a \cdot \mathrm{ISS} \cdot \arctan(b \cdot \mathrm{CFDD} \cdot \mathrm{ISS}^{\gamma})$	
26	$a \cdot \mathrm{ISS} \cdot \mathrm{CFDD}^{\gamma} \cdot \arctan\left(b \cdot \mathrm{CFDD} \cdot \mathrm{ISS}^{-1}\right)$	
30	$a \cdot \tanh(b \cdot \mathrm{CFDD})$	Chosen function
31	$a \cdot \mathrm{ISS} \cdot \tanh\left(b \cdot \mathrm{CFDD} \cdot \mathrm{ISS}^{-1}\right)$	
32	$a \cdot \tanh(b \cdot \mathrm{CFDD}) + c \cdot \mathrm{ISS}$	

REFERENCES

Benetatos, C., Eleftheratos, K., Gierens, K., and Zerefos, C.: A statistically significant increase in ice supersaturation in the atmosphere in the past 40 years, Scientific Reports, 14, 24760, doi: 10.1038/s41598-024-75756-9, 2024.

Bickel, M., Ponater, M., Bock, L., Burkhardt, U., and Reineke, S.: Estimating the effective radiative forcing of contrail cirrus, Journal of Climate, 33, 1991–2005, doi: 10.1175/JCLI-D-19-0467.1, 2020.

Bier, A. and Burkhardt, U.: Variability in contrail ice nucleation and its dependence on soot number emissions, Journal of Geophysical Research: Atmospheres, 124, 3384–3400, doi: 10.1029/2018JD029155, 2019.

Bier, A. and Burkhardt, U.: Impact of parametrizing microphysical Processes in the jet and vortex phase on contrail cirrus properties and radiative forcing, Journal of Geophysical Research: Atmospheres, 127, doi: 10.1029/2022JD036677, 2022.

Bier, A., Unterstrasser, S., Zink, J., Hillenbrand, D., Jurkat-Witschas, T., and Lottermoser, A.: Contrail formation on ambient aerosol particles for aircraft with hydrogen combustion: a box model trajectory study, Atmospheric Chemistry and Physics, 24, 2319–2344, doi: 10.5194/acp-24-2319-2024, 2024.

Bock, L. and Burkhardt, U.: Reassessing properties and radiative forcing of contrail cirrus using a climate model, Journal of Geophysical Research: Atmospheres, 121, 9717–9736, doi: 10.1002/2016JD025112, 2016a.

Bock, L. and Burkhardt, U.: The temporal evolution of a long-lived contrail cirrus cluster: Simulations with a global climate model, Journal of Geophysical Research: Atmospheres, 121, 3548–3565, doi: 10.1002/2015JD024475, 2016b.

Bock, L. and Burkhardt, U.: Contrail cirrus radiative forcing for future air traffic, Atmospheric Chemistry and Physics, 19, 8163–8174, doi: 10.5194/acp-19-8163-2019, 2019.

Bruder, H., Thor, R. N., Niklaß, M., Dahlmann, K., Eichinger, R., Linke, F., Grewe, V., Matthes, S., and Unterstrasser, S.: The DLR CO2-equivalent estimator FlightClim v1.0: an easy-to-use estimation of per flight CO2 and non-CO2 climate effects, Geoscientific Model Development, 19, 3551–3567, doi: 10.5194/gmd-19-3551-2026, 2026.

Burkhardt, U. and Kärcher, B.: Process-based simulation of contrail cirrus in a global climate model, Journal of Geophysical Research, 114, D16201, doi: 10.1029/2008JD011491, 2009.

Burkhardt, U. and Kärcher, B.: Global radiative forcing from contrail cirrus, Nature Climate Change, 1, 54–58, doi: 10.1038/nclimate1068, 2011.

Burkhardt, U., Bock, L., and Bier, A.: Mitigating the contrail cirrus climate impact by reducing aircraft soot number emissions, npj Climate and Atmospheric Science, 1, 37, doi: 10.1038/s41612-018-0046-4, 2018.

Dahlmann, K., Grewe, V., Frömming, C., and Burkhardt, U.: Can we reliably assess climate mitigation options for air traffic scenarios despite large uncertainties in atmospheric processes?, Transportation Research Part D: Transport and Environment, 46, 40–55, doi: 10.1016/j.trd.2016.03.006, 2016.

Dischl, R., Märkl, R., Sauer, D., Voigt, C., Harlaß, T., Scheibe, M., Hahn, V., Kaufmann, S., Marsing, A., Dörnbrack, A., Roiger, A., Yu, F., Gauthier, M., Renard, C., Swann, P., Johnson, M., Ahrens, D., Sallinen, R., Eckel, G., and Le Clercq, P.: Fuel sulfur content can modulate contrail ice crystal numbers, Communications Earth & Environment, 6, 902, doi: 10.1038/s43247-025-02951-5, 2025.

Grewe, V. and Stenke, A.: AirClim: An efficient tool for climate evaluation of aircraft technology, Atmospheric Chemistry and Physics, 8, 4621–4639, doi: 10.5194/acp-8-4621-2008, 2008.

Grewe, V., Bock, L., Burkhardt, U., Dahlmann, K., Gierens, K., Hüttenhofer, L., Unterstrasser, S., Gangoli Rao, A., Bhat, A., Yin, F., Reichel, T. G., Paschereit, O., and Levy, Y.: Assessing the climate impact of the AHEAD multi-fuel blended wing body, Meteorologische Zeitschrift, 26, 711–725, doi: 10.1127/metz/2016/0758, 2017.

Grewe, V., Gangoli Rao, A., Grönstedt, T., Xisto, C., Linke, F., Melkert, J., Middel, J., Ohlenforst, B., Blakey, S., Christie, S., Matthes, S., and Dahlmann, K.: Evaluating the climate impact of aviation

emission scenarios towards the Paris agreement including COVID-19 effects, Nature Communications, 12, 3841, doi: 10.1038/s41467-021-24091-y, 2021.

Hersbach, H., Bell, B., Berrisford, P., Hirahara, S., Horányi, A., Muñoz-Sabater, J., Nicolas, J., Peubey, C., Radu, R., Schepers, D., Simmons, A., Soci, C., Abdalla, S., Abellan, X., Balsamo, G., Bechtold, P., Biavati, G., Bidlot, J., Bonavita, M., De Chiara, G., Dahlgren, P., Dee, D., Diamantakis, M., Dragani, R., Flemming, J., Forbes, R., Fuentes, M., Geer, A., Haimberger, L., Healy, S., Hogan, R. J., Hólm, E., Janisková, M., Keeley, S., Laloyaux, P., Lopez, P., Lupu, C., Radnoti, G., De Rosnay, P., Rozum, I., Vamborg, F., Villaume, S., and Thépaut, J.: The ERA5 global reanalysis, Quarterly Journal of the Royal Meteorological Society, 146, 1999–2049, doi: 10.1002/qj.3803, 2020.

Irvine, E. A. and Shine, K. P.: Ice supersaturation and the potential for contrail formation in a changing climate, Earth System Dynamics, 6, 555–568, doi: 10.5194/esd-6-555-2015, 2015.

Kleine, J., Voigt, C., Sauer, D., Schlager, H., Scheibe, M., Jurkat-Witschas, T., Kaufmann, S., Kärcher, B., and Anderson, B. E.: In situ observations of ice particle losses in a young persistent contrail, Geophysical Research Letters, 45, doi: 10.1029/2018GL079390, 2018.

Kärcher, B., Burkhardt, U., Bier, A., Bock, L., and Ford, I. J.: The microphysical pathway to contrail formation, Journal of Geophysical Research: Atmospheres, 120, 7893–7927, doi: 10.1002/2015JD023491, 2015.

Lee, D., Fahey, D., Skowron, A., Allen, M., Burkhardt, U., Chen, Q., Doherty, S., Freeman, S., Forster, P., Fuglestvedt, J., Gettelman, A., De León, R., Lim, L., Lund, M., Millar, R., Owen, B., Penner, J., Pitari, G., Prather, M., Sausen, R., and Wilcox, L.: The contribution of global aviation to anthropogenic climate forcing for 2000 to 2018, Atmospheric Environment, 244, 117 834, doi: 10.1016/j.atmosenv.2020.117834, 2021.

Lottermoser, A. and Unterstrasser, S.: Modeling the impact of alternative fuels and hydrogen propulsion on contrail-cirrus: A parameter study, Journal of Geophysical Research: Atmospheres, 131, e2025JD044 604, doi: 10.1029/2025JD044604, 2026.

Marenco, A., Thouret, V., Nédélec, P., Smit, H., Helten, M., Kley, D., Karcher, F., Simon, P., Law, K., Pyle, J., Poschmann, G., von Wrede, R., Hume, C., and Cook, T.: Measurement of ozone and water vapor by Airbus in-service aircraft: The MOZAIC airborne program, an overview, Journal of Geophysical Research: Atmospheres, 103, 25 631–25 642, doi: 10.1029/98JD00977, 1998.

Matthes, S., Lim, L., Burkhardt, U., Dahlmann, K., Dietmüller, S., Grewe, V., Haslerud, A. S., Hendricks, J., Owen, B., Pitari, G., Righi, M., and Skowron, A.: Mitigation of non-CO2 aviation's climate impact by changing cruise altitudes, Aerospace, 8, 36, doi: 10.3390/aerospace8020036, 2021.

Megill, L. and Grewe, V.: Investigating the limiting aircraft-design-dependent and environmental factors of persistent contrail formation, Atmos. Chem. Phys., 25, 4131–4149, doi: 10.5194/acp-25-4131-2025, 2025.

Märkl, R. S., Voigt, C., Sauer, D., Dischl, R. K., Kaufmann, S., Harlaß, T., Hahn, V., Roiger, A., Weiß-Rehm, C., Burkhardt, U., Schumann, U., Marsing, A., Scheibe, M., Dörnbrack, A., Renard, C., Gauthier, M., Swann, P., Madden, P., Luff, D., Sallinen, R., Schripp, T., and Le Clercq, P.: Powering aircraft with 100% sustainable aviation fuel reduces ice crystals in contrails, Atmospheric Chemistry and Physics, 24, 3813–3837, doi: 10.5194/acp-24-3813-2024, 2024.

Petzold, A., Thouret, V., Gerbig, C., Zahn, A., Brenninkmeijer, C. A. M., Gallagher, M., Hermann, M., Pontaud, M., Ziereis, H., Boulanger, D., Marshall, J., Nédélec, P., Smit, H. G. J., Friess, U., Flaud, J.-M., Wahner, A., Cammas, J.-P., Volz-Thomas, A., and Team, I.: Global-scale atmosphere monitoring by in-service aircraft – current achievements and future prospects of the European Research Infrastructure IAGOS, Tellus B: Chemical and Physical Meteorology, 67, 28 452, doi: 10.3402/tellusb.v67.28452, 2015.

Roeckner, E., Bäuml, G., Bonaventura, L., Brokopf, R., Esch, M., Giorgetta, M., Hagemann, S., Kirchner, I., Kornblueh, L., Manzini, E., Rhodin, A., Schlese, U., Schulzweida, U., and Tompkins: The atmospheric general circulation model ECHAM5. Part 1: Model description, Tech. Rep. 349, Max-Planck-Institut für Meteorologie, Hamburg, ISSN 0937-1060, 2003.

Roeckner, E., Brokopf, R., Esch, M., Giorgetta, M., Hagemann, S., Kornblueh, L., Manzini, E., Schlese, U., and Schulzweida, U.: Sensitivity of simulated climate to horizontal and vertical resolution in the ECHAM5 atmosphere model, Journal of Climate, 19, 3771–3791, 2006.

Rubin-Zuzic, M., Bugliaro, L., Marsing, A., Wang, Z., Voigt, C., Simson, C., Kaiser, S., and Ziegler, P.: Reduced contrail radiative effect for fleets with low soot and water vapour emissions, Atmospheric Environment: X, 27, 100 353, doi: 10.1016/j.aeaoa.2025.100353, 2025.

Stier, P., Feichter, J., Kinne, S., Kloster, S., Vignati, E., Wilson, J., Ganzeveld, L., Tegen, I., Werner, M., Balkanski, Y., Schulz, M., Boucher, O., Minikin, A., and Petzold, A.: The aerosol-climate model ECHAM5-HAM, Atmospheric Chemistry and Physics, 5, 1125–1156, doi: 10.5194/acp-5-1125-2005, 2005.

Teoh, R., Engberg, Z., Schumann, U., Voigt, C., Shapiro, M., Rohs, S., and Stettler, M. E. J.: Global aviation contrail climate effects from 2019 to 2021, Atmospheric Chemistry and Physics, 24, 6071–6093, doi: 10.5194/acp-24-6071-2024, 2024.

Unterstrasser, S.: Properties of young contrails – a parametrisation based on large-eddy simulations, Atmospheric Chemistry and Physics, 16, 2059–2082, doi: 10.5194/acp-16-2059-2016, 2016.

Unterstrasser, S. and Görsch, N.: Aircraft-type dependency of contrail evolution, Journal of Geophysical Research: Atmospheres, 119, 14,015–14,027, doi: 10.1002/2014JD022642, 2014.

Voigt, C., Kleine, J., Sauer, D., Moore, R. H., Bräuer, T., Le Clercq, P., Kaufmann, S., Scheibe, M., Jurkat-Witschas, T., Aigner, M., Bauder, U., Boose, Y., Borrmann, S., Crosbie, E., Diskin, G. S., DiGangi, J., Hahn, V., Heckl, C., Huber, F., Nowak, J. B., Rapp, M., Rauch, B., Robinson, C., Schripp, T., Shook, M., Winstead, E., Ziemba, L., Schlager, H., and Anderson, B. E.: Cleaner burning aviation fuels can reduce contrail cloudiness, Communications Earth & Environment, 2, 114, doi: 10.1038/s43247-021-00174-y, 2021.

Voigt, C., Märkl, R., Sauer, D., Dischl, R., Renard, C., Seeliger, K., Yu, F., Kaufmann, S., Bräuer, T., Jurkat-Witschas, T., Le Chenadec, G., Moreau, J., Requena-Esteban, E., Bonne, N., Vals, M., Roche, A., Zelina, J., Dörnbrack, A., Eirenschmalz, L., Heckl, C., Horst, E., Lichtenstern, M., Marsing, A., Neumann, G., Roiger, A., Scheibe, M., Stock, P., Giez, A., Eckel, G., and Le Clercq, P.: Substantial aircraft contrail formation at low soot emission levels, Nature, 652, 112–118, doi: 10.1038/s41586-026-10286-0, 2026.

Zink, J., Unterstrasser, S., and Jurkat-Witschas, T.: On the potential role of lubrication oil particles in contrail formation for kerosene and hydrogen combustion, Journal of Geophysical Research: Atmospheres, 130, doi: 10.1029/2025jd043487, 2025.

Addicted to flying.

restless morning sky,
another thin white line,
chasing one more flight.

— LM

6

ANALYSIS OF ICAO AVIATION SCENARIOS WITH OPENAIRCLIM

Data and code available at:

Megill, L.: Data and code underlying the ICAO scenario analysis with OpenAirClim, 4TU.ResearchData, doi: 10.4121/f016041d-5c71-430e-9358-24b2d5bc5403, 2026.

ABSTRACT

The aviation industry expects high growth in demand and is simultaneously one of the most challenging sectors to decarbonise. In addition to carbon dioxide, aviation contributes to anthropogenic climate change through non-CO_2 effects, which dominate warming in the short term. The assessment of long-term climate impacts from aviation thus requires integrated and internally consistent scenarios that consider future pathways for technology, operations and fuels. In analysing the feasibility of long-term aspiration goals for the aviation industry, the International Civil Aviation Organization (ICAO) developed a set of detailed, integrated global aviation scenarios. In this study, we harmonise these scenarios for use with the response model OpenAirClim. We perform an integrated model test of the OpenAirClim model and demonstrate its ability to simulate complex, multi-fuel and multi-aircraft scenarios. Across the scenario ensemble, the simulated global mean temperature change from net CO_2 and contrails increases through 2070, with no scenario achieving stabilisation within the study horizon, backing up a similar study by Aamaas et al. (2025). In the most ambitious pathways, as the use of alternative aviation fuels increases, net CO_2 warming trends towards stabilisation but contrail-induced warming continues to rise. This increases the value of further research into contrail formation and properties in the low-soot regime. Our results show that to reduce the climate impact of aviation effectively, the switch to alternative fuels must be coupled with dedicated non-CO_2 mitigation measures.

6.1. INTRODUCTION

International civil aviation has grown rapidly over the past decades and is expected to continue expanding as global demand for mobility increases (Leipold et al., 2021; Lee et al., 2021; Grewe et al., 2021). At the same time, aviation is widely regarded as one of the most challenging sectors to decarbonise: Aircraft have long service lives, infrastructure turnover is slow and many mitigation options require coordinated changes across technology, fuels, and operations. In addition, the industry's climate impact is not limited to CO_2. Non-CO_2 effects such as contrail-cirrus contribute substantially to near-term warming (Kärcher, 2018; Bock and Burkhardt, 2019; Teoh et al., 2022a) and require different mitigation measures and considerations (Matthes et al., 2021; Sausen et al., 2024; Dischl et al., 2025; Voigt et al., 2026). Robust long-term assessments therefore require scenario frameworks that treat aircraft, fuels and operations in a consistent and

integrated manner.

The 40th session of the ICAO Assembly initiated an analysis of the feasibility of a Long-Term global Aspiration Goal (LTAG) for international civil aviation. A dedicated task group from ICAO's Committee on Aviation Environmental Protection (CAEP) consulted a wide range of industry stakeholders to gather evidence on prospective developments within the industry. The result was a set of three integrated global aviation scenarios (ICAO, 2022): internally consistent combinations of assumptions on pathways for aircraft technology, operations and fuel demand and availability. A key feature of these scenarios is the explicit treatment of alternative aviation fuels in a global context using a well-to-wake life-cycle assessment, accounting for upstream emissions from extraction, production and energy mixes, rather than only considering tailpipe CO_2 emissions. Their internal consistency makes the scenarios attractive for climate impact assessments, but also increases the complexity of translating them into inputs compatible with climate models. Furthermore, the scenarios did not focus on non-CO_2 emissions and effects, so any study of these effects requires further data and a large set of assumptions.

The objective of this chapter is to use the ICAO scenarios as a demanding use case to test and demonstrate the ability of OpenAirClim to simulate multi-aircraft emission inventories and scenarios. This is the first test case of the model at this scale. Since, at the time of writing, the majority of the OpenAirClim modules are not available or fully validated, our analysis thus focuses only on net CO_2 (treated consistently with the life-cycle framework) and contrails.

An important point of reference is Aamaas et al. (2025), which was published during the preparation of this work. They also assessed the ICAO scenarios, using the reduced complexity climate model CICERO-SCM (Sandstad et al., 2024). Their study provides an opportunity for a direct comparison of the global mean temperature change estimates for each scenario and sensitivity to various underlying assumptions. However, their approach does not resolve different aircraft categories and types using an emission inventory. This is a key element of the OpenAirClim approach, particularly for contrails, where the emission location and aircraft characteristics influence the likelihood of formation and climate impact.

The following section describes how the ICAO scenarios are harmonised for use with OpenAirClim, including the conversion of fuel pathways to net-CO_2 emissions and the generation of compatible emission inventories. The results of the study are presented in Section 6.3, compared with Aamaas et al. (2025) in Section 6.4 and discussed in Section 6.5. We also provide a number of improvement ideas and suggestions for the OpenAirClim model based on the experience gained during this first integrated model test.

6.2. HARMONISING THE ICAO SCENARIOS WITH OPENAIRCLIM

A dedicated scenario and set of emission inventories are required to simulate the climate effects of aviation using OpenAirClim. This includes a number of assumptions regarding aircraft and fuel types, aircraft emission characteristics and fleet composition. Ideally, a dedicated set of emission inventories are created that directly correspond to the research question. If this is not possible, existing inventories can be modified.

In this section, using the ICAO scenarios[1], we demonstrate the steps required to create consistent and compatible scenarios and emission inventories, which can be used as a guide for future users of OpenAirClim. The harmonisation of the ICAO scenarios is not a simple undertaking, because the scenarios are complex and highly integrated. Furthermore, the scenarios are CO_2-focused and do not include a number of parameters required for estimating the non-CO_2 impact. A number of assumptions thus had to be made, which are all described below. The OpenAirClim-compatible scenarios are driven by an Excel sheet and a Jupyter notebook, both provided in the supplementary material of this work.

The section begins by defining the ICAO scenarios (Section 6.2.1). The fuel demand and CO_2 emissions, including assumptions on life cycle emissions, is described in Section 6.2.2. Time-dependent assumptions on aircraft emission characteristics and fleet composition are discussed in Section 6.2.3, followed by the development of compatible emission inventories in Section 6.2.4. Finally, the OpenAirClim simulation setup is described in Section 6.2.5.

6.2.1. SCENARIO DEFINITIONS

ICAO defines three Integrated Scenarios (IS), which include assumptions about the development of technology (TECH), operations (OPS) and fuel availability (FUEL). The three integrated scenarios are:

- **IS1 – low/nominal scenario:** Requires the lowest delivery effort and foresees no significant infrastructure changes. The future fleet is assumed to consist entirely of improved tube-and-wing aircraft using drop-in fuels. There are few policy incentives for SAF (Sustainable Aviation Fuel) and LCAF (Lower Carbon Aviation Fuel); SAF blend levels remain below 50 %.
- **IS2 – increased ambition scenario:** Requires medium delivery effort. It foresees significant step-changes in efficiency at the airframe and propulsion level, for example through the replacement of conventional tube-and-wing aircraft with advanced concepts. The use of drop-in fuels from a variety of feedstocks, including carbon capture, is widespread and an approval

[1]The underlying ICAO data can be found at https://www.icao.int/LTAG-data-spreadsheet [Last accessed: 15/01/2026]

for 100 % SAF blends is assumed. Phase-out of conventional, fossil-based jet fuel is expected by 2050 (no phase-out of LCAF).

- **IS3 – speculative scenario:** Requires maximum policy enablers and the highest delivery effort. Significant changes in airport and fuelling infrastructure is required to handle advanced concept aircraft with significant step-changes in performance and capability. Widespread use of drop-in fuels as well as non-drop-in fuels for all aircraft categories is assumed, with a phase-out of conventional, fossil-based jet fuel by 2040 (phase-out of LCAF by 2045).

The OPS and FUEL sub-scenarios are directly linked to the integrated scenarios; TECH includes two aspects: which technologies will be introduced (linked directly to the integrated scenarios) and the technology confidence level (LOWER, MEDIUM, HIGHER; not linked). In addition, each integrated scenario has three traffic forecasts (LOW, MID, HIGH). Therefore, in this study we define a "scenario" as a unique combination of IS, traffic forecast and technology confidence level – 27 scenarios in all.

6.2.2. FUEL DEMAND AND CO_2 EMISSIONS

The global fuel demand is provided by ICAO for each combination of IS and traffic forecast (nine independent fuel demand forecasts in all) between 2020 and 2070 for the MEDIUM technology confidence level (so-called "priority runs", see Table 7 in Appendix M1 of ICAO, 2022). To supplement this with historical data, we multiply the global flown distance reported by airlines.org[2] (see also Figure 3.1) by estimated global averaged fuel efficiency values. We use the Grewe et al. (2021) method for this, linearly interpolating between $8\,\mathrm{kg\,km^{-1}}$ in 1940 and $4.61\,\mathrm{kg\,km^{-1}}$ in 2020. All fuel before 2020 is assumed to be Jet A/A-1. The resulting global fuel demand is used to develop an OpenAirClim-compatible normalisation file – we use one file per scenario for convenience, even though the fuel demand does not depend on the technology confidence level.

Six fuels are considered for future air traffic. Next to conventional fossil jet fuels (Jet A/A-1) are Lower Carbon Aviation Fuels (LCAFs). These fuels are also obtained from petroleum, but use various greenhouse gas mitigation methods such as low-carbon electricity use, control of methane leakages, hydro treatment and carbon capture to reduce the well-to-wake carbon intensity to below $80.1\,\mathrm{gCO_2e/MJ}$[3]. Sustainable Aviation Fuels (SAFs) are split into three categories:

[2]https://www.airlines.org/dataset/world-airlines-traffic-and-capacity/ [Last accessed: 26/11/2025]

[3]The method with which CO_2-equivalent emissions are calculated is not clearly defined. Since the Jing et al. (2020) study is referenced, we assume a Global Warming Potential (GWP) with a 100-year time horizon is used. Although "wake" suggests the products of combustion are considered, non-CO_2 emissions and effects such as NO_x and contrails are not mentioned in the ICAO reports and thus also assumed not to be part of the carbon intensity value.

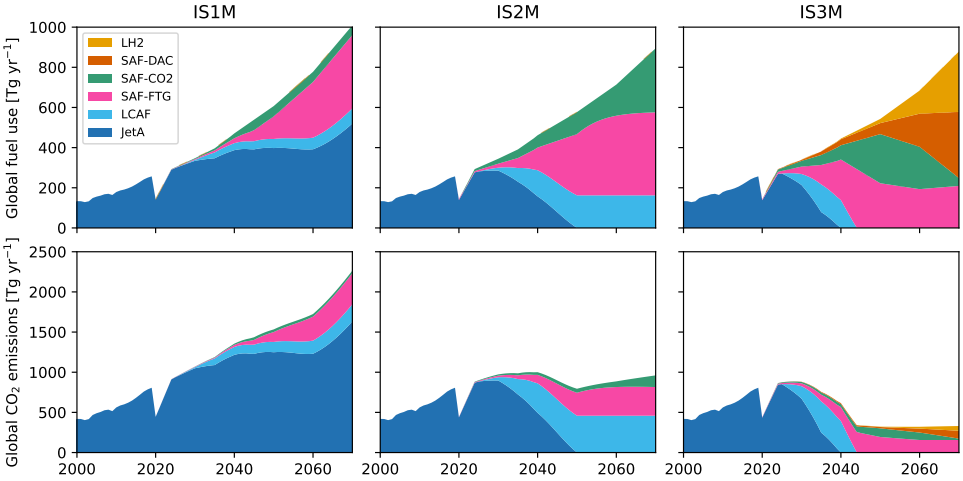


Figure 6.1: Global fuel demand and CO_2 emissions for the three integrated ICAO scenarios. Assumed are a MID traffic forecast and MEDIUM technology confidence level.

SAF-FTG[4] from biomass and solid/liquid wastes, SAF-CO_2 from (industrial) waste CO_2 and SAF-DAC from Direct Air Capture of atmospheric CO_2. Finally, liquid hydrogen (LH2) is the only non-drop-in fuel considered at scale, assumed to only be used in direction combustion in a gas turbine (fuel cells were not within scope). Gaseous hydrogen storage was deemed infeasible due to its low volumetric energy density.

A well-to-wake life cycle assessment (LCA) is used by ICAO to determine CO_2 emissions from each fuel. This assessment considers all upstream emissions from fuel production as well as the combustion itself. Since all drop-in fuels have similar carbon contents, in this study we assume that Jet A/A-1, LCAF and all SAF have identical tailpipe emissions: $3.14\,\mathrm{kg(CO_2)/kg(fuel)}$. As CO_2 is a well-mixed greenhouse gas, the location of emission and capture can be safely ignored. Therefore, we define net CO_2 emissions as the tailpipe CO_2 emissions multiplied by the ratio of the LCA value of the fuel and the LCA value of the reference Jet A/A-1 ($89.0\,\mathrm{gCO_2e/MJ}$). This method is also applied to LH2, which has zero tailpipe CO_2 emissions, but has an energy intensive creation process that often relies on non-renewable energy sources. We note that the fuel demand of LH2 is always given in Jet A/A-1-equivalent mass units, which enables this simple usage.

The fuel demand of all fuels and corresponding net CO_2 emissions over time

[4]SAF-FTG refers to fuels from biomass and solid/liquid wastes that were investigated by the ICAO Fuels Task Group, now called CAEP Working Group 5. See: https://www.icao.int/CAEP/WG5 [Last accessed: 25/03/2026]. More information on the FTG fuels is provided in Attachment A to Appendix M5 of the LTAG Report, available using the Wayback Machine: https://www.icao.int/environmental-protection/LTAG/Documents/ICAO_LTAG_Report_AppendixM5_AttachmentA.pdf [Last available snapshot at archive.org: 05/02/2024].

Table 6.1: Aircraft category definitions for the ICAO scenarios. The categories are adapted from the DLR WeCare project and harmonised with the three ICAO aircraft categories. The aircraft wingspans are assumed based on the aircraft in each category and are used to post-process the RF values in OpenAirClim. EIS is the year in which an aircraft of that category first entered commercial service (underlined aircraft). *For scenario development, we assume that early jet-powered aircraft such as the DH 106 Comet and Tu-104 are narrowbody aircraft, even though their seat numbers are significantly lower – see the main text for details.

	Cat.	Seats	Span	EIS	Example aircraft
RJ	1	75 (20–50)	26	1968	Yak-40, CRJ 100/200, ERJ 135/140/145, D328
	2	(51–100)		1965	BAC-111, Tu-134, F28, CRJ 550–1000, E-Jets, C909
NB	3	150 (101–150)	36	1952*	DH 106*, Tu-104*, B727, DC-9, B737, A318, A319, A220
	4	(151–200)		1958	B707, DC-8, Il-62, B737, Tu-154, B757, A320, A321
WB	5	300 (201–250)	65	1972	L-1011, B767, A310, A330
	6	(251–300)		1971	DC-10, A300, A340, A350, B787
	7	(301+)		1970	B747, Il-86, B777, A380

are shown in Figure 6.1 for the medium traffic forecast and all integrated scenarios. The fuel demand is expected to increase by a factor of between 5 and 6 from 2000 to 2070. The IS2 and IS3 scenarios show a slight reduction in fuel demand due to the introduction of generally more fuel efficient aircraft (see the following Section and the expected fuel composition in Figure 6.2) and, due to the higher uptake of low-carbon fuels, a large reduction in net CO_2 emissions. IS3 in particular demonstrates the benefit of phasing out higher carbon fuels such as Jet A/A-1 and LCAF, resulting in 85 % less net CO_2 emissions in 2070 compared to IS1.

6.2.3. AIRCRAFT DEFINITIONS

The scenarios differentiate between three aircraft categories: Regional Jets (RJ) – reference: Embraer E190E2; Narrowbodies (NB) – reference: Airbus A320neo; and Widebodies (WB) – reference: Airbus A350-900. As described in Section 6.2.4, the emission inventories used in this analysis are based on the results of the DLR WeCare project (Grewe et al., 2017a). In that study, air traffic in the year 2012 was analysed and split into seven distinct categories depending on their seat number. Table 6.1 thus shows the harmonisation of these two category definitions.

We define representative seat numbers, representative wingspans and example aircraft for each category, in order of entry into commercial service (EIS). The EIS of each category is the year in which an aircraft of similar size and with similar range to modern aircraft within the category entered commercial service. This categorisation is not perfect: We assume that early jet aircraft, such as the DH 106 Comet and Tu-104, are defined as narrowbodies, even though their seat numbers are significantly lower than the other aircraft in the NB category. This is done because the aircraft and their comparatively high mission ranges (in particular compared to the first dedicated RJ aircraft) more closely resemble present day NB aircraft. Dedicated RJ aircraft are introduced in the mid-1960s with the

BAC-111 and Yak-40. The WB category is assumed to enter service in 1971.

This data is used to make an estimation of the fuel share between the three aircraft categories over time. We assume 100 % NB aircraft until the introduction of RJ aircraft in 1965. In 1970, we assume a global fuel share of 10 % RJ and 90 % NB aircraft. The share of WB aircraft is assumed to increase until 1992, where we assume the WeCare fuel share of 7.3 % RJ, 42.8 % NB and 49.9 % WB. This is generally in line with air traffic in both 1992 (Baughcum et al., 1996) and 2019 (Randt, 2016). Since ICAO do not provide any information on the fuel share between the categories, we maintain this share until 2070.

The TECH sub-scenarios define three aircraft types within each category: ATW-T1, ACA-T2 and ACA-T3. The Advanced Tube and Wing (ATW) is part of the TECH sub-scenario T1 and present in all scenarios. It corresponds to aircraft that are the result of incremental improvements in today's aircraft designs that can use any drop-in fuels – up to a 50 % blend in IS1 and up to 100 % in IS2 and IS3. In comparison, the Advanced Concept Aircraft (ACA) refers to aircraft using novel technologies such as lifting bodies, active boundary layer control and additive manufacturing, among many others. The technologies considered depend on the TECH sub-scenario (T2 in IS2 and T3 in IS3). The ACA are assumed to either use drop-in fuels (ACA-T2) or both drop-in and non-drop-in fuels such as hydrogen (ACA-T3).

The fleet composition is determined by ICAO for each scenario using proprietary software from Boeing and Airbus. Likely for this reason, the scenarios only provide the number of deliveries of each aircraft type over time (the "flow"). Therefore, to obtain the fleet composition ("stock"), we use ICAO's estimate for the number of aircraft within each category in 2025[5] and assume a 25-year service life with no hull losses for all aircraft. We note that since non-drop-in fuel can only be used by ACA-T3 (in IS3) and the estimated fleet composition is not perfectly aligned with that underlying ICAO's models, in the first one or two years after the introduction of non-drop-in fuel, we are unable to fully match the non-drop-in fuel demand with the available ACA-T3 aircraft. This difference is, however, only in the order of 0.1 % of the global fuel demand and thus deemed negligible.

The resulting fleet compositions of each category for IS2 and IS3 are shown in Figure 6.2. IS1 wholly consists of ATW-T1 aircraft and is thus not shown for brevity. Earliest fleet replacement begins in 2035 for RJ and NB aircraft and in 2040 for WB aircraft. Non-drop-in fuels (ACA-T3) are not expected to enter the WB fleet until 2050 in IS3. The highest degree of fleet replacement by 2070 is found in the RJ category. However, the fastest rate of fleet replacement is found in the WB category, where replacement begins later.

The TECH sub-scenarios differentiate between three technology confidence

[5]https://www.iata.org/en/iata-repository/publications/economic-reports/the-global-commercial-aircraft-fleet/, their Chart 2 [Last accessed: 02/01/2026]

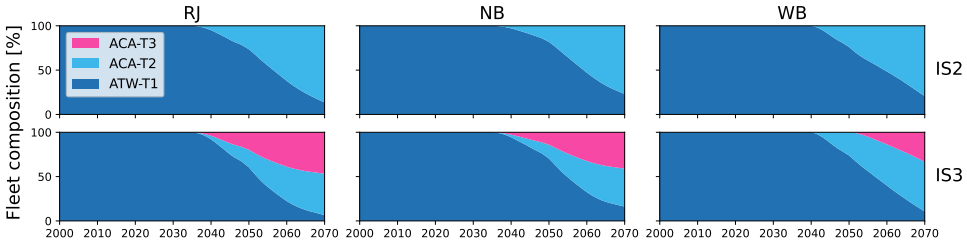


Figure 6.2: Fleet composition of each aircraft category in scenarios IS2 (top row) and IS3 (bottom row). The introduction year of each ACA aircraft depends on the aircraft category and scenario. Non-drop-in fuels are only considered in the IS3 scenario. Scenario IS1 wholly consists of ATW-T1 aircraft and is thus not shown.

levels (LOWER, MEDIUM, HIGHER). For each category and aircraft type there is an associated, estimated yearly improvement in fuel burn per Available Tonne Kilometre (ATK) until an assumed technology freeze from 2050 onwards. We need the time-dependent values of fuel efficiency (used to determine the flown distance from the fuel burn) and overall propulsion efficiency η (used in contrail calculations, see Section 5.3.2). We assume that all categories had identical historical fuel efficiency and η values until 2018 – the reference year for the ICAO scenarios. The historical fuel efficiency is again taken from Grewe et al. (2021) and linearly interpolated from $8\,\mathrm{kg\,km^{-1}}$ in 1940 to $4.61\,\mathrm{kg\,km^{-1}}$ in 2020. The historical η is determined by setting $\eta = 0.30$ in 2018 (a global mean value from Teoh et al., 2022a) and back-calculating the values using the same yearly improvement as the fuel efficiency. From 2018 onwards, we assume that the yearly improvement in fuel burn per ATK can be used for both parameters. The resulting fuel efficiency for all aircraft and technology confidence levels is shown in Figure 6.A.1.

The fuel demand is only provided by ICAO for the MEDIUM technology confidence level (see Table 7 in Appendix M1 of ICAO, 2022). Therefore, for each year, we determine a global average fuel efficiency based on the corresponding fleet composition. For the LOWER and HIGHER technology confidence levels, we then use the ratio of this value to the global average fuel efficiency for the MEDIUM confidence level to scale the global fuel demand. The global fuel demand, CO_2 emissions and flown distance thus also depend on the technology confidence level.

Finally, the relative nvPM emissions, required for the calculation of the contrail climate impact, are assumed to depend only on the fuel used. Unfortunately, few studies have been conducted on historic and future nvPM emissions, so our assumptions have a high degree of uncertainty. We assume a historical global soot number emission index $\mathrm{EI_s}$ (for Jet A/A-1) of $7.5 \times 10^{15}\,\mathrm{kg^{-1}}$ in 1952 (due to the prevalence of turbojet engines), $3 \times 10^{15}\,\mathrm{kg^{-1}}$ in 1972 and $2 \times 10^{15}\,\mathrm{kg^{-1}}$ in 1992. In 2019, we introduce the other fuels: Jet A-A/1 and LCAF are estimated at $1 \times 10^{15}\,\mathrm{kg^{-1}}$, SAF fuels at $1 \times 10^{14}\,\mathrm{kg^{-1}}$ and LH2 at $0\,\mathrm{kg^{-1}}$. The $\mathrm{EI_s}$ is linearly

improved until 2050 (Jet A/A-1 and LCAF: $7.5 \times 10^{14}\,\mathrm{kg}^{-1}$; SAFs $1 \times 10^{13}\,\mathrm{kg}^{-1}$) and then 2100 (Jet A/A-1 and LCAF: $5 \times 10^{14}\,\mathrm{kg}^{-1}$; SAFs $1 \times 10^{12}\,\mathrm{kg}^{-1}$). The simulations are conducted with the low-soot methods "MID" and "HIGH" (see Section 5.3.5).

6.2.4. DEVELOPING COMPATIBLE EMISSION INVENTORIES

The 3D emission inventories used for this analysis are developed from the WeCare emission inventory (Grewe et al., 2017a). The seven WeCare aircraft categories are combined into the three ICAO categories (RJ, NB, WB) as shown in Table 6.1, resulting in the vertical and latitudinal profiles in Figure 6.A.2.

A separate set of emission inventories is created for each scenario (unique combination of three integrated scenarios, three traffic forecasts and three technology confidence levels). Each emission inventory consists of multiple aircraft identifiers of the form *CAT_AC_YR_FUEL*: *CAT* corresponds to the category (RJ, NB, WB); *AC* to the aircraft type (ATW-T1, ACA-T2, ACA-T3); *YR* to the inventory year; and *FUEL* to the fuel used (Jet A/A-1, LCAF, SAF-FTG, SAF-CO_2, SAF-DAC, LH2). Each emission inventory thus has between one and 54 unique aircraft identifiers. The 3D sub-inventories for each aircraft identifier are created by scaling the fuel burn, distance flown and net CO_2 emissions of the corresponding combined *CAT* inventories to the right level according to the scenario. The distance flown by each aircraft is determined by multiplying the fuel burn by the relevant fuel efficiency (in $\mathrm{kg\,km}^{-1}$).

At the time of writing, it is not possible to input multiple evolution files into OpenAirClim[6]. Such a capability would be very beneficial for this use case, because it would allow the aircraft-specific parameters, such as the overall propulsion efficiency, to be modified over time. In lieu of this capability, we introduce generations of aircraft at regularly spaced intervals throughout the simulation. These generations do not correspond with actual aircraft; rather, they reflect the current average aircraft definition. This methodology is shown in Figure 6.3. To model the overall propulsion efficiency of NB aircraft ("actual"), generations of aircraft are introduced in specific years, shown by the cross markers. The dashed line ("approximated") is then the average overall propulsion efficiency (weighted by the flown distance). The lower plot shows how each generation (colours) is linearly introduced and removed – this is done automatically by OpenAirClim. Since the additive, proportional attribution method is used, the results can be arbitrarily combined, for example per aircraft category. The parameters for each aircraft ID required to run the contrail module are compiled into csv files that can be loaded into OpenAirClim separately.

The aircraft generations are introduced using the emission inventories. We thus create inventories for 15 different years: 1952 (only NB), 1964 (only NB), 1970

[6]"Evolution file" refers to an OpenAirClim input file that allows for various parameters to be modified over time. Allowing multiple files, for example one per aircraft type, to be inputted is currently not possible but under development at the time of writing.

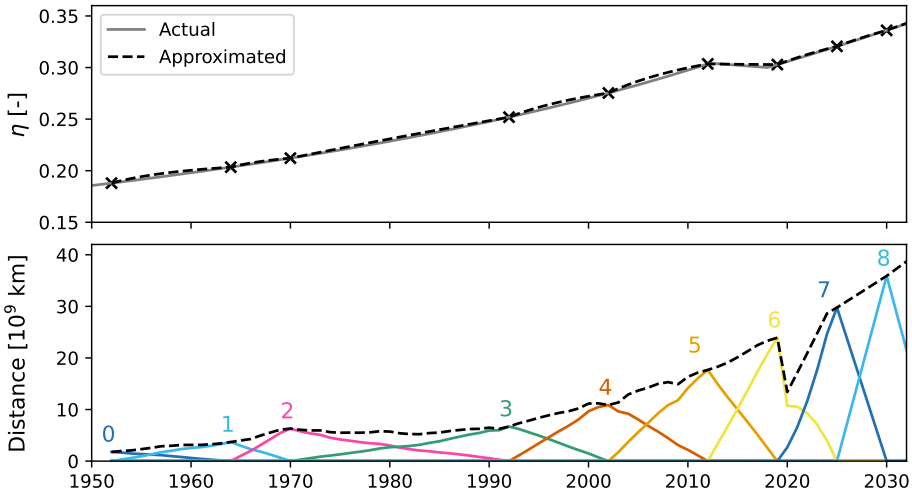


Figure 6.3: Demonstration of creating aircraft generations in lieu of providing evolution files per aircraft. The upper plot compares the overall propulsion efficiency η defined by ICAO ("actual") compared to the average η in the OpenAirClim simulation ("approximated"). This average value is obtained by introducing new generations of aircraft over time (numbering and colours in the lower plot). See the main text for more details.

(RJ and NB), 1992, 2002, 2012, 2019, 2025, 2030, 2035, 2040, 2045, 2050, 2060 and 2070. The inventories in years 1964 and 1970 are used to direct OpenAirClim to introduce a new aircraft category from the following year (RJ and WB respectively); in 2019 to introduce SAF; in 2035 to introduce ACA-T3 aircraft; in 2040 and 2050 to phase out Jet A/A-1; and in 2045 to phase out LCAF.

6.2.5. OPENAIRCLIM SIMULATION SETUP

OpenAirClim v0.13.0 is used for this analysis, coupled with the new contrail module described in Chapter 5[7]. The simulation is run from 1952 (introduction of first jet-powered aircraft) until 2070 (end of ICAO scenario). Only CO_2 and contrails are simulated in this study since the other modules are still under development. The default OpenAirClim setup and values are used. For CO_2, the Sausen and Schumann (2000) method is used to determine concentration changes; the Etminan et al. (2016) method for Radiative Forcing. To determine the temperature change for both CO_2 and contrails, we make use of Boucher and Reddy (2008) method with their implicit climate sensitivity $\lambda_{CO_2} = 1.06$ and the contrail efficacy $r_{\text{cont}} = 0.59$ from Ponater et al. (2006, their Table 1). The emission inventories, time evolution files and configuration files used for the analysis are available in the linked dataset.

[7]This custom OpenAirClim setup can be replicated with v0.15.0 (released Mar. 18, 2026, which introduced the new contrail module) and above. At the time of writing, only the high-soot regime is publicly available.

6.3. RESULTS

We find increasing temperature change from CO_2 and contrails over time in all ICAO scenarios, as shown in Figure 6.4. No scenario results in temperature stabilisation until the year 2070, even with the most optimistic assumptions (IS3L). For 2019, before the scenarios diverge, we find a CO_2 RF of $28.6\,\mathrm{mW\,m^{-2}}$, on the lower end of the best estimate of Lee et al. (2021), and a contrail RF of $54.6\,\mathrm{mW\,m^{-2}}$, significantly lower than their best estimate but still within their large uncertainty range (see also the discussion in Sections 3.3 and 5.4). This results in a temperature change of $15.3\,\mathrm{mK}$ and $17.6\,\mathrm{mK}$ respectively, similar to the estimates of Aamaas et al. (2025) ($12\,\mathrm{mK}$ and $21\,\mathrm{mK}$).

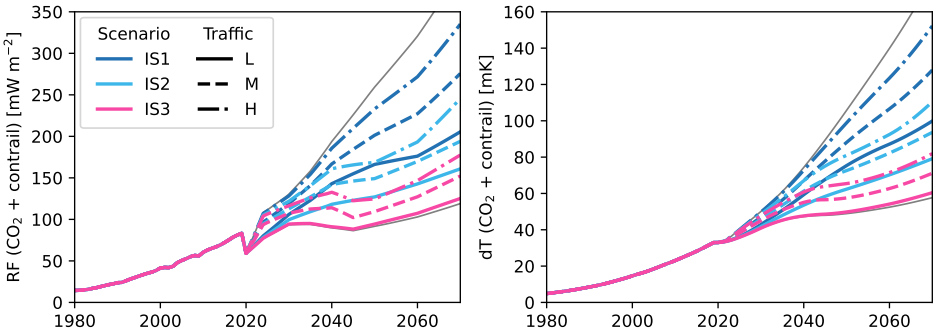


Figure 6.4: Radiative Forcing and temperature change from CO_2 and contrails for the ICAO scenarios. The colours correspond to the integrated scenarios, the line styles to the traffic forecasts (low, medium, high). The SSP2-4.5 background scenario, medium technology confidence level and low soot case MID are assumed. The thin, grey lines correspond to the limits of all sub-scenario combinations.

The three integrated scenarios differ notably in their expected temperature change. Between IS1 and IS3, the radiative forcing and temperature in 2070 are approximately halved, even though the total global fuel use of IS3 is only around 13 % lower than IS1 (Figure 6.1). This clearly demonstrates the importance of switching to alternative aviation fuels.

We find temperature change due to aviation CO_2 to have increased to between 25.4 and $89.1\,\mathrm{mK}$ (32.9 and $153.8\,\mathrm{mW\,m^{-2}}$) in 2070. This estimate is higher than Aamaas et al. (2025), who find 21 to $35\,\mathrm{mK}$ across all scenarios for the MID traffic forecast (other values were not reported). This is due to the difference in assumed climate sensitivity (see Section 6.4).

The two studies find similar temperature change for contrail-cirrus. Using OpenAirClim, we find between 30.0 and $95.1\,\mathrm{mK}$ (82.4 and $272.7\,\mathrm{mW\,m^{-2}}$) in 2070; from their Table S1, we can calculate that Aamaas et al. (2025) find between 14 and $71\,\mathrm{mK}$ across all three scenarios with a MID traffic forecast and accounting

for their upper/lower bounds for contrail ERF from alternative fuels. However, the close alignment of the temperature change is likely a coincidence in how the simulation parameters were chosen, rather than a result of similar modelling setups. Notably, the underlying (effective) radiative forcing values differ significantly between the two studies. The comparison is not straightforward, because ERF values are used as an input to CICERO-SCM, but by using the inverse of the ERF/RF ratio reported by Lee et al. (2021), it is possible to estimate Aamaas et al. (2025)'s contrail-cirrus RF range in 2070 to be 48 to 783 $\mathrm{mW\,m^{-2}}$ (IS3L and IS1H respectively). The model differences are discussed in more detail in Section 6.4.

We show the temperature change over time for the three integrated scenarios in Figure 6.5, assuming a medium traffic forecast, medium technology confidence, low soot case MID and the SSP2-4.5 background scenario. The results for low soot case HIGH are provided in Figure 6.A.3 for comparison. If we consider the contribution of CO_2 and contrails individually, we can identify that the temperature change from CO_2 emissions in IS3 almost reaches stabilisation (top row of Figure 6.5). Were the scenario to be continued beyond 2070, it is likely that the temperature change from CO_2 would begin to decline, in particular as more aircraft use SAF-DAC (assumed LCA value of 8.39 $\mathrm{gCO_2e/MJ}$, compared to 89.0 $\mathrm{gCO_2e/MJ}$ for Jet A/A-1) and LH2 (5.6 $\mathrm{gCO_2e/MJ}$).

However, the temperature change from contrails continues to increase. This is because while the CO_2 climate impact is reduced by increasing fuel efficiency and by switching to alternative fuels, the same is not necessarily true for contrails. As aircraft engines become more efficient, they are able to extract more energy from the exhaust, reducing its temperature. As a result, the Schmidt-Appleman slope, and hence likelihood of persistent contrail formation, increases (see Section 4.3.1). SAF generally has a higher Schmidt-Appleman slope than conventional kerosene due to a higher water vapour emission index (slightly offset by a larger lower heating value); this effect is of course even larger for hydrogen. For alternative fuels, the soot number emission index and how the low soot regime is treated are also vitally important.

The result is that by 2070, the RF for aircraft powered by alternative fuels is dominated by contrails: for low soot case MID, the contrail RF is approximately larger than the CO_2 by 3 times for SAF-FTG, 21 times for SAF-DAC and 45 times for LH2; for low soot case HIGH, this approximately doubles for SAF-FTG and SAF-DAC (LH2 remains effectively unchanged because zero nvPM emissions are treated differently – see Section 5.3.5). Therefore, as the flown distance continues to increase beyond 2070, the contrail climate impact can be assumed to also continue to increase in tandem. Further reduction of the contrail climate effect per flown distance would require changes to operations, notably contrail avoidance, which is not considered in this study.

The sensitivity of the temperature change from contrails on the low soot case is shown in Figure 6.6. The cases are described in more detail in Section 5.3.5: Low soot case HIGH attempts to replicate the latest findings of Voigt et al. (2026,

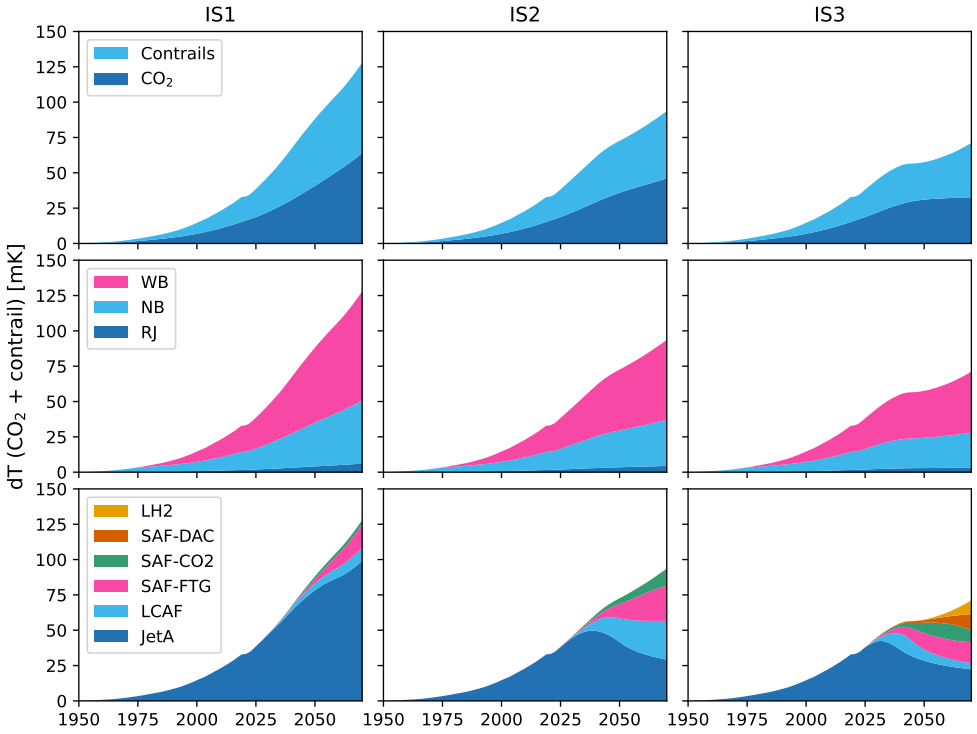


Figure 6.5: Temperature change for the ICAO scenarios split by source, aircraft category and fuel used. The medium traffic forecast, medium technology confidence, low soot case MID and the SSP2-4.5 background scenario are assumed.

$s_\tau = 0.8$), who find a significant increase in contrail ice crystals in the low soot regime due to volatile aerosols; case MID assumes a constant number of contrail ice crystals within the low soot regime ($s_\tau = 0.385$), approximately equivalent to the lowest value in the high soot regime. Hydrogen-powered aircraft are handled identically in both cases, at the same level as the rest of the low soot regime in case MID ($s_\tau = 0.385$).

The result of this assumption is that hydrogen-powered aircraft have a higher contrail-induced climate effect than SAF aircraft in case MID, since the probability of persistent contrail formation is higher for these aircraft (see Chapter 4). This is reversed in case HIGH, where the significant increase in ice crystal number densities erode the majority of the contrail climate advantage of SAF compared to conventional kerosene. The difference between the integrated scenarios is thus lower for low soot case HIGH than for case MID, so much so that the contrail-induced temperature change of IS1 and IS2 are almost identical, even though the relative SAF usage in IS2 is around double that in IS1. This only further underlines the importance of further research in the low soot regime.

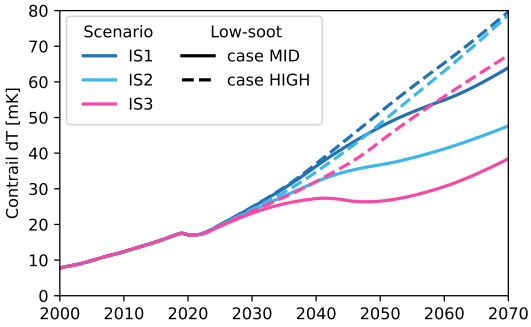


Figure 6.6: Sensitivity of the contrail-induced temperature change to the low soot case. The colours correspond to the integrated scenario, the line styles to the case. See Figure 5.7 for the definition of the low soot cases.

Widebody aircraft dominate the temperature change in all scenarios (middle row of Figure 6.5). However, when comparing different aircraft categories to one another, it is generally more interesting to consider the climate impact with respect to the Available Seat Kilometres (ASKs). This value is estimated by multiplying the flown distance by the number of passengers per category (Table 6.1). A better metric would be the Revenue Passenger Kilometre (RPK), which considers the load factor of each aircraft; in other words how many paying passengers are on board each aircraft. However, we do not have any meaningful historical data for the load factor and contemporary literature does not seem to show a significant difference between the load factors of various aircraft sizes (e.g. Hameed and Rutherford, 2025, their Table 4). Since our objective is to compare the aircraft categories to one another, these assumptions are considered sufficiently accurate.

The Radiative Forcing per ASK for both CO_2 and contrails is shown in Figure 6.7. Regional jet aircraft have the highest CO_2 impact per ASK, WB aircraft the lowest. Therefore, although the climate impact of WB aircraft is high, per ASK these aircraft are very effective from a climate perspective. Regional aircraft have the largest reduction potential of CO_2 RF per ASK, likely because of the large fleet replacement expected in the category (see Figure 6.2). The large peak in 2020 is due to the dramatic reduction in flown distance because of the COVID-19 pandemic. This is not seen in the contrail results because contrails are a short-lived climate forcer with lifetimes well below the OpenAirClim time step of one year, whereas the CO_2 RF results from all previous emissions.

The contrail RF per ASK is very similar across the categories. Since the nvPM emissions are assumed not to depend on the category, the differences can be attributed to differences in overall propulsion efficiency and emission location. Here, it is important to note that RJ aircraft fly at similar altitudes to NB and WB

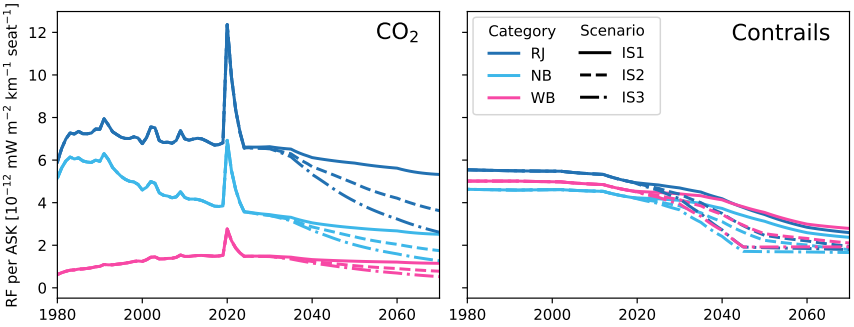


Figure 6.7: Radiative Forcing from CO_2 and contrails per Available Seat Kilometre. The colours correspond to the aircraft category (RJ, NB, WB), the line styles to the integrated scenario. Assumed are the medium traffic forecast, medium technology confidence, SSP2-4.5 and the low soot case MID.

aircraft – the results would look significantly different if only turboprop aircraft were considered as regional aircraft, because the likelihood of persistent contrail formation significantly reduces at lower altitudes.

6

The sensitivity of background emissions on the temperature change from aviation CO_2 emissions is around ± 10 % (Figure 6.A.4). In the context of rapidly increasing background emissions, such as in SSP5-8.5, the temperature change attributed to aviation is lower. On the other hand, if other industries significantly reduce their emissions, the relative contribution from aviation increases. The contrail-induced temperature change does not depend on the background emissions scenario.

Finally, the sensitivity of the technology confidence level on the temperature change is marginal (Figure 6.A.5). A higher technology confidence level means more efficient aircraft, which have a lower fuel burn and hence CO_2 impact. However, as discussed above, more efficient aircraft are more likely to form persistent contrails and hence have a higher contrail impact, assuming, as we do in this study, no corresponding changes in the soot emission index due to the engine efficiency. We find these effects to be approximately equal and opposite (approximately ± 6 % compared to MEDIUM in 2070), resulting in a net insensitivity to the technology confidence level. Of course this is simply a coincidence and would no longer be the case if other non-CO_2 species were also to be considered.

6.4. CONTEXTUALISATION OF THE RESULTS

This study generally backs up the findings of Aamaas et al. (2025), which was published during the preparation of this study. Compared to that study, we find

generally higher temperature change from CO_2, but similar temperature change from contrails. The difference in CO_2 temperature change is primarily because of the differing model setups and climate sensitivities used (see also Section 2.1.1): $\lambda_{CO_2} = 1.06\ \mathrm{K/(W\ m^{-2})}$ (OpenAirClim, implicitly through the use of the Boucher and Reddy (2008) temperature method[8]) vs. $\lambda_{CO_2} = 0.61$ (CICERO-SCM). We highly recommend performing a dedicated model intercomparison for simple and response models to better understand the model differences.

The difference in contrail temperature change is attributable to at least four main effects. The first two effects are related to a lower baseline RF and are straightforward to quantify. (1) Bier and Burkhardt (2022), which underpins the ECHAM5-CCMod simulations used to develop the OpenAirClim contrail module, find 22 % lower RF than the Lee et al. (2021) estimate. Since Aamaas et al. (2025) use this estimate and linearly scale the contrail ERF by fuel use over time, this difference is directly applicable. (2) The second effect relates to the use of track rather than slant distance (see Appendix 3.A): by using track distance, OpenAirClim's RF values are expected to be 12 % lower.

The third effect relates to differences in the climate sensitivity and efficacy values used in OpenAirClim and CICERO-SCM. This effect is difficult to quantify, because the two studies use very different model setups: OpenAirClim directly calculates RF and then uses the Boucher and Reddy (2008) method to calculate a temperature change, whereas Aamaas et al. (2025) used the ERF values over time as an input perturbation to CICERO-SCM. Nevertheless, at a high-level, following Eq. 2.2, the relationship between RF and ΔT is proportional to $r \cdot \lambda_{CO_2}$. Therefore, for OpenAirClim, $0.59 \cdot 1.06 = 0.62$. Since Aamaas et al. (2025) use the ERF as an input (with an assumed ERF-based efficacy $r' = 1.0$), but define λ_{CO_2} with respect to RF, we need to use the ERF/RF ratio found by Lee et al. (2021), i.e.: $r' \cdot (\mathrm{ERF/RF}) \cdot \lambda_{CO_2} = 0.42 \cdot 0.61 = 0.26$. For the same RF, OpenAirClim's temperature change is thus expected to be 142 % higher.

The fourth main effect relates to the non-linear saturation behaviour of contrail RF for future air traffic growth. As Figure 5.14 shows, a simple, linearised contrail model begins to overestimate RF beyond approximately $200\ \mathrm{mW\ m^{-2}}$. Using their Eq. (5) and the ERF/RF ratio as above, we can reverse-calculate RF values from Aamaas et al. (2025) of up to $783\ \mathrm{mW\ m^{-2}}$. This is well within the range where saturation effects matter: At $783\ \mathrm{mW\ m^{-2}}$, the RF is overestimated compared to literature (notably Bickel et al., 2020) by 89 %. OpenAirClim captures non-linear effects for future air traffic better, as demonstrated by Figure 5.10. Therefore, as air traffic increases, OpenAirClim will estimate significantly lower RF values than CICERO-SCM, but quantifying this is not possible without a dedicated analysis.

Other effects are likely to play a role, but also cannot be quantified here. Of particular importance is how alternative fuels are considered in the two studies.

[8] Until the release of OpenAirClim v0.18.0, the λ_{CO_2} selected by the user in the configuration file had no effect. See also Issue dlr-pa/oac/#129.

Aamaas et al. (2025) scale the ERF by the fuel use and by factors corresponding to the relative change in ERF per unit fuel energy compared to conventional kerosene. In comparison, in this study we adapt the aircraft designs and soot emissions over time.

In total, therefore, effects 1 and 2 are in the order of 10-20 %, effects 3 and 4 are much larger but opposite, and further effects (notably how alternative fuels are considered) are unknown. The net effect is that both studies produce similar temperature change values for contrail-cirrus in the year 2070. However, this must be seen as a coincidence due to the choice of simulation parameters (efficacy, climate sensitivity) rather than as a result of similar modelling strategies. Nevertheless, the core message of both studies is the same: no ICAO scenario achieves temperature stabilisation within the study horizon.

6.5. DISCUSSION AND CONCLUSION

The assessment of long-term aviation climate impacts requires integrated and internally consistent scenarios that consider future pathways for technology, operations and fuels. This study focused on the scenarios created by the International Civil Aviation Organization (ICAO) in support of an assessment into the feasibility of a Long-Term global Aspiration Goal (LTAG) for international civil aviation. The global mean radiative forcing and surface temperature change were estimated for all scenarios using the response model OpenAirClim. This study marks the first integrated model test of the OpenAirClim framework and demonstrates its ability to simulate complex, multi-fuel and multi-aircraft scenarios. Furthermore, a detailed overview of the scenario and emission inventory harmonisation process is provided to aid future users to perform similar studies using OpenAirClim.

The analysis presented in this chapter underscores how challenging the transition to more sustainable aviation is. We find that no ICAO scenario results in a temperature stabilisation from CO_2 and contrails until 2070, even with the most optimistic assumptions. The switch to alternative fuels, generally seen as the primary means of reducing the industry's climate impact, is challenging technologically and a number of open questions remain regarding the climatic benefits the switch would bring. For net CO_2, viewed from a life-cycle perspective, it is a clear win: Phasing out fossil fuels (Jet A/A-1 and LCAF) as soon as possible is vital, because CO_2 Radiative Forcing remains for a long time. For contrails, however, it is more difficult. As we demonstrate, the benefit in switching to SAF really depends on the definition of the low-soot regime. If, as the latest studies suggest (Voigt et al., 2026), the total number of ice crystals do not reduce at significantly lower soot emission levels because of volatile particles in the exhaust and surrounding air (modelled with low-soot case HIGH), the difference in climate impact compared with conventional fossil fuel will, unfortunately, be small.

The ICAO scenarios are highly complex and integrated. Their analysis is certainly interesting, but, because many parameters change simultaneously, not fit-for-purpose if the goal is to understand individual effects. Since the scenarios were not designed with non-CO_2 effects in mind, a number of high-level assumptions were required to harmonise the scenarios with OpenAirClim. One major assumption relates to the fleet composition: Since this data was not provided by ICAO, likely because the analysis was performed with proprietary software, we assume a fixed split in the aircraft categories from 1992 onwards. This is important because widebody aircraft are found to have a significantly lower climate impact per ASK than narrowbodies and regional jets. The scenarios also did not consider any operational strategies for reducing non-CO_2 climate effects, such as climate optimised routing and contrail avoidance (Grewe et al., 2017b; Niklaß et al., 2021; Sausen et al., 2024), flying higher/lower (Matthes et al., 2021) and targeted SAF usage (Teoh et al., 2022b; Woeldgen et al., 2025). Since the implementation of such strategies is likely feasible within the scenario time frame (until 2070), the temperature changes found by this study could potentially be significantly reduced.

This chapter is the first demonstration of OpenAirClim for complex, integrated scenarios. During preparation of the study, a number of improvements and suggestions for future development of the model were identified. The first is an improved flexibility in the creation of time evolution files. It would be highly beneficial for the contrail module to allow aircraft characteristics to change over time; and for the main model to be able to define normalised or scaled fuel use, emission index and flown distance for sub-inventories (e.g. corresponding to a single aircraft identifier). In this way, the number of emission inventory years could have been reduced, significantly cutting down computation time. The second recommendation is to work on the development of a Graphical User Interface (GUI) with which the full OpenAirClim scenario can be viewed, and perhaps subsequently simulated. This could allow obvious mistakes in the configuration files to be more easily detected. Finally, a dedicated comparison to other models will be paramount to understanding the functioning of OpenAirClim.

This study could be improved by including further emission species, in particular NO_x and water vapour. New emission inventories, separated by aircraft type or category, could also be developed, designed specifically for future air traffic and perhaps including other aircraft categories such as business jets and turboprops, which were considered by ICAO but not included in WeCare. However, the largest uncertainties in this study relate to the contrail calculations, specifically the contrail efficacy, assumed future soot emissions and the treatment of the low-soot regime. Particularly relevant would be a dedicated analysis, for example using a Monte Carlo method, to quantify the uncertainties inherited from the base model (ECHAM5-CCMod) and those introduced by the parameterisations of the OpenAirClim contrail module.

6.A. APPENDIX

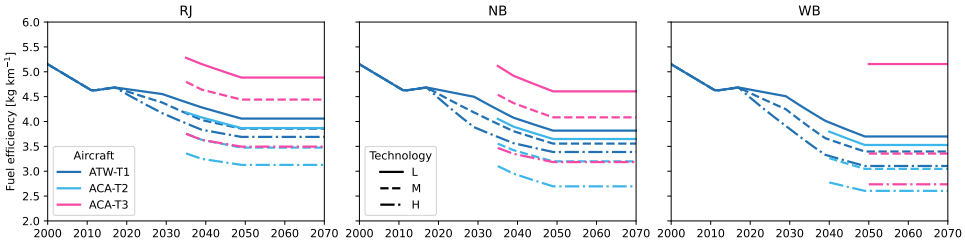


Figure 6.A.1: Assumed fuel efficiency values for ICAO scenarios. The colours correspond to the aircraft types; the line styles to the technology confidence levels. At lower technology confidence, the fuel efficiency of the ACA-T3 – novel technologies and non-drop-in fuels – is assumed to be worse (higher value) than the ATW-T1.

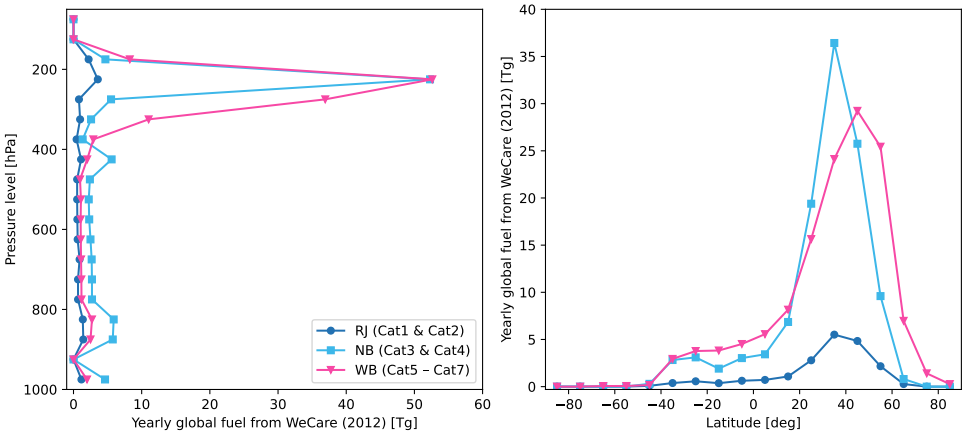


Figure 6.A.2: Vertical and latitudinal profiles of the aircraft categories used in this study. The three categories (RJ, NB and WB, see main text) are combinations of the WeCare dataset of seven aircraft categories (Cat1 – Cat7).

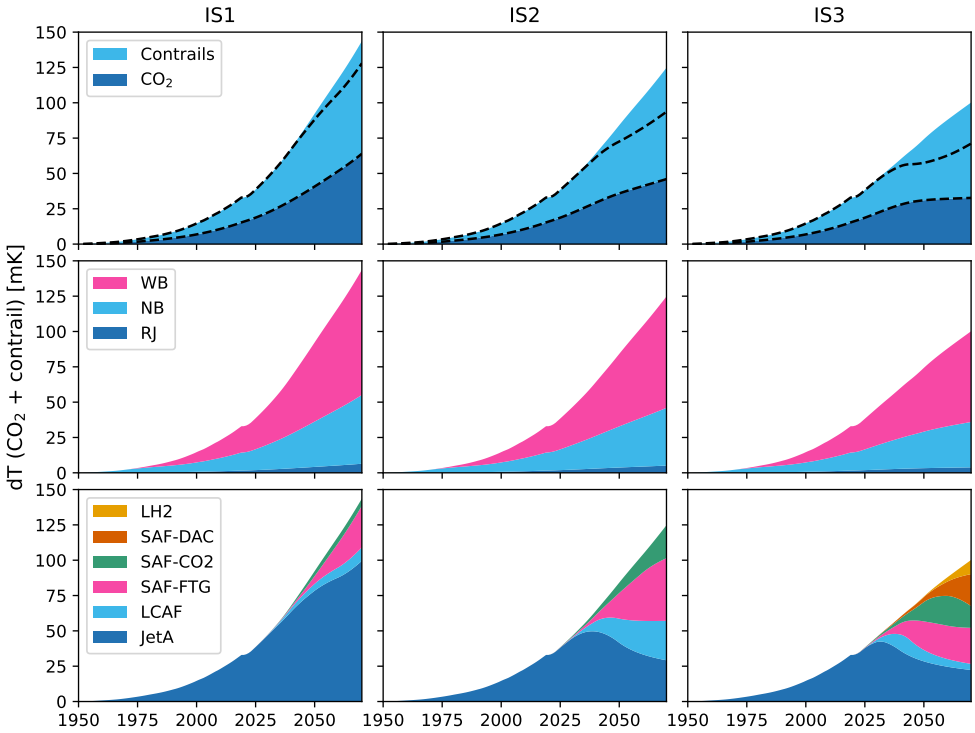


Figure 6.A.3: Temperature change for the ICAO scenarios split by source, aircraft category and fuel used. The medium traffic forecast, medium technology confidence, low soot case HIGH and the SSP2-4.5 background scenario are assumed. The results for low soot case MID are shown by the black dashed line.

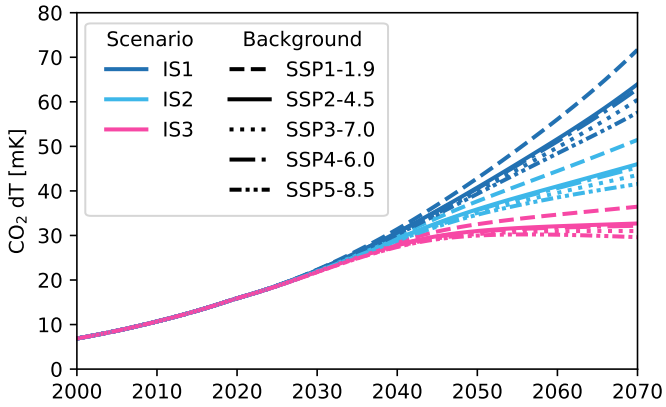


Figure 6.A.4: Sensitivity of the background emission scenario on the temperature change from aviation CO_2 emissions. The colours correspond to the integrated scenario, the line styles to the background scenario. Assumed are the medium traffic forecast and medium technology confidence.

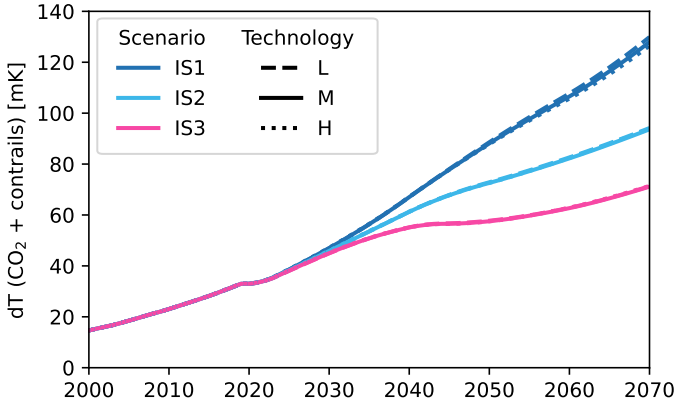


Figure 6.A.5: Sensitivity of the technology confidence level on the temperature change. The colours correspond to the integrated scenario, the line styles to the technology confidence level. Assumed are the low soot case MID, the medium traffic forecast and the SSP2-4.5 background emissions.

REFERENCES

Aamaas, B., Lund, M. T., Fuglestvedt, J. S., Totterdill, A., Owen, B., Skowron, A., and Lee, D. S.: Continued global warming from aviation even under high-ambition mitigation scenarios, One Earth, 101451, doi: 10.1016/j.oneear.2025.101451, 2025.

Baughcum, S. L., Tritz, T. G., Henderson, S. C., and Pickett, D. C.: Scheduled civil aircraft emission inventories for 1992: Database development and analysis, Tech. Rep. CR-4700, NASA, 1996.

Bickel, M., Ponater, M., Bock, L., Burkhardt, U., and Reineke, S.: Estimating the effective radiative forcing of contrail cirrus, Journal of Climate, 33, 1991–2005, doi: 10.1175/JCLI-D-19-0467.1, 2020.

Bier, A. and Burkhardt, U.: Impact of parametrizing microphysical Processes in the jet and vortex phase on contrail cirrus properties and radiative forcing, Journal of Geophysical Research: Atmospheres, 127, doi: 10.1029/2022JD036677, 2022.

Bock, L. and Burkhardt, U.: Contrail cirrus radiative forcing for future air traffic, Atmospheric Chemistry and Physics, 19, 8163–8174, doi: 10.5194/acp-19-8163-2019, 2019.

Boucher, O. and Reddy, M.: Climate trade-off between black carbon and carbon dioxide emissions, Energy Policy, 36, 193–200, doi: 10.1016/j.enpol.2007.08.039, 2008.

Dischl, R., Märkl, R., Sauer, D., Voigt, C., Harlaß, T., Scheibe, M., Hahn, V., Kaufmann, S., Marsing, A., Dörnbrack, A., Roiger, A., Yu, F., Gauthier, M., Renard, C., Swann, P., Johnson, M., Ahrens, D., Sallinen, R., Eckel, G., and Le Clercq, P.: Fuel sulfur content can modulate contrail ice crystal numbers, Communications Earth & Environment, 6, 902, doi: 10.1038/s43247-025-02951-5, 2025.

Etminan, M., Myhre, G., Highwood, E. J., and Shine, K. P.: Radiative forcing of carbon dioxide, methane, and nitrous oxide: A significant revision of the methane radiative forcing, Geophysical Research Letters, 43, doi: 10.1002/2016gl071930, 2016.

Grewe, V., Bock, L., Burkhardt, U., Dahlmann, K., Gierens, K., Hüttenhofer, L., Unterstrasser, S., Gangoli Rao, A., Bhat, A., Yin, F., Reichel, T. G., Paschereit, O., and Levy, Y.: Assessing the climate impact of the AHEAD multi-fuel blended wing body, Meteorologische Zeitschrift, 26, 711–725, doi: 10.1127/metz/2016/0758, 2017a.

Grewe, V., Matthes, S., Frömming, C., Brinkop, S., Jöckel, P., Gierens, K., Champougny, T., Fuglestvedt, J., Haslerud, A., Irvine, E., and Shine, K.: Feasibility of climate-optimized air traffic routing for trans-Atlantic flights, Environmental Research Letters, 12, 034 003, doi: 10.1088/1748-9326/aa5ba0, 2017b.

Grewe, V., Gangoli Rao, A., Grönstedt, T., Xisto, C., Linke, F., Melkert, J., Middel, J., Ohlenforst, B., Blakey, S., Christie, S., Matthes, S., and Dahlmann, K.: Evaluating the climate impact of aviation emission scenarios towards the Paris agreement including COVID-19 effects, Nature Communications, 12, 3841, doi: 10.1038/s41467-021-24091-y, 2021.

Hameed, M. and Rutherford, D.: Fuel burn of new commercial jet aircraft: 1960 to 2024, Tech. Rep. 287, Internationl Council on Clean Transportation, https://theicct.org/wp-content/uploads/2025/02/ID-287-%E2%80%93-Jet-aircraft_working-paper_final.pdf, 2025.

ICAO: Report on the Feasibility of a Long-Term Aspirational Goal (LTAG) for International Civil Aviation CO2 Emission Reductions, Tech. rep., ICAO (Committee on Aviation Environmental Protection), https://www.icao.int/sites/default/files/sp-files/environmental-protection/LTAG/Documents/REPORT%20ON%20THE%20FEASIBILITY%20OF%20A%20LONG-TERM%20ASPIRATIONAL%20GOAL_en.pdf, 2022.

Jing, L., El-Houjeiri, H. M., Monfort, J.-C., Brandt, A. R., Masnadi, M. S., Gordon, D., and Bergerson, J. A.: Carbon intensity of global crude oil refining and mitigation potential, Nature Climate Change, 10, 526–532, doi: 10.1038/s41558-020-0775-3, 2020.

Kärcher, B.: Formation and radiative forcing of contrail cirrus, Nature Communications, 9, 1824–1824, doi: 10.1038/s41467-018-04068-0, 2018.

Lee, D., Fahey, D., Skowron, A., Allen, M., Burkhardt, U., Chen, Q., Doherty, S., Freeman, S., Forster, P., Fuglestvedt, J., Gettelman, A., De León, R., Lim, L., Lund, M., Millar, R., Owen, B., Penner, J., Pitari, G., Prather, M., Sausen, R., and Wilcox, L.: The contribution of global aviation to

anthropogenic climate forcing for 2000 to 2018, Atmospheric Environment, 244, 117 834, doi: 10.1016/j.atmosenv.2020.117834, 2021.

Leipold, A., Aptsiauri, G., Ayazkhani, A., Bauder, U., Becker, R.-G., Berghof, R., Claßen, A., Dadashi, A., Dahlmann, K., Dzikus, N., Flüthmann, N., Grewe, V., Göhlich, L., Grimme, W., Günther, Y., Jaksche, R., Jung, M., Knabe, F., Kutne, P., Le Clercq, P., Pabst, H., Poggel, S., Staggat, M., Wicke, K., Wolters, F., Zanger, J., and Zill, T.: DEPA 2050 – Development Pathways for Aviation up to 2050 (Final Report), Tech. rep., DLR, Köln, https://elib.dlr.de/142185/, 2021.

Matthes, S., Lim, L., Burkhardt, U., Dahlmann, K., Dietmüller, S., Grewe, V., Haslerud, A. S., Hendricks, J., Owen, B., Pitari, G., Righi, M., and Skowron, A.: Mitigation of non-CO2 aviation's climate impact by changing cruise altitudes, Aerospace, 8, 36, doi: 10.3390/aerospace8020036, 2021.

Niklaß, M., Grewe, V., Gollnick, V., and Dahlmann, K.: Concept of climate-charged airspaces: a potential policy instrument for internalizing aviation's climate impact of non-CO2 effects, Climate Policy, 21, 1066–1085, doi: 10.1080/14693062.2021.1950602, 2021.

Ponater, M., Pechtl, S., Sausen, R., Schumann, U., and Hüttig, G.: Potential of the cryoplane technology to reduce aircraft climate impact: A state-of-the-art assessment, Atmospheric Environment, 40, 6928–6944, doi: 10.1016/j.atmosenv.2006.06.036, 2006.

Randt, N. P.: Aircraft Technology Assessment Using Fleet-Level Metrics, Ph.D. thesis, Technische Universität München, 2016.

Sandstad, M., Aamaas, B., Johansen, A. N., Lund, M. T., Peters, G. P., Samset, B. H., Sanderson, B. M., and Skeie, R. B.: CICERO Simple Climate Model (CICERO-SCM v1.1.1) – an improved simple climate model with a parameter calibration tool, Geoscientific Model Development, 17, 6589–6625, doi: 10.5194/gmd-17-6589-2024, 2024.

Sausen, R. and Schumann, U.: Estimates of the climate response to aircraft CO2 and NOx emissions scenarios, Climatic Change, 44, 27–58, doi: 10.1023/A:1005579306109, 2000.

Sausen, R., Hofer, S., Gierens, K., Bugliaro, L., Ehrmanntraut, R., Sitova, I., Walczak, K., Burridge-Diesing, A., Bowman, M., and Miller, N.: Can we successfully avoid persistent contrails by small altitude adjustments of flights in the real world?, Meteorologische Zeitschrift, 33, 83–98, doi: 10.1127/metz/2023/1157, 2024.

Teoh, R., Schumann, U., Gryspeerdt, E., Shapiro, M., Molloy, J., Koudis, G., Voigt, C., and Stettler, M. E. J.: Aviation contrail climate effects in the North Atlantic from 2016 to 2021, Atmospheric Chemistry and Physics, 22, 10 919–10 935, doi: 10.5194/acp-22-10919-2022, 2022a.

Teoh, R., Schumann, U., Voigt, C., Schripp, T., Shapiro, M., Engberg, Z., Molloy, J., Koudis, G., and Stettler, M. E. J.: Targeted use of sustainable aviation fuel to maximize climate benefits, Environmental Science & Technology, 56, 17 246–17 255, doi: 10.1021/acs.est.2c05781, 2022b.

Voigt, C., Märkl, R., Sauer, D., Dischl, R., Renard, C., Seeliger, K., Yu, F., Kaufmann, S., Bräuer, T., Jurkat-Witschas, T., Le Chenadec, G., Moreau, J., Requena-Esteban, E., Bonne, N., Vals, M., Roche, A., Zelina, J., Dörnbrack, A., Eirenschmalz, L., Heckl, C., Horst, E., Lichtenstern, M., Marsing, A., Neumann, G., Roiger, A., Scheibe, M., Stock, P., Giez, A., Eckel, G., and Le Clercq, P.: Substantial aircraft contrail formation at low soot emission levels, Nature, 652, 112–118, doi: 10.1038/s41586-026-10286-0, 2026.

Woeldgen, E., Teoh, R., Stettler, M. E. J., and Malina, R.: Sustainable Aviation Fuel deployment strategies in Europe: Supply chain implications and climate benefits, Environmental Science & Technology, 59, 12 447–12 457, doi: 10.1021/acs.est.5c02364, 2025.

Waiting.

the world warms,
we argue the metric,
crickets tonight.

— LM

7

ANALYSIS OF CLIMATE METRICS

This chapter has been published and reproduced with permission from Springer Nature as:

Megill, L., Deck, K. and Grewe, V.: Alternative climate metrics to the Global Warming Potential are more suitable for assessing aviation non-CO_2 effects, Communications Earth & Environment, 5, 249, doi: 10.1038/s43247-024-01423-6, 2024.

It also contains elements from:

de Haes, V., ..., **Megill, L.**, et al.: Support for establishing a monitoring, reporting and verification system for non-CO2 effects in aviation, stemming from the revision of the ETS Directive. Final Report, 2025.

Grewe, V., Zhukovska, S., ..., **Megill, L.**, et al.: Review of methods for assessing the climate impacts of aviation technologies and the resulting best practices, CEAS Aeronautical Journal, doi: 10.1007/s13272-026-00980-0, 2026

Data and code available at:

Megill, L., Deck, K. and Grewe, V.: Data and code underlying the publication "Alternative climate metrics to the Global Warming Potential are more suitable for assessing aviation non-CO2 effects", 4TU.ResearchData, doi: 10.4121/344e24ad-b2f5-4ed9-8d49-6efa2081d30c, 2024.

ABSTRACT

A growing body of research has highlighted the major contribution of aviation non-CO_2 emissions and effects to anthropogenic climate change. Regulation of these emissions, for example in the EU Emissions Trading System, requires the use of a climate metric. However, choosing a suitable climate metric is challenging due to the high uncertainties of aviation non-CO_2 climate impacts, their variability in atmospheric lifetimes and their dependence on emission location and altitude. Here we use AirClim to explore alternatives to the conventional Global Warming Potential (GWP) by analysing the neutrality, temporal stability, compatibility and simplicity of existing climate metrics and perform a trade-off. We find that using the temperature-based Average Temperature Response (ATR) or using an Efficacy-weighted GWP (EGWP) would enable a more accurate assessment of existing as well as future aircraft powered by novel aviation fuels.

7.1. INTRODUCTION

The EU Parliament recently adopted legislation (Directive 2023/958 of 10 May 2023 amending Directive 2003/87/EC) that aims to revise the EU Emissions Trading System (ETS) for aviation, inter alia requiring the European Commission to include aviation non-CO_2 effects in a monitoring, reporting and verification (MRV) framework and, if deemed appropriate, expand the scope of the ETS to include aviation non-CO_2 effects by the end of 2027[1]. Such implementation requires the use of a climate metric, which relates non-CO_2 emissions and effects to their consequences on the climate and/or on society (Fuglestvedt et al., 2003, 2010; Wuebbles et al., 2010; Tanaka et al., 2010). To maintain compatibility with market-based or offsetting schemes such as the ETS, climate metrics are often used as exchange rates, expressing non-CO_2 emissions on a common scale with CO_2 emissions. This single-basket approach can simplify climate negotiations and the implementation of climate policies (Tanaka et al., 2010).

However, establishing an adequate equivalence is not trivial and there is currently no consensus on which climate metric is most appropriate for aviation. In international climate policy, the most commonly used climate metric is the Global Warming Potential (GWP; Rodhe, 1990; Fuglestvedt et al., 2003), although it has been heavily criticised, primarily due to its dependence on the time horizon (Manne and Richels, 2001; Shine et al., 2007; Allen et al., 2016; Ocko et al., 2017).

[1]The analysis of climate metrics specifically for use in the MRV was conducted as part of this PhD research. The results of this analysis are discussed in Section 7.4.1.

The choice of climate metric for aviation climate policy is further complicated because aviation non-CO_2 emissions and effects have highly varying atmospheric lifetimes (see Section 2.1.2) and efficacies (Ponater et al., 2006), are dependent on the emission time, altitude and location (Frömming et al., 2021; Lund et al., 2017) and their impacts on the climate have a high degree of uncertainty (Lee et al., 2010, 2021). Furthermore, since each climate metric uses a different climate indicator (e.g. stratospheric-adjusted radiative forcing or global mean near-surface temperature change) and calculation method (Grewe and Dahlmann, 2015), a climate metric can inherently and inadvertently place emphasis on certain aircraft design choices, emission species or effects. The choice of climate metric is thus an important consideration for all stakeholders to ensure that the implementation of climate policy results in the desired reduction of the aviation industry's impact on climate and on society (Tanaka et al., 2010; Grewe and Dahlmann, 2015).

In this chapter, we explore the applicability of existing, physical climate metrics to the aviation industry. Specifically, we analyse the compatibility to aircraft design and aviation policy, methodological simplicity, neutrality and stability of the following conventional climate metrics (see Section 2.3): Radiative Forcing (RF) and the Radiative Forcing Index (RFI - relative RF; IPCC, 1999; Forster et al., 2006), GWP (Rodhe, 1990; Fuglestvedt et al., 2003), Global Temperature Change Potential (GTP; Shine et al., 2005), Integrated GTP (iGTP; Peters et al., 2011) and Average Temperature Response (ATR; Dallara et al., 2011). The performance of a recently proposed, unconventional method that relates the changes in emission rates of short-lived species to pulses of CO_2, denoted GWP* (Allen et al., 2018; Cain et al., 2019; Smith et al., 2021), is also evaluated. We further analyse derivatives of the GWP and GWP* that are weighted by the efficacy, which we denote the Efficacy-weighted Global Warming Potential (EGWP) and EGWP* respectively.

The chapter is set up as follows. Section 7.2 describes the methodology, including the climate metric calculation methods, requirements and aircraft design. The results per requirement are presented in Section 7.3, along with an overview of the performance of each climate metric and the choices that need to be made in the selection. Feedback on Megill et al. (2024), upon which this chapter is based, was obtained during the EU MRV project[2] as well as at a dedicated workshop in June 2024 in Hamburg as part of the CLAIM project[3]. This feedback is presented and discussed in Section 7.4. Finally, the results are discussed in Section 7.5.

[2]Support for establishing a monitoring, reporting and verification system for non-CO_2 effects in aviation, stemming from the revision of the ETS Directive, CLIMA/2023/OP/0005

[3]Clean Aviation Support for Impact Monitoring, HORIZON-JU-CLEAN-AVIATION-2023-02-CSA-01, https://www.claim-project.eu/

7.2. METHODS

This section outlines the data and methods used to analyse the performance of climate metrics for aviation. Section 7.2.1 outlines the four requirements for aviation climate metrics, which correspond to the analyses in Section 7.3. The fuel scenarios and aircraft designs are described in Sections 7.2.2 and 7.2.3 respectively. The metric calculation methods are provided in Section 2.3.2.

7.2.1. DEVELOPMENT OF CLIMATE METRIC REQUIREMENTS

Climate metrics are used in both their absolute form and relative to CO_2. In aviation, absolute climate metrics have two primary use cases: in trajectory optimisation, where aircraft are re-routed to avoid climate sensitive regions (Niklaß et al., 2021; Grewe et al., 2014); and in aircraft design, where the climate metric can be part of the design trade-off process (e.g. Proesmans and Vos, 2022). Relative metrics are primarily used at a policy level, notably to calculate CO_2-equivalent emissions and multipliers in single-basket emissions trading schemes such as the ETS (Tanaka et al., 2010; Fuglestvedt et al., 2003).

From these use cases, we identify the following main requirements for climate metrics used for aviation. Aviation climate metrics shall:

1. **Neutrally represent the chosen climate indicator (REQ 1)**
   Rogelj and Schleussner (2019); Grewe and Dahlmann (2015)
   Value judgements should be left to policymakers and should not be built into climate metrics. Therefore, a climate metric should not exhibit any inherent bias towards specific aircraft design changes.

2. **Be temporally stable (REQ 2)**
   Meinshausen and Nicholls (2022)
   For aviation policy, it should be possible to use climate metrics to monitor how well the industry is performing through annual and quarterly reports. The results shown by a climate metric, and thus the emission offsetting cost, should not vary to the extent that policymakers cannot gauge the effectiveness of their policies, and airlines and other stakeholders cannot estimate their offsetting cost.

3. **Be compatible with existing climate policy (REQ 3)**
   Meinshausen and Nicholls (2022)
   A new climate metric must still be able to perform the same functions in the current climate policy context.

4. **Be simple to understand and implement (REQ 4)**
   Meinshausen and Nicholls (2022); Wuebbles et al. (2010); Fuglestvedt et al. (2010)

Non-specialists should be able to understand how a climate metric is calculated and be able to correctly interpret what its results show.

In Section 7.3, we analyse each requirement individually and recommend the best-suited climate metric based on the results. We also analyse the impact of the time horizon on the results. For the purposes of analysing climate metrics with time horizons in the order of years, the responses of other very short-lived species such as aerosols are expected and assumed to be qualitatively the same as for contrails. Note that in this study, we add an A to denote an absolute climate metric (i.e. AGWP, AEGWP, AGTP, iAGTP) and use rATR to denote the relative ATR (to CO_2). The GWP* and EGWP* do not have absolute and relative forms. Where necessary for clarification, we also use P-, F- and S- to denote climate metrics calculated using a pulse, fleet or total aviation industry emission scenario respectively.

7.2.2. DEVELOPMENT OF FUEL SCENARIOS

This research is based on the CORSIA and Flightpath 2050 (FP2050) fuel scenarios developed by Grewe et al. (2021). Since time horizons of up to 100 years are analysed, the scenarios needed to be extended. For this research, they have been extended until the year 2200, assuming a 0.5% annual growth rate after the year 2100. The scenarios are developed to test climate metrics and have not been evaluated for reliability and accuracy.

7.2.3. DEVELOPMENT OF AIRCRAFT DESIGNS

The fleets used in this research are theoretical and characterised with a set of input parameters in AirClim, chosen uniformly from the ranges shown in Table 7.1. The parameter ranges are based on expected technological pathways developed by Grewe et al. (2021), by the Clean Sky 2 Technology Evaluator (Gelhausen et al., 2022) and by the Hydrogen-Powered Aviation report (Fuel Cells and Hydrogen 2 Joint Undertaking, 2020).

Table 7.1: Ranges of fleet design parameters for the fleet pairing analysis simulations. See the accompanying text for a more detailed description of the contrail distance modifier, and Table 7.2 for the impact of different fuels.

Parameter	Range	Reference	Minimum	Maximum
Fuel burn (40% of category) [Tg]	70 - 100%	100%	70%	100%
NO_xemission [Tg]	70 - 100%	100%	70%	100%
Cruise pressure [hPa]	80 - 120%	100%	120%	80%
Contrail distance modifier [km]	40 - 100%	100%	40%	100%
Fuel used [-]	Jet-A1, SAF, H_2	Jet-A1	H_2(FC)	Jet-A1
Year of fleet introduction [yr]	2030 - 2050	2030	2030	2030
Background emissions [-]	SSP1 - SSP5	SSP2-4.5	SSP2-4.5	SSP2-4.5

The contrail distance modifier mentioned in the Table is a multiplier for the total cruise distance over which contrails form, which is an AirClim input. In this context, a factor below unity corresponds to aircraft flying further to avoid climate sensitive regions and, therefore, contrail formation. As a result, the reduction in contrail distance is coupled with an increase in fuel burn, estimated from Yin et al. (2018) to be of the ratio -15%:1% contrail distance to fuel burn up to a contrail distance reduction of 60% (contrail distance modifier of 40%), which is approximately the end of the quasi-linear region of the Pareto fronts calculated.

For fleets using fuels other than Jet-A1, the emissions parameters are further modified according to Table 7.2. Here, the contrail reduction is assumed to correspond to changes in the exhaust composition due to the use of different fuels. We note that the data in both tables are a simplification and that comprehensive data is not yet available for different fuel types. However, since our objective is to provide a wide range of potential future fleets, this simplification is deemed appropriate and should not affect the results of this research.

Table 7.2: Assumed change of in-flight emissions and emission-related effects for Sustainable Aviation Fuel (SAF) and hydrogen. The values are taken from the Hydrogen-Powered Aviation report (Fuel Cells and Hydrogen 2 Joint Undertaking, 2020). Note that these values cannot currently be corroborated through other studies and are, therefore, only used to provide a wide spectrum of potential future fleets.

Fuel	CO_2	NO_x	H_2O	Contrails	Total
SAF	-65-80%[4]	-0%	-0%	-10-40%	-30-60%
Hydrogen combustion	-100%	-50-80%	+150%	-30-50%	-50-75%
Hydrogen fuel cell	-100%	-100%	+150%	-60-80%	-75-90%

For each fleet, a constant production rate is assumed, expected to last 30 years. Production is assumed to begin after 2030, approximately on par with the expected introduction of the next generation of single-aisle aircraft and new fuels such as hydrogen according to the analyses of Grewe et al. (2021). The exact year of introduction of new fleets is, however, not relevant to the outcome of this study and is thus varied. Each aircraft is further assumed to have a lifetime of 35 years with no hull losses. A single-aisle aircraft about the size of the Airbus A320 is chosen for reference. For simplicity, the fuel use of this fleet is taken to be 40% of Category 4 of the DLR WeCare project (Grewe et al., 2017), characterised by aircraft with seat numbers between 152 and 201. A total of 10 000 fleets are simulated using AirClim.

7.3. RESULTS

This section presents the performance of the climate metrics with respect to the four requirements set in Section 7.2.1. The results of each analysis are shown in Sections 7.3.1-7.3.4. We provide an overview of the requirements and discuss the

choice of climate metric and time horizon in Section 7.3.5.

7.3.1. REQ 1: CLIMATE METRIC NEUTRALITY WITH RESPECT TO AVIATION EMISSIONS

To assess the neutrality of climate metrics for aircraft design, the peak and average total temperatures and climate metric values of potential future fleets are compared. A wide range of narrowbody fleets are generated using a Monte Carlo simulation of various high-level aircraft parameters, including the use of conventional as well as novel aviation fuels such as SAF and hydrogen and analysed using AirClim (see Section 7.2.3).

The neutrality of each climate metric is gauged by the frequency f of incorrect fleet pairs - defined here as when the signs of the differences in peak/average temperature (ΔT) and total climate metric value (CM) between any two fleets i and j do not match - compared to the total number of fleet pairs (see also the method used by Grewe et al., 2010):

$$f(H) = \frac{1}{C(N,2)} \sum_{i=1}^{N} \sum_{j=1,j\neq i}^{N} \begin{cases} 1 & \text{if } (\mathrm{CM}_{H,j} - \mathrm{CM}_{H,i}) \times (\Delta T_j - \Delta T_i) < 0 \\ 0 & \text{otherwise} \end{cases} \tag{7.1}$$

where N = 10000 is the total number of fleets. Figure 7.2 shows the frequency of incorrect fleet pairs as a function of the time horizon H; example results for a single time horizon H = 100 are shown in Figure 7.1.

In general, the similarity shown in Figure 7.2 between the results for all climate metrics and climate objectives suggest that the peak temperature is also a good indicator for the average temperature and vice versa over a wide range of time horizons. The endpoint climate metrics F-RF and F-AGTP show a clear dependence on the time horizon and hence shape of the temporal emission profile (temporal evolution of yearly emissions per species). This demonstrates that a single value of radiative forcing or temperature at a time in the future is not a good indicator of the peak or average temperature. Since the radiative forcing from a number of aviation non-CO_2 effects, such as the warming effect from the NO_x-induced short-term increase in ozone (e.g. Lee et al., 2021), has dissipated at large time horizons, the F-RF in particular can have low or altogether no sensitivity to a number of aircraft and engine design changes, leading to a high rate of incorrect fleet pairs. The integrated climate metrics F-AGWP, F-AEGWP and F-iAGTP/F-ATR, in comparison, have a memory of these previous emissions and are less dependent on the temporal emission profile.

The F-AGWP and F-GWP* show largely linear responses for peak and average temperature, particularly for time horizons above 60 years, but in general have higher frequencies of incorrect fleet pairs than climate metrics based on temperature or using efficacy. The F-EGWP* has a similarly low dependence

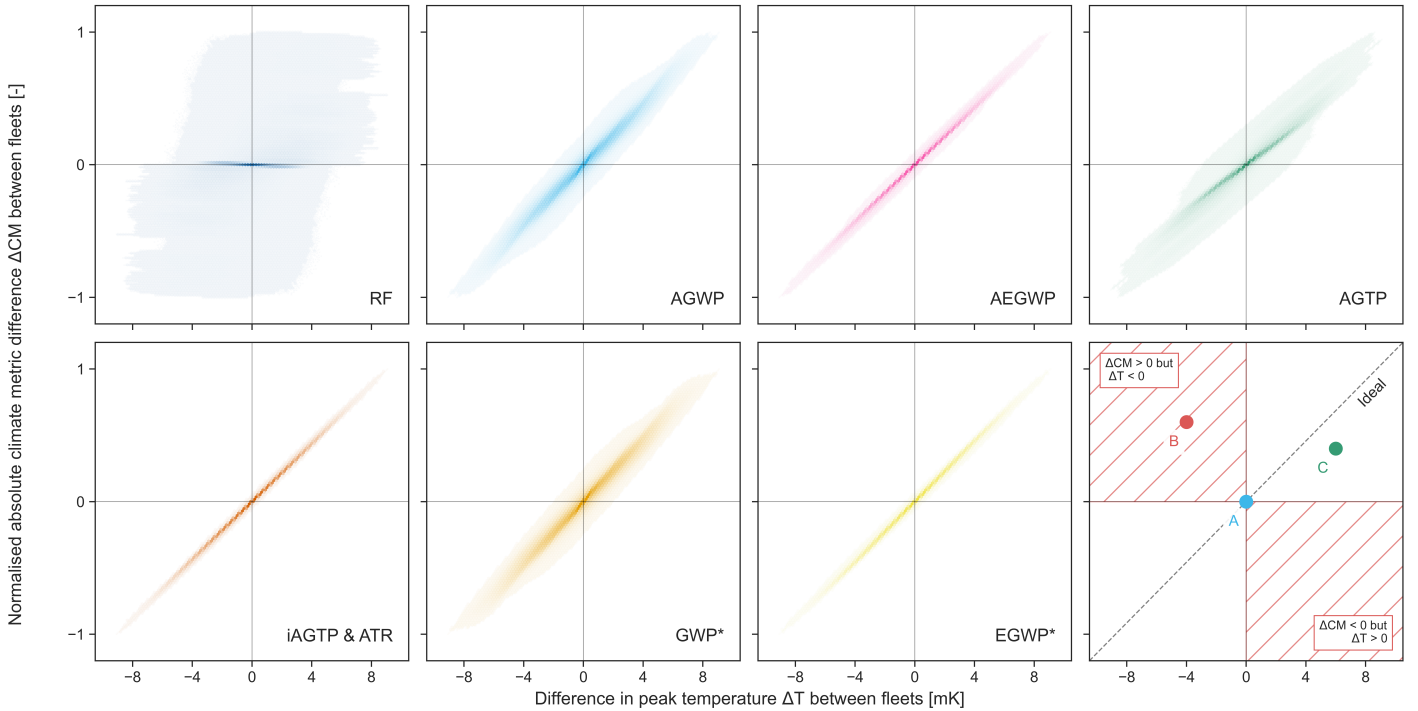


Figure 7.1: Results of the peak temperature pairwise analysis of all fleets for each climate metric with a time horizon of 100 years. Each fleet pairing is represented by a point on the scatter plot, shown in the background with low opacity. A 2D histogram is overlaid to show the regions of most fleet pairings - larger opacity corresponds to a larger number of fleet pairings within each hexagonal bin. An example fleet pairing is shown in the bottom-right panel: Compared to fleet A, fleet B has a higher climate metric value but lower peak temperature and is hence classed as "incorrect", whereas fleet C has both a higher climate metric and peak temperature. An ideal climate metric for the peak temperature climate indicator would show a diagonal line through the bottom-left to top-right quadrants, as depicted by the dashed line.

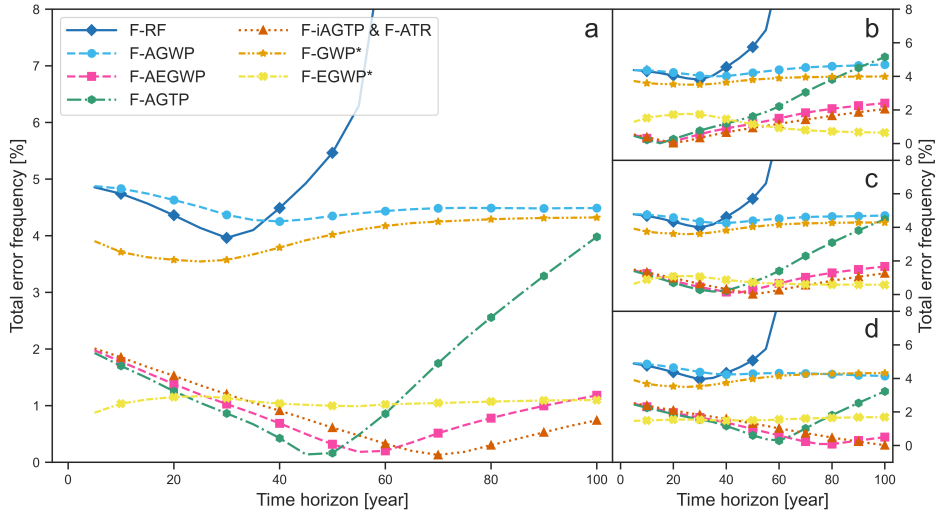


Figure 7.2: Comparison of the neutrality of different climate metrics to changes in aircraft design. Shown is the frequency of incorrect fleet pairs, corresponding to those where the signs of the peak/average temperature change and climate metric change do not match, as a function of the time horizon for the peak temperature (**a**) and 20-, 50- and 100-year average temperature (**b-d**) climate objectives. Each climate metric is represented by a different combination of colour, line style and marker. Values are available between 5 and 100 years with a time horizon step of 5 years; however, markers are shown every 10 years for clarity.

on the time horizon with a lower frequency of incorrect fleet pairs, demonstrating almost ideal behaviour in this context. Whilst the F-iAGTP/F-ATR has a clear minimum at 70 years for peak temperature and at 20, 50 and 100 years for the corresponding average temperatures, it generally has a frequency of incorrect fleet pairs of less than 2%. The F-AEGWP performs very similarly, surpassing 2% error frequency only for the 20-year average temperature, and has clear minima at slightly lower time horizons: 55, 15, 45 and 80 years respectively.

7.3.2. REQ 2: TEMPORAL STABILITY

The temporal stability of climate metrics is judged using CO_2-eq trajectories for the full aviation industry. In this work, we use the CORSIA and FP2050 scenarios developed by Grewe et al. (2021) as examples. The CORSIA scenario assumes business as usual, but that CO_2 emissions are offset beyond 2020; whereas the FP2050 scenario makes use of the Flightpath 2050 targets: 75% CO_2 and 90% NO_x reduction by 2050. Figure 7.3 shows the CO_2-eq emissions calculated for both scenarios using each climate metric with a 100-year time horizon. Two elements of the responses are highlighted here.

First, the total CO_2-eq values calculated using the endpoint S-RFI and S-GTP

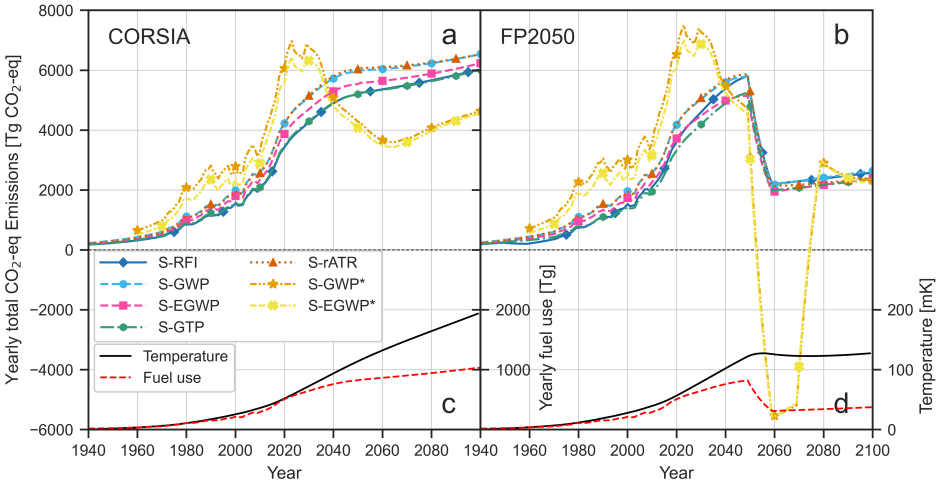


Figure 7.3: Comparison of the climate metric responses for full aviation emission scenarios. Shown are the CO_2-eq emissions calculated using each climate metric with a 100-year time horizon for the CORSIA (**a**) and FP2050 (**b**) scenarios. Each climate metric is represented by a different combination of colour, line style and marker for clarity. Also shown is the fuel use (red dashed line) and temperature (solid black line) response for each emission species calculated using AirClim for the CORSIA (**c**) and the FP2050 (**d**) scenarios. All values are calculated on a yearly basis - the markers for each species are differently spaced such that overlapping lines can more easily be identified.

climate metrics are very similar, although as the emission rate (rate of change of yearly emissions over time) reduces around the year 2020 in the FP2050 scenario, the results begin to drift apart. The RFI and GTP can thus be seen to be stable for the analysed full aviation emissions. However, both climate metrics can struggle to show qualitatively the same response for pulse and constant emissions (see e.g. Dahlmann (2011), their Figure 3.3), depending on the chosen time horizon.

The S-GWP and S-iGTP/S-rATR show very similar responses; the S-EGWP also produces similar, albeit generally lower results. The similarity between the S-GWP and S-iGTP/S-rATR potentially allows for species-dependent conversion factors and reduces the political capital required to switch from the standard GWP to either the iGTP or rATR in climate policy. This is a somewhat surprisingly result, since the bases for the climate metric calculations differ, affecting the contributions of individual species to the total CO_2-eq: The GWP is RF-based, whereas the ATR is temperature-based. As a result, the GWP emphasises contrail-cirrus, and the ATR the warming effect of NO_x-induced ozone (see Figure 7.A.1). Nevertheless, for full aviation scenarios assuming Jet-A1 fuel, the differing contributions seem to balance out. It is, however, likely that the introduction of novel propulsion technologies and fuels, which change the emission indices relative to one another, will result in a divergence of the total CO_2-eq emissions calculated by both metrics. The rATR would then likely more closely

match the EGWP than the GWP. Further research could analyse the response from different models and emission inventories to check the validity of conversion factors, in particular for novel aviation fuels.

A second noticeable element is the rapid deviation of the S-GWP* and S-EGWP* from the response shown by all other climate metrics in both scenarios. The GWP* calculation method uses an average of the previous 20 years of radiative forcing and is closely tied to the emission rate given by the scenario. Therefore, small changes in the emission rate, in the years 2020 and 2050 in the CORSIA scenario, result in large changes in the CO_2-eq trajectory. A policymaker using the GWP* or EGWP* method to monitor CO_2-eq emissions between 2030 and 2050 could incorrectly assume that the impact of aviation is reducing, when in actuality only the emission rate has decreased.

This instability is particularly problematic for the FP2050 scenario. Whilst the values from all other climate metrics largely correspond to the reducing fuel use, the S-GWP* and S-EGWP* show negative CO_2-eq emissions between 2050 and 2080. Whilst this behaviour is useful for representing the temperature using a cumulative integral, negative CO_2-eq values could easily be misinterpreted as a sign that aviation is causing an active cooling. The magnitude of the negative CO_2-eq values is also disproportionately large compared to the shallow peak shown in the temperature.

7.3.3. REQ 3: BE COMPATIBLE WITH EXISTING CLIMATE POLICY

To be compatible with existing climate policy means that a climate metric can be used in current climate frameworks and methods. These have generally been established on the basis of the GWP, which has become the most commonly used climate metric. There is thus a natural bias towards climate metrics that behave in a similar manner to the GWP. For aviation, this functionally means that any alternative to the GWP must be able to 1) calculate the temporal trajectories of CO_2-eq emissions; and 2) calculate single values for fleets and individual flights, the latter of which is necessary for the introduction of aviation non-CO_2 emissions into the ETS. The climate metrics RF, GWP, EGWP, GTP, iGTP and ATR are able to perform these functions. However, the GWP* and EGWP* struggle to provide a single value for an individual fleet or flight.

Rather than providing a single value for a given time horizon, the GWP* method provides a temporal trajectory for each emission species, as shown in Figure 7.4 for a simple fleet temporal emission profile. If used as a climate metric, for example to compare this fleet to another, there is no obvious point along the temporal trajectory to choose. Indeed, the choice of which point to use is itself a trade-off between different emission species. Therefore, whilst the GWP* method is useful for certain certain technical discussions, it should be seen as a model rather than a metric, as previously argued by Meinshausen and Nicholls (2022), and should not be viewed as a potential replacement for the GWP in aviation policy.

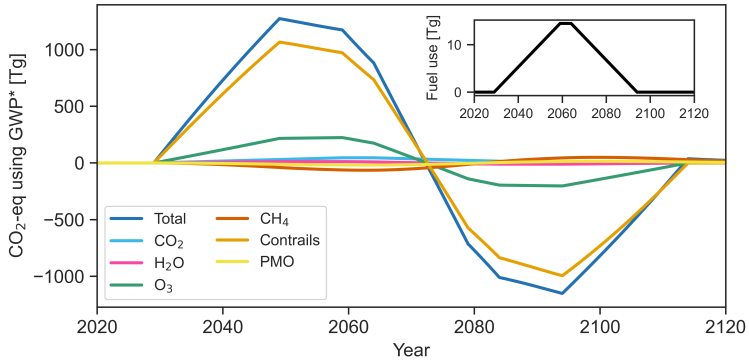


Figure 7.4: CO_2-eq emissions calculated using the GWP*$_{100}$ method for an example fleet demonstrating the flow-based nature of the GWP*. The inset figure shows the temporal emission profile; the main figure the CO_2-eq response for each species (colours). For the comparison of fleets in this study (F-GWP*), the peak total value is used, in this example occurring in the year 2050. Note that the total value is dominated by the contrail impact and that different species have their peaks at later times. Therefore, the choice of which value to use is itself a trade-off between different emission species.

7.3.4. REQ 4: BE SIMPLE TO UNDERSTAND AND IMPLEMENT

The endpoint climate metrics RF and GTP are clearly the easiest to understand. It is straightforward to determine how these climate metrics behave for different time horizons, background emissions scenarios and fuel scenarios. Integrated climate metrics - GWP, EGWP, iGTP and ATR - are more complex and it can be difficult to ascertain the impacts of individual effects and species on the results. Least simple to understand and implement are the GWP* and EGWP*: Their behaviour can be puzzling even for simple temporal emission profiles and can show initially counter-intuitive results, such as the negative emissions in Figure 7.3.

In comparison to temperature-based climate metrics (GTP, iGTP, ATR), climate metrics based on radiative forcing (RF, GWP) are easier to implement since they do not need a full climate or carbon-cycle model. The EGWP requires efficacy values and is thus more complex. However, the demand on computational time depends on which model is used to calculate the climate metric values. The GWP* and EGWP* are RF-based climate metrics, but they do use the AGWP for CO_2, which would need to be defined as a standard value or calculated for a given scenario. Additionally, these metrics require the temporal emission profile twenty years prior to any value, since the method uses a 20-year running average. This could potentially complicate the implementation of the GWP* method.

7.3.5. CHOICE OF CLIMATE METRIC AND TIME HORIZON

An overview of the performance of all analysed climate metrics is shown in Table 7.3. It is clear that the choice of climate metric must be the result of a trade-off. Based on our analysis and definition of requirements, the ATR and EGWP can be seen to perform best. Here, we inspect in more detail the advantages and disadvantages of these metrics in comparison to the GWP and investigate their dependence on the time horizon. We note that the ATR and iAGTP differ only in the division of the time horizon; in their relative forms, the rATR and iGTP are identical. However, the ATR is chosen rather than the iAGTP because the division by the time horizon improves the stability of the absolute climate metric responses.

Table 7.3: Overview of the performance of the analysed climate metrics with respect to each requirement. "Generally stable" refers to the finding that the RF and GTP are stable for full aviation emission scenarios, but can struggle to show qualitatively the same response for pulse and constant emissions (see e.g. Figure 3.3 of Dahlmann, 2011)

	Neutrality (REQ 1)	Stability (REQ 2)	Compatibility (REQ 3)	Simplicity (REQ 4)
RF	Very low neutrality	Generally stable	Compatible	Simple to understand and implement
GWP	Low, but consistent neutrality	Stable	Compatible	Complex to understand, simple to implement
EGWP	High neutrality	Stable	Compatible	Complex to understand and implement
GTP	Low, but inconsistent neutrality	Generally stable	Compatible	Simple to understand, complex to implement
ATR & iGTP	High neutrality	Stable	Compatible	Simple/complex to understand, complex to implement
GWP*	Low, but consistent neutrality	Highly unstable	Not compatible	Highly complex to understand and implement
EGWP*	High and consistent neutrality	Highly unstable	Not compatible	Highly complex to understand and implement

The ATR and EGWP perform similarly well in the pairwise fleet analysis (REQ 1) for the peak and average temperature climate indicators, as well as in analysis on temporal stability (REQ 2). The $rATR_{100}$ produces CO_2-eq emissions that very closely match those calculated using the GWP_{100}, potentially easing the introduction of the ATR in climate policy (REQ 3); introduction of the EGWP is even simpler since it is only a derivative of the GWP. Finally, although the concept of an average temperature change is simple to understand for non-specialists, it can be difficult to identify the impacts of specific effects on results. In comparison to the GWP, the EGWP and in particular the ATR as a temperature-based metric, include more climatic processes, but thus also more assumptions and uncertainties. Implementation of both climate metrics can thus be seen as complex (REQ 4). Further work is required to better understand the benefits and potential downsides of the EGWP in other contexts. Further research into best estimates of the efficacy would also be beneficial.

The dependence of the GWP, EGWP and ATR on the time horizon is shown

in Figure 7.5 for three different emission scenarios. Individual overviews for each of these metrics and the GTP are provided in Figures 7.A.2-7.A.5. The inclusion of the efficacy in the EGWP is evident from the lower panel of the figure, affecting the relative importance of ozone and contrails in particular. The results of the RF-based EGWP now much more closely match those of the temperature-based ATR. Nevertheless, the total relative metric values and thus calculated CO_2-eq emissions of the GWP, EGWP and ATR are very similar, especially for large time horizons. In general, the sensitivity of all three metrics to the time horizon, represented by the gradient of the relative metric values, decreases with increasing time horizon. Using a low time horizon, for example 20 years, would require particular justification: Why was 20 years chosen rather than say 15, 25 or even 19 years? Instead, the responses suggest that larger time horizons are most suitable for integrated climate metrics, greater than around 70 years. This is particularly true for the ATR, which requires larger time horizons to properly account for the delay in the temperature response of the atmosphere.

7.4. FEEDBACK FROM THE COMMUNITY

Since the publication of Megill et al. (2024), we have received comments and feedback from various sources. Two notable instances are described here. Firstly, the results of the study were used to inform EU policy on the inclusion of non-CO_2 effects in the EU ETS. Secondly, the study was used as the basis of a dedicated workshop on climate metrics for aviation as part of the CLAIM (Clean Aviation Support for Impact Monitoring) project[5] project, which included a number of industry stakeholders. The feedback received from these two sources is described in this chapter.

7.4.1. NON-CO_2 MRV

With the adoption of European Union Directive 2023/958 of 10 May 2023, the European Commission was given a mandate to create a Monitoring, Reporting and Verification (MRV) framework for non-CO_2 aviation emissions and effects. The objective of the MRV is to collect sufficient information from aircraft operators to calculate CO_2-eq emissions per flight. Then, if deemed appropriate, by the end of 2027 and based on the results of the MRV, the Commission should submit a legislative proposal to expand the scope of the EU ETS to cover aviation non-CO_2 emissions and effects.

The objective of the subsequent tender CLIMA/2023/OP/0005 was to provide an overview of existing models and metrics, provide advice on data needs and develop an IT tool for data collection. I led the tendering process on behalf of the DLR. The consortium, consisting of To70 with the DLR and AerLabs as subcon-

[5]https://www.claim-project.eu/post/claim-project-hosts-international-workshop-on-climate-metrics-and-impact-assessment-of-aviation [Last accessed: 30/03/2026].

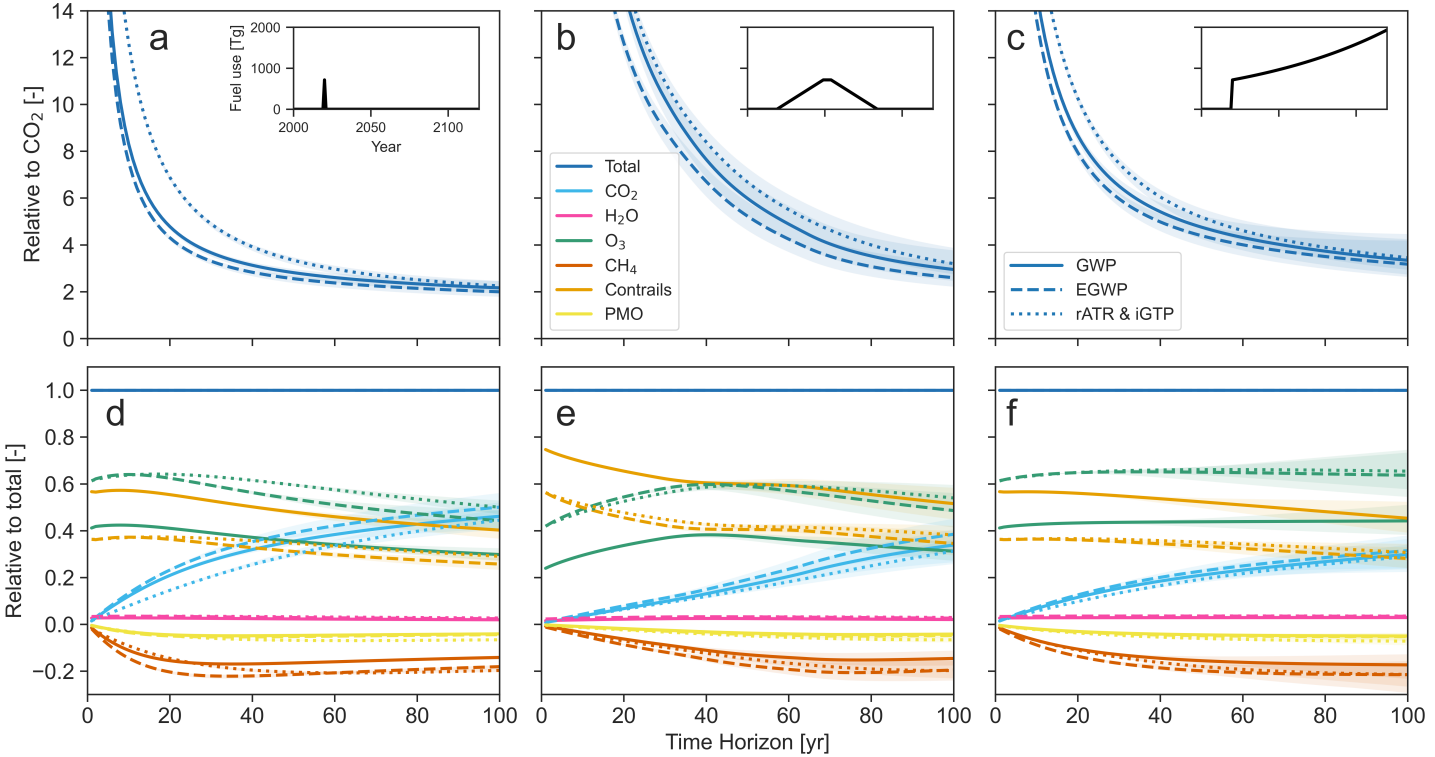


Figure 7.5: Comparison of the GWP, EGWP and ATR responses for time horizons between 0 and 100 years. Shown are the responses from the GWP (solid line), EGWP (dashed line) and rATR (dotted line), which in its relative form is equivalent to the iGTP. The top row shows the total metric value relative to CO_2; the bottom row the responses calculated for each species (colours) relative to the total. Three temporal emission profiles are used, for which the fuel usage profiles are shown in the inset plots: a pulse emission (P-) in **a** and **d**; a fleet emission (F-) in **b** and **e** and a 1% increasing emission (I-) in **c** and **f**. Each response is shown for the Shared Socioeconomic Pathway SSP2-4.5 with margins (shading) for scenarios SSP1 to SSP5, which are used as the background emissions scenarios in AirClim.

tractors, went on to win the tender. Within Work Package 1, I was responsible for providing an overview of and analysing the suitability of climate metrics for use in the MRV. Through this process, I was able to interact with many industry stakeholders, including airlines, aircraft manufacturers, government and Commission representatives as well as other researchers.

In general, there was a clear desire to stick with the GWP framework. The clear advantage of the GWP is "its compatibility with the implementation of the Paris Agreement" (Directorate-General for Research and Innovation, DG RTD). DG RTD also noted the risks associated with using one metric in Europe if another one is used at the international level (referring, for example, to the Paris Agreement). The European Aviation Safety Agency (EASA) also emphasised the need for climate metric consistency between European aviation policy measures and international agreements (Paris Agreement), frameworks (e.g. EU ETS) and studies (IPCC reports).

The European Commission was open to including the efficacy, even though a number of commenters - from industry, academia and governments - were against doing so due to the uncertainty. Ultimately, the Commission Implementing Regulation (EU) 2024/2493 of 23 September 2024[6] included the following paragraph, which stipulates the use of what we refer to as the EGWP (GWP with applied efficacy):

(28) The calculation of the CO_2(e) per flight should be done using the Global Warming Potential (GWP) metric in three time horizons GWP_{20}, GWP_{50} and GWP_{100}, to better understand those impacts on the climate, applying efficacy, as defined in Implementing Regulation (EU) 2018/2066, and the Commission's non-CO_2 aviation effects tracking system (NEATS), to refine the GWP metric.

7.4.2. CLAIM

The CLAIM (Clean Aviation Support for Impact Monitoring) project is an EU-funded project under the Clean Aviation programme, coordinated by the DLR. Its goal is to bridge the gap between climate and technology impact monitoring by reviewing literature, discussing climate metrics, uncertainties, dependencies and assessment challenges with all aviation stakeholders. The focus of the second CLAIM workshop, held between 17-18 June 2024 in Hamburg, was on climate metrics. In total, 32 participants from 14 institutions and institutes took part. The objective was, using the Megill et al. (2024) study as the basis, to obtain feedback from industry stakeholders on:

- the list of (weighted) requirements that a climate metric should consider;
- the procedure on how climate metrics can be tested against those require-

[6]http://data.europa.eu/eli/reg_impl/2024/2493/oj [Last accessed: 06/03/2026]

ments;
- research gaps that are associated with the choice of usage of climate metrics; and
- implications of a climate metric choice on the technology assessment.

In the following, I describe and discuss the results of the workshop and the recommendations of the participants from my perspective, guided by the analyses performed in this chapter. The workshop participants rated the neutrality requirement (REQ 1) as most important, followed by temporal stability (REQ 2). However, it was recommended to rename both requirements for ease of understanding: REQ 1 to "Representative of scenario temperature change"; REQ 2 to "Not sensitive to small changes in the time horizon". The workshop participants also pointed out that it is not clear for whom a climate metric should be simple to understand (REQ 4). An educated user is meant, so this should also be specified.

I do not support the renaming of REQ 2. The main aim of REQ 2 is to ensure that it is possible to use climate metrics to monitor how well the industry is performing. It is undesirable for a climate metric to vary to the extent that policymakers cannot gauge the effectiveness of their policies, as the GWP* tends to do (see Section 7.3.2). Sensitivity to the choice of time horizon is potentially a separate requirement, but it is not equivalent to REQ 2.

The workshop participants also identified other aspects that were not covered by the four requirements defined by Megill et al. (2024). These included that the climate metric should 1) be in line with the Paris Agreement; 2) focus on longer time horizons; 3) be robust; 4) be able to represent or implement new findings; and 5) be compatible with all technologies, fuels and species. Further research into efficacy and the limits of climate metric used was also recommended. Nevertheless, the assessment methodology was deemed to be sound with no need for major improvements. The error frequency used for the analysis of REQ 1 could, however, be revised into a weighted error frequency that considers how wrong a fleet pairing is, rather than just whether or not it is.

My most important take-away from the workshop is to always ensure a clear differentiation between climate models and climate metrics. Many of the problems that the workshop participants identified were actually related to the climate model rather than the climate metric. This is because the boundary between model and metric is often blurry - see for example the discussion on the GWP* in Section 7.3.3. In this work, we assume that a climate metric takes as an input a time-series of radiative forcing or temperature change (Section 2.3.2). A climate model is used to generate this time-series. Therefore, all climate metrics are able to represent or implement new findings (point 4) - the real question is whether the climate models can do so. Similarly for point 5 about compatibility with different technologies, fuels and species. Ultimately, climate metrics inherit their uncertainties from the models upon which they are based. It is, therefore, vital to differentiate between them.

7.5. DISCUSSION AND CONCLUSION

Our analyses demonstrate that the selection of a climate metric plays a crucial role in ensuring that implemented climate policies effectively reduce the aviation industry's impact on the climate. In the fleet pairing analysis, we illustrate that climate metrics can have inherent trade-offs and favour certain aircraft designs over others. These inherent biases are undesirable since value judgements should be left to policy decision-making and not embedded into climate metrics.

The choice of climate metric is always the result of a trade-off. Due to the historical dominance of the GWP, there is a natural bias towards climate metrics that behave in a similar manner. However, our research clearly suggests that there are derivatives and alternatives that outperform the GWP for aviation. We require that a suitable climate metric displays neutrality with respect to different emission species; exhibits temporal stability; is compatible with existing climate policy; and is simple to understand and implement. These requirements are in line with those stated by others (Fuglestvedt et al., 2010; Meinshausen and Nicholls, 2022). Based on these requirements, we identify the Efficacy-weighted Global Warming Potential (EGWP) and Average Temperature Response (ATR) as the most appropriate climate metrics for aircraft design and aviation policy. Both metrics are stable and can monitor the impact of the aviation industry using CO_2-equivalents effectively. They also do not favour specific emission species for both peak and average temperature climate indicators across a wide range of time horizons and emission scenarios.

While the ATR as a temperature-based climate metric has the potential to include more climatic processes and be more relevant for temperature-based targets than the GWP, the larger number of assumptions and uncertainties must also be considered. The EGWP may, therefore, be a useful compromise for policymakers, in that it can more accurately represent the climate impact of aviation whilst still using the GWP methodology. If the ATR were to be chosen, it would benefit from the close match of the total CO_2-eq emissions calculated by the S-rATR$_{100}$ and S-GWP$_{100}$, despite the differences in contributions of individual species. The S-EGWP$_{100}$, for its part, also produces similar results. However, it is likely that the total emissions calculated by the ATR and GWP will diverge with the introduction of novel propulsion technologies and fuels such as hydrogen since the relative contributions of the non-CO_2 emissions will change.

Determining an appropriate time horizon for both the EGWP and ATR remains a challenge. The time horizon is a trade-off between incorporating the long-term response to an emission and ensuring predictability and accuracy of a future emission scenario. We find that integrated climate metrics generally require larger time horizons to account for the atmospheric radiative forcing and temperature adjustment. If a short time horizon is chosen, policymakers must provide sufficient justification for the choice. Alternatively, values for different time horizons could be provided together, as proposed by Ocko et al. (2017), al-

though this complicates the calculation of CO_2-eq emissions, for example in the upcoming ETS revision.

The accuracy of our results could be improved by using real aircraft designs: Since design parameters are chosen randomly within a given range, some fleets may not be physically feasible. However, since we used the same method of randomly choosing parameters, any additional incorrect fleet pairings caused by this limitation are assumed to cancel out and not impact our conclusions. Similarly, given the wide range of potential aircraft designs analysed in this study, it is unlikely that the choice of climate model, AirClim, has influenced the results significantly. Verification with another climate model may enhance our understanding of the results.

Ultimately, the most suitable climate metric and corresponding time horizon must be determined by policymakers depending on the policy and climate objective, the emission scenario, and whether a relative or absolute climate metric is required. Based on a general set of requirements suitable for policy-making, our findings endorse the use of the ATR and EGWP with a time horizon greater than 70 years for aircraft design and aviation policy to assess the long-term climate impact of aviation. However, the choice of climate metric does not have to be contentious or controversial: As our analysis and the numerous previous studies have demonstrated, tools exist with which the performance of any climate metric can be analysed and potential shortcomings and pitfalls identified, such that these can be addressed in climate policy.

7.A. APPENDIX

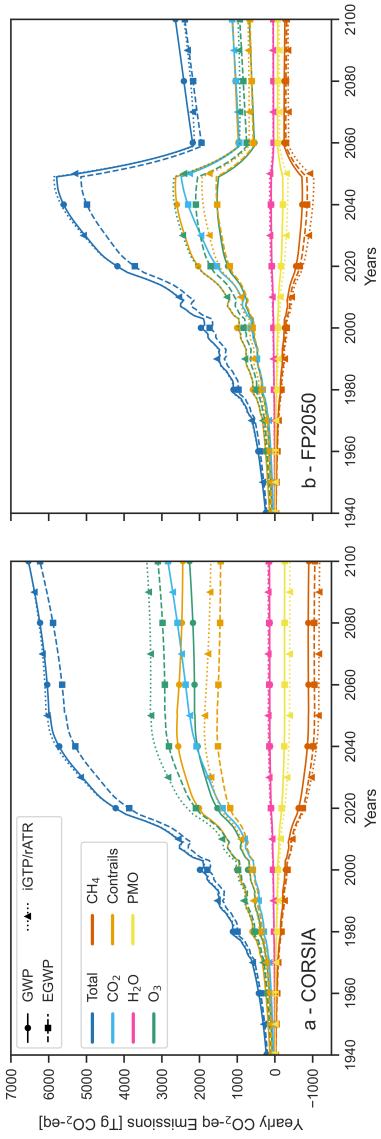


Figure 7.A.1: Comparison of the GWP, EGWP and rATR responses for the CORSIA and FP2050 full aviation emission scenarios. CO_2-eq emissions calculated using each climate metric with a 100-year time horizon for the CORSIA (a) and FP2050 (b) scenarios, demonstrating the differences in contributions of individual species to the total CO_2-eq emissions between the three climate metrics.

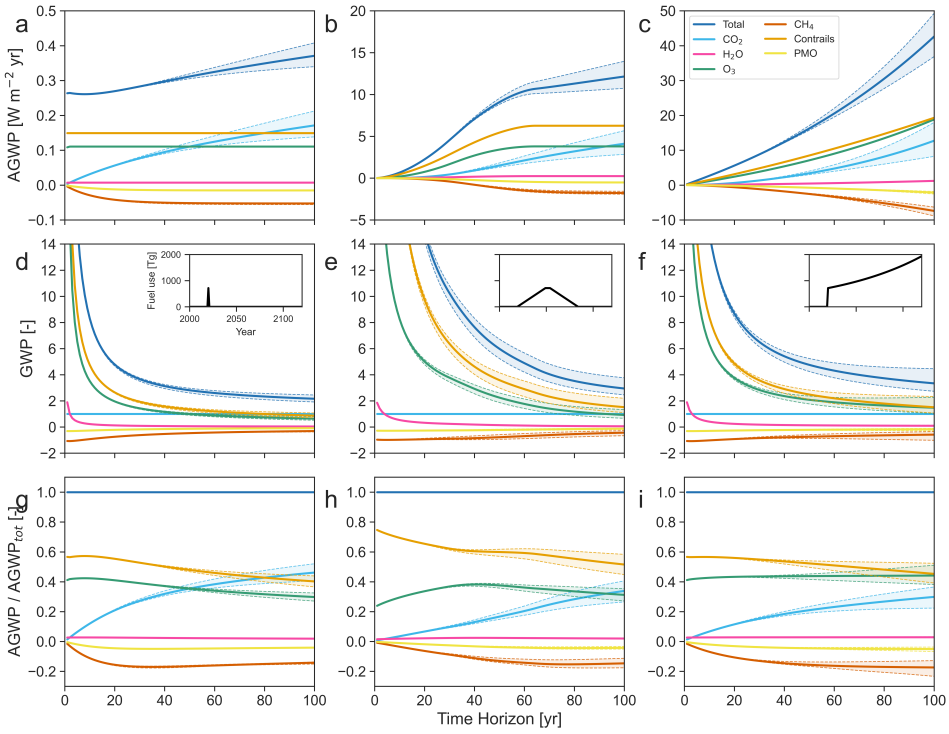


Figure 7.A.2: Time horizon analysis of the GWP. AGWP (top row), GWP (middle row) and AGWP relative to total AGWP (bottom row) responses for each species (colours) plotted against the time horizon for (**a**, **d**, **g**) a pulse emission (P-GWP), (**b**, **e**, **h**) a fleet emission (F-GWP) and (**c**, **f**, **i**) a 1% increasing emission (I-GWP) for background emissions scenario SSP2-4.5 with margins for scenarios SSP1 to SSP5. The inset plots show the yearly fuel use for each temporal emission profile.

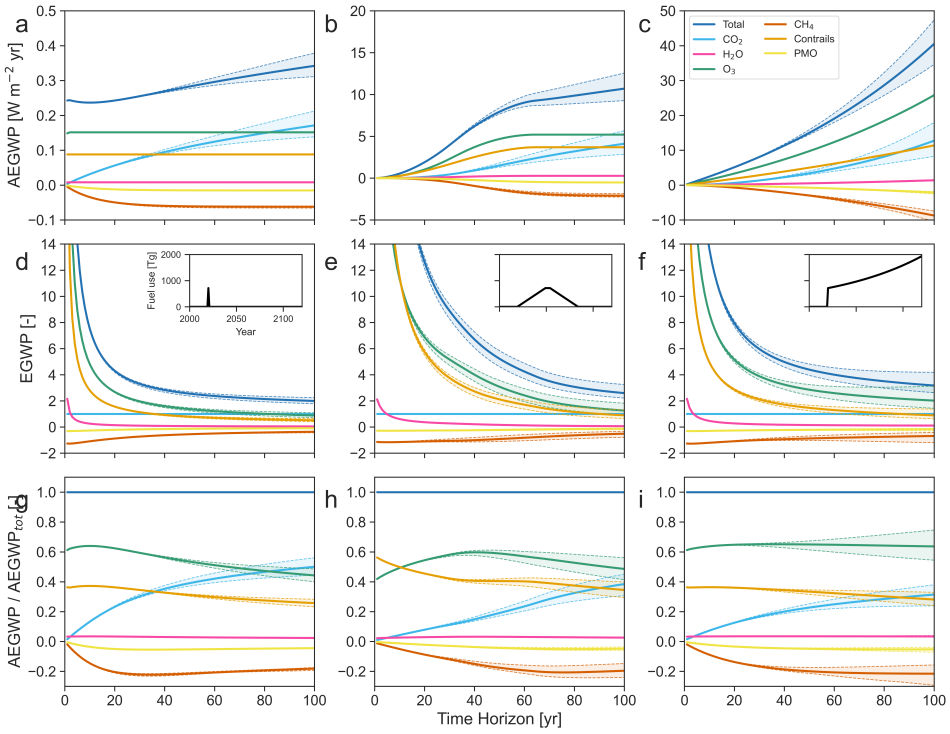


Figure 7.A.3: Time horizon analysis of the EGWP. AEGWP (top row), EGWP (middle row) and AEGWP relative to total AEGWP (bottom row) responses for each species (colours) plotted against the time horizon for (**a**, **d**, **g**) a pulse emission (P-EGWP), (**b**, **e**, **h**) a fleet emission (F-EGWP) and (**c**, **f**, **i**) a 1% increasing emission (I-EGWP) for background emissions scenario SSP2-4.5 with margins for scenarios SSP1 to SSP5. The inset plots show the yearly fuel use for each temporal emission profile.

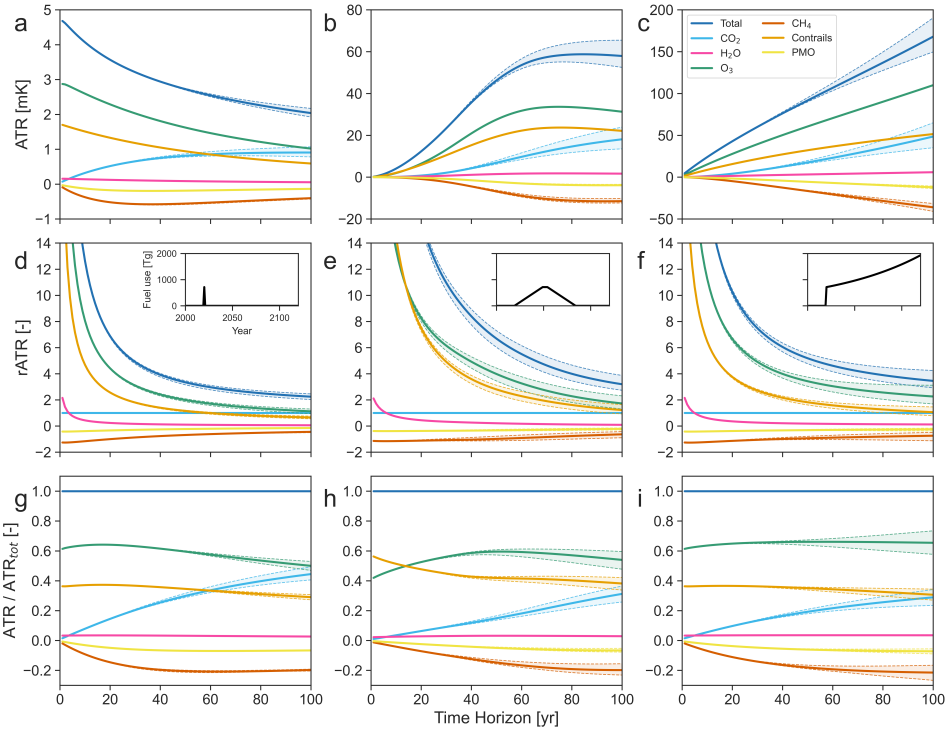


Figure 7.A.4: Time horizon analysis of the ATR. ATR (top row), rATR (middle row) and ATR relative to total ATR (bottom row) responses for each species (colours) plotted against the time horizon for (**a**, **d**, **g**) a pulse emission (P-ATR), (**b**, **e**, **h**) a fleet emission (F-ATR) and (**c**, **f**, **i**) a 1% increasing emission (I-ATR) for background emissions scenario SSP2-4.5 with margins for scenarios SSP1 to SSP5. The inset plots show the yearly fuel use for each temporal emission profile.

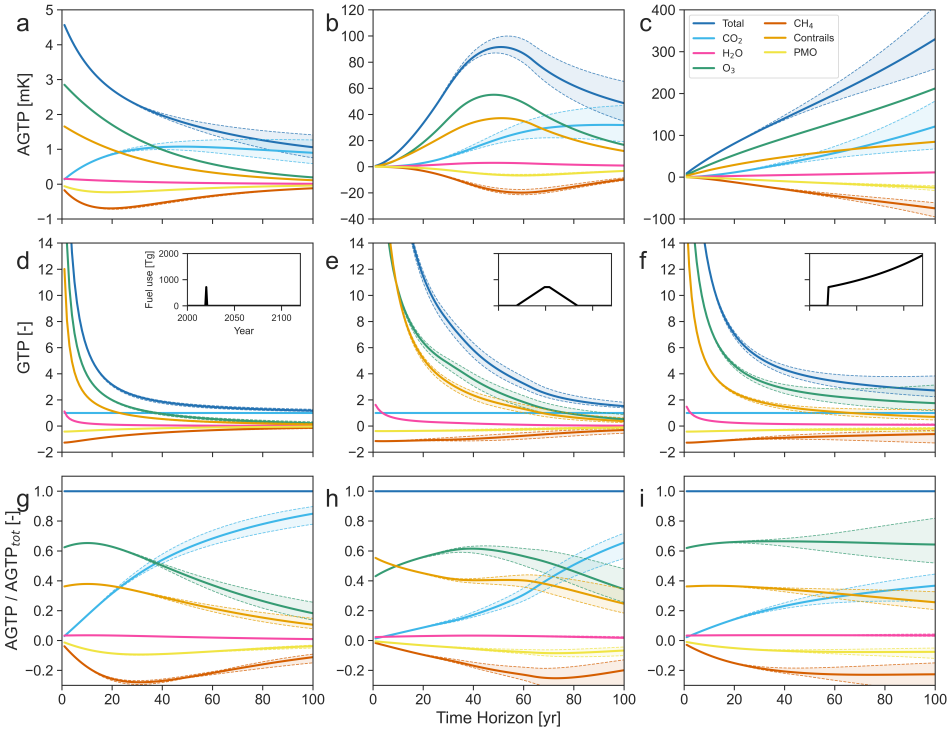


Figure 7.A.5: Time horizon analysis of the GTP. AGTP (top row), GTP (middle row) and AGTP relative to total AGTP (bottom row) responses for each species (colours) plotted against the time horizon for (**a**, **d**, **g**) a pulse emission (P-GTP), (**b**, **e**, **h**) a fleet emission (F-GTP) and (**c**, **f**, **i**) a 1% increasing emission (I-GTP) for background emissions scenario SSP2-4.5 with margins for scenarios SSP1 to SSP5. The inset plots show the yearly fuel use for each temporal emission profile.

REFERENCES

Allen, M. R., Fuglestvedt, J. S., Shine, K. P., Reisinger, A., Pierrehumbert, R. T., and Forster, P. M.: New use of global warming potentials to compare cumulative and short-lived climate pollutants, Nature Climate Change, 6, 773–776, doi: 10.1038/nclimate2998, 2016.

Allen, M. R., Shine, K. P., Fuglestvedt, J. S., Millar, R. J., Cain, M., Frame, D. J., and Macey, A. H.: A solution to the misrepresentations of CO2-equivalent emissions of short-lived climate pollutants under ambitious mitigation, npj Climate and Atmospheric Science, 1, doi: 10.1038/s41612-018-0026-8, 2018.

Cain, M., Lynch, J., Allen, M. R., Fuglestvedt, J. S., Frame, D. J., and Macey, A. H.: Improved calculation of warming-equivalent emissions for short-lived climate pollutants, npj Climate and Atmospheric Science, 2, 29, doi: 10.1038/s41612-019-0086-4, 2019.

Dahlmann, K.: Eine Methode zur effizienten Bewertung von Maßnahmen zur Klimaoptimierung des Luftverkehrs, Ph.D. thesis, Ludwig-Maximilians-Universität München, München, doi: 10.5282/edoc.14199, 2011.

Dallara, E. S., Kroo, I. M., and Waitz, I. A.: Metric for comparing lifetime average climate impact of aircraft, AIAA Journal, 49, 1600–1613, doi: 10.2514/1.J050763, 2011.

Forster, P. M. d. F., Shine, K. P., and Stuber, N.: It is premature to include non-CO2 effects of aviation in emission trading schemes, Atmospheric Environment, 40, 1117–1121, doi: 10.1016/j.atmosenv.2005.11.005, 2006.

Frömming, C., Grewe, V., Brinkop, S., Jöckel, P., Haslerud, A. S., Rosanka, S., van Manen, J., and Matthes, S.: Influence of weather situation on non-CO2 aviation climate effects: the REACT4C climate change functions, Atmospheric Chemistry and Physics, 21, 9151–9172, doi: 10.5194/acp-21-9151-2021, 2021.

Fuel Cells and Hydrogen 2 Joint Undertaking: Hydrogen-powered aviation: A fact-based study of hydrogen technology, economics, and climate impact by 2050, Tech. rep., Publications Office, Brussels, Belgium, ISBN 978-92-9246-342-7, https://doi.org/10.2843/471510, 2020.

Fuglestvedt, J., Shine, K., Berntsen, T., Cook, J., Lee, D., Stenke, A., Skeie, R., Velders, G., and Waitz, I.: Transport impacts on atmosphere and climate: Metrics, Atmospheric Environment, 44, 4648–4677, doi: 10.1016/j.atmosenv.2009.04.044, 2010.

Fuglestvedt, J. S., Berntsen, T. K., Godal, O., Sausen, R., Shine, K. P., and Skodvin, T.: Metrics of climate change: assessing radiative forcing and emission indices, Climatic Change, 58, 267–331, doi: 10.1023/A:1023905326842, 2003.

Gelhausen, M. C., Grimme, W., Junior, A., Lois, C., and Berster, P.: Clean Sky 2 Technology Evaluator - results of the first air transport system level assessments, Aerospace, 9, 204, doi: 10.3390/aerospace9040204, 2022.

Grewe, V. and Dahlmann, K.: How ambiguous are climate metrics? And are we prepared to assess and compare the climate impact of new air traffic technologies?, Atmospheric Environment, 106, 373–374, doi: 10.1016/j.atmosenv.2015.02.039, 2015.

Grewe, V., Stenke, A., Plohr, M., and Korovkin, V. D.: Climate functions for the use in multi-disciplinary optimisation in the pre-design of supersonic business jet, The Aeronautical Journal, 114, 259–269, doi: 10.1017/S0001924000003705, 2010.

Grewe, V., Frömming, C., Matthes, S., Brinkop, S., Ponater, M., Dietmüller, S., Jöckel, P., Garny, H., Tsati, E., Dahlmann, K., Søvde, O. A., Fuglestvedt, J., Berntsen, T. K., Shine, K. P., Irvine, E. A., Champougny, T., and Hullah, P.: Aircraft routing with minimal climate impact: the REACT4C climate cost function modelling approach (V1.0), Geoscientific Model Development, 7, 175–201, doi: 10.5194/gmd-7-175-2014, 2014.

Grewe, V., Dahlmann, K., Flink, J., Frömming, C., Ghosh, R., Gierens, K., Heller, R., Hendricks, J., Jöckel, P., Kaufmann, S., Kölker, K., Linke, F., Luchkova, T., Lührs, B., Van Manen, J., Matthes, S., Minikin, A., Niklaß, M., Plohr, M., Righi, M., Rosanka, S., Schmitt, A., Schumann, U., Terekhov, I., Unterstrasser, S., Vázquez-Navarro, M., Voigt, C., Wicke, K., Yamashita, H., Zahn, A., and Ziereis, H.: Mitigating the climate impact from aviation: achievements and results of the DLR WeCare project, Aerospace, 4,

34, doi: 10.3390/aerospace4030034, 2017.

Grewe, V., Gangoli Rao, A., Grönstedt, T., Xisto, C., Linke, F., Melkert, J., Middel, J., Ohlenforst, B., Blakey, S., Christie, S., Matthes, S., and Dahlmann, K.: Evaluating the climate impact of aviation emission scenarios towards the Paris agreement including COVID-19 effects, Nature Communications, 12, 3841, doi: 10.1038/s41467-021-24091-y, 2021.

IPCC: Aviation and the Global Atmosphere, Cambridge University Press, Cambridge, United Kingdom and New York, NY, USA, 1999.

Lee, D., Pitari, G., Grewe, V., Gierens, K., Penner, J., Petzold, A., Prather, M., Schumann, U., Bais, A., and Berntsen, T.: Transport impacts on atmosphere and climate: Aviation, Atmospheric Environment, 44, 4678–4734, doi: 10.1016/j.atmosenv.2009.06.005, 2010.

Lee, D., Fahey, D., Skowron, A., Allen, M., Burkhardt, U., Chen, Q., Doherty, S., Freeman, S., Forster, P., Fuglestvedt, J., Gettelman, A., De León, R., Lim, L., Lund, M., Millar, R., Owen, B., Penner, J., Pitari, G., Prather, M., Sausen, R., and Wilcox, L.: The contribution of global aviation to anthropogenic climate forcing for 2000 to 2018, Atmospheric Environment, 244, 117 834, doi: 10.1016/j.atmosenv.2020.117834, 2021.

Lund, M. T., Aamaas, B., Berntsen, T., Bock, L., Burkhardt, U., Fuglestvedt, J. S., and Shine, K. P.: Emission metrics for quantifying regional climate impacts of aviation, Earth System Dynamics, 8, 547–563, doi: 10.5194/esd-8-547-2017, 2017.

Manne, A. S. and Richels, R. G.: An alternative approach to establishing trade-offs among greenhouse gases, Nature, 410, 675–677, doi: 10.1038/35070541, 2001.

Megill, L., Deck, K., and Grewe, V.: Alternative climate metrics to the Global Warming Potential are more suitable for assessing aviation non-CO2 effects, Communications Earth & Environment, 5, 249, doi: 10.1038/s43247-024-01423-6, 2024.

Meinshausen, M. and Nicholls, Z.: GWP* is a model, not a metric, Environmental Research Letters, 17, 041 002, doi: 10.1088/1748-9326/ac5930, 2022.

Niklaß, M., Grewe, V., Gollnick, V., and Dahlmann, K.: Concept of climate-charged airspaces: a potential policy instrument for internalizing aviation's climate impact of non-CO2 effects, Climate Policy, 21, 1066–1085, doi: 10.1080/14693062.2021.1950602, 2021.

Ocko, I. B., Hamburg, S. P., Jacob, D. J., Keith, D. W., Keohane, N. O., Oppenheimer, M., Roy-Mayhew, J. D., Schrag, D. P., and Pacala, S. W.: Unmask temporal trade-offs in climate policy debates, Science, 356, 492–493, doi: 10.1126/science.aaj2350, 2017.

Peters, G. P., Aamaas, B., Berntsen, T., and Fuglestvedt, J. S.: The integrated global temperature change potential (iGTP) and relationships between emission metrics, Environmental Research Letters, 6, 044 021, doi: 10.1088/1748-9326/6/4/044021, 2011.

Ponater, M., Pechtl, S., Sausen, R., Schumann, U., and Hüttig, G.: Potential of the cryoplane technology to reduce aircraft climate impact: A state-of-the-art assessment, Atmospheric Environment, 40, 6928–6944, doi: 10.1016/j.atmosenv.2006.06.036, 2006.

Proesmans, P.-J. and Vos, R.: Airplane design optimization for minimal global warming impact, Journal of Aircraft, 59, 1363–1381, doi: 10.2514/1.C036529, 2022.

Rodhe, H.: A comparison of the contribution of various gases to the greenhouse effect, Science, 248, 1217–1219, doi: 10.1126/science.248.4960.1217, 1990.

Rogelj, J. and Schleussner, C.-F.: Unintentional unfairness when applying new greenhouse gas emissions metrics at country level, Environmental Research Letters, 14, 114 039, doi: 10.1088/1748-9326/ab4928, 2019.

Shine, K. P., Fuglestvedt, J. S., Hailemariam, K., and Stuber, N.: Alternatives to the Global Warming Potential for comparing climate impacts of emissions of greenhouse gases, Climatic Change, 68, 281–302, doi: 10.1007/s10584-005-1146-9, 2005.

Shine, K. P., Berntsen, T. K., Fuglestvedt, J. S., Skeie, R. B., and Stuber, N.: Comparing the climate effect of emissions of short- and long-lived climate agents, Philosophical Transactions of the Royal Society A: Mathematical, Physical and Engineering Sciences, 365, 1903–1914, doi: 10.1098/rsta.2007.2050, 2007.

Smith, M. A., Cain, M., and Allen, M. R.: Further improvement of warming-equivalent emissions calculation, npj Climate and Atmospheric Science, 4, 19, doi: 10.1038/s41612-021-00169-8, 2021.

Tanaka, K., Peters, G. P., and Fuglestvedt, J. S.: Policy Update: Multicomponent climate policy: why do emission metrics matter?, Carbon Management, 1, 191–197, doi: 10.4155/cmt.10.28, 2010.

Wuebbles, D., Forster, P., Rogers, H., and Herman, R.: Issues and uncertainties affecting metrics for aviation impacts on climate, Bulletin of the American Meteorological Society, 91, 491–496, doi: 10.1175/2009BAMS2840.1, 2010.

Yin, F., Grewe, V., Frömming, C., and Yamashita, H.: Impact on flight trajectory characteristics when avoiding the formation of persistent contrails for transatlantic flights, Transportation Research Part D: Transport and Environment, 65, 466–484, doi: 10.1016/j.trd.2018.09.017, 2018.

Bright outlook.

the sun rises,
nothing to model today,
only blue.

— LM

8

CONCLUSION AND OUTLOOK

International civil aviation is the cornerstone of global mobility and trade, but also presents a distinct challenge for climate mitigation. While carbon dioxide (CO_2) emissions remain the dominant driver of long-term warming, a substantial share of aviation's climate impact arises from non-CO_2 emissions and effects, notably the increased cloudiness due to contrails. These non-CO_2 effects have a highly heterogeneous impact on the atmosphere and climate and are sensitive to aircraft design, fuel composition and operational choices. Quantifying aviation's full climate impact and accounting for it within existing policy frameworks therefore requires transparent, efficient and adaptable analytical tools.

This dissertation addresses this challenge by linking contrail formation theory, response modelling and climate metric design within a consistent analytical framework. Reanalysis data are used to identify the key environmental and aircraft-design-dependent factors governing persistent contrail formation, revealing robust relationships suitable for climatological parameterisation. Building on this foundation and using simulations with the general circulation model ECHAM5-CCMod, a new contrail module is developed for the open-source response model OpenAirClim. The module enables the efficient simulation and attribution of the contrail-induced stratospheric-adjusted radiative forcing and surface temperature change across a wide range of existing and future aircraft designs and aviation fuels and includes a first representation of the low-soot regime.

Application of OpenAirClim to the ICAO integrated aviation scenarios illustrates that no scenario achieves temperature stabilisation within the study horizon, demonstrating that to reduce the climate impact of aviation effectively, the switch to alternative fuels must be coupled with dedicated non-CO_2 mitigation measures. To compare CO_2 and non-CO_2 emissions and effects on a common scale, a climate metric is required. Therefore, finally, the suitability of climate metrics for representing aviation-specific emissions and effects is systematically evaluated, highlighting limitations with the conventional Global Warming Potential (GWP) and identifying alternative efficacy-weighted or temperature-based metrics that more closely align with aviation policy.

This chapter relates the key findings of this work to the research questions posed in the introduction, identifies the scientific and methodological contributions of the work and discusses its limitations and implications for future research and aviation climate policy.

8.1. ANSWERING THE RESEARCH QUESTIONS

Research Question 1: What aircraft-dependent and environmental factors govern persistent contrail formation and how do they vary spatially and seasonally? *Addressed by Chapter 4 and published as Megill and Grewe (2025).*

The relationship between aircraft-dependent and environmental factors on the formation process and probability of persistent contrail formation is explored using ERA5 reanalysis data from the 2010 decade. While some previous studies addressed individual case studies for dedicated technologies (e.g. Gierens, 2021; Kaufmann et al., 2024; Hofer et al., 2024a), this work aims to understand the interplay between these factors in a systematic and generalised manner.

Persistent contrail formation is limited by three factors: droplet formation, droplet freezing and persistence. Of these, persistence (ice supersaturation) is found to be the most limiting across all aircraft and fuel types. The droplet freezing and persistence factors together determine an upper bound of potential persistent contrail formation regions, which vary with latitude, altitude and season. Droplet formation, governed by the slope of the Schmidt-Appleman mixing line, controls the proportion of each region within which contrails can actually form. The vast majority of region boundaries are defined by ice supersaturation, regardless of the mixing line slope, indicating that contrail formation regions are largely contiguous in space. Consequently, when a conventional or future aircraft begins producing a persistent contrail without changing its operating condition, it is generally because it has entered an ice supersaturated air mass. This finding underscores the importance of accurately forecasting ice supersaturated regions (see also Gierens et al., 2020; Hofer et al., 2024b), in particular for operational contrail mitigation strategies.

The introduction of novel aviation fuels and propulsion technologies will have a major impact on persistent contrail formation. Hydrogen-powered aircraft could increase the formation of persistent contrails by around 50 % relative to contemporary state-of-the-art aircraft along representative flight tracks, whereas water vapour emission reduction systems could feasibly reduce formation by up to 85 %. Mitigating persistent contrail formation by changing the mixing line slope is most effective at lower altitudes and for mixing line slopes similar to conventionally fuelled aircraft.

The climatological probability of persistent contrail formation can be robustly expressed for any given conventional cruise pressure level as a function of the mixing line slope only. Although additionally resolving the latitude could refine this representation, it comes at the cost of higher seasonal dependence.

Persistent contrail formation is not synonymous with contrail climate impact, because alternative fuels are expected to have different optical and radiative properties. Nonetheless, this study points to a clear potential to significantly reduce persistent contrail formation using targeted technologies and is a key first step for the development of a computationally inexpensive method to analyse the contrail climate impact of aviation pathways (RQ2).

Research Question 2: How can the climate impact of contrails be evaluated within a computationally efficient response modelling framework? *Addressed by Chapter 5.*

The OpenAirClim contrail module, developed in this work, allows the efficient evaluation of the contrail climate impact for existing and future aircraft and fuels within a climatological framework by decomposition into a modelling chain: emission inventory → persistent contrail formation → contrail-cirrus coverage → radiative forcing. The relationship between persistent contrail formation and contrail-cirrus coverage is strongly non-linear and is robustly captured using a hyperbolic tangent parameterisation. Contrail-cirrus coverage and radiative forcing are linked through regionally resolved power-law relationships for four broad domains (Americas, EMEA, Asia and Australia, Pacific). The OpenAirClim contrail module also integrates attribution methodologies to enable the simulation of multiple aircraft and fuels within a single scenario, enabling the analysis of multi-fuel aviation pathways. The treatment of the low-soot regime remains a first-order approximation and is thus a priority for further refinement.

Comparison with published studies finds that the contrail module is able to capture differences between emission inventories and saturation behaviour under very high future air traffic scenarios. In contrast to simple, linearised, distance-based radiative forcing formulations such as that used by Lee et al. (2021), the OpenAirClim approach remains valid beyond present-day traffic levels. The new module finds a best estimate of contrail radiative forcing of $48.7\,\mathrm{mW\,m^{-2}}$ for air traffic in 2018, 56.3 % lower than the median best estimate of Lee et al. (2021) but in line with more recent literature (e.g. Bier and Burkhardt, 2022; Teoh et al., 2024). The OpenAirClim contrail module also estimates lower radiative forcing than its predecessor AirClim 2.1, primarily because the simulations underlying the development of AirClim allowed contrails to form within the stratosphere, thereby overestimating contrail formation in the extratropics.

Development and validation were constrained by the limited availability of dedicated and globally representative ECHAM5-CCMod simulations. Regional-only simulations exhibited insufficient signal-to-noise ratios and the lack of long-range aircraft resulted in an absence of data in a few important high air traffic regions such as the North Atlantic. Validation against previous published global studies demonstrated that the model is nonetheless able to capture the impact

of this air traffic, but future model development should focus on using dedicated ECHAM5-CCMod or alternative simulations to improve the model response in these areas. In addition, the aircraft size correction currently relies on a simplified relationship derived from a small set of Large-Eddy simulations for conventional kerosene-powered aircraft. Further work should thus include extending the domain of validity of this correction to include a broader range of aircraft designs, fuels and atmospheric conditions.

Research Question 3: How do alternative aviation fuel pathways affect the relative contributions of contrails and CO_2 to future radiative forcing and temperature change? *Addressed by Chapter 6.*

The assessment of long-term climate impacts from aviation requires integrated and internally consistent scenarios that consider future pathways for technology, operations and fuels. In analysing the feasibility of long-term aspirational goals for the aviation industry, the International Civil Aviation Organization (ICAO) developed a set of global aviation scenarios, which explicitly treat the introduction of alternative aviation fuels in a global context. These scenarios are investigated using OpenAirClim, including the contrail module developed in RQ2, to compare the contributions of contrails and CO_2 to future radiative forcing and temperature change.

Global mean temperature change from contrails and CO_2 does not stabilise within the study horizon for any of the ICAO scenarios, even under the most ambitious transition pathways. Contrails and CO_2 exhibit opposing long-term trends. Improvements in aircraft and engine efficiency and the increasing use of alternative aviation fuels reduce lifecycle CO_2 emissions, gradually trending to temperature stabilisation beyond the study horizon. The rapid phase-out of fossil-based aviation fuels thus remains essential given the long atmospheric lifetime and cumulative nature of CO_2 emissions.

However, at the same time, these technological and fuel transitions tend to increase the probability of persistent contrail formation. As a result, in the analysed scenarios, the contrail contribution to radiative forcing of aircraft powered by alternative aviation fuels exceeds the contribution of CO_2 by 2070. Unlike CO_2, contrail-induced radiative forcing does not exhibit a comparable tendency toward stabilisation. The contrail climate impact of fuels such as SAF and hydrogen is, therefore, highly sensitive to modelling assumptions of the low-soot regime. If recent in-situ measurements of lean-burn technology (Voigt et al., 2026) are indicative of future low-soot fuels, the anticipated contrail-induced climate advantage may be substantially lower than often assumed. This clearly underscores the need for improved research into the microphysical pathways for ice crystal formation in the low-soot regime and the effect of fuel and exhaust composition.

The study of the ICAO scenarios demonstrates the ability of the OpenAirClim response modelling framework to efficiently simulate and attribute the contrail and CO_2 climate impacts of realistic, multi-fuel transition pathways. The harmonisation process revealed that applying non-CO_2 assessment tools such as OpenAirClim to scenarios not originally designed for such analysis requires a number of high-level assumptions, particularly regarding fleet composition and the choice of emission inventory. A number of limitations and opportunities for improvement could also be identified, in addition to those already found by RQ2. Most notably, the OpenAirClim framework would benefit from a more flexible representation of evolving fleet characteristics and fuel use within sub-inventories over time.

Research Question 4: Are alternative climate metrics more suitable for assessing aviation CO_2 and non-CO_2 effects? *Addressed by Chapter 7 and published as Megill et al. (2024).*

The regulation of aviation non-CO_2 emissions, for example in emissions trading schemes, requires the use of a climate metric, which can express these emissions on a common scale with CO_2 (Fuglestvedt et al., 2003). However, choosing a suitable climate metric is challenging due to the high uncertainties of aviation non-CO_2 climate impacts, their highly variable atmospheric lifetimes and their dependence on the emission location, altitude and time of day (e.g. Ponater et al., 2006; Lund et al., 2017; Frömming et al., 2021). To answer this research question, a set of four requirements for climate metrics are established and the responses of a range of alternative climate metrics are analysed from simulations using AirClim (Grewe and Stenke, 2008; Dahlmann et al., 2016).

All climate metrics are found to embed implicit trade-offs between CO_2 emissions and non-CO_2 emissions and effects. The radiative and temperature changes from aviation non-CO_2 are comparable in magnitude to those from CO_2. The choice of climate metric thus plays a key role in ensuring that climate policies reach their intended objectives.

Due to the historical dominance of the Global Warming Potential (GWP), there is a natural bias to select climate metrics that behave similarly. However, there are derivatives and alternatives that outperform the GWP for aviation policy and aircraft design. The Average Temperature Response (ATR) provides a more direct representation of aviation's contribution to global mean temperature change and is thus closer to temperature-based targets such as those set by the Paris Agreement. It also has the potential to include more climatic processes, at the expense of a larger number of assumptions and uncertainties. The Efficacy-weighted Global Warming Potential (EGWP) is a useful compromise for policymaking since it retains the methodological familiarity of the GWP framework whilst better reflecting the temperature response. However, it too requires estimates for the ef-

ficacy, which for non-CO_2 species and effects remain uncertain (Lee et al., 2021; Bickel et al., 2025). Nevertheless, both the EGWP and ATR demonstrate better neutrality, stability and policy relevance for aviation than the conventional GWP.

There is no single, general optimal value for the time horizon. Shorter time horizons emphasise short-lived non-CO_2 effects but risk undervaluing the cumulative nature of CO_2; longer time horizons better capture long-term responses but are subject to higher uncertainty and depend on the choice of emission scenario. Integrated climate metrics such as the EGWP and ATR require longer time horizons, generally above 70 years, to account for atmospheric radiative and temperature adjustments, but depending on the objective a short time horizon can also be justified. The choice of time horizon is thus not an optimisation problem, but a policy decision that should depend on the policy and climate objectives.

Non-CO_2 emissions and effects are increasingly being considered by climate policy, notably within the European Union's Monitoring, Reporting and Verification (MRV) framework for aviation non-CO_2 effects. The evaluation of climate metrics presented in this dissertation thus has direct regulatory relevance. Discussions with policymakers and industry stakeholders highlighted the need to clearly differentiate between climate models and metrics since their effects and uncertainties are often conflated and misunderstood.

8.2. OUTLOOK

The contrail modelling and metrics framework presented by this work enables the consistent assessment of aviation climate impacts across existing and future fuels and technologies. At the same time, the answers to the research questions reveal uncertainties and limitations that confine its current range of validity. This section therefore outlines key avenues for future research to strengthen the physical basis and robustness of the framework, extend its applicability to evolving fleet and operational concepts and enhance its policy relevance.

The contrail modelling framework, integrated into OpenAirClim and presented in Chapters 4 and 5, is a significant advancement that enables OpenAirClim to flexibly model future multi-fuel aviation scenarios. However, the ICAO scenario analysis in Chapter 6 demonstrated how sensitive the model is to the definition of the low-soot regime. Additionally, the current contrail module only posits a relationship between the soot number emission index and contrail optical depth, which requires further research and validation. This work clearly underscores the need for better understanding of ice crystal formation in the low-soot regime as well as the influence of other combustion and ambient aerosols. A key next step would thus be to investigate the link between soot and other combustion and ambient aerosols on the optical depth to improve and validate the modelling approach. The ultimate goal should be to directly link fuel composition to its effects

on physical and optical contrail properties.

A straightforward area of improvement relates to the validity range of the contrail module. The current version was developed using simulations for regional and short-/medium-range aircraft only. As a result, the underlying simulations did not consider air traffic over certain areas, notably the Atlantic and Pacific oceans. Comparison with a simulation that did include this traffic did not identify any discrepancies. However, the module would certainly benefit from dedicated ECHAM5-CCMod simulations to cover this air traffic and hence extend the validity range. By using multipliers, the same simulations could also be used to further validate the model for scenarios with highly increased air traffic, for which published data is currently lacking. A systematic comparison of the OpenAirClim contrail module to other models such as CoCiP/pycontrails would also be of interest.

A question identified by this work is whether the Schmidt-Appleman theory, which is based on thermodynamic assumptions, is applicable to all aircraft. In this research, the theory was amended for high-G aircraft to more closely align with recent literature (Chapter 4), but this change has not been validated using a more comprehensive framework. Integrating recent studies (notably Ponsonby et al., 2025; Richardson, 2025; Hillenbrand and Unterstrasser, 2026) into the OpenAirClim contrail module would increase its flexibility for use with novel aviation fuels and propulsion designs, and is hence a good direction for further development.

The utility of OpenAirClim for analysing future aviation scenarios would be improved by introducing parameterisations for operational mitigation strategies. Contrail avoidance and climate-optimised routing in particular include inherent trade-offs between CO_2 and non-CO_2 emissions and effects. Extending OpenAirClim to include parameterisations for weather-based altitude and flight path adjustments would allow the long-term effectiveness of various strategies to be evaluated. Similarly, it could allow the assessment of targeted SAF deployment, where the limited available SAF is distributed to airports or flights to maximise its climate benefits. The analysis of more speculative concepts such as formation flying or multi-fuel aircraft architectures (e.g. combining combustion with a fuel cell) would require additional, dedicated simulations to understand interactions within the exhaust plumes and the influence on physical and optical contrail properties. Incorporating these updates into the OpenAirClim framework would allow such operational strategies to be considered within long-term integrated aviation scenarios.

The climate metric study has already informed aviation climate policy, most notably through the Non-CO_2 MRV. The MRV will be a good test case for the use of the newly developed EGWP, which must be reported on a per-flight basis over 20-, 50- and 100-year time horizons. The use of this climate metric clearly benefits from further research into efficacy values for non-CO_2 emissions and effects, in particular for contrails given its high level of uncertainty. The results of

the study could also be compared using another model, including OpenAirClim once all non-CO_2 modules are ready.

Overall, this dissertation advances the climatological modelling and assessment of aviation climate impacts by linking contrail formation theory, response modelling and climate metric evaluation within a coherent analytical framework. A central outcome is the OpenAirClim contrail module, a transparent and computationally efficient tool that can easily be adapted and extended following scientific advancements. This work, along with accompanying, ongoing model development, will allow OpenAirClim to provide consistent assessments of aviation climate impacts across a wide range of fuels, propulsion technologies and transition pathways. Finally, the systematic evaluation of climate metrics identified alternatives that are more suited for ensuring aviation climate policy achieves its stated objectives. Together, these contributions help establish a physically grounded foundation for advancing the sustainable transformation of the aviation sector.

REFERENCES

Bickel, M., Ponater, M., Burkhardt, U., Righi, M., Hendricks, J., and Jöckel, P.: Contrail cirrus climate impact: from radiative forcing to surface temperature change, Journal of Climate, 38, 1895–1912, doi: 10.1175/JCLI-D-24-0245.1, 2025.

Bier, A. and Burkhardt, U.: Impact of parametrizing microphysical Processes in the jet and vortex phase on contrail cirrus properties and radiative forcing, Journal of Geophysical Research: Atmospheres, 127, doi: 10.1029/2022JD036677, 2022.

Dahlmann, K., Grewe, V., Frömming, C., and Burkhardt, U.: Can we reliably assess climate mitigation options for air traffic scenarios despite large uncertainties in atmospheric processes?, Transportation Research Part D: Transport and Environment, 46, 40–55, doi: 10.1016/j.trd.2016.03.006, 2016.

Frömming, C., Grewe, V., Brinkop, S., Jöckel, P., Haslerud, A. S., Rosanka, S., van Manen, J., and Matthes, S.: Influence of weather situation on non-CO2 aviation climate effects: the REACT4C climate change functions, Atmospheric Chemistry and Physics, 21, 9151–9172, doi: 10.5194/acp-21-9151-2021, 2021.

Fuglestvedt, J. S., Berntsen, T. K., Godal, O., Sausen, R., Shine, K. P., and Skodvin, T.: Metrics of climate change: assessing radiative forcing and emission indices, Climatic Change, 58, 267–331, doi: 10.1023/A:1023905326842, 2003.

Gierens, K.: Theory of contrail formation for fuel cells, Aerospace, 8, 164, doi: 10.3390/aerospace8060164, 2021.

Gierens, K., Matthes, S., Rohs, S., and Susanne Rohs: How well can persistent contrails be predicted, Aerospace, 7, 169, doi: 10.3390/aerospace7120169, 2020.

Grewe, V. and Stenke, A.: AirClim: An efficient tool for climate evaluation of aircraft technology, Atmospheric Chemistry and Physics, 8, 4621–4639, doi: 10.5194/acp-8-4621-2008, 2008.

Hillenbrand, D. and Unterstrasser, S.: Contrail formation: generalised theory and a mitigation proposition for fuel-cell-propelled aircraft, The Aeronautical Journal, pp. 1–26, doi: 10.1017/aer.2026.10185, 2026.

Hofer, S., Gierens, K., and Rohs, S.: Contrail formation and persistence conditions for alternative fuels, Meteorologische Zeitschrift, 33, 43–49, doi: 10.1127/metz/2024/1178, 2024a.

Hofer, S., Gierens, K., and Rohs, S.: How well can persistent contrails be predicted? An update, Atmospheric Chemistry and Physics, 24, 7911–7925, doi: 10.5194/acp-24-7911-2024, 2024b.

Kaufmann, S., Dischl, R., and Voigt, C.: Regional and seasonal impact of hydrogen propulsion systems on potential contrail cirrus cover, Atmospheric Environment: X, 24, 100 298, doi: 10.1016/j.aeaoa.2024.100298, 2024.

Lee, D., Fahey, D., Skowron, A., Allen, M., Burkhardt, U., Chen, Q., Doherty, S., Freeman, S., Forster, P., Fuglestvedt, J., Gettelman, A., De León, R., Lim, L., Lund, M., Millar, R., Owen, B., Penner, J., Pitari, G., Prather, M., Sausen, R., and Wilcox, L.: The contribution of global aviation to anthropogenic climate forcing for 2000 to 2018, Atmospheric Environment, 244, 117 834, doi: 10.1016/j.atmosenv.2020.117834, 2021.

Lund, M. T., Aamaas, B., Berntsen, T., Bock, L., Burkhardt, U., Fuglestvedt, J. S., and Shine, K. P.: Emission metrics for quantifying regional climate impacts of aviation, Earth System Dynamics, 8, 547–563, doi: 10.5194/esd-8-547-2017, 2017.

Megill, L. and Grewe, V.: Investigating the limiting aircraft-design-dependent and environmental factors of persistent contrail formation, Atmos. Chem. Phys., 25, 4131–4149, doi: 10.5194/acp-25-4131-2025, 2025.

Megill, L., Deck, K., and Grewe, V.: Alternative climate metrics to the Global Warming Potential are more suitable for assessing aviation non-CO2 effects, Communications Earth & Environment, 5, 249, doi: 10.1038/s43247-024-01423-6, 2024.

Ponater, M., Pechtl, S., Sausen, R., Schumann, U., and Hüttig, G.: Potential of the cryoplane technology to reduce aircraft climate impact: A state-of-the-art assessment, Atmospheric Environment, 40, 6928–6944, doi: 10.1016/j.atmosenv.2006.06.036, 2006.

Ponsonby, J., Teoh, R., Kärcher, B., and Stettler, M. E. J.: An updated microphysical model for particle activation in contrails: the role of volatile plume particles, Atmospheric Chemistry and Physics, 25, 18 617–18 637, doi: 10.5194/acp-25-18617-2025, 2025.

Richardson, E. S.: Contrail Formation Criterion for Assessment of Alternative Propulsion Technologies, Journal of Propulsion and Power, 41, 264–276, doi: 10.2514/1.B39430, 2025.

Teoh, R., Engberg, Z., Schumann, U., Voigt, C., Shapiro, M., Rohs, S., and Stettler, M. E. J.: Global aviation contrail climate effects from 2019 to 2021, Atmospheric Chemistry and Physics, 24, 6071–6093, doi: 10.5194/acp-24-6071-2024, 2024.

Voigt, C., Märkl, R., Sauer, D., Dischl, R., Renard, C., Seeliger, K., Yu, F., Kaufmann, S., Bräuer, T., Jurkat-Witschas, T., Le Chenadec, G., Moreau, J., Requena-Esteban, E., Bonne, N., Vals, M., Roche, A., Zelina, J., Dörnbrack, A., Eirenschmalz, L., Heckl, C., Horst, E., Lichtenstern, M., Marsing, A., Neumann, G., Roiger, A., Scheibe, M., Stock, P., Giez, A., Eckel, G., and Le Clercq, P.: Substantial aircraft contrail formation at low soot emission levels, Nature, 652, 112–118, doi: 10.1038/s41586-026-10286-0, 2026.

A

OPENAIRCLIM CONTRAIL MODULE

Parts of this chapter have been published at:

https://openairclim.org/background/contrails.html [last accessed 18/05/2026].

This chapter provides a concise overview of the methods and functions underlying the OpenAirClim Contrail Module (oac.cont). Its purpose is to provide a quick reference, next to the official documentation[1]. More detail about the modelling approach and validation is provided in Chapter 5.

The objective of the OpenAirClim contrail module is to calculate the changes in the contrail-induced global annual mean stratospheric-adjusted radiative forcing due to an input emission inventory and scenario. The high-level setup is in line with AirClim 2.1 (Dahlmann et al., 2016; Grewe et al., 2017) and can be represented as: emission inventory → contrail formation → contrail-cirrus coverage → radiative forcing. An overview of the module is provided by Figure A.1.

The emission inventory and simulation configuration is described in Section A.1. The contrail formation, contrail-cirrus coverage and radiative forcing parameterisations are shown in Sections A.2 to A.4. Finally, Sections A.5 and A.6 describe the post-processing and attribution processes respectively.

A.1. EMISSION INVENTORY AND SIMULATION CONFIGURATION

The OpenAirClim emission inventory files are in netCDF format and consist of yearly aggregated emission data for each species and corresponding emission locations (latitude, longitude, pressure level). Emission data may be provided on either regular or irregular grids and for multiple different years. OpenAirClim either interpolates between the input emission inventories, or scales the results following a time evolution defined by the user. See the upcoming main OpenAirClim publication and the OpenAirClim documentation for more detail.

For the calculation of the contrail climate impact, the yearly aggregated, 3D-resolved distance flown is required. If multiple aircraft are present within the emission inventory, each entry in the inventory must be accompanied by an identifier (variable `ac` in the netCDF file). The user is free to choose appropriate labels for the inventory in question. For example, the labels could correspond to the aircraft type (e.g. `A320` or `B737`) or to the propulsion technology (e.g. `SAF` or `H2C`). Important is only that all identifiers in the emission inventories are defined in the simulation configuration – the OpenAirClim documentation provides more detail on how to do this. To calculate a contrail climate impact, the following contrail-relevant parameters must be defined for each identifier. Further parameters may be added in future updates.

- G_{250}: Slope of the mixing line G at $250\,\mathrm{hPa}$ in $\mathrm{Pa\,K^{-1}}$. Valid range: $\geq 0.48\,\mathrm{Pa\,K^{-1}}$. Alternatively, the necessary parameters to calculate the slope can be provided, using equations (1) to (4) in Megill and Grewe (2025);

[1] https://openairclim.org [Last accessed: 09/03/2026]

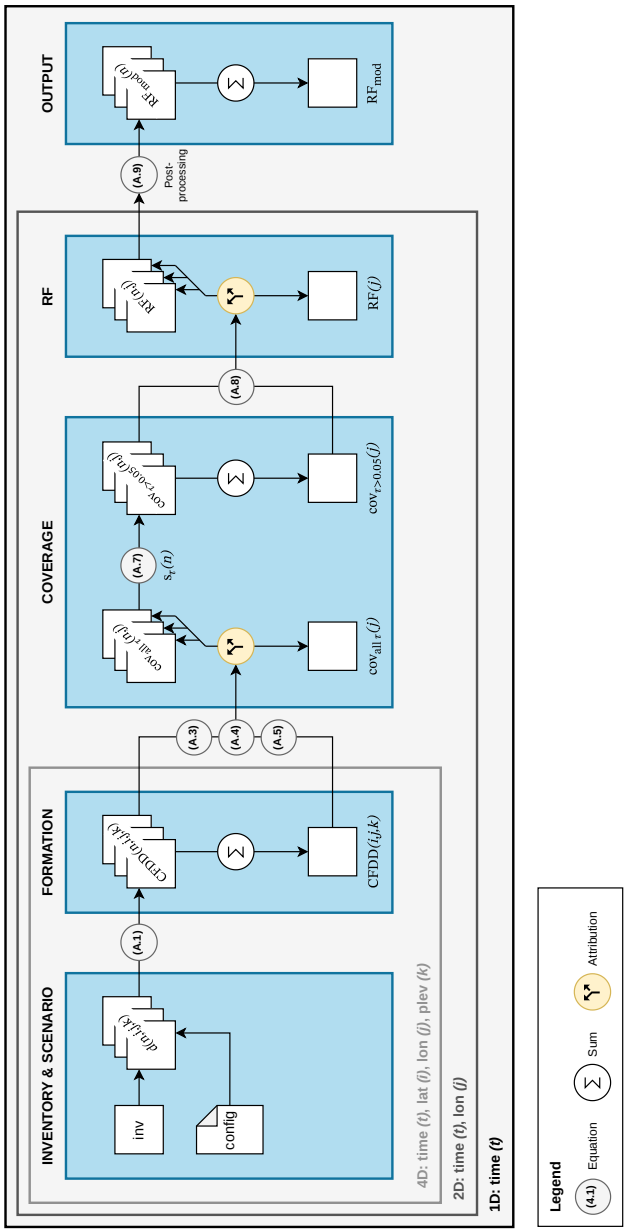


Figure A.1: Overview of the OpenAirClim Contrail Module.

- $\mathrm{EI_s}$: Soot number emission index in $\mathrm{kg^{-1}}$. Valid range[2]: $\geq 0.0\ \mathrm{kg^{-1}}$;
- b: Wing span in m. Valid range (high soot regime only): [20 m, 80 m] (defaults to 35 m).

A.2. CONTRAIL FORMATION

Persistent contrail formation is represented using the Contrail Flight Distance Density (CFDD), which is calculated for each fleet n in the emission inventory and in all three spatial dimensions,

$$\mathrm{CFDD}(n,i,j,k) = \frac{d(n,i,j,k)}{A(i,j)} \cdot p_{\mathrm{pcf}}(G_{250}(n),i,j,k) \tag{A.1}$$

where $d(n,i,j,k)$ is the slant (3D) distance flown (km) in each grid box (aircraft, latitude, longitude, pressure level); $A(i,j)$ is the horizontal area of each grid column ($\mathrm{km^2}$); and $p_{\mathrm{pcf}}(G_{250}(n),i,j,k)$ is the probability of persistent contrail formation in each grid box ($\in [0,1]$) for an aircraft n with a Schmidt-Appleman mixing line slope G_{250} at $250\,\mathrm{hPa}$. The pressure level $250\,\mathrm{hPa}$, corresponding to Flight Level 340, or $34000\,\mathrm{ft}$ in the International Standard Atmosphere, is chosen as the reference pressure level.

The p_{pcf} values are pre-calculated for 13 aircraft designs with G_{250} values between 0.48 and $15.82\,\mathrm{Pa\,K^{-1}}$ following the Megill and Grewe (2025) methodology (Chapter 4) and interpolated along modified logistic functions of the form,

$$\overline{p_{\mathrm{pcf}}}(G) = \frac{L_1}{1+\mathrm{e}^{-k_1(G-G_{0,1})}} + \frac{L_2}{1+\mathrm{e}^{-k_2(G-G_{0,2})}} + d \tag{A.2}$$

where $\overline{p_{\mathrm{pcf}}}$ is the global, area-weighted average p_{pcf}. The function parameters are dependent on the pressure level and are available in the dataset accompanying this dissertation.

A

A.3. CONTRAIL-CIRRUS COVERAGE

Two different measures of contrail-cirrus coverage are considered by OpenAirClim: total coverage across all optical depths ($\mathrm{cov_{all\ \tau}}$) and optically thick coverage ($\mathrm{cov_{\tau>0.05}}$). The contrail-cirrus coverage submodule is split into two steps: calculating $\mathrm{cov_{all\ \tau}}$ from CFDD using a dedicated parameterisation; and calculating $\mathrm{cov_{\tau>0.05}}$ from $\mathrm{cov_{all\ \tau}}$ using the scaling factor s_τ, derived from literature.

[2]Until publication of the underlying ECHAM5-CCMod simulation data, the publicly available valid range is limited to $\geq 1.5 \times 10^{14}\,\mathrm{kg^{-1}}$

The relationship between CFDD and $\mathrm{cov}_{\mathrm{all}\ \tau}$ is strongly non-linear. It is represented by a hyperbolic tangent function of the form,

$$\mathrm{cov}_{\mathrm{all}\ \tau}(n,i,j,k) = a \cdot \tanh\left(b \cdot \mathrm{CFDD}(n,i,j,k)\right) \tag{A.3}$$

where parameter $a = 0.0772$ controls the asymptotic maximum coverage and $b = 132.3\,\mathrm{km}$ the sensitivity to the CFDD. The coverage is then combined vertically using a random overlap assumption, i.e. assuming statistical independence between vertical layers k,

$$\mathrm{cov}_{\mathrm{all}\ \tau}(n,i,j) = 1 - \prod_k \left(1 - \mathrm{cov}_{\mathrm{all}\ \tau}(n,i,j,k)\right) \tag{A.4}$$

and then area-weighted over the latitude i,

$$\mathrm{cov}_{\mathrm{all}\ \tau}(n,j) = \frac{\sum_i \mathrm{cov}_{\mathrm{all}\ \tau}(n,i,j) \cdot A(i,j)}{\sum_i A(i,j)} \tag{A.5}$$

A scaling factor s_τ is applied to obtain an estimate of optically thick contrail-cirrus coverage $\mathrm{cov}_{\tau>0.05}$. This scaling factor is currently only a function of the soot number emission index $\mathrm{EI_s}$, but further dependencies could be added in future updates. The function is defined for both the high- and low-soot regimes. The parameter x corresponds to the $\mathrm{EI_s}$ relative to the reference $1.5 \times 10^{15}\,\mathrm{kg}^{-1}$. In the high-soot regime ($x \geq x_0$, where $x_0 = 0.1$), a single arctangent form is derived from literature. In the low-soot regime ($0 < x < x_0$), a set of three cases are introduced using composite logistic-beta functions that smoothly connect the low- and high-soot regimes at x_0. Mathematically, s_τ is defined as,

$$s_\tau = \begin{cases} 0.91 \cdot \arctan\left(1.96 \cdot x^{0.58}\right) & \text{for } x \geq 0.1 \\ c_0 + (y_0 - c_0) \cdot w(x) - d \cdot h(x) & \text{for } 0 < x < 0.1 \\ 0.385 & \text{for } x = 0 \end{cases}$$

$$w = \frac{2\,u^k}{1+u^k}, \quad \text{where } u = \frac{x}{x_0} \tag{A.6}$$

$$h = u^p \cdot (1-u)$$

$$d = x_0\left(y_0' - \frac{1}{2}(y_0 - c_0) \cdot \frac{k}{x_0}\right)$$

where $c_0 = \lim_{x\to 0+} s_\tau(x)$ is the value as x approaches 0 for a given case, $y_0 = s_\tau(x_0)$ is the value of the high-soot fit at the transition point and y_0' is its derivative

(also at x_0). The parameter c_0 describes the limiting behaviour as $x \to 0^+$, while the discrete value at $x = 0$ is imposed independently. The transition function w controls the monotonic transition between the limiting value c_0 and the transition point y_0, while the term involving h introduces a local curvature adjustment near x_0, allowing the gradient of the composite function to match that of the high-soot fit. The parameters k and p control the steepness of the transition and the shape of the curvature adjustment, respectively.

Three sets of parameters are implemented at the time of writing, shown in Table A.1. Case MID aligns with the ECHAM5-CCMod hydrogen simulations (see Section 5.2) as $x \to 0$ and is currently used by default by oac.cont. Cases LOW and HIGH are designed to define lower and upper boundaries, following Rubin-Zuzic et al. (2025) and Voigt et al. (2026) respectively. Further work is required to better constrain the low-soot regime.

Table A.1: Parameters for the low-soot regime modelling cases.

	c_0	k	p
Case MID	0.385	2.0	2.5
Case LOW	0.08	1.0	0.3
Case HIGH	0.8	3.5	1.2

For a given aircraft n, the optically thick contrail-cirrus coverage is then calculated using,

$$\mathrm{cov}_{\tau>0.05}(n, j) = \mathrm{cov}_{\mathrm{all}\ \tau}(n, j) \cdot s_\tau(n) \tag{A.7}$$

A.4. RADIATIVE FORCING

Separate relationships are derived between $\mathrm{cov}_{\tau>0.05}$ and RF for four regions defined by longitude (see also Supplementary Figure 5.A.2): Americas (235, 330]; Europe, Middle-East and Africa (330, 60]; Asia and Australia (60, 160]; and Pacific (160, 235]. Within each region, RF is determined using a power-law relationship of the form,

$$\mathrm{RF}(j) = c_j \cdot \mathrm{cov}_{\tau>0.05}(j)^{\gamma_j} \tag{A.8}$$

where $\mathrm{cov}_{\tau>0.05}(j)$ is the area-weighted optically thick contrail-cirrus coverage for longitude band j, and c_j and γ_j are region-specific fit parameters (derived using the CCMod simulation results). The range of validity differs depending on the region due to data availability (see the right side of Figure 5.9). OpenAirClim therefore checks whether input coverage values fall outside the fitted range and issues a warning if extrapolation occurs. The fit parameters and validity ranges

are provided in Table A.2.

Table A.2: Radiative forcing model fit parameters and validity ranges. The values are given for each region (defined by longitude) as well as for the global fit. The maximally valid contrail-cirrus coverage [%] is given for each region.

Region	Longitude	c	γ	Max. $\mathrm{cov}_{\tau>0.05}$
EMEA	(330, 60]	9.64	1.02	1.52 %
Asia & Austr.	(60, 160]	10.81	1.00	1.03 %
Pacific	(160, 235]	1.93	0.81	0.21 %
Americas	(235, 330]	20.33	1.14	2.91 %
Global	(0, 360]	25.04	1.20	2.91 %

Because the model grid uses equal longitudinal spacing, each band contributes equally to the global mean RF. The global RF is thus simply the mean of $\mathrm{RF}(j)$.

A.5. POST-PROCESSING

The contrail module currently has a single post-processing step for the resulting RF, which depends on the size of the aircraft in the emission inventory. Large aircraft tend to produce contrails with a higher number of ice crystals, resulting in overall deeper contrails. Therefore, the simple relationship presented by Bruder et al. (2026, see their Supplementary Section S1) is applied,

$$\mathrm{RF}_{\mathrm{mod}}(n) = \mathrm{RF}(n) \cdot \frac{v + w \cdot b(n)}{v + w \cdot b_{\mathrm{ref}}} \tag{A.9}$$

where $b(n) \in [20\ \mathrm{m}, 80\ \mathrm{m}]$ is the wingspan of fleet n, $w = 0.0287\ \mathrm{m}^{-1}$ and $v = 0.396$. If no wingspan is given, OpenAirClim defaults to $b_{\mathrm{ref}} = 35\ \mathrm{m}$. Currently, the correction is not valid for the low-soot regime – within this regime, $b(n)$ is assumed to be equal to b_{ref}.

A.6. ATTRIBUTION

The contrail module implements proportional attribution, consistent with the tagging-based approach used in other OpenAirClim modules (Völk et al., in prep.). In proportional attribution, the contribution of each aircraft identifier to the output variable is determined from its fractional contribution to the input variable. Specifically, the contribution of identifier n to $\mathrm{cov}_{\mathrm{all}\ \tau}$ is determined from its relative contribution to CFDD, and the contribution to RF is determined from its relative contribution to $\mathrm{cov}_{\tau>0.05}$.

REFERENCES

Bruder, H., Thor, R. N., Niklaß, M., Dahlmann, K., Eichinger, R., Linke, F., Grewe, V., Matthes, S., and Unterstrasser, S.: The DLR CO2-equivalent estimator FlightClim v1.0: an easy-to-use estimation of per flight CO2 and non-CO2 climate effects, Geoscientific Model Development, 19, 3551–3567, doi: 10.5194/gmd-19-3551-2026, 2026.

Dahlmann, K., Grewe, V., Frömming, C., and Burkhardt, U.: Can we reliably assess climate mitigation options for air traffic scenarios despite large uncertainties in atmospheric processes?, Transportation Research Part D: Transport and Environment, 46, 40–55, doi: 10.1016/j.trd.2016.03.006, 2016.

Grewe, V., Bock, L., Burkhardt, U., Dahlmann, K., Gierens, K., Hüttenhofer, L., Unterstrasser, S., Gangoli Rao, A., Bhat, A., Yin, F., Reichel, T. G., Paschereit, O., and Levy, Y.: Assessing the climate impact of the AHEAD multi-fuel blended wing body, Meteorologische Zeitschrift, 26, 711–725, doi: 10.1127/metz/2016/0758, 2017.

Megill, L. and Grewe, V.: Investigating the limiting aircraft-design-dependent and environmental factors of persistent contrail formation, Atmos. Chem. Phys., 25, 4131–4149, doi: 10.5194/acp-25-4131-2025, 2025.

Rubin-Zuzic, M., Bugliaro, L., Marsing, A., Wang, Z., Voigt, C., Simson, C., Kaiser, S., and Ziegler, P.: Reduced contrail radiative effect for fleets with low soot and water vapour emissions, Atmospheric Environment: X, 27, 100 353, doi: 10.1016/j.aeaoa.2025.100353, 2025.

Voigt, C., Märkl, R., Sauer, D., Dischl, R., Renard, C., Seeliger, K., Yu, F., Kaufmann, S., Bräuer, T., Jurkat-Witschas, T., Le Chenadec, G., Moreau, J., Requena-Esteban, E., Bonne, N., Vals, M., Roche, A., Zelina, J., Dörnbrack, A., Eirenschmalz, L., Heckl, C., Horst, E., Lichtenstern, M., Marsing, A., Neumann, G., Roiger, A., Scheibe, M., Stock, P., Giez, A., Eckel, G., and Le Clercq, P.: Substantial aircraft contrail formation at low soot emission levels, Nature, 652, 112–118, doi: 10.1038/s41586-026-10286-0, 2026.

B

CURRICULUM VITÆ

W. A. (Liam) Megill

12-02-1997 Born in Vancouver, Canada.

EDUCATION

2013–2016 Abitur
Städtisches Gymnasium Goch, Goch, Germany

2016–2020 Bachelor of Science in Aerospace Engineering
Delft University of Technology, Delft, The Netherlands

2020–2023 Master of Science in Aerospace Engineering
Delft University of Technology, Delft, The Netherlands

2023–2026 PhD candidate
Delft University of Technology, Delft, The Netherlands
Thesis: Assessing Contrail Climate Impacts and Metrics with OpenAirClim
Promotor: Prof.dr. V. Grewe

AWARDS

2023 Ivar Isaksen Early Career Researcher Prize

Aviation's climate impact extends well beyond CO_2. Contrails alone are estimated to account for over one-third of the effective radiative forcing from aircraft operations. However, as policymakers begin to fold non-CO_2 effects into regulation, they face a difficult problem: contrail impacts are highly uncertain and vary sharply with where, when and how aircraft fly.

This dissertation develops a new contrail module for the climate response model OpenAirClim, enabling computationally inexpensive estimates of contrail impacts across a wide range of aircraft and fuels. Application to the ICAO LTAG scenarios reveals that alternative aviation fuels alone will not sufficiently curb the industry's climate impact; their introduction must be coupled with dedicated non-CO_2 measures.

This dissertation also finds the conventional Global Warming Potential not suitable for aircraft design trade-offs and aviation policy. Efficacy-weighted and temperature-based metrics are proposed instead, which align more closely with international climate agreements.

TU Delft

DLR

